FLOW PATTERNS
ON SIEVE TRAYS

VOLUME I

A THESIS SUBMITTED

BY

SIMON CHAMBERS B.Sc. Dip.Ind.

A candidate for the degree of

Doctor of Philosophy

DEPARTMENT OF CHEMICAL ENGINEERING
AND
APPLIED CHEMISTRY

UNIVERSITY OF ASTON IN BIRMINGHAM

MAY 1993

CERTIFICATE

CONTAINS DISKETTE

UNABLE TO COPY

CONTACT UNIVERSITY

IF YOU WISH TO SEE

THIS MATERIAL

The University of Aston in Birmingham

FLOW PATTERNS ON SIEVE TRAYS

A Thesis submitted by

Simon Chambers B.Sc. Dip.Ind.

A candidate for the degree of Doctor of Philosophy

May 1993.

THESIS SUMMARY

Studies into gas-liquid flow patterns were carried out on commercial scale sieve trays where the ratio of froth depth to flow path length is typical of that found in practice. Experiments were conducted on a 2.44 m diameter air-water distillation simulator, in which flow patterns were investigated by direct observation, using directional flow pointers; by water cooling, to simulate mass transfer; and by height of clear liquid measurements across the tray using manometers. The flow rates used are typical of those found in practice.

The approach adopted was to investigate the effect of the gas flow on the liquid flow by comparing water only flow patterns across an unperforated tray with air-water flow patterns on perforated trays. Initial gas-liquid contacting experiments on the 6.35 mm hole tray showed that under certain conditions, the gas flow pattern beneath the test tray, can have a significant effect on the tray liquid flow pattern such that gas-driven liquid circulation was produced. This was found to be a function of this particular air-water simulator design, and as far as is known this is the first time that this phenomenon has been observed. Consequently non-uniform gas flow effects were removed by modification of the gas distribution system.

By eliminating gas circulation effects, the effect of the gas flow on the separation of liquid flow was similar to that obtained on the 1.0 mm hole tray (Hine, 1990). That is, flow separation occurred at the ends of the inlet downcomer which produced large circulating zones along the tray segments both on the non-perforated and perforated trays. The air when forced through the liquid, inhibited circulating flow such that it only occurred at high water inlet velocities. With the 6.35 mm hole tray, the growth and velocity of circulating flow was reduced at high superficial air velocities, and in the experiments to simulate distillation, liquid was in forward flow over most of the tray.

For all experiments, water cooling and the measurement of clear liquid heights were used to show the effect of flow patterns on mass transfer and on the liquid head gradient across the tray. In most cases, including gas-driven liquid circulation and the simulation of distillation, there were colder liquid regions on the tray where circulating or slower moving liquid has a longer residence time. This in turn had an adverse effect on the calculated tray efficiencies. The height of clear liquid of the slower moving or circulating liquid on the sides of the tray at the ends of the inlet downcomer was greater than that for the faster moving liquid along the middle.

Studies into gas-liquid interactions on two trays, set at a spacing of 300 mm, showed that the gas flow did not change the direction of liquid flow on the second tray in the same way as that observed on the one tray. Furthermore the flow patterns on the second tray were, on the whole, superior to that produced on the one tray in that the size and velocity of reverse or circulating flow was less compared to those on the one tray.

Overall the experiments have shown that the presence of gas-driven liquid circulation ocurred on the one tray only. Hence, in a real tray column, gas-influenced liquid flow patterns may only occur on the first tray above the vapour feed inlet. Nevertheless it is quite possible that the inter-tray gas flow pattern may change the liquid flow on all trays within a column, at higher tray spacings. This is the subject of further research at Aston University.

Keywords: DISTILLATION, SIEVE TRAYS, FLOW PATTERNS, GAS DISTRIBUTION, CIRCULATION, MASS TRANSFER.

ACKNOWLEDGEMENTS

I would like to express my sincere gratitude to the following:-

Professor K. E. Porter, for his enlightening supervision, constant encouragement and stimulating ideas throughout the course of the research program.

The workshop technicians; Ian Murkett, Roger Wheeler, Maurizio Santoro, Bill Curtis, and Pete Green, for their exellent practical help, advice and assistance, particularly during the careful modification of the distillation simulator facility.

The departmental technicians and secretarial staff for their valuable help and advice throughout the programme of research and preparation of the thesis.

Mr. M.J. Griffiths for his guidance and expertise during my training at BP Chemicals Ltd., Belgrave House, London.

The Science and Engineering Research Council (SERC), and BP Chemicals Ltd. for their funding of the CASE award.

My family and friends for their constant support.

And finally, to my wife Jacky for her valued expertise in the typing of the thesis, as well as for her enormous patience, constant encouragement and understanding particularly at difficult times.

LIST OF PUBLICATIONS

1. Chambers, S. and Porter, K.E., 1991, " Liquid distribution and mass transfer on a 2.44 m diameter distillation tray. ", Poster presented at the I.ChemE Research Event, University of Cambridge, Cambridge. (Work based on Chapters 6 and 8).

2. Porter, K.E., Yu, K.T., Chambers, S. and Zhang, M.Q., 1992, " Flow patterns and temperature profiles on a 2.44 m sieve tray ", I.ChemE Symposium Series No. 128: A257. (Work based on Chapters 8 and 9).

3. Porter, K.E., Yu, K.T., Chambers, S. and Zhang, M.Q., 1992, " Flow patterns and temperature profiles on a 2.44 m sieve tray ", I.ChemE Trans.,Vol. 70, Part A. (Work based on Chapters 8 and 9).

TABLE OF CONTENTS

LIST OF FIGURES

LIST OF TABLES

LIST OF FIGURES IN APPENDICES IN VOLUME II

LIST OF TABLES IN APPENDICES IN VOLUME II

CHAPTER 1

INTRODUCTION

Distillation in many ways resembles the motor industry in that it is a mature business which is constantly being driven by market forces and is often led by research and development (Porter, 1992). Thus the assertion that distillation is a fully mature technology and lacking the potential for further improvement, can be dispelled by the fact that it is the most frequently used process for separating fluid mixtures and that more sophisticated distillation technology is continually being developed. For instance, the petrochemical industry, in terms of tonnage throughput, is by far the largest user of distillation technology, so much so that the total amount of distillation capacity in oil refineries is in excess of five billion tons per annum (Darton, 1992).

However, the main drawback of distillation is that it consumes large quantities of energy. In a recent survey (Report on Energy Consumption in the U.K. Chemical Industry, Legg, 1986), presented in Table 1.1, distillation accounted for 13% of the total energy consumption in the U.K. chemical industry and this results in high running costs.

	Industrial Operation	Energy Usage - %
Breakdown of the energy use for the chemical industry	Process Heating	40
	Distillation	13
	Compressors	10
	Drying	10
	Pumping	6
	Refrigeration	5
	Evaporation	4
	Space Heating	4
	Comminution	2
	Drive Motors	2
	Fans and Blowers	2
	Mixing	2

Table 1.1 Summary of the total energy consumption by various operations in the chemical industry.

Thus any improvements in the overall distillation technology, however small, may produce substantial rewards in energy and financial savings. In 1979, Rush demonstrated that for most cases, it would not be economically viable to use an alternative method of separation. Furthermore, he stated that there was a need to design distillation

columns 'leaner and harder', at a time when energy conservation and power savings were top priority.

In fact, the most significant energy savings (and thus a reduction in the capital and overall running costs) can be achieved in the immediate future by operating existing distillation equipment more efficiently. That is, by operating columns at a lower reflux ratio close to the pinch point. However, this approach increases the risk of distillation columns not performing to the required design specifications, and thus any unexpected loss in column efficiency may have large adverse effects. Hence a thorough understanding of vapour-liquid contacting devices, be they trays or packings, is clearly needed so as to improve column performance.

Originally, the use of trays were favoured over packings since trays were less expensive to manufacture and there was considerable uncertainty in the performance of scaled-up packed columns. This was in spite of the fact that the pressure drop of packings are approximately one-fifth that of trays, (Lockett, 1986). However, developments in modern structured packings have made possible a reduction in the column size and recent advancements in vapour and liquid distributor technology have overcome the problem of scale-up effects. Furthermore, it may be that equipment costs in the future will become similar to that used for trays.

Nevertheless, trays remain a popular column internal device for use in new plants because of the reduced initial cost. However, in the longer term, trays may be replaced by packings if the overall plant running costs need to be decreased. Despite this, the possibility of developing new trays, with an increased throughput and a high operating efficiency, exists on the basis of a better understanding of the fluid mechanics of two phase flows over a tray.

It was Porter and Jenkins (1979), who explained the reasons for correlating past experience empirically, and that this inhibited new developments in tray design owing to a lack in the scientific understanding of how trays operate under various flow conditions. (The use of empirical design methods increase the risk of column under- or over-design or even failure). Thus a thorough understanding of the flow phenomena and it's effect on mass transfer on distillation trays, beginning with sieve trays, is needed. The simple shape of sieve trays and ease of manufacture made them a popular choice for research and use in industrial scale columns. However, initial research into sieve tray performance did not keep pace with the continuous evolution of new trays of increasing diameter. A lack of data on the behaviour of vapour-liquid traffic in large diameter columns, and attempts

to apply data from small scale laboratory equipment for use in industrial scale columns led to serious discrepancies.

Thus over a period of many years, attempts have been made to relate the flow phenomena and mass transfer performance, i.e., tray efficiency, by the use of theoretical models. The prediction of flow patterns and their effect on tray and overall column performance were proposed by Kirshbaum (1934), Lewis (1936), Gerster (1958), Porter et al., (1972), Bell and Solari (1974), Sohlo and Kouri (1982), and Yu et al., (1990, 1991).

In general, the models are based on the concepts of a plug (unmixed) flow of liquid across a tray, or well mixed liquid pools with an interchange of liquid flow between them, or an imposed backmixing mechanism on the plug flow of liquid, or diffusional mixing within the liquid flow across circular trays. These theories assume that predicted liquid concentration changes only occur in the direction of liquid flow whilst remaining constant perpendicular to the direction of flow. This can be described as one dimensional modelling.

During the early 1970's, theoretical models which accounted for non-uniform liquid flow and mixing on a tray (Porter et al., 1972) were proposed on the basis of a limited amount of evidence concerning the existence of greater non-uniform liquid flow with increasing column diameter. The implications of the modelled hypothetical flow patterns, such as liquid channelling associated with stagnant regions at the sides of the tray, are a serious loss in tray efficiency and scale-up failures on large trays. This was subsequently confirmed on large single pass trays, of diameter 7.6 m, at the Union Carbide Company, Linde Division (Smith and Delnicki, 1975). Thus it became necessary to develop a two or three-dimensional modelling approach as well as the need for experimental data on trays of a commercially significant size. The most recent example of the modern approach to modelling is the three-dimensional non-equilibrium pool model (Yu et al., 1991), which predicts concentration changes and inter-diffusional mixing in two dimensions, in both the liquid and vapour mixing pools.

However, it should be noted that the above studies were based on hypothetical flow patterns, sometimes modelled on single phase flow, and would lead to some uncertainty in tray design since it is still not known how close the hypothetical liquid flow patterns are to reality. Hence, current research is directed towards the identification of the physical principles which are valid in a new branch of fluid mechanics, recently defined by Porter (1992) as "Open Channel Two Phase Flow". This phenomenon has been investigated at The University of Aston in Birmingham in cooperation with the National

Distillation Laboratory headed by Professsor K T Yu in the P.R. China. The new theory may permit the prediction of two phase flow patterns that are likely to occur in industrial-scale practical distillation.

Before any theoretical description of two phase flows across a distillation tray can be developed, a comprehensive set of flow patterns needs to be determined on trays of various hole sizes using flow conditions similar to those used in practice. Some progress in this area has been made using the 2.44 diameter simulator column at Aston in which distillation is simulated by forcing air (vapour) through a water (liquid) flow on commercial sized trays where the ratio of froth depth to flow path length is typical of that found in practice.

The overall experimental approach was to determine the effect of the gas flow on the liquid flow by comparing water-only flow patterns with those obtained by air-water contacting on perforated trays of various hole sizes. These include 1.0 mm holes, used in air-separation processes; intermediate hole size trays ranging from 4.50 mm to 6.35 mm, used in the chemical industry; and 12.7 mm hole trays, which are the most widely used trays in the petrochemical industry. The chemical and petrochemical industries utilize large hole trays since they are less prone to fouling compared with small hole trays.

Results from water-only flow experiments and air-water contacting on a 1.0 mm hole tray (Hine, 1990) showed that flow separation at the ends of the inlet downcomer occurred on both trays, thus causing large circulating zones at the sides. However, the air, when forced through the liquid flow, inhibited flow separation and circulating flow such that it only occurred at much higher water inlet velocities than with no air flow.

At this point, it is worth noting that intermediate sized hole trays, such as 6.35 mm holes, can have a peculiar effect on two phase flow patterns in that the gas flow can sometimes change the direction of liquid flow. For instance, Porter et al., (1987) reported severely distorted liquid flow patterns, in the form of highly "U -shaped" water temperature profiles from water-cooling experiments, on a 4.5 mm hole sieve tray, of diameter 1.22 m, compared to that obtained on 1.0 and 12.0 mm hole trays at the same operating conditions. In addition the effect of the gas flow, beneath a 6.0 mm hole tray (of diameter 2.44 m), on changing the direction of liquid flow was first reported by Ayvaz (1990). Under certain conditions, it was observed that the gas forced the liquid to circulate on the tray outlet. Thus it was established that non-uniform liquid flow, on trays of hole diameters 4.50-6.35 mm, may have been caused by gas flow effects and as far as is known this is the first time that this phenomenon has been observed.

With this in mind, gas-liquid contacting studies are to be carried out to determine the effect of the gas flow on the developed liquid flow pattern. Does the gas flow pattern change the direction of liquid flow such that it forces the liquid to circulate in a similar manner to that observed by Ayvaz (1990)? Or, does the gas flow pattern inhibit the separation of liquid flow in a similar manner to that observed on the 1.0 mm hole tray?

If the gas flow changes the direction of liquid flow on the tray, how does the direction of gas flow beneath the tray influence the tray liquid flow pattern? Does the gas distributor (i.e., chimney tray) have an effect on the gas flow pattern beneath the test tray? If this is the case, does the gas distribution system need to be modified so as to eliminate the effects of gas-influenced liquid flow patterns?

It is quite possible that the effect of the gas flow on the separation of liquid flow on a 6.35 mm hole tray may be similar to that observed on the 1.0 mm hole tray. Thus, under what conditions does the gas flow inhibit the onset of flow separation? If circulating flow is produced on the 6.35 mm hole tray, does it occupy the whole of the tray segments with increasing liquid velocity from small clearance heights beneath the inlet downcomer? Furthermore, is the velocity of circulating flow the same as that produced on the 1.0 mm hole tray ? Finally, are the developed two phase flow patterns similar to the hypothetical flow pattern developed in the stagnant regions model (Porter et al., 1972)?

An extension of the above set of investigations is to determine whether any flow separation occurs using flow conditions that simulate distillation in practice. That is, by selecting flow rates to simulate distillation at three different operating pressures, does circulating flow occur, or is the liquid in forward flow at all points on the tray?

If it is established that the direction of the gas flow beneath one tray changes the direction of liquid flow, does the gas flow emerging from the liquid movement on one tray influence the direction of liquid flow on a second tray placed directly above? It is important to address this problem since this will influence the way in which future theoretical models are developed to explain the flow patterns that occur in practical distillation columns. There are two possible alternatives:-

a) If the gas flow pattern changes the direction of liquid flow on more than one tray, then the new theoretical description will need to take into account the fluid mechanics of the vapour-liquid interactions throughout the column as a whole.

b) Alternatively, if the gas flow changes the direction of liquid flow on only the one tray, then this may be the result of gas entrance effects from the vapour feed inlet to

the column. Hence, the theoretical description will only need to concentrate on the fluid mechanics of liquid only flow on trays placed one above the other in a column.

The experimental results collected from this and other research programmes will be incorporated in an open channel two phase flow theoretical model during the next stage of tray research at Aston University. This more mechanistic model will be used to describe the controlling phenomena for any test system and tray configuration, which is necessary for the more scientific approach required for the design of new trays.

To answer the above questions, the structure of the thesis is set out in the following manner. A concise review of the literature, selected for evidence of the existence of gas flow effects on liquid flow patterns and flow patterns that are representative of that found in practice, will be followed by an overview of the overall programme of experiments used to study the behaviour of flow patterns on 6.35 mm hole trays. The following chapters will be concerned with describing in detail the apparatus, the experimental methods, and the appropriate modifications for the installation of two trays as well as procedures used for the presentation of results.

The series of investigations discussed in the following set of experimental chapters can be summarised as follows.

1) Experiments to determine the effect of gas flow, below the 6.35 mm hole test tray, on the liquid flow pattern and the removal of these effects by modification of the gas distributor.

2) Studies of non-separated and separated liquid flow patterns, by simple gas-liquid contacting experiments, and by simulating distillation at different pressures, on the single tray set up in which gas flow pattern effects below the tray have been removed.

3) Observations of liquid flow patterns on two 6.35 mm hole trays.

For each investigation the objectives of each experiment are stated along with a discussion of the results at the end of each section. Results of all the experiments are collected and discussed, in order to determine the implications for industrial-scale practical distillation. Finally, the major findings from the work are summarised in the main conclusions followed by recommendations for future work.

CHAPTER 2

A SURVEY OF PREVIOUS WORK

2.1 Introduction

Distillation is a mature unit operation which enjoyed a rapid growth in popularity during the establishment of the petrochemical industry over the past seventy years. However, the main problem to upgrade tray technology in order to meet increasing demands of the consumer was the enormous difficulty in testing full scale distillation columns such that negligible plant data was published over a period of many years.

Initial research was confined to defining stable operating conditions on small laboratory scale distillation trays, and mathematical models were formulated to predict the effect of liquid flow on mass transfer efficiency. In addition tray design was, and still is, based on empirical (trial and error) correlations and past experience.

The theoretical origins of many of these empirical correlations and simple models for tray design were incorrect (Porter and Jenkins, 1979), and raised the question of whether tray performance would have been greatly enhanced through a better understanding of the controlling phenomena. It was through the rapid increase in the scale of trayed columns, brought about by economic pressures and the need for cost effective design, that serious discrepancies were revealed between the simple tray theories and what was happening in reality. Since the 1970's experimental work on commercial scale trays and a new generation of theoretical models have given a better insight into the complex vapour-liquid behaviour on trays and its effect on performance. However, a considerable amount of work remains to be done for a complete understanding of tray hydraulics and flow patterns in order to improve current tray design procedures and column performance.

The purpose of this literature review is to place the studies, presented in this thesis, into context with the work of the past by identifying those areas which require a better understanding of the controlling phenomena on trays. Hence, the structure of this chapter consists of the following topics for discussion.

a) A brief description of the current state of the art for tray design and the effect of different flow regimes on tray flow patterns provides a basis for the simulation of distillation experiments contained in Chapter 9.

b) It will be shown that on reviewing the experimental work on commercial scale trays and modelled hypothetical liquid flow patterns, that the flow phenomenon is a two phase flow problem. This justifies the gas-liquid contacting experiments required to investigate the effect of flow conditions and tray configuration on the two phase flow pattern. These are detailed in Chapters 8, 9 and 10.

c) The study of the theoretical models on the effect of liquid flow patterns on tray efficiency will show that they are mainly based on single phase flow. Thus, the physical principles which are valid for open channel two phase flow need to be identified to determine which two phase flow patterns are likely to occur in practice.

d) Since the two phase flow phenomena requires an understanding of the fluid mechanics of both the vapour and liquid flow patterns, it is necessary to review the work, if any, on the effect of vapour distribution on the liquid flow pattern. Does the vapour action improve the liquid distribution on a tray or is the direction of liquid flow changed so as to produce a different liquid flow distribution? If so does the vapour distribution need to be improved by distributor design? Work on this subject is contained in Chapters 6 and 7.

e) Finally, a concise outline of the methods used to improve tray performance by the use of flow control devices and the design of novel trays is also given.

It is worth noting that all the notation presented in this chapter is defined in the nomenclature section at the end of the thesis.

2.2 Conventional Procedures for Sieve Tray Design

A complete distillation column design must satisfy two requirements. These are the ability to perform the separation task safely at the specified throughputs, and that the design must be economically viable such that the whole process can be operated profitably. Set out below are the essentially empirical methods used in tray design.

2.2.1 Background Approach to Design

In the design of sieve trays, the main objective is to calculate tray bubbling area, downcomer area, and the number of passes on a tray in order to minimise the column diameter (and hence costs) for a given separation duty. The usual strategy is to design the sieve tray at 80% of total flooding so as to "force" the maximum vapour and liquid

throughputs through the smallest possible distillation column, in terms of diameter and height. Furthermore, based on the engineering judgement of the tray designer, the material costs of fabricating the column must be kept at a minimum whilst at the same time, a minimum safety factor needs to be incorporated into the overall design.

The information required for the design of a tray, are the vapour and liquid mass flow rate specifications, and the vapour and liquid phase density ratio. It was noted (Porter and Jenkins, 1979), that as the physical properties change according to whether the column is to be designed for vacuum or a high pressure duty, they can all be approximately correlated against each other. That is, they can be correlated in terms of the vapour and liquid phase densities, and in particular (ρ_V/ρ_L) since this is incorporated into the flow parameter correlation [$= L/V(\rho_V/\rho_L)^{0.5}$].

Occasional experience of column failures proves that for some systems, the design methods have produced an under-design and a derating factor, S, must be incorporated in the design methods. The effect of this 'ignorance derating factor' is that it is used to reduce the "flood factor" F' (= S.F.). In tray design, S is usually set at 1.0, but can be as low 0.5. For example a high pressure debutaniser distillation column is derated by a factor of 0.9. The effect of the S factor is that a larger diameter column is required for the same separation duty. This emphasises the empirical nature of tray design procedures which are briefly outlined below.

2.2.2 Calculation Procedure for Tray Design

The procedures for a typical tray design are as follows:

a) Estimate the column diameter from either the flooding correlation based on entrainment (Fair, 1961), or the total flows chart based on an 80% flood single pass sieve tray at a spacing of 600 mm, and of hole diameter 12.5 mm (Porter and Jenkins, 1979). In this review the method of Porter and Jenkins will be considered.

   This method involves the calculation of the total volumetric vapour and liquid flow rates from the following relations,

$$\text{Vapour Load: } \overline{V} = V\cdot\left(\frac{\rho_V}{\rho_L - \rho_V}\right)^{0.5} \qquad \text{Liquid Load: } Q_L = \frac{W_L}{\rho_L} \qquad (2.1)$$

   which are then used to look up column diameter and the number of passes required for the tray at 80 % flood using the above mentioned total flows chart. That is,

$$D = 2\cdot\sqrt{\frac{A_T}{\pi}} \quad \text{where } A_T \text{ is the column cross-sectional area} \qquad (2.2)$$

b) Calculate the downcomer area, A_D, in order to evaluate the downcomer velocity, U_{DF}, at 80% flood (Q_L/F), since $A_D = Q_L/U_{DF}.F$. (F is the flood factor). The following empirical relations may be used to calculate the downcomer velocity,

$U_{DF} = 0.17\ ms^{-1}$: $U_{DF} = 0.007(\rho_L - \rho_V)^{0.5}\ ms^{-1}$:

$U_{DF} = 0.008[T.S.(\rho_L - \rho_V)]^{0.5}\ ms^{-1}$, where T.S. = Tray Spacing (2.3)

Calculate the tray bubbling area A_B (= A_T - $2A_D$); and the bubbling area load factor, C_{SB}, where,

$$C_{SB} = u_{SB}\cdot\left(\frac{\rho_V}{\rho_L - \rho_V}\right)^{0.5} = \frac{W_G}{A_B[\rho_V(\rho_L - \rho_V)]^{0.5}} \qquad (2.4)$$

c) In the tray design, a weir load, b, needs to be specified at the calculated values of A_T and A_D. Thus calculate the weir load, $q/b = Q_L/F.b.N$, where N is the number of passes. It is usual practice that b is not less than $0.6D_T$, since this prevents severe liquid channelling and loss of efficiency. Like the derating factor, b (= $0.6D_T$) is an empirical limit.

d) Using the jet flooding curve shown in Figure 2.1, identify C_{SBf} at the weir load q/b and calculate the vapour fractional flood. (Porter and Jenkins plotted this diagram using the experimental data of Sakata and Yanagi, (1979), for a 12.5 mm hole tray at a spacing of 600 mm, and a hole area of 8%.)

In Figure 2.1, note that the two operating lines , drawn from the origin to bisect the jet flood curve, represent the flow conditions of a tray for a particular system in which the throughput changes, according to the boil-up rate, at a constant reflux ratio. That is, C_{SB} = (constant of operating line) x q/b. Thus it is convenient to locate operating systems on the jet flood diagram. High pressure systems appear towards the right,where the ρ_L/ρ_V ratio is small, while low pressure systems appear towards the left where the ρ_L/ρ_V ratio is greater. In general, vacuum distillation systems are low weir load systems and pressure systems are high weir load systems.

e) Alter the design to produce the same fraction of flood for the bubbling area and downcomer. Compare this fraction of flood with that specified, and readjust the design until the specification is satisfied. For example, if the weir load is high,

increase the number of passes by increasing the total weir length,b, which at the same time results in a slight decrease in A_B and an increase in $\dot{C}_{SB}$.

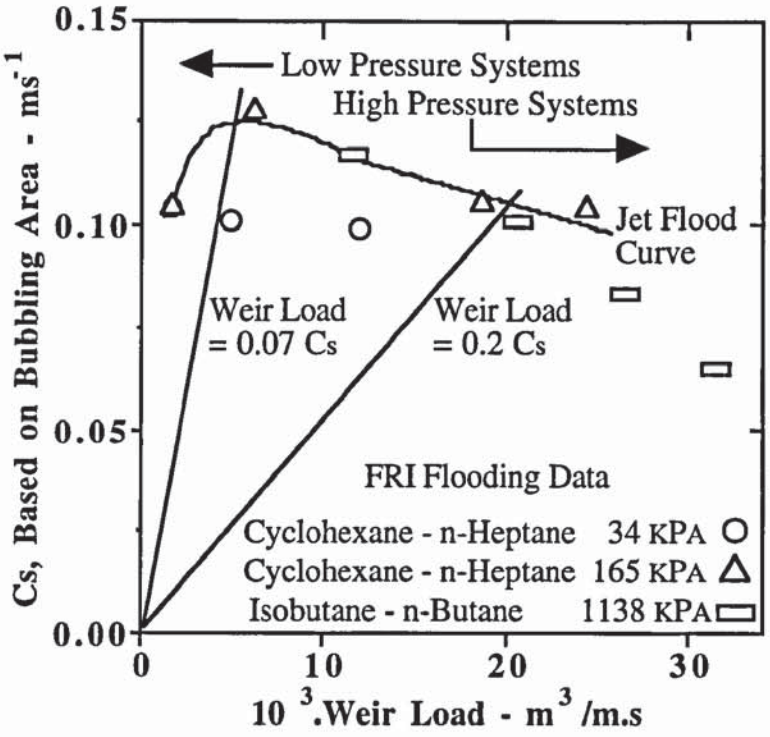

Figure 2.1 Maximum capacity for an FRI sieve tray as a jet flood verses weir load plot.

The overall aim at this stage is to achieve a balanced design by adjusting A_D and b in order to modify A_B so as to produce the same percent flood both in the downcomer and on the tray bubbling area. If necessary alter the column diameter and repeat the above steps until a balanced design is achieved.

2.2.3 Conclusions on Tray Design

This section has shown that empirical methods used in tray design are based on the satisfactory operation of columns in the past. Although these methods will produce a trayed column that will cope with the specified duty, it is sometimes over or under - designed and can lead to performance failure.

At this stage it is worth noting that trays are designed in terms of capacity followed by an estimation of the efficiency in which the column is expected to perform. However, the scope of this work presented in this thesis is concerned with the study of flow patterns and their effect on the efficiencies of trayed columns when operated under different flow conditions. At present, it is difficult to predict the efficiency of a process at the design stage, particularly with large diameter columns which, in turn, may be significantly

different to the actual column efficiency when in full operation.

It should be noted that the jet flood diagram, described in this section, forms the basis of selecting flow conditions for the simulation of distillation at different flow regimes and operating pressures, details of which are contained in Chapter 9.

Additional factors which are of importance to the final tray design are flow regimes, produced under different operating conditions; the vapour - liquid flow patterns; and a measure of the driving force necessary for the separation process to occur efficiently. These topics are the subject of discussion in the following sections.

2.3 Flow Regimes on Sieve Trays

The structure of vapour-liquid dispersions, or flow regimes, on a sieve tray, exist in several different forms. The purpose of this section is to describe each flow regime, and identify the operating conditions in which they exist.

There are three main reasons why flow regimes are of importance. Firstly, the hydrodynamic behaviour on a tray depends upon the flow regime. For instance, different correlations in each regime, such as dispersion density, are required to examine the effect of dispersion density on entrainment or weeping, since this will affect column throughputs. The second reason is that some flow regimes need to be avoided. For example, foaming is aggravated in the emulsion flow regime and entrainment rapidly increases in the spray regime. The final reason is that there is some evidence of improvements in tray efficiency which can be achieved by designing the tray to operate in a particular regime, (Porter et al., 1975, 1977; Raper et al., 1984). A number of these points will be discussed later in this section.

From here on the terms "gas" and "vapour" are used interchangeably in which the latter is mainly used in distillation, while the former is usually used in non-boiling systems.

2.3.1 Spray Regime

Spray regime is a gas phase-continuous dispersion and is produced at high gas flow rates and low liquid rates. The liquid phase is 'atomised', by the gas emerging with a high velocity from the perforations, into a fluidised bed of small liquid droplets of various sizes, (see Figure 2.2). The dispersion has no observable upper surface.

Figure 2.2 Schematic diagram of the biphase dispersion in the spray regime.

The first experimental observations of spray were made by De Goederen (1965) from simple air-water contacting experiments. These observations were confirmed by Porter and Wong (1969), in which the effects of gas density, liquid density, liquid viscosity and surface tension on the spray dispersion were examined. Porter and Wong reported that for a fixed gas velocity, spray was produced at low clear liquid heights which slowly transformed into a bubbly mixture on increasing the height of clear liquid. The objective was to determine this parameter at the spray to bubbly froth (or vice versa) transition point, and it was on that basis that the experimental results were correlated from,

$$\frac{h_{cl}}{d_h} = \text{function of, } f\left[u_G\sqrt{\frac{\rho_G}{\rho_L}}\right] \quad \text{or, } f\,(C_{SB}) \tag{2.5}$$

In simple terms, this shows that spray is associated with large diameter holes, large hole gas velocities, and low clear liquid heights.

Subsequent work on the spray to bubbly froth transition (Payne and Prince, 1977; Pinczewski and Fell, 1977; Hofhuis and Zuiderweg, 1979; Lockett, 1981) resulted in the formulation of alternative spray to bubbly froth transition models, all of which were based on descriptions of flow through a single orifice. These models were tested by correlation of the Porter and Wong experimental results, and thus produced various correlations that were all fairly similar.

2.3.2 Mixed Froth Regime

This is an intermediate regime between the spray and bubbling regimes in which the dispersion close to the tray deck is predominantly a bubbly regime while at the top, the dispersion moves towards the spray regime. Gas passes through the liquid as jets and bubbles, the shape of which are ill-defined and undergo continuous changes in size. The irregular bubbles subsequently burst into a large shower of liquid fragments and coarse

spray droplets. The mixed regime structure is depicted in Figure 2.3.

A limited amount of information on the mixed froth regime is available in the open literature (Hofhuis and Zuiderweg, 1979) and can be summarised as follows. At low gas flow rates a variety of irregular shaped bubbles are hindered from rapidly bursting through the liquid surface by other bubbles. To a certain extent this can be overcome by circulating froth bubbles which travel up to the liquid surface in the middle of the column and downwards at the wall.

Figure 2.3 Schematic diagram of the biphase dispersion in the mixed froth regime.

At some point, this process is exceeded such that bubble-bubble coalescence occurs which increases the size of a certain fraction of bubbles and thus the velocity of their buoyancy-rise increases. As the gas velocity is increased further, the situation changes to gas jetting which completely penetrates the liquid depth to the open space above particularly at low heights of clear liquid. The frequency of jetting increases with increasing gas flow rate until at the transition point to spray, all the holes transport jets through the froth depth.

2.3.3 Emulsion Flow Regime

This flow dispersion, characterised by Hofhuis and Zuiderweg (1979) on cross flow trays, consists of a large number of small bubbles (1 to 3 mm) which are 'emulsified' in the liquid phase, and can be described as a continuous gas-in-liquid flow. It is thought that these bubbles formed are sheared off in the direction of flow by a horizontal liquid shear force which is favoured by a high horizontal liquid momentum compared with the vertical gas momentum. A simplified diagram of the emulsion flow regime is presented in Figure 2.4.

Figure 2.4 Schematic diagram of the biphase dispersion in the emulsion flow regime.

2.3.4 Relating Flow Regimes to the Operation of Trays

With the exception of Hofhuis and Zuiderweg (1979), many of the above experimental results for the different flow regimes were obtained on "non-crossflow" trays. Thus it seemed logical to transfer these results to the conditions of liquid cross flow on real sieve trays where the clear liquid height depends on weir load and occasionally weir height. This was done for the spray-to-mixed and the spray-mixed-emulsified flow regimes by Hofhuis and Zuiderweg, who formulated a height of clear liquid correlation,

$$h_L = 0.6 \cdot \psi^{0.25} \cdot h_w^{0.5} \cdot \rho^{0.25} \qquad (2.6)$$

which can be used with correlations of other workers, (e.g. Porter and Wong, 1969; Pinczewski and Fell, 1977; Hofhuis and Zuiderweg, 1979; Lockett, 1981) to predict which regime the tray is operating in. It was found that spray is a low weir load duty and emulsion flow is a high weir load duty.

An alternative approach for predicting flow regimes on operating trays was the relation of the spray/bubbly transition to entrainment for cross flow sieve trays, (Lockett, Spiller and Porter, 1976). This was later used by Porter and Jenkins (1979) to shape the jet flood curve. The diagram was used to show that for optimal tray design it was desirable to operate trays at the spray to bubbly transition since entrainment was less than that in the low weir load spray regime and at the higher weir load bubbly regime. (Bubbly regime has more recently been split into the mixed and emulsion flow regimes, by Hofhuis and Zuiderweg, 1979). Overall Porter and Jenkins explained the maximum shape of the jet flood diagram by describing flow conditions to the left of the maximum as spray regime, and those to the right as the mixed or emulsion flow regimes.

These arguments can be applied to the mixed to emulsion flow transition. This transition was characterised by Hofhuis and Zuiderweg (1979) who suggested that it depended on

the weir load and the ratio of the liquid momentum to that of the vapour rising through it. That is, at high weir loadings, the emulsion flow regime is all bubbly liquid with no spray whereas the mixed regime is a bubbly dispersion in which a lot of splashing occurs.

Up to this point, the work mentioned above has been concerned with selecting the appropiate flow regime and operating pressure for the tray in order to improve tray capacity. However, there has been very little work on the study of flow patterns in which the liquid flows in a certain manner across the tray i.e., in the form of a spray, a bubbly mixture, or a transition flow regime. Nevertheless, it is possible to comment, at this stage, on what is known about the properties of flow regimes in terms of the manner in which liquid flows over the outlet weir. This may be of significance in the development of the two phase flow pattern, and its effect on the mass transfer efficiency.

Hofhuis and Zuiderweg (1979), found that at high weir loads, the emulsion flow regime was transported over the outlet weir in a similar manner to liquid only flow. In a high pressure column, this can lead to entrainment of froth containing large quantities of vapour into the outlet downcomer, thus increasing the vapour load on the bubbling area which, in turn, may have an adverse effect on tray efficiency.

At lower weir loads, it was observed that liquid was projected straight into the outlet downcomer by splashing and the movement of drops in the spray and mixed flow regimes. This flow behaviour was predicted to be independent of the outlet weir (Pinczewski and Fell, 1972: Lockett, 1981). To avoid this in practice, weirs are partially blocked so as to produce an increased clear liquid height on the tray at very low weir loads and thus prevent liquid being blown off the tray as fine drops.

In general it has been suggested (Porter and Jenkins, 1979), that the above problems may be avoided by operating trays at weir loads corresponding to the spray to mixed or mixed to emulsion flow regimes. This optimises the vapour throughput by "controlling" the rate of vapour or liquid entrainment, according to the distillation pressure for the separation duty, and is further evidence of the empiricism of procedures used in practical distillation.

The above observations raise questions concerning the function of the outlet weir and how does this, together with the nature of the flow dispersion influence the development of the liquid flow pattern across the tray? To respond to this question, a complete understanding of gas-liquid contacting, in the form of liquid splashing and drop movement aswell as liquid flow through a bubbly mixture on trays, is needed. Thus, a theoretical model is required to predict the height of the two phase mixture, and the rate at

which one phase is entrained into the other phase passing through it. Furthermore, a description of two phase flow across and around the tray from the liquid inlet to the outlet downcomer will not only help in predicting mass transfer efficiency, but may provide an insight as to why tray efficiency has a certain value for a particular set of conditions.

Some progress has been made towards achieving this objective and is reviewed in the following sections. Furthermore this justifies the two phase flow pattern studies presented in this thesis.

2.3.5 Flow Regimes and Liquid Flow Patterns

For some time, a number of researchers, (Porter et al., 1975, 1977; Hofhuis and Zuiderweg, 1979), have noted that the flow regime may affect the way in which liquid flows across a tray from the inlet downcomer to the outlet weir. This seems possible since the divergent/convergent shape of a distillation tray means that the tray cross section through which the liquid flows is never constant.

On single pass trays with straight chordal weirs, there is some evidence of liquid channelling associated with circulating flow at the sides. Porter and Lockett, (1975) suggested that this may occur in flow regimes in which the flow of froth is very similar to that of liquid only flow. This flow pattern is the result of the high horizontal momentum of the liquid, within the froth, as it enters the tray from the inlet downcomer, while circulating flow to some extent is caused by reflection of liquid elements by the outlet weir. This flow pattern has a detrimental effect on tray efficiency, especially for large diameter single pass trays (see Section 2.7).

However, Bell and Solari (1974), reported that liquid channelling occurred at very low vapour velocities but diminished at "commercial vapour flow rates". Porter (1975) suggested that this may have been the result of the tray being operated in the spray regime. Spray is produced at high vapour and low liquid flow rates such that the liquid can be considered to be randomly dispersed by the vapour flow to prevent channelling.

As a result of this, liquid flow in the spray regime was explained in terms of a diffusion model (Porter, Safekourdi and Lockett, 1977), such that the clear liquid height at any point on the tray was analogous to drop concentration in molecular diffusion. However experimental measurements of the eddy diffusivity, which gives a measure of the liquid mixing on the tray, showed that there is a limit to the way in which liquid can flow by "spray diffusion". This raised the question of "how does liquid flow in the spray regime?", which as far as is known has yet to be answered.

Nevertheless, research into flow regimes and flow patterns has shown that they may well be of importance in developing future theoretical models so as to predict, more accurately, the flow phenomena occurring in real trayed columns and their effect on tray efficiency.

2.3.6 Conclusion of Flow Regimes

The review on flow regimes has shown that the gas-liquid dispersion on a sieve tray is of importance for tray design and overall column performance. In addition, it has been suggested that flow regimes may be of significance on the manner in which the liquid crosses the tray, and that a non-uniform liquid flow might be improved upon by changing the operating regime. This provides a basis for describing flow regimes and their effect on the developed flow patterns in the simulation of distillation (Chapter 9) and the fundamental gas-liquid contacting experiments (Chapters 6, 8 and 10).

In addition, the formation of liquid flow patterns in a particular flow regime is expected to have significant implications on tray efficiency. The flow of liquid in the bubbly or spray regime, currently forms an integral part of many theoretical models for the prediction of tray efficiency. However, only a limited amount of work has been carried out to study liquid flow patterns. Consequently, efficiency models have been formulated from hypothetical flow patterns, some of which were based on a limited number of experimental observations. A number of these points are discussed in the following sections.

2.4 Experimental Investigations into Liquid Flow Patterns on Commercial Scale Trays

A lack of data from full scale plants and the over simplified mathematical models using rectangular channels of uniform width, made it difficult to predict the nature of flow patterns produced on circular trays and their effect on tray efficiency (Lockett, 1986). This led to intensive studies into how liquid flows across circular trays with the experimental results being incorporated into a new generation of theoretical models to explain liquid flow on a tray and its effect on tray efficiency. Examples of hypothetical flow patterns are discussed in Section 2.5.

In this section, procedures used to determine liquid flow patterns experimentally on sieve trays will be analysed. The techniques presented demonstrate the existence of non-uniform flow across the tray which was interpreted qualitatively, by some researchers,

for use in theoretical modelling of the flow pattern, whilst others determined the liquid flow pattern quantitatively in terms of RTD profiles. A concise description of each experiment will be followed by ways in which the results are interpreted and used.

2.4.1 Camera Recording of Coloured Dye

The monitoring of liquid flow across a circular tray using a coloured dye, with straight sided chordal weirs, was a highly popular technique among several workers (Aleksandrov and Vybronov, 1971; Weiler et al., 1971, 1973; Porter et al., 1972; Solari et al., 1982; Ani, 1988; Hine, 1990). The technique used to show flow non-uniformities on a tray involved the continuous injection of dye from the inlet downcomer until the whole of the single liquid phase or biphase was completely coloured. On stopping the dye injection, the coloured dye in the liquid was removed by fresh clear liquid entering the tray. The rate of coloured dye removal was monitored by camera which showed non-uniform flow as well as regions of longer residence time on the tray.

More recently, Ani (1988) and Hine (1990) observed the movement of purple dye discharged from a solenoid controlled pulse injection system fitted across the length of the inlet downcomer. In these experiments the coloured dye moved faster in the middle of the tray, whilst at the sides of the tray, it moved very slowly or was forced to circulate.

Dye injection was favoured by Weiler et al., (1971, 1973), Porter et al., (1972) and Solari et al., (1982) to obtain results by direct-observation for the formulation of hypothetical liquid flow patterns.

In Weiler's experiments, the width of the dye line steadily increased by forward and backward movements about it's concentration centre point to form a dye band as the biphase flowed across the 7.6 m diameter tray. This gives a measure of the extent of diffusional mixing and a plot of the centre line at numerous times after discharge defines the extent of bulk flow velocity variations. The measured 'break through' times for the first and last elements of the dye band to reach the outlet together with an arbitrary residence time for the cumulative fraction of liquid flow parameter, led to cumulative plots of RTD profiles.

The results showed that the liquid residence time distribution became highly irregular with increasing liquid flow rate. This resulted in greater flow non-uniformity and caused a significant reduction in tray efficiency when evaluated by numerical computation.

2.4.2 Pulsed Coloured Dye Injection and Sampling

The technique of discharging a pulse of dye uniformily across the flow stream at the inlet downcomer was also used by Aleksandrov and Vybronov (1971). Tests were carried out on 1.22 m concurrent and ballast valve trays. In this experiment, liquid samples were extracted downstream near the outlet weir at three evenly spread locations across the weir length. On mixing samples together, a photocolorimeter was used to measure dye concentration and the results used to establish liquid RTD response curves for the whole tray. Overall the RTD for the entire operating range showed highly complex flow patterns with various degrees of completely mixed liquid along the flow path length as well as a backmixing, dead zones, and circulating liquid at the tray outlet. However, no generalised liquid flow pattern was proposed and no efficiencies were reported.

2.4.3 Cine Photography of Floating Balls

This technique was used to study single phase flow in the absence of liquid mixing caused by the bubbling action of the gas, Porter et al., (1972). The presence of non-uniform liquid flow was illustrated by observing the motion of semi-buoyant table tennis balls on the surface of liquid in a 2.1 m wooden open channel water flume in the form of a single pass tray. The results were recorded by cine-photography which showed that water rapidly flowed across the horizontal plane between the downcomers whilst in the diverging/converging sections of the tray near the walls, the water was either stagnant (non-moving) or slowly recirculating within a closed area. The experimental results were used by Porter et al., (1972); Lim et al., (1974); and Lockett et al., (1976), to develop theoretical models or test new tray designs.

A similar procedure was used by Sohlo and Kinnumen (1977) who attempted to measure froth velocities by timing the movement of floating cork balls on a 0.5 m perforated tray.

2.4.4 Fibre Optic Technique

Further information on flow non-idealities on single pass trays was provided by Bell (1972a, 1972b), in which a fibre optic technique to measure RTDs was developed. The procedure involved the use of several fibre optic probes for detecting fluorescent tracers when injected into an n-hexane/toluene binary system on a 2.44 m diameter sieve tray. The rapid activation and decay time of the fluorescent tracer uranine was utilized as follows. By splitting the probes into two separate detectors, one was used to conduct light from a mercury light source, through a 'tunnel' and into the probe tip submerged in the liquid. Tracers which passed through the fibre tip absorbed the transmitted light and

on de-exitation, fluoresence occurred which was conducted by the second detector and relayed to a photomultiplier tube. The raw data signals were processed to give flourescent emission spectra. The main advantage of this method is that it can be used safely in real columns processing hazardous liquid mixtures.

Using several probes on a rectangular grid over the tray, RTD profiles and the variance of dye residence at each probe were obtained from fluorescent responses of the dye crossing the tray. The results led to the suggestion (Bell 1972) that the liquid flow consisted of a rapid forward flow along the centre of the tray, (fairly short U-shaped RTD), with retrograde flow at the sides, (extended RTD from the outlet weir to the wall at the sides).

Bell extended these studies further using a flow visualisation water only experiment on a 2.44 m diameter tray which showed circulating liquid, and led to the suggestion of fluid circulation about a 'line of rotation'. However, this phenomenon was not reproduced on five 1.22 m trays using a modified version of the fibre optic technique (Solari and Bell 1986). Instead, stagnant zones with a certain element of backmixing was reported.

The experimental results were used to formulate a square tray mathematical model with recirculation for the prediction of tray efficiency (Bell and Solari, 1974). However, the effects of scale-up on, for example, 'the width of the mixing zone' concept devised by Porter et al., (1972), within the recirculating liquid was unaccounted for in the model.

2.4.5 Salt Tracer and Electrode Potential Conductivity Cells

RTD profiles on a 2.44 m half tray and 1.22 m sieve trays were evaluated from concentration measurements of a salt tracer injected into a liquid flow (Yu et al., 1982, 1986, 1990). Over the years, Yu has used several devices to measure the salt tracer concentration: the most recent technique being the use of thin sensitive electrode potential conductivity cells. By pulsed injection of sodium chloride into the liquid at the inlet downcomer, tracer concentrations are measured using fifteen pre-standardised Cl^- | AgCl,Ag conductivity cells. The voltage measured across each cell, representing the change in conductivity with time in the liquid, is amplified and relayed to a transducer. Signals are discharged to an on-line computer, via an analogue-to-digital converter from which displays of concentration verses time response curves are produced.

The sampling time for each cell is approximately 1/30th of second so that data acquisition from all fifteen electrodes could be considered as simultaneous For each test run, the liquid flow across the tray changes and to accomodate for this, 8-12 replica runs are taken and their average value computed as the original RTD profile. The moment of such RTD

data at each point is considered to be the mean residence time of the liquid from the inlet to that particular position. Cross plotting the mean residence time from various sampling points yields a mean of residence time distribution (MRTD) for the whole tray. In all of his works, Yu compares experimental MRTD with the computed MRTD obtained from mathematical models where liquid velocity, liquid concentration and diffusional mixing change in two dimensions rather than one.

2.4.6 Heat Transfer by Water-Cooling

Heat transfer experiments involve the cooling of hot water by cold air in which a small fraction of water is evaporated. When this technique is applied to a cross flow tray, liquid flow patterns are investigated using an analogy between heat and mass transfer to simulate distillation. Water-cooling is monitored by measuring the water temperature using an array of temperature measuring devices from which lines of constant temperature (isotherms) are constructed. These are related to concentration profiles found in distillation. The coldest liquid on the tray corresponds to extended liquid residence times.

The technique was first used by Stichlmair et al., (1973, 1985, 1987) to investigate the effects of weir configurations, baffles within the biphase and tray tilting on liquid channelling. Experiments were conducted on 2.3 m diameter bubble cap and sieve trays from which temperature isotherms were obtained from 182 thermocouples and interpreted as lines of constant residence time. This method was replaced with the more effective technique of thermography. This yielded temperature "maps" of the tray in which regions of constant temperature show the same colour.

Porter et al., (1982) and his subsequent co-workers (Enjugu, 1986; Ani, 1988; Hine, 1990) developed a method of interpreting the temperature isotherms in terms of enthalpy driving forces for the calculation of thermal point and tray efficiencies. Overall it was shown that severely distorted or "U-shaped" isotherms represent liquid channelling on the horizontal plane between the downcomers with slow moving, stagnant, or circulating liquid at the sides of the tray. These effects have a detrimental effect on tray efficiency. The overall aim of this and future work is to incorporate all the flow phenomena in a new theory of "Open Channel Two Phase Flow" in order to predict two phase flow patterns and their effect on tray efficiency in full scale distillation columns.

2.4.7 Direction of Flow Experiments Using Flow Pointers

The use of several directional flow pointers partially submerged in the froth on a sieve tray (Hine 1990), is a quick and sensitive visual assessment of the extent of non-uniform

biphase flow. The experimental results were not used to calculate RTD data. Directional flow pointers are based on the principle of a weather vane used to show the direction of the wind. They consist of thin light weight aluminium sheets with a painted arrow indicator loosely hinged to a vertical rod. These are supported above the tray deck with a spacer so that they can freely rotate and become aligned with the direction of flow. All observed flow patterns are recorded using an overhead video camera.

Hine (1990) showed that liquid channelling and circulating flow occurred at high water inlet velocities produced from small inlet gap heights beneath the inlet downcomer. The results will form part of a comprehensive set of flow patterns from trays of different hole sizes so as to model two phase flow on trays.

2.4.8 Froth Velocity Measurements

The direct froth velocity measurement technique, developed by Biddulph and Bultitude (1990), gives a direct assessment of the local froth velocity. The technique involves the froth momentum producing a strain onto a flat titanium probe which is installed in the froth. An array of strain gauges on the probe converts the strain into an electrical signal, the magnitude of which is related to the froth velocity. Calibration data are used to convert the electrical signal into froth velocity measurements.

2.4.9 Conclusions

From the above evidence, it appears that significant flow non-uniformities exist on commercial scale trays and that a number of factors influence tray flow patterns.

In general , non-uniform liquid flow consists of an "active region" between the weirs (Porter et al., 1972), with a superimposed velocity gradient, and a region of constantly changing width between the boundary of the "active region" and the column wall. The liquid that spreads into this region can be considered as stagnant, slowly moving forward, or slowly recirculating depending upon the flow conditions and tray geometry.

Many researchers recognise that the liquid velocity distribution itself is very difficult to determine because of the complex behaviour of the two phase dispersion. Instead, several hypothetical flow patterns have been derived, both from direct-observation experiments and from experimentally determined RTD, in order to gain an insight into the velocity gradient within a non-uniform liquid flow across the tray. Examples of the hypothetical flow patterns are presented in the next section.

2.5 Theoretical Development of Maldistributed Liquid Flow Patterns

Liquid flow across a tray consists of an underlying bulk velocity profile onto which the random movement of liquid flow by gas bubbling is superimposed. This determines the liquid residence time distribution (RTD) on a tray. If the liquid distribution was the same at all points on the tray, the RTD profiles such as concentration profiles would be straight and parallel to the tray downcomers. This would produce the same vapour-liquid residence time over the whole tray and thus yield an optimum mass transfer efficiency (Lockett, 1976). Below is a selection of hypothetical flow patterns some of which were derived from experimental observations described in Section 2.4, where the liquid flow was far from ideal.

2.5.1 Stagnant Regions Model or SRM (Porter et al., 1972)

The SRM consists of preferential liquid flow across the shortest flow path from the inlet downcomer to the outlet downcomer. As the tray is a diverging/converging open channel, there is very little tendency to flow sideways across the longer liquid flow path around the columns walls. This leaves two stagnant regions, at the sides of the tray, in which liquid is in between slow forward moving or reverse flow.

The SRM assumes no circulating eddies and bulk flow of liquid into the stagnant regions. However, random vapour-liquid agitation into the stagnant zones by transverse diffusional mixing occurs over a limiting distance, calculated to be 0.30 - 0.60 m, and is independent of column diameter. The concept of a mixing zone is important when considering the effects of scale-up on tray efficiency (see Section 2.7.1). For small diameter trays, stagnant zones are smaller than the mixing zone such that volatile material is continuously replenished as it is stripped by the vapour. This is repeated on larger diameter trays, except that the stagnant zones are much larger with the liquid reaching equilibrium as the vapour passes through it. Further vapour passage through the stagnant liquid undergoes no composition changes and thus leads to a fall-off in tray efficiency.

Composition changes are depicted as concentration profiles which are a measure of the driving force for mass transfer. For various tray geometries, these are "U-shaped" which indicates rapid depletion of the volatile component in the stagnant zones. A typical example of concentration profiles, predicted for a 6.0 m diameter tray, from the SRM are presented in Figure 2.5. These are similar to the experimental liquid composition profiles, measured on a 2.44 m diameter tray by Bell (1972), in that they both show the

characteristic U-shape, in spite of the differences in tray geometry. (It is worth noting that no concentration profiles from the SRM were predicted for a 2.44 m diameter tray).

Later Porter and Lockett (1975) suggested that the SRM flow pattern occurs in the mixed or bubbly regime since it behaves in a similar manner to liquid only flow. With this in mind, Porter et al., (1975, 1977) hypothesised that flow patterns may well depend on the flow regime and that liquid channelling might not occur in the spray regime.

Figure 2.5 Comparison of predicted concentration profiles from a) the SRM (Porter et al., 1972), with b) experimentally measured concentration (RTD) profiles (Bell, 1972).

Liquid flow in the spray regime was modelled in terms of a spray diffusion model which utilizes point heights of clear liquid on the tray that are analagous to concentration in molecular diffusion. The predicted concentration profiles, shown in Figure 2.6, indicate a more uniform liquid flow distribution compared with that predicted using the SRM in that there are no stagnant zones produced at the sides of the tray. However, experimental determination of the diffusion coefficient shows that there is a limit to liquid flow by spray diffusion, where the Peclet Number in the spray regime ,N_{Pes}, is less than 1.25.

The SRM was reconsidered by Yu et al., (1983) in which the stagnant regions were divided into a slowly forward flow zone, close to the boundary of the active region; a backward flow close to the column wall; and a backmixing region in front of the inlet downcomer. In addition, it was suggested that the liquid flow was not unidirectional between the downcomers and that the bulk flow contained a non-uniform velocity distribution.

Figure 2.6 Calculated drop concentration profiles and liquid concentration profiles (x) from the spray diffusion model (Porter et al., 1977).

2.5.2 Retrograde Flow Model

From the experimentally measured RTD data, Bell (1972), made an approximate estimation of local froth velocities within the non-uniform liquid flow pattern. The results showed that the velocity along the centre line was more than twice that near the walls which was in reverse or retrograde flow.

Retrograde flow assumes two regions of forward and reverse flow which are separated by a "flow boundary line" where the velocity is zero. The forward flow path occupies a significant fraction of the total tray area whilst a small proportion of liquid flow towards the outlet is transferred to the retrograde (reverse) flow channels near the column wall.

2.5.3 Bulk Liquid Velocity Profiles

Non-uniform liquid flow was predicted from bulk liquid velocity profile measurements (Solari et al., 1982) which became increasingly severe as the outlet weir height was increased and as the vapour flow rate was reduced. Examples of the measured bulk liquid velocity profiles are presented in Figure 2.7.

The liquid velocity profile of Figure 2.7 b is very similar to the SRM (Porter et al., 1972), whilst Figure 2.7 c is similar to the retrograde flow pattern (Bell, 1972).

Figure 2.7 Schematic diagram of the experimental bulk liquid velocity profiles measured by Solari et al., (1982).

2.5.4 Turbulent Two-Dimensional Liquid Phase Flow

Since direct measurement of liquid velocity is very difficult it would be advantageous to predict liquid velocity profiles and RTD data by computational fluid dynamics. Some progress has been made in this area (Yu and Zhang, 1991; Yu, 1992; Porter et al., 1992) with the development of a liquid flow mathematical model in which the rising vapour provides a resisting force to liquid flow. To simulate two-dimensional flow on a large diameter tray, relationships, which are valid for single phase turbulent flow, were applied to a situation where turbulence and mixing is produced by a continuous vapour stream passing through the liquid (i.e., treat the biphase as a homogeneous fluid). Development of the model is outlined below.

The basic equations representing the turbulent liquid flow on a tray are composed of the Reynolds equation which is derived from the Navier-Stokes equation, and the continuity equation as follows:

$$u_j \cdot \frac{\partial u_i}{\partial x_j} = \frac{1}{\rho} \cdot \frac{\partial}{\partial x_j} \cdot \left[- p\delta_{ij} + D \cdot \left(\frac{\partial u_i}{\partial x_j} + \frac{\partial u_j}{\partial x_i} \right) - \rho \overline{u_i' u_j'} \right] \qquad (2.7)$$

$$\frac{\partial u_j}{\partial x_j} = 0 \qquad (2.8)$$

In applying equation (2.7) to the flow of turbulent liquid on a tray, the vertically rising vapour may be regarded as a part of the overall resistance to the liquid flow, thus an additional term representing the vapour resistance term is added. This is obtained by assuming that, as a result of momentum transfer from the liquid to the vapour, the vapour

leaving the top of the froth attains a horizontal velocity component, which in both magnitude and direction, is equal to that of the local liquid flow. Thus the resisting force to the liquid flow caused by the rising vapour is expressed as:

$$F_{vi} = \rho_g u_s u_i dxdy \tag{2.9}$$

By adding this resisting force into the Reynolds equation and rearranging, equation (2.7) becomes:

$$u_j \cdot \frac{\partial u_i}{\partial x_j} = \frac{1}{\rho} \cdot \frac{\partial}{\partial x_j} \cdot \left[-p\delta_{ij} + D \cdot \left(\frac{\partial u_i}{\partial x_j} + \frac{\partial u_j}{\partial x_i} \right) - \rho \overline{u_i u_j} \right] - \frac{\rho_g u_s}{\rho h} u_i \tag{2.10}$$

The Reynold's stress, $(-\rho \overline{u_i u_j})$, in equation (2.10) may be replaced by the multiple of an eddy viscosity D_e and a velocity gradient, that is:

$$-\rho \overline{u_i u_j} = D_e \cdot \left(\frac{\partial u_i}{\partial x_j} + \frac{\partial u_j}{\partial x_i} \right) \tag{2.11}$$

Substituting equation (2.11) into equation (2.10) and making the reasonable assumption that, $D << D_e$, the following equation of motion is obtained:

$$u_j \cdot \frac{\partial u_i}{\partial x_j} = \frac{1}{\rho} \cdot \frac{\partial}{\partial x_j} \cdot \left[-p\delta_{ij} + D_e \cdot \left(\frac{\partial u_i}{\partial x_j} + \frac{\partial u_j}{\partial x_i} \right) \right] - \frac{\rho_g u_s}{\rho h} u_i \tag{2.12}$$

Due to the vigorous agitation of the liquid by the rising vapour, it is assumed that any variation in liquid velocity with liquid depth may be neglected. The flow of liquid on the tray is considered to be two-dimensional and the following equations apply:

$$u \cdot \frac{\partial u}{\partial x} + v \cdot \frac{\partial u}{\partial y} = -\frac{1}{\rho} \cdot \frac{\partial p}{\partial x} + \frac{\partial}{\partial x}\left(D_e \cdot \frac{\partial u}{\partial x} \right) + \frac{\partial}{\partial y}\left(D_e \cdot \frac{\partial u}{\partial y} \right) - \frac{\rho_g u_s}{\rho h} u \tag{2.13}$$

$$u \cdot \frac{\partial v}{\partial x} + v \cdot \frac{\partial v}{\partial y} = -\frac{1}{\rho} \cdot \frac{\partial p}{\partial y} + \frac{\partial}{\partial x}\left(D_e \cdot \frac{\partial v}{\partial x} \right) + \frac{\partial}{\partial y}\left(D_e \cdot \frac{\partial v}{\partial y} \right) - \frac{\rho_g u_s}{\rho h} v \tag{2.14}$$

and the equation of continuity:

$$\frac{\partial u}{\partial x} + \frac{\partial v}{\partial y} = 0 \tag{2.15}$$

Additional relationships required to solve these equations are taken from those used in the computation of single phase flow patterns. A two equation flow model is chosen comprising of a transport equation for the kinetic energy of turbulence, k:

$$u_j \cdot \frac{\partial k}{\partial x_j} = \frac{\partial}{\partial x_j} \cdot \left(\frac{D_e}{\sigma_k} \frac{\partial k}{\partial x_j} \right) + G - \varepsilon \tag{2.16}$$

where

$$G = D_e \cdot \left(\frac{\partial u_i}{\partial x_j} + \frac{\partial u_j}{\partial x_i} \right) \cdot \frac{\partial u_i}{\partial x_j} \tag{2.17}$$

and a transport equation for the dissipation rate of turbulence energy,

$$u_j \cdot \frac{\partial \varepsilon}{\partial x_j} = \frac{\partial}{\partial x_j} \cdot \left(\frac{D_e}{\sigma_s} \frac{\partial \varepsilon}{\partial x_j} \right) + (C_1 G - C_2 \varepsilon) \frac{\varepsilon}{k} \tag{2.18}$$

In addition, the turbulent viscosity D_e is related by:-

$$D_e = C_\mu \cdot \frac{k^2}{\varepsilon} \tag{2.19}$$

Launder et al., (1972, 1974) proposed the following values for the constants based on a large amount of experimental work.

$$C_m = 0.09 \quad C_1 = 1.44 \quad C_2 = 1.92 \quad \sigma_k = 1.00 \quad \sigma_s = 1.30 \tag{2.20}$$

For the two-dimensional model, equation (2.16) becomes:

$$u \frac{\partial k}{\partial x} + v \frac{\partial k}{\partial y} = \frac{\partial}{\partial x} \cdot \left(\frac{D_e}{\sigma_k} \cdot \frac{\partial k}{\partial x} \right) + \frac{\partial}{\partial y} \cdot \left(\frac{D_e}{\sigma_k} \cdot \frac{\partial k}{\partial y} \right) + G - \varepsilon \tag{2.21}$$

and equation (2.18) becomes:

$$u \frac{\partial \varepsilon}{\partial x} + v \frac{\partial \varepsilon}{\partial y} = \frac{\partial}{\partial x} \cdot \left(\frac{D_\varepsilon}{\sigma_s} \cdot \frac{\partial \varepsilon}{\partial x} \right) + \frac{\partial}{\partial y} \cdot \left(\frac{D_\varepsilon}{\sigma_k} \cdot \frac{\partial \varepsilon}{\partial y} \right) + (C_1 G - C_2 \varepsilon) \frac{\varepsilon}{k} \tag{2.22}$$

The velocity field is calculated by solving equations (2.13), (2.14), (2.15), (2.19), (2.21), and (2.22).

The theoretical liquid velocity field is symmetrical with respect to the centre line of the tray perpendicular to the downcomers. Thus:

$$\frac{\partial u}{\partial y} = 0, \quad v = 0, \quad \frac{\partial k}{\partial y} = 0, \quad \frac{\partial \varepsilon}{\partial y} = 0$$

Theoretically, the boundary condition of no slip at the column wall is set, where $u = 0$, $v = 0$, $k = 0$, and ε is a finite value. To simplify the computation in the wall region

where the velocity gradient becomes very steep, a wall function taken from single phase flow theory was introduced.

The inlet boundary condition was set at, u_{in} =L/h; v_{in} =0. This implies that the liquid velocity entering the tray is equal to that of the froth near the inlet downcomer.

The method of finite volume was chosen for the computation such that the results are in effect not influenced by the outlet boundary condition, and the outlet flow conditions may be taken as if the flow is unidirectional.

The computed flow pattern, presented in Figure 2.8 shows the two-dimensional velocity distribution in which a number of velocity profiles represent forward flow from downcomer to downcomer, as well as reverse flow in the segmental regions at the side. The liquid velocity remains uniform in the main flow region between downcomers but diminishes sharply in the segmental regions, whilst in the converging tray section, the velocity distribution becomes parabolic owing to mixing of the contracted flow of liquid from the segmental region.

The assumptions and simplifications used in the theoretical model are open to question and need to be tested experimentally in order to determine their validity. These include, the use of a boundary layer in the liquid close to the tray floor and column wall, and the use of equations relating to longitudinal flow if instantaneous velocity and pressure values are known. Furthermore, eddy kinematic viscosity needs to be defined in order to simplify and solve the equations by computer in a reasonable time.

Figure 2.8 Typical computed velocity distribution produced from the $\kappa - \varepsilon$ turbulent liquid phase flow model (Yu et al., 1991).

Nevertheless, computation of flow patterns provides a promising start for a new interpretation of tray and column performance based on the fluid mechanics of two phase flow in an open channel.

2.5.6 Conclusions on Theoretical Non-Idealised Liquid Flow

The hypothetical flow patterns consists of a region of forward flow with a superimposed velocity distribution profile between the downcomers, in which the faster moving liquid occurs along the centreline, and stagnant zones. Liquid in these zones may be slow moving, stagnant or recirculating at the sides of the tray.

Hence, with the establishment of non-uniform liquid flow on circular trays, both theoretically and by experiment, the next section assesses these effects on tray efficiency beginning with the definition of efficiency terms used in the theoretical models.

2.6 Definition of Efficiency Terms

The term efficiency is a measure of the rate of mass transfer in tray design, and is dependent on several factors such as liquid film and gas film resistances. For the prediction of overall column efficiency, use is made of point and tray efficiencies as shown in Figure 2.9. There are a number of tray definitions, the most common being that defined by Murphree (1925), since it is the most widely comprehended parameter and is relatively easy to calculate.

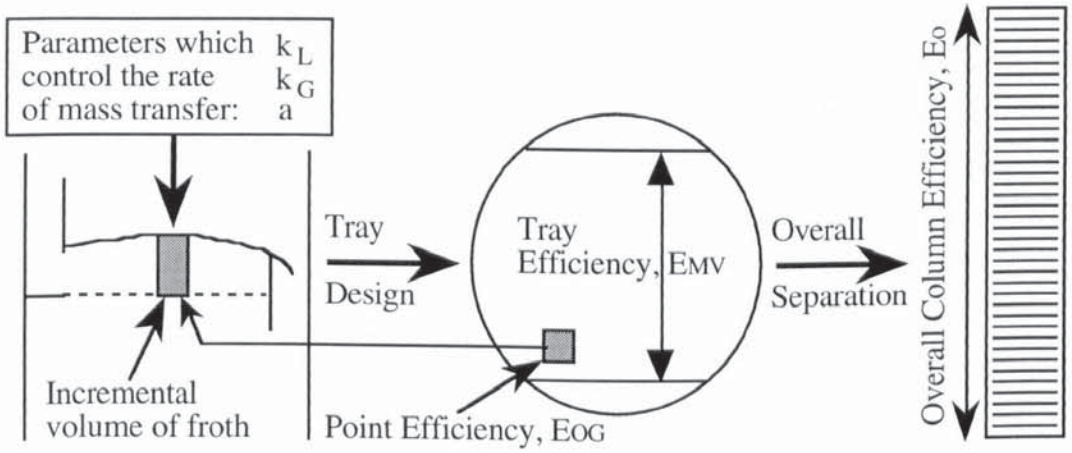

Figure 2.9 Schematic diagram of the relation between point, tray, and overall column efficiency (simplified).

The definition of point and tray efficiencies are best explained by means of a vapour-

liquid composition diagram, (see Figure 2.10). For a binary system, efficiencies can be defined in terms of either the least or most volatile component. It is more convenient to define efficiencies in terms of the least volatile component (lvc), since the concentration of the lvc in the liquid,x, increases as it crosses the tray. In addition it is mathematically convenient to define efficiencies in this manner since it removes the use of several minus signs during the derivation of efficiencies of theoretical analyses.

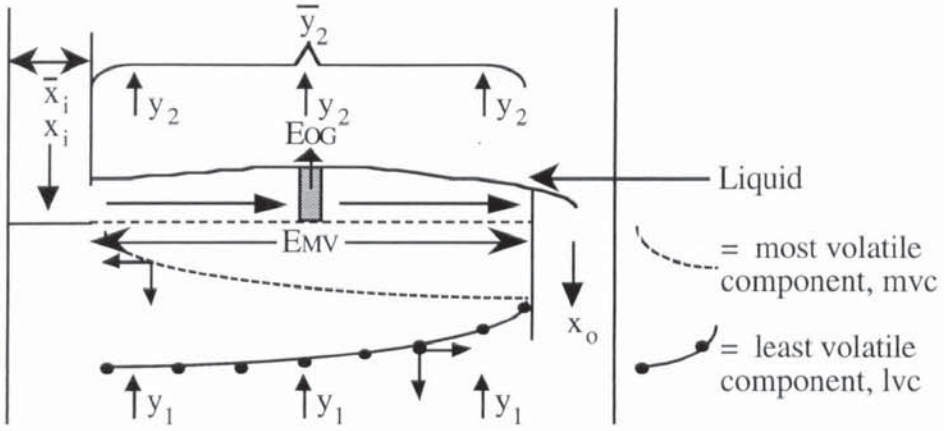

Figure 2.10 Schematic diagram of the concentration profile of vapour and liquid streams entering and leaving the tray.

2.6.1 Definition of Murphree Point Efficiency E_{OG}

From Figure 2.10, E_{OG} is defined in terms of the mole fraction of the vapour and liquid streams entering and leaving the tray. The compositions of the vapour entering and leaving the tray are y_1 and y_2 respectively. Similarly, the liquid phase enters the tray from that above it with a composition x_i and leaves the tray with a composition x_o. In an ideal situation, the composition of the vapour, y^*, is assumed to be in equilibrium with the liquid composition at a point being considered on the tray. However, in reality, this is not the case and the non-equilibrium froth element on the tray can be described in terms of a local or point efficiency. Thus the fractional approach to equilbrium is given by,

$$E_{OG} = \frac{\text{actual concentration change at point i}}{\text{maximum possible concentration change at point i}} = \frac{y_1 - y_2}{y_1 - y^*} \qquad (2.23)$$

where y_1 is assumed to be of uniform composition when entering the tray. The term OG indicates that point efficiency has been defined in terms of the overall resistance to mass transfer based on vapour phase driving forces. The same argument applies to the less commonly used E_{OL} which is based on liquid phase driving forces. That is,

$$E_{OL} = \frac{x_0 - x_i}{x^* - x_i} \tag{2.24}$$

where x^* is the liquid composition in equilibrium with the vapour composition, y_2, leaving the tray at the point being considered.

2.6.2 Definition of Murphree Tray Efficiency E_{MV}

To define Murphree tray efficiency, the overall composition of the vapour entering and leaving the tray in question, are y_1 and $\overline{y_2}$ respectively, whereas the overall liquid phase composition entering and leaving the tray can be defined as $\overline{x_i}$ and x_0 respectively. The composition of the vapour, y_0^*, is in equilibrium with the liquid leaving the tray for an ideal situation; that is, $y_0^* = mx_o + c$. Thus in reality the driving force behind the deviation from the ideal equilibrium condition is measured by the Murphree tray efficiency defined as,

$$E_{MV} = \frac{\text{actual overall concentration change}}{\text{maximum possible concentration change}} = \frac{y_1 - \overline{y_2}}{y_1 - y_0^*} \tag{2.25}$$

The subscript MV indicates the Murphree efficiency for the whole tray on the basis of the vapour concentrations. In contrast the less commonly used E_{ML} is based on the liquid concentrations such that,

$$E_{ML} = \frac{x_0 - \overline{x_i}}{x_0^* - \overline{x_i}} \tag{2.26}$$

where x_0^* is the equilibrium liquid concentration with the overall vapour composition $\overline{y_2}$.

The above definitions of point and tray efficiency are used in theoretical models for binary systems described in the next section.

2.7 Theoretical Modelling of Tray Efficiency from Liquid Flow Patterns

Development of theoretical analyses to predict tray efficiency became necessary since the availability of full scale column data was scarce. Thus, numerous mathematical models for the calculation of Murphree tray efficiency, E_{MV}, from point efficiency, E_{OG}, were derived which incorporate hypothetical liquid flow patterns on a tray, based on

experimental observations described in Section 2.4.

Initially, Murphree (1925) assumed a completely mixed tray in which the vapour entering and leaving the tray was completely mixed, and that the liquid composition at any point was equal to that leaving the tray (i.e., $E_{MV} = E_{OG}$). Kirschbaum (1934) found that this was not true, since he reported the existence of liquid concentration gradients on small scale trays. This effect was incorporated into subsequent theoretical models whereby a hypothesised liquid flow pattern was used to calculate tray efficiency. Two categories of theoretical models were devised. That is, the steady change in liquid concentration across the tray approach, and the 'stepwise' concentration change in a series of well defined mixed pools method.

The steady liquid concentration change approach to theoretical modelling was initiated by Lewis (1936), who introduced the concept of plug flow between the inlet and outlet downcomers on a tray, with no axial mixing. The idea of 'stepwise' concentration changes in a series of mixed pools, introduced by Kirschbaum (1948), was developed mathematically by Gautreaux and O'Connell (1955) for the case of a simple flow pattern in order to calculate tray efficiency. However, the main disadvantage of this approach at the time was how to calculate the appropiate number of mixed pools for use in modelling.

The concept of plugflow (Lewis, 1936), was further developed by Gerster (1958) by superimposing a backmixing mechanism on plug flow, which, for the first time, was described in terms of an eddy diffusion coefficient. This model was recommended by the AIChE as the primary method for calculating tray efficiency using the AIChE Bubble Tray Design Manual (1958).

Ashley and Haselden (1970) highlighted an interrelationship between the Peclet number and the number of mixing pools, by suggesting that they were effectively measuring the same flow phenomena, observed from different aspects, which is the degree of mixing. Furthermore, they proposed a method whereby the number of mixed pools for use in mathematical modelling could be found from tracer experiments. This removed one of the main disadvantages of using mixed pool models.

As a result of increasing column diameters in the petro-chemical and associated industries, large discrepancies between actual tray efficiencies and those predicted by the AIChE method were reported. This was explained in a modified eddy diffusion model, or Stagnant Regions Model (SRM), on a circular tray (Porter et al., 1972). The model predicted serious losses in tray efficiency on large diameter single pass trays from the

hypothetical flow pattern of 'liquid channelling associated with stagnant regions'. This was the first time that changes in the liquid concentration were considered in two dimensions on the tray as opposed to one. Several other diffusional mixing models were proposed for the prediction of tray efficiency, (Bell and Solari, 1974; Sohlo and Kouri, 1982: Kouri and Sohlo, 1985), which, on the whole differ in minor detail from the stagnant regions model (Porter et al., 1972). That is, differential changes in composition of the liquid have a significant effect on tray efficiency.

Bruin and Freije, (1974) applied the mixed pool analysis to a tray containing stagnant regions by introducing side mixing pools. The results were remarkably similar to that calculated by Porter et al., (1972). Kafarov et al., (1979) proposed a unified model which incorporated both diffusional mixing and mixed pools, but was considered too complicated for practical use. Throughout the 1980's Yu et al., (1982, 1986, 1991) has used the concept of mixing pools, in which the liquid concentration, liquid velocity and eddy diffusional mixing all change in two dimensions on the tray as opposed to one. The most recent theoretical model developed was the three-dimensional non-equilibrium pool model with partial mixing.

Below are a selection of differential concentration change and mixed pool theoretical models which are described in more detail.

2.7.1 Examples of Theoretical Models to Calculate Tray Efficiency

Lewis (1936)

Flow pattern effects for the prediction of tray performance were first accounted for by Lewis (1936) in which unidirectional or plug flow of liquid was assumed. Analytical relationships for the calculation of E_{MV} from E_{OG} were formulated for three different cases of plug flow as shown in Figure 2.11. For each case, it was assumed that there was no liquid mixing perpendicular to the direction of flow, the tray is a rectangular channel of constant uniform width, the vapour and liquid flow rates are constant, and point efficiency is constant across the whole tray.

Case I

The first case assumes that the vapour is completely mixed between trays and the liquid flow on successive trays is unmixed. The simple relation to calculate E_{MV} is given by,

$$E_{MV} = \frac{1}{\lambda} \cdot [\exp(\lambda E_{OG}) - 1] \qquad (2.27)$$

Case II

For the second case, there is no vapour mixing between trays while liquid flows in the same direction on successive trays. Expressions for the calculation of E_{MV} are given by,

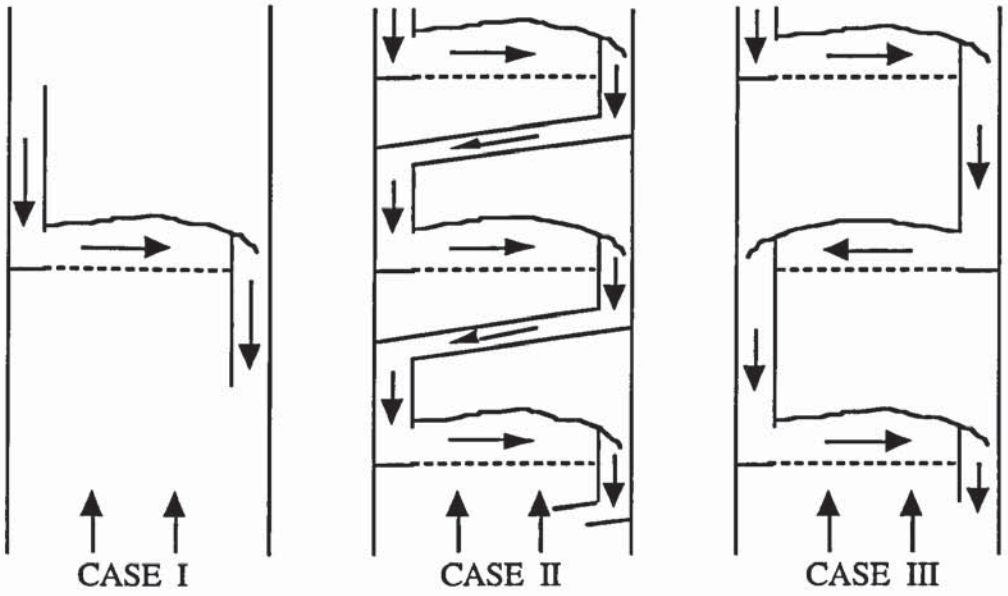

Figure 2.11 Representation of the flow schemes for the three cases of the Lewis models.

$$E_{MV} = \frac{\alpha - 1}{\lambda - 1} = \frac{\alpha - 1}{\left[\left(\frac{1}{E_{OG}} - \frac{1}{\alpha - 1}\right)\ln \alpha\right] - 1} \tag{2.28}$$

$$\text{where} \quad \lambda = \left[\frac{1}{E_{OG}} - \frac{1}{\alpha - 1}\right] \tag{2.29}$$

Case III

The calculation of E_{MV} in the third case assumes that there is no vapour mixing between trays while liquid flows in alternate directions on a sequence of trays. The resultant equations for this case are,

$$E_{MV} = \frac{\alpha - 1}{\lambda - 1} \tag{2.30}$$

where , if $\alpha > 1$,

$$\lambda = \sqrt{\left[\frac{\alpha^2 - (1 - E_{OG})^2}{E_{OG}^2(\alpha^2 - 1)}\right]} \cosh^{-1}\left[1 + \frac{(\alpha - 1)(\alpha - 1 + E_{OG})}{\alpha(2 - E_{OG})}\right] \tag{2.31}$$

and, if $\alpha < 1$,

$$\lambda = \sqrt{\left[\frac{\alpha^2 - (1 - E_{OG})^2}{E_{OG}^2 (1 - \alpha^2)}\right]} \cos^{-1}\left[1 - \frac{(1-\alpha)(\alpha - 1 + E_{OG})}{\alpha (2 - E_{OG})}\right] \qquad (2.32)$$

For the second and third cases, α is defined as the concentration similarity ratio and for all three cases, $\lambda = mG/L$.

In general, Lewis showed that tray efficiencies with parallel flow (Case II), are greater than those where the liquid flows in opposite directions as it descends from tray to tray (Case III). Overall, the effect of direction of flow on tray efficiency shows that for the conventional opposite direction tray design, E_{MV} with no vapour mixing, (Case III) is less than that with complete vapour mixing (Case I).

The problem with Lewis's equations is that a maximum possible tray efficiency was found to be greater than that in practice. Real tray efficiencies are less than the maximum value because of liquid mixing, vapour mixing, non-uniform liquid flow across the tray, non-uniform flow of vapour through the tray, entrainment and weeping. The mathematical analyses described below incorporate some or all of these factors.

Kirschbaum (1948)

The presence of liquid concentration gradients on small diameter trays was recognised by Kirschbaum (1934) who later formulated a scheme (1948) in which the liquid changed composition by movement between a series of well defined mixing cells, of length 600 mm, across the tray. The model was quite flexible in that mixing pools were linked by interpool liquid flow and that this could be adjusted. Unfortunately, the analysis was too complex and found little application.

Gautreaux and O'Connell (1955)

The mixed pools theory was explained mathematically (Gautreaux and O'Connell, 1955) by deriving an expression which relates the effect of liquid flow path length on the number of mixed pool stages, to the overall tray efficiencies. Tray efficiency was defined in terms of λ, E_{OG} and the number of mixed pool stages, n, thus:

$$\frac{E_{MV}}{E_{OG}} = \frac{1}{\lambda E_{OG}}\left[\left(1 + \frac{\lambda E_{OG}}{n}\right)^n - 1\right] \qquad (2.33)$$

The pool nearest to the inlet downcomer is defined as n = 1, whereas n = n is the final pool at the outlet downcomer. If the tray consisted of one completely mixed pool, (i.e.,

completely mixed tray) then $E_{MV} = E_{OG}$. If, on the other hand, the tray consisted of an infinite number of mixed pools then the tray is operating under plug flow conditions and is similar to the Lewis Case I in that the liquid is unmixed.

Gerster (1958), AIChE Method

The use of eddy diffusion theory to describe liquid cross-flow effects on tray efficiency was used for the first time (Gerster, 1958) to formulate the most widely used model of "plug flow plus backmixing". The model was recommended by the AIChE as the principle method for calculating tray efficiency.

Detailed below are the concepts involved for the cases of plug flow with no backmixing and the simple backmixing mechanism imposed on plug flow. For each case the rate of mixing of a component is proportional to the changes in the local concentration of that component and that these effects are considered in the direction of the flow path length (Z) only.

For both models, the calculation of E_{MV} is based on overall concentration changes in the vapour and liquid phases. Hence, the following assumptions are made:

i) The analysis is limited to binary mixtures and so assume that the "equilibrium-curve" is a straight line across the whole tray, that is $y = mx+c$.

ii) Assume that the vapour entering the tray is completely mixed and of uniform composition y.

iii) The liquid entering the tray at the inlet is completely mixed and of uniform composition x.

iv) As the liquid crosses the tray, the liquid concentration changes from x_i at the inlet to x_o at the outlet. The liquid is assumed to be completely mixed on leaving the tray.

v) In the vertical direction the liquid is assumed to be completely mixed at any point on the tray (i.e., no vertical concentration gradient).

In setting up the analysis, the liquid flows across a rectangular channel of uniform width as shown in Figure 2.12.

The use of a rectangular flow path means that a uniform concentration across the width of the channel in the (W+D)/2 direction can be assumed.

Thus, the E_{MV}/E_{OG} equation to describe plugflow on a tray with no backmixing is,

$$E_{MV} = \frac{1}{\lambda}\,[\exp(\lambda E_{OG}) - 1] \quad \text{or,} \quad \frac{E_{MV}}{E_{OG}} = \frac{1}{\lambda E_{OG}}\,[\exp(\lambda E_{OG}) - 1] \qquad (2.34)$$

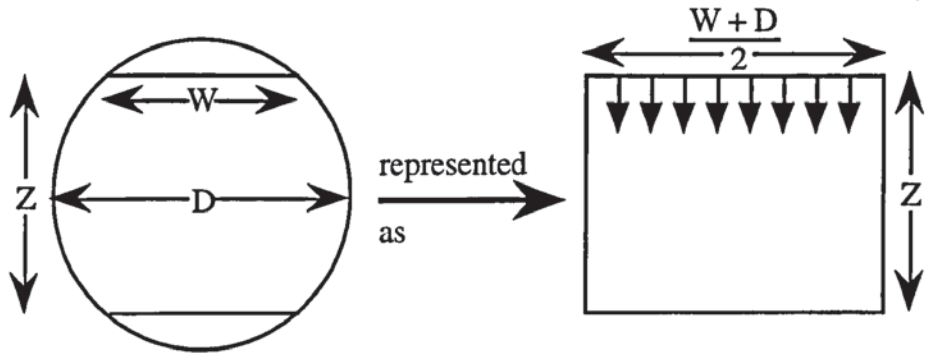

W = Weir length D = Column diameter Z = Liquidflowpath length

Figure 2.12 Representation of the circular tray as a rectangular flow path of uniform width in the plug flow plus back-mixing model.

which is independent of the flow path length and is the same as Lewis case I

For this situation, E_{MV} is always greater than E_{OG} since the enhancement is caused by the concentration change in plug flow. Consequently, the extent of enhancement increases with E_{OG} and in many cases predicts an E_{MV} greater than 100%.

The analysis below considers backmixing on plug flow which is brought about by the vigorous mixing of the liquid by the vapour in all directions, including backwards and forwards in the direction of liquid flow. By maintaining a rectangular flow channel, the backward and forward mixing process only occurs in the z direction. Backmixing has been measured experimentally using non-volatile tracer methods that are well documented in the open literature in which the results have been described in terms of a diffusion coefficient, D_E. In brief, diffusion of liquid components occurs by means of a diffusive flux, N, through the froth cross-section, based on a cross-sectional area per unit width A, perpendicular to the direction of flow, and is given by,

$$N = -D_E \cdot h_F \frac{dx}{dz} \qquad (2.35)$$

For this and subsequent analyses, the influence of diffusional mixing on tray efficiency is established by means of a differential equation of the form,

$$a\frac{d^2X}{dz^2} + b\frac{dX}{dz} + cX = 0 \qquad (2.36)$$

The solution to the equation is obtained from the roots, m_1 and m_2, which in turn are incorporated into the concentration profile solution $X = A \exp(m_1) Z + B \exp(m_2) Z$. By substitution of the appropriate boundary conditions, the constants A and B may be determined.

With this in mind the backmixing analysis begins with a mass balance over an increment of froth in the Z direction. By using mass transfer in - mass transfer out = 0, the mass balance equation is given by,

$$D_E \frac{d^2x}{dz^2} - \frac{L}{h_F \rho_L \rho_F} \frac{dx}{dz} + (y_1 - y_2) \frac{G}{h_F \rho_L \rho_F} = 0 \qquad (2.37)$$

To produce a differential equation of the form outlined in equation (2.36), equation (2.37) is rearranged in terms of the Peclet Number, N_{Pe}, which is a measure of the effect of mixing, thus causing a deviation from plug flow. N_{Pe} is related to the total flow path length, Z, the froth velocity V_F, and the diffusive mixing coefficient D_E, such that,

$$N_{Pe} = \frac{Z V_F}{D_E} \qquad (2.38)$$

By using assumptions from an overall mass balance, mathematical simplifications and the definition of point efficiency, equation (2.37) can be re-arranged to,

$$\frac{1}{N_{Pe}} \frac{d^2X}{dz^2} - \frac{dX}{dz} - \lambda E_{OG} X = 0 \qquad (2.39)$$

in which the following mathematical simplifications are made:

Let $Z^* = z/Z$, (z = tray length), $dZ^* = dz/Z$,
Set, $X = x^* - x$, $dX = -dx$, and define $\lambda = mG/L$

Equation (2.43) is solved using $(1/N_{Pe}) m^2 - m - \lambda E_{OG} = 0$. The roots are obtained from

$$m_1, m_2 = 1 \pm \frac{\sqrt{(-1)^2 - 4(1/N_{Pe})(-\lambda E_{OG})}}{2(1/N_{Pe})} \qquad (2.40)$$

By re-arrangement and making the appropriate substitutions, the final expression for the enhancement ratio, E_{MV}/E_{OG} is,

$$\frac{E_{MV}}{E_{OG}} = \frac{1 - \exp\left[-(\eta + N_{Pe})\right]}{(\eta + N_{Pe})\cdot\left(1 + \dfrac{\eta + N_{Pe}}{\eta}\right)} + \frac{\exp(\eta - 1)}{\eta\cdot\left(1 + \dfrac{\eta}{\eta + N_{Pe}}\right)} \qquad (2.41)$$

$$\text{where} \quad \eta = \frac{N_{Pe}}{2}\cdot\left[\sqrt{1 + \frac{4\,\lambda E_{OG}}{N_{Pe}}} - 1\right]$$

The result can be presented graphically, in terms of an E_{MV}/E_{OG} verses λE_{OG} plot. This shows that for long liquid flow paths (i.e., large diameters) and high liquid rates, the extent of backmixing has a negligible effect on the liquid concentration profile. That is, when N_{Pe} tends to infinity the plug flow limiting solution applies. In practice plug flow is achieved at Peclet numbers of 20 or above.

At the other extreme, short flow path lengths with low liquid cross flow velocities suffer from backmixing which in general occurs over a distance of 300 to 600 mm, (the length of a mixed pool), but can extend over a greater distance. Thus the concentration of all the lvc/mvc components are more or less uniform over the tray. If the liquid concentration across the whole tray is uniform, such that it is equal to the liquid concentration x_o leaving the tray, and the vapour concentrations entering and leaving the tray (y_1 and y_2) are uniform, then E_{OG} is equal to E_{MV}. This is described as the "completely mixed" tray.

"Plug flow" and "completely mixed" represent the two limiting solutions for the general backmixing theory and is summarised graphically in Figure 2.13.

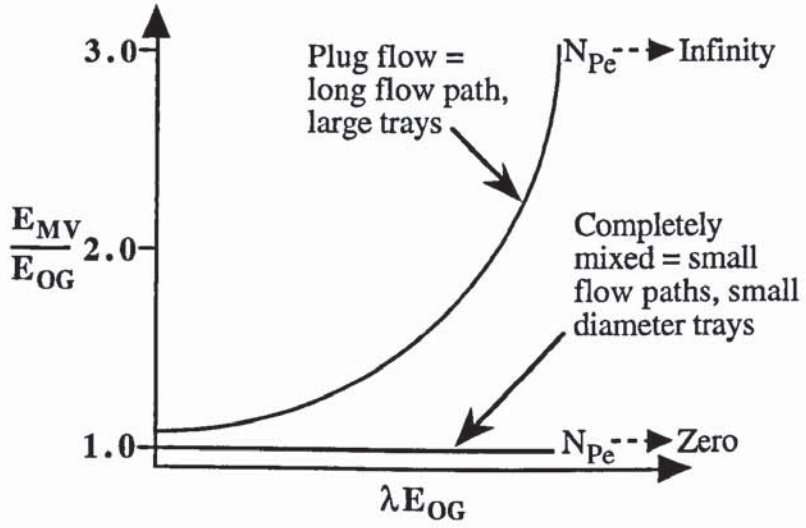

Figure 2.13 Graph of the two limiting solutions, "plug flow" and "completely mixed" for the general plug flow plus back-mixing theoretical model.

To predict E_{MV}/E_{OG} in between the two limiting solutions, use is made of equation

(2.41) or a more detailed version of Figure 2.13.

The main drawback of the "plug flow plus backmixing" model is that it over predicts E_{MV} as a result of using rectangular channels. Thus both experimental and theoretical investigations of flow patterns generated on circular trays and their effect on tray efficiency, were pursued. An example of such an approach is the stagnant regions model which is described below.

Porter and Lockett Models

From the observation of liquid channelling associated with stationary or slowly circulating regions on single and two pass trays, a series of theoretical analyses were devised, to calculate tray efficiency from the hypothesised flow patterns (Porter et al., 1972; Locket et al., 1973; Lim et al., 1974; Lockett et al., 1975). The flow patterns have been idealised by neglecting circulation in the stagnant regions and by separating the various tray geometries into the active and stagnant regions as shown in Figure 2.14.

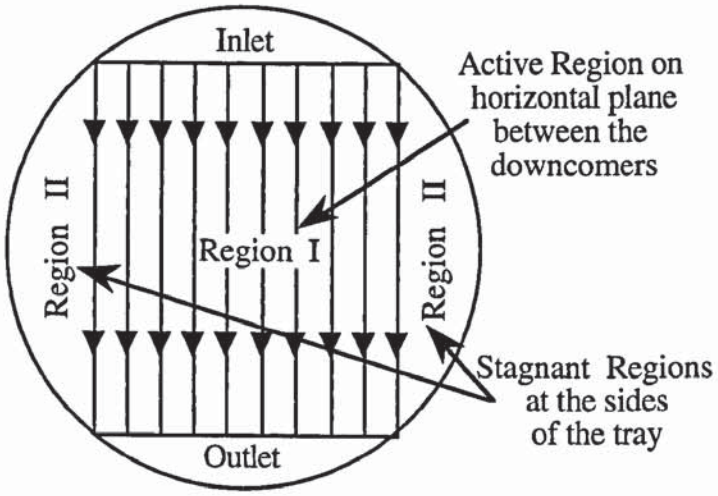

Figure 2.14 Schematic diagram of the assumed liquid flow pattern on a single pass tray (Stagnant Regions Model).

Incorporated into the overall flow pattern is the random transportation of liquid caused by the gas bubbling through it which produces backmixing in the active regions (similar to the AIChE model). In addition, liquid interchange between the active and stagnant regions is attained by the bubbling action of the gas. The above phenomena are explained in terms of eddy diffusion and the analysis starts with a number of simplifications, some of which are identical to the "plug flow plus backmixing" method (see previous section). Additional assumptions which are specific to the Porter/Lockett models are:

a) In the active region, the liquid flow is uniform at all points on per unit width, that is, $L' = L/W$.

b) The liquid flow in the stagnant zone is zero,

c) The eddy diffusion coefficient, D_E, is assumed to be the same in all directions.

To calculate tray efficiency, concentration profiles for various tray geometries are predicted, which in turn are mapped onto a coordinate system diagram as shown in Figure 2.15. Since the concentration profiles are symmetrical about the XX axis, calculations are confined to half of the tray on the right handside.

The liquid composition in the active and stagnant regions are calculated from differential equations derived from a material balance over an increment of froth, of area dw'dz', on the tray for mass transfer which is specific to a binary system. The material balance presented in Figure 2.16 accounts for one component transfer to the vapour passing through the elemental area, mixing of the liquid by the vapour, and one component transfer by the liquid through the froth on the elemental area, in the active region. For the stagnant region the first two factors apply.

Figure 2.15 Schematic diagram of the coordinate system used in the formulation of the Stagnant Regions Model (Porter et al., 1972).

Hence the mass balance, for the active region, yields,

$$D_E\left(\frac{\partial^2 x}{\partial w'^2}+\frac{\partial^2 x}{\partial z'^2}\right)-\frac{L}{h_F\cdot\rho_L'\cdot\rho_F}\frac{\partial x}{\partial z'}+(y_1-y_2)\frac{G'}{h_F\cdot\rho_L'\cdot\rho_F}=0 \qquad (2.42)$$

whereas for the stagnant region, in which the liquid flow term is zero,

$$D_E\left(\frac{\partial^2 x}{\partial w'^2}+\frac{\partial^2 x}{\partial z'^2}\right)+(y_1-y_2)\frac{G'}{h_F\cdot\rho_L'\cdot\rho_F}=0 \qquad (2.43)$$

The concentration profile and subsequent tray efficiency equations, are a function of the dimensionless terms λ, E_{OG}, N_{Pe}, DW/A, and by assuming that changes in bulk liquid flow occur in the z' direction only.

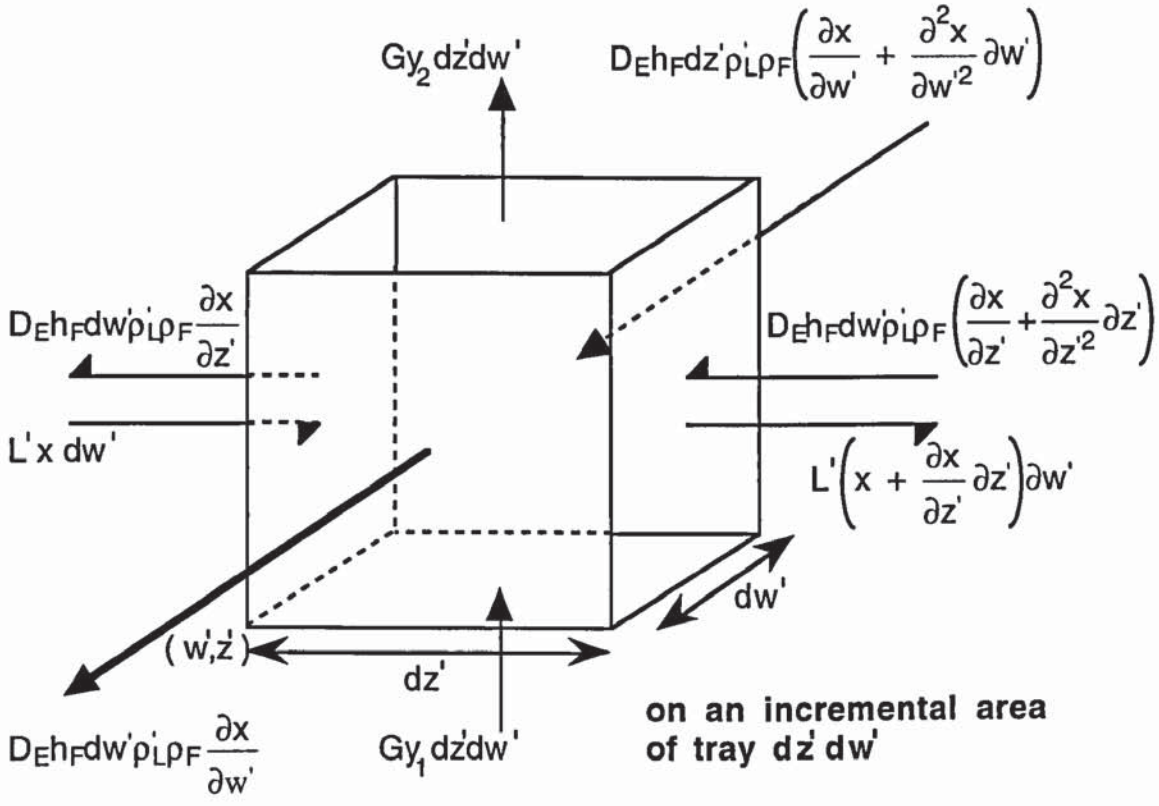

Figure 2.16 Schematic diagram of a mass balance over an element of froth on incremental area of tray.

Thus, by re-arrangement and the use of simple mathematical relationships outlined below, the concentration profile differential equations, (2.42) and (2.43), are made dimensionless such that,

$$\frac{1}{N_{Pe}}\left(\frac{\partial^2 X}{\partial w^2}+\frac{\partial^2 X}{\partial z^2}\right)-\frac{\partial X}{\partial z}-\lambda E_{OG}\cdot\left(\frac{WD}{A}\right)\cdot X=0 \qquad (2.44)$$

$$\frac{1}{N_{Pe}}\left(\frac{\partial^2 X}{\partial w^2}+\frac{\partial^2 X}{\partial z^2}\right)-\lambda E_{OG}\cdot\left(\frac{WD}{A}\right)\cdot X = 0 \qquad (2.45)$$

where; $X = \dfrac{x - x_e^*}{x_1 - x_e^*}$ $\quad N_{Pe} = \dfrac{LD}{W\cdot h_F\cdot \rho_L'\cdot \rho_F\cdot D_E}$ $\quad \lambda = \dfrac{mG}{L}$

$z = z'/D$ $\quad w = w'/D$ $\quad L' = L/W$

$z_1 = z/D$ $\quad w_1 = w/D$ $\quad G' = G/A$

The equations are solved by incorporating the boundary conditions, presented in Figure 2.15, and by numerical computation which involves the finite difference technique. (Lim, 1973).

With the concentration profiles known from the hypothetical stagnant regions flow pattern, E_{MV} is calculated by summing the changes in vapour concentration over the bubbling area for the whole tray. The mean vapour concentration change is obtained from,

$$\overline{y}_2 - y_1 = \frac{m\cdot E_{OG}}{A}\int_A (x - x_e^*)\, dA \qquad (2.46)$$

Now E_{MV} in terms of the most volatile component is defined as:

$$E_{MV} = (\overline{y}_2 - y_1) / (y_2^* - y_1) \qquad (2.47)$$

Where y^*_2 is the vapour concentration in equilibrium with the average liquid composition leaving the tray, $\overline{x}_2$,

$$y_2^* = \frac{1}{W}\int_{-W/2}^{+W/2} (m\overline{x}_2 + b)\, dw' \qquad (2.48)$$

Since y_1, x_1, x_e, m and b are all assumed to be constant, the calculation of E_{MV} from E_{OG}, on rearranging equations (2.46), (2.47) and (2.48), gives

$$\frac{E_{MV}}{E_{OG}} = \left[\frac{1}{A}\int_A X\, dA\right] \Big/ \left[\frac{1}{W}\int_{-W/2}^{+W/2} X_2\, dw'\right] \qquad (2.49)$$

Equation (2.49) is a function of the dimensionless groups λ, E_{OG}, N_{Pe} and DW/A. Since A is proportional to D^2, the latter term DW/A, with some simplification can be expressed as W/D. With the exception of W/D, which gives a measure of the stagnant region compared to the active region, λ, E_{OG}, and N_{Pe} appear in the plug flow plus

backmixing method. Hence by defining, in mathematical terms, a very large tray where W/D approaches unity, and assuming a very high N_{Pe}, the limiting solution of tray efficiency reduces to that of the "plugflow plus backmixing" equation, i.e., equation (2.41) from the AIChE method. Overall, the predicted tray efficiencies from the stagnant regions model, or SRM, are less than those calculated from the AIChE method.

When the weir length is decreased such that W/D reaches the minimum design specification of 0.6, a remarkable fall-off in tray efficiency may occur due to the increased size of the stagnant regions. A simple explanation is that since there is no bulk flow of liquid through these zones, they quickly reach equilibrium with the rising vapour passing through them. Further vapour flow through the stagnant zones undergoes no composition change, and since the duty of the tray is to change the vapour composition, this is detrimental to tray efficiency.

However the random movement of liquid can transport volatile material from the active region into the stagant region . This transverse mixing only occurs over a limited distance since the mvc is being simultaneously stripped by the action of the vapour. Hence it is over this distance that liquid mixing from the active region continuously replenishes the stagnant liquid with volatile material, and is commonly known as the 'width of a mixing zone'. This was calculated to cover a distance of 300 to 600 mm (Porter et al., 1972) and since this distance is independent of tray diameter, it has very important consequences for tray efficiency on scaled-up trays.

For small diameter trays, the width of the mixing zone is greater than the stagnant regions, so that transverse mixing is sufficient to overcome adverse effects on tray efficiency. On larger diameter trays however, the size of the stagnant regions increases which cause insufficient transverse mixing and thus has a detrimental effect on tray efficiency. The 'width of the mixing zone' concept is summarised in Figure 2.17.

Solutions to the tray efficiency equations were obtained by numerical computation and applied to the following situations.

a) One single pass tray, completely mixed vapour, of various diameters (Porter et al., 1972).

b) Several single pass trays, of various diameters, in a column, unmixed vapour (Lockett et al., 1973).

c) Several two pass trays of various diameters in a column, unmixed vapour (Lim et al.,

1974).

d) Vapour mixing effects on several single pass trays in a column (Lockett et al., 1975).

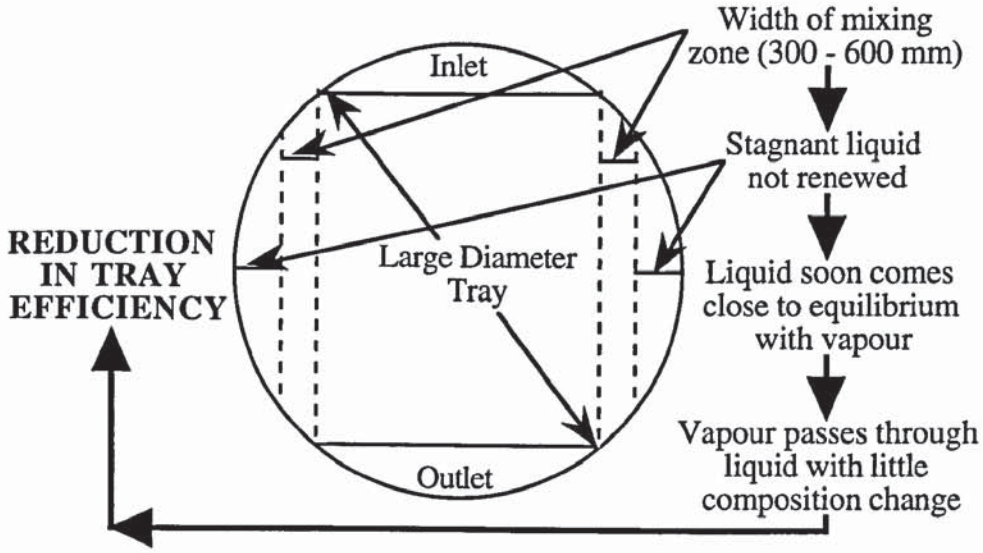

Figure 2.17 Schematic diagram of the detrimental effect of stagnant regions on tray efficiency.

Solutions to the tray efficiency equations were obtained by numerical computation and For the case of single pass trays, the predicted E_{MV} from E_{OG} increases steadily for small diameter trays up to approximately 1.5 m because of the increase in flow path length and sufficient transverse mixing into the stagnant regions. The stagnant regions are small compared to the width of the transverse mixing zone and have a negligible effect. By increasing the column diameter, the stagnant zones become large enough to permit vapour passage through the non-moving liquid with little composition change (i.e., vapour bypassing) and thus causes a steady decline in tray efficiency.

This effect is exacerbated when several single pass trays are stacked in a column such that the stagnant regions lie directly above each other, (see Figure 2.18). That is, on scaling-up the column diameter, the vapour may pass through the trays with no concentration change on passing from one stagnant zone to another, such that in effect the vapour is in equilibrium with the liquid composition of the reboiler. Thus if the column diameter exceeds 3.6 m and is fitted with ten single pass trays such that the size of the stagnant regions is significant, the predicted tray efficiency is less than the point efficiency.

When two pass trays are incorporated into a column, stagnant zones only appear on every other tray where the liquid is in diverging flow from the sides to the centre. The size of stagnant regions on two pass trays are less than that on single pass trays of the same

diameter. Thus the effect of stagnant zones on tray efficiency for scaled-up two pass trays is less severe.

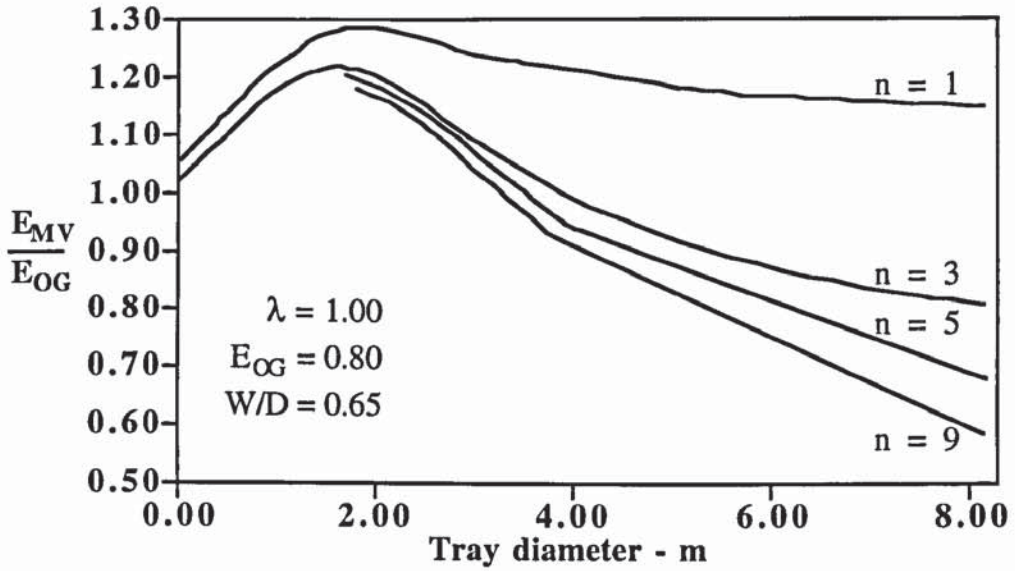

Figure 2.18 Variation in Murphree tray efficiency over point efficiency with column diameter for a multiple of trays in a column.

The effect vapour mixing was predicted to have little significance on the efficiency of large diameter trays (see Section 2.8).

Overall, Porter and Lockett (1975) suggested that liquid channelling with stagnant zones may occur for flow regime on trays which behave in a similar fashion to liquid only flow, such as the froth regime. This type of flow pattern in the froth regime has a detrimental effect on tray efficiency and that this effect increases with increasing column diameter.

However, (Porter et al., 1977) hypothesised that if a tray was operated in the spray regime, this may prevent liquid channelling with stagnant zones and thus produce higher efficiences. The spray regime flow pattern was modelled using "spray diffusion" theory, by assuming that the liquid momentum was negligible and that liquid transportation only occurred by the random movement of liquid droplets. The main conclusion is that the extent of liquid mixing required to transport liquid over the whole tray is such that the enhancement of E_{MV} over E_{OG} is comparatively small for most systems operating in the spray regime. (That is, the flow of spray by diffusion was only valid for $N_{Pes} < 1.25$).

On the whole, the Porter/Lockett models demonstrated the urgent need for experiments on commercial scale trays in order to predict and understand the controlling phenomena on flow patterns and their effect on efficiency. To this effect, the theory outlined in the

stagnant regions model above was used in Section 9.4 of Chapter 9 to calculate concentration profiles on a 2.44 m diameter tray and compare them with temperature profiles produced from water-cooling experiments.

Yu et al., (1991)

In previous theoretical analyses, the assumption of completely mixed vapour and liquid streams entering and leaving a tray in equilibrium was used, in which there was a uniform composition change in one dimension only. For each tray, a set of **M** (material balance), **E** (equilibrium relationship), **S** (summation of mole fractions), **H** (heat balance) equations are established and solved numerically. The disadvantage of this method is that trays are not in vapour-liquid equilibrium, and with the exception of a few cases, idealised liquid flow is assumed on the trays.

These deficiencies were exploited by Yu et al., (1982, 1986, 1990, 1991) by modelling full scale trayed columns with consideration for liquid velocity profiles and diffusional mixing in two dimensions as a opposed to one. Recently a three-dimensional model with partial mixing was formulated, Yu et al., (1991), in which it was claimed that tray efficiency and the concentration profile of a trayed column, calculated from the point efficiency, are in good agreement with published data from industrial columns.

The three-dimensional mixed pool with partial mixing model is the most advanced theoretical pool model to date and is considered here in more detail. In the development of the model, the tray bubbling area is split into a number of square mixing pools such that interpool liquid flow and diffusional mixing occurs in both the w- and z- directions. Liquid flow to and from each pool is in connection with four adjacent pools as shown in Figure 2.19. By considering the size of a liquid pool and the region on the tray in which perfect mixing can occur, seven liquid pools were chosen to represent one half of a commercial scale tray. This is also shown in Figure 2.19.

Above each liquid pool is the addition of a vapour pool such that there is material and heat transfer from the liquid phase to the vapour phase, aswell as interpool vapour diffusional mixing. The two main features of this model are:

a) The pool model is a two-dimensional problem, instead of a one-dimensional study, so that more complex liquid flow patterns on large trays can be closely simulated by adjusting the interpool flow between mixing pools in both the z- and w- directions.

b) Since diffusional mixing is taken into account in two dimensions, the number of

mixing pools on a tray is fixed instead of changing them as in previous mixed pool models. This permits the use of matrix computation.

Figure 2.19 Schematic diagram of two-dimensional pools with super-imposed interpool liquid flow and diffusional mixing on a single tray (Yu et al., 1991).

Thus for each pool, as shown in Figure 2.20, a set of **MPSH** equations can be established: **M** (material balance, see Figure 2.20), **P** (non-equilibrium relationship between liquid and vapour), **S** (summation of mole fraction), and **H**, (heat balance). To assist with computation, the theoretical distribution of velocities are taken as initial values in the z- and w- directions with the corresponding eddy diffusivities determined from either correlations based on experimental RTD data (Yu, 1992), or by computation using a turbulent liquid flow model (Yu, 1992; Porter et al., 1992). These can described as interpool flow patterns.

With these parameters established, the **MPSH** equations can then be derived for each tray. Since the reboiler and condenser are each regarded as equilibrium pool stages, sets of **MESH** (reboiler) and **MSH** (condenser) equations can be derived in a similar manner to that obtained for the trays in the column. This forms the basis of the mathematical model for the three-dimensional simulation of a tray column.

By noting the methods to obtain interpool liquid flow velocities and eddy diffusivity in the z- and w- directions, as well as measures to calculate point efficiency, the

computation procedure is as follows. Iteration methods are used to solve the **M-P** equations of each component by determining the compositions in all the liquid and vapour pools. **S**-equations are used to correct the pool temperature followed by the **H**-equations which are used to adjust the total flow of the liquid and vapour. Successive iterations eventually yield the final concentration, flow rate and temperature in all pools so that three-dimensional profiles of the vapour-liquid compositions and tray temperature for a multicomponent distillation process in a tray column are obtained.

Figure 2.20 Schematic diagram of a material and heat balance around a liquid pool and a vapour pool (Yu et al., 1991).

The three-dimensional model can be simplified, so as to emulate other models such as Gautreaux and O'Connell (1955), Porter et al., (1972) and Bruin and Freije (1974), by selecting the apppropiate number of pools in the z- and w- directions. On the whole, it was claimed that the three-dimensional model produced more accurate tray efficiencies over point efficiencies compared with that produced from the emulated models.

2.7.2 Conclusions on Tray Efficiency Models

It has long been known that liquid flow patterns have a significant effect on tray efficiency, but it was not until the early 1970's that tray efficiencies were rigorously modelled on commercial scale trays by predicting the flow pattern that was likely to occur for a particular tray geometry. The stagnant regions model (Porter et al., 1972) predicted that large diameter trays would suffer serious reductions in tray efficiency as a result of maldistributed liquid flow across the tray. The prediction of scale up failures were subsequently confirmed for large diameter trays (Smith and Delnicki, 1975). Although improvements in the modelling and simulation of real tray columns have been made, (e.g. Yu et al., 1991) in which good agreement with plant data was claimed, the overall view of many authors was the need for greater experimental work on commercial trays of various geometries.

With this in mind, it is worth raising the question of what are the real flow patterns encountered in practice, and how does this change with operating conditions? To help answer this question, has there been previously a comprehensive investigation into the development of liquid flow patterns on a commercial size tray?

Since the flow phenomenon on real trays is a two phase flow problem, the following section reviews the work on the vapour distribution effects on the tray liquid flow pattern.

2.8 Effect of Vapour Flow on Liquid Flow Patterns

Over the years, there has been little research into vapour distribution and its effect on liquid flow patterns. Initially, research was mainly concerned with vapour mixing and whether it produced a more uniform liquid flow pattern and thus improve tray efficiency.

For the case of uniform liquid flow, it was shown by Katayama and Imoto, (1972) that if the Peclet number for horizontal vapour mixing, N_{PeG}, is greater than 50, the vapour is considered to be unmixed with regards to influencing tray efficiency. So what is the effect of vapour mixing on non-uniform liquid flow such as that predicted by the SRM? Based on the maximum possible vapour mixing, Lockett et al., (1975) reported that for small diameter columns, with small stagnant zones, there was only a small increase in tray efficiency caused by vapour mixing as opposed to unmixed vapour. This however is ineffective in reducing the adverse effects of vapour bypassing through the stagnant

regions found on large diameter trays. Thus it was suggested that, the vapour should be considered to be unmixed in the design of large diameter trays.

Evidence of vapour maldistribution and its effect on liquid flow patterns is very scarce. It is known that there is preferential vapour flow through the liquid close to the outlet weir so as to overcome the hydraulic gradient (Lockett, 1986), which depends both on tray pressure drop and the total pressure drop in the column. This causes a reduction in the vapour contact time and thus decreases point efficiency. However, (Lockett and Dhulesia, 1980) reported that this type of vapour maldistribution has little effect on the predicted E_{MV}/E_{OG} ratio . On the other hand, Vybornov et al., (1971) reported a significant reduction in tray efficiency because of vapour maldistribution perpendicular to the direction of flow although this was attributed to tray out-of-levelness or column tilt.

Thus, until recently, there have been no studies into the effect of gas distribution on the liquid distribution such that it can change the direction of liquid flow. Some peculiar but remarkable two phase flow patterns have been reported on large hole trays in which the gas flow beneath the trays forced the liquid to recirculate on 1.22 m and 2.44 m diameter trays (Ayvaz, 1990; Porter and Lan, 1991). It is not yet understood what causes gas induced liquid flow patterns and thus more experimental work is required in this area.

2.8.1 Conclusions

Up to now, there have been no investigations into the effect of gas distribution on the liquid flow pattern such that it is possible to change the direction of liquid flow. Hence, to predict two phase flow patterns that are likely to occur in practice, more investigations into vapour interactions with the tray liquid flow pattern are required to find out under what conditions gas-influenced liquid circulation occurs. In a real tray column, this phenomenon may occur on the first tray above the vapour feed inlet from the reboiler, or it may be reproduced on a series of trays where one is placed above the other. An attempt to answer these questions by experiment is described in Chapters 6 and 10.

The assumption of unmixed vapour plug flow between trays is too idealistic for predicting real vapour-liquid interactions in a trayed column with confidence.

Sufficient evidence on the adverse effects of vapour and liquid flow maldistribution on tray efficiency led to the suggestion (Sohlo and Kouri, 1982) that the most obvious method of overcoming these effects was the improvement of the liquid velocity profile itself. Below is a description of flow control devices used to improve the flow pattern and restore the expected tray efficiency.

2.9 Control of Vapour and Liquid Non-Uniformities

The prediction of failure to achieve separation in large diameter columns from the tray efficiency models, as a result of severe non-uniform flow, prompted the establishment of several methods to restore the expected tray efficiencies by improving the liquid flow pattern. These include modifications of the tray bubbling area and the inlet downcomer apron. Presented below are examples of corrective flow pattern devices in which higher tray efficiencies from an improved liquid distribution are claimed.

2.9.1 UOP Slotted Sieve Tray

The UOP Process Equipment Group (formerly Union Carbide) has produced a variety of slotted sieve trays (Williams and Yendall, 1963, 1968; Matsch, 1973; Kirkpatrick and Weiler, 1978). In order to overcome the adverse effects of unbalanced vapour-liquid contacting for mass transfer and flow maldistribution, slotted trays incorporate raised slots punched into the tray deck with an opening on one side. Proper angling and distribution of these slots directs a small vapour fraction horizontally along the tray deck and transmits sufficient momentum to the liquid such that it is propelled into stagnant or circulating regions, thus producing a more uniform liquid distribution.

The advantages of slotted trays over conventional sieve trays claimed by UOP are:

a) Non-uniform liquid flow and unbalanced vapour-liquid contacting are minimised by the horizontal liquid propulsion mechanism from the tray slots.

b) Control of the liquid residence time to give maximum efficiency is achieved.

c) Complete vapour-liquid agitation over the tray bubbling area is produced by an inlet bubble promoter, and that single or two pass versions are available depending upon the weir load.

d) High tray efficiencies are reported in which parallel flow trays achieve a high efficiency followed by cross flow trays.

2.9.2 Kuhni Slit Tray

The column-internals vendors Kuhni developed a slit tray which operates on the principle that liquid flow is in the same direction on all trays (see Figure 2.21). This is achieved by a central downcomer combined with a liquid distribution network of radial pipes to direct liquid to the outer edge of the tray below. The tray bubbling area consists of slits rather

than sieve tray perforations which produces a horizontal distribution of vapour into the liquid flow thus providing the biphase with a flat trajectory for reducing the levels of entrainment. In addition the tray design permits intensive vapour-liquid mixing as well as long contact times.

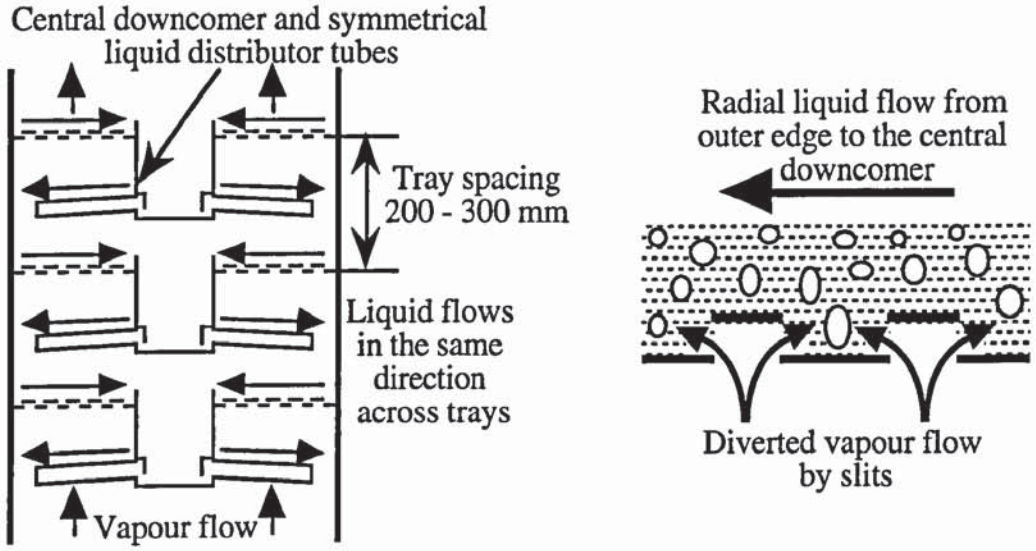

Figure 2.21 Schematic diagram the Kuhni slit tray (an example of Lewis's case 2).

Advantages of the slit tray claimed by Kuhni are:

a) Vapour passage through the parallel flow of liquid on successive trays (Lewis Case II) yields a high tray efficiency. When combined with a low tray spacing, this gives a high number of theoretical stages per metre of trayed height.

b) A high efficiency and a low pressure drop is achieved over a wide operating range at very low tray spacings of between 200 and 400 mm.

c) The turndown range is greater than that for conventional sieve trays.

2.9.3 Double Expanded Metal (BOC) Tray

The Flow Control tray consists of a fine expanded metal mesh to support the biphase, and a coarse grid attached on top. This was designed for cryogenic distillation of air (BOC Cryoplants Ltd., Biddulph, 1990), which requires a low tray spacing and pressure drop.

Operation of the tray involves vapour issuing through fine slots of the bottom metal mesh, by slot alignment away from the inlet downcomer, to assist liquid cross flow from the inlet to the outlet. The coarse grid permits long vapour-liquid contact times for mass transfer by maintaining a uniform height of clear liquid across the tray. The Flow Control

tray, like the UOP slotted tray was designed to overcome non-uniform liquid flow and thus high efficiencies were claimed at a low pressure drop over a wide operating range (Urua et al., 1992).

2.9.4 Downcomer Modifications

Several downcomers have been designed to improve the liquid flow distribution on entering the tray at the inlet.

The FRI downcomer improves flow distribution by preferential liquid flow at certain positions along the length of the inlet and outlet weirs (Keller, 1973; Yanagi and Scott, 1973). This is achieved by incorporating several metal strips on the inlet downcomer apron in order to attain a greater clearance at the sides of the inlet, with a smaller clearance along the centre, as well as using a notched weir at the outlet. It appears that this arrangement is specific to particular flow rates and that uniform liquid distribution may not be achieved for other flow rates.

Downcomers that were designed to produce a more even liquid distribution at the inlet and prevent channelling associated with stagnant regions at the sides of the tray, include the step flow downcomer (Porter, 1973) and the winged downcomer (Lavin, 1986). The cylindrical tube of the step flow downcomer and the greatly increased length of the winged downcomer were both designed to provide liquid flow around the sides of the tray and thus produce a more uniform liquid distribution from the inlet to the oulet.

2.9.5 Conclusions on Controlling Vapour and Liquid Uniformity

The continuous development of flow control devices suggests that improving the liquid flow pattern maybe of considerable importance in optimizing tray and column performance, although they are not widely used at present. However, the above examples are only corrective measures for controlling the liquid flow at the inlet downcomer and dispersing vapour-liquid flow into stagnant or circulating regions. It is unclear how well these methods work under different flow regimes as well as controlling the flow patterns developed over a range of throughputs.

Ideally, it would be desirable to design trays where corrective methods are unnecessary. However, if this was impossible, a method needs to be developed to predict when such flow control measures are required. To this effect, a fundamental study into enhancing our understanding of the controlling phenomena of two-phase flow patterns, started by Hine (1990), needs to be extended to other commercial trays with larger size holes.

2.10 Overall Conclusion on Literature Survey

From the literature review, it is clear that tray design methods are empirical. This increases the risk of under or over-design and inhibits tray development which at present must occur by trial and error since there is no scientific foundation for tray design. A fundamental scientific approach is therefore needed to design columns so as to move away from the need to develop new trays by trial and error, and gain the necessary knowledge needed to produce more sophistcated trays which give a better performance. This requires the establishment of a "flow pattern data bank" when the tray is operating in a particular regime so as to identify those flow conditions in which non-uniform liquid flow occurs, thus reducing tray efficiency. For example, if liquid channelling associated with circulating flow occurs on a tray operating in the emulsion flow or froth regimes, it may in some circumstances be avoided by operating in the spray regime. However, the question of how spray flows across a tray has yet to be answered.

Despite a significant amount of experimental and theoretical work into the effects non-uniform liquid flow on tray efficiency, it is still not possible to predict liquid velocity profiles when changes are made to the tray geometry and the vapour-liquid flowrates. Thus, a number of methods have been devised to improve the liquid flow pattern and restore the expected tray efficiency by incorporating corrective measures which may only work for a particular operating condition. It should also be noted that gas flow effects on tray liquid flow patterns, such that it changes the direction of flow, may occur on the bottom tray in a distillation column or on all of the trays placed one above the other. The overall conclusion from the above evidence is that previous studies were based on hypothetical flow patterns modelled mainly on single phase flow and may not give a true representation of what is happening in practice.

In order to understand, from first principles, the complex two-phase flow behaviour on a tray, a comprehensive set of experiments are required to study the effect of a vertical gas flow through the liquid flow over a tray. This was started by Hine (1990) in which two phase flow patterns on a 1.0 mm tray were compared with water only on an unperforated tray. This approach needs to be extended to larger hole trays in order to establish the parameters required for a new theory of open channel two phase flow and assess their effect on subsequent new tray efficiency models. This should lead to a better understanding of tray hydraulics and thus greatly improve tray design procedures.

CHAPTER 3

APPROACH TO THE PROBLEM

It has already been established that biphase flow patterns on sieve trays are highly complex as a result of the bubbling action of the vapour when forced through a horizontal liquid cross flow. To simplify the study of two phase flow patterns, the effect of the gas flow on the liquid flow pattern can be investigated by comparing water only flow across an unperforated tray with air-water flow patterns produced on a perforated tray. This approach is part of a long term project in which the effect of the gas flow on liquid flow patterns is to be investigated on sieve trays of various hole diameters.

The work, started on 1.0 mm hole trays (Hine, 1990), used in air-separation, is to be extended to 6.35 mm hole trays, typical of that found in the petrochemical industry, with the results being presented in this thesis. At some future stage, it is envisaged that the effect of the gas flow on the liquid flow will be investigated on 12.7 mm hole trays since they are the most widely used trays in the chemical and petrochemical industries. As mentioned in Chapter 1, the chemical and petrochemical industries tend to use large hole trays since they are less prone to fouling and corrosion compared with small hole trays.

The research programme was pursued using a 2.44 m diameter test facility for the study of air-water flow patterns using a range of experimental techniques. (It is necessary to work at this scale to reproduce the flow patterns that are likely to occur on commercial scale distillation trays which vary from 1.0 to 10.0 m in diameter). The techniques used for the experimental investigations described in this thesis are as follows:-

a) Direct-observation of two phase flow patterns using directional flow pointers partially submerged in the froth or spray which behave in a similar way to that of weather vanes used to show the direction of the wind. To observe air only flow patterns in the inter-tray spacing, ribbon flow pointers were used.

b) Heat transfer by water-cooling was applied to the single tray experiments. Hot water is fed onto the tray and the rising air evaporates a small fraction of the water causing localised cooling. When compared with distillation, air enthalpy is analagous to vapour concentration and water temperature is analagous to liquid concentration on the tray. In these experiments, the water temperature is measured at 108 equally

spaced positions on the tray, to produce lines of constant temperature (isotherms). The temperature profile isotherms are sensitive to changes in the flow pattern, which in turn, have a significant effect on mass transfer.

c) The effect of the biphase flow pattern on the liquid head variation across the tray is determined by measurement of the clear liquid height. This is achieved using manometers attached to thirty two pressure tappings evenly spread across the tray. Like the water-cooling experiments, the height of clear liquid data is computer processed to yield three-dimensional liquid head surface profiles.

The series of investigations outlined below involved the use of one or a combination of all three experimental techniques. The investigations are as follows:-

1) Direct observation experiments are used to determine the effect of gas flow, below the 6.35 mm hole test tray, on the liquid flow pattern and the removal of these effects by modification of the gas distributor. Water cooling is used to determine whether the existence of gas-influenced liquid flow patterns have a significant effect on mass transfer and tray efficiency.

2) Studies of non-separated and separated liquid flow patterns, by simple gas-liquid contacting experiments, and by simulating distillation at different pressures, on the test tray in which gas flow pattern effects below the tray had been removed. In these experiments all three techniques are used. Direct observation is used to show the presence of circulating/non-circulating flow patterns, which in turn will have a significant effect on the driving force for mass transfer, during water cooling, and on the variation in liquid head during the clear liquid height measurements.

3) Observations of liquid flow patterns on two 6.35 mm hole trays, to determine whether the gas flow emerging from the liquid flow on one tray changes the direction of liquid flow on a second tray placed directly above. Information can be obtained qualitatively by direct observation and by the measurement of the clear liquid height. Are the flow patterns on two trays the same or different to that produced on one tray given that the inlet downcomer to the bottom tray contains no sparge pipe and random packing system to provide a uniform liquid flow to this tray?

Complete details of the programme of experiments including the objectives of each investigation along with a discussion of results are contained in subsequent chapters. Descriptions of the apparatus as well as the experimental techniques and processing of results, are contained in the next two sections.

CHAPTER 4

DESCRIPTION OF THE APPARATUS

4.1 Introduction

In order to permit the experimental investigation of two phase flow patterns on larger hole sieve trays, the following chapters are concerned with detailed descriptions of the apparatus and the experimental methods used for this research programme. Experimental procedures and the processing of results are contained in Chapter 5.

This chapter is concerned with describing the air - water simulator column, which incorporates an air supply from an industrial scale fan and a water heating facility for heat transfer experiments to measure tray efficiency. Details of the air, water and heating circuits; the associated instrumentation for measuring flow rates; and the level of accuracy of measured variables are presented. Furthermore, details of changes to the gas distribution system are given and this section concludes with the modification of the simulator to permit the investigation of biphase flow patterns on two trays.

4.2 Overall Test Facility

The industrial scale distillation test plant incorporates a 2.44 m diameter air-water simulator column; a 150 HP air fan; and a 1.2 MW water heating supply in the form of two gas fired process boilers and a steam top up facility. The test facility is equipped for the direct-observation of liquid flow patterns; the investigation into the effect of liquid flow patterns on mass transfer by the heat transfer water-cooling technique; and the use of several manometers to measure liquid head variation on the test tray(s). A schematic diagram of the overall distillation test plant is shown in Figure 4.1.

The procedures used in the design and construction of the 2.44 m diameter distillation simulator are detailed elsewhere (Hine, 1990), with the overall design specifications of the peripheral components, that make up the overall test plant, summarised in Table 4.1. A brief description of the air, water and heating supply facilities is in the following subsections.

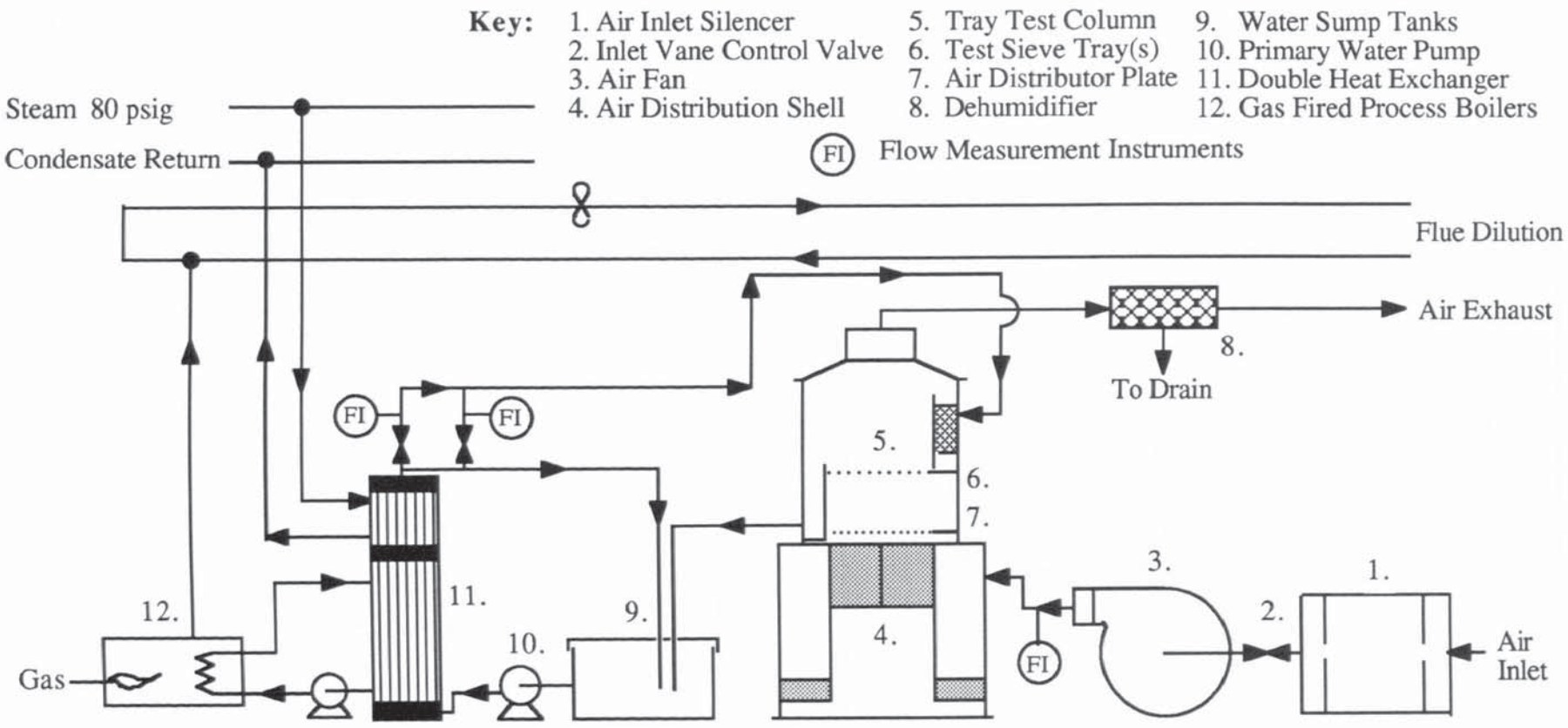

Figure 4.1 Schematic diagram of the air -water distillation test plant

Ancillary Units		Design Specifications		
Air Equipment	Number 48 "Mistral Backward Inclined" Air Fan	Max. Air Flowrate - m^3/s		14.38
		Pressure Head - mH_2O		0.51
		Electric Motor - HP		150.0
	Air Inlet Ducting	Dimensions - m^2		0.978 x 0.622
Water Equipment	Two Sump Tanks	Total Capacity - m^3		5.448
	Main Centrifugal Water Pump	Max. Water Flowrate - m^3/s		0.055
		Pressure Head - mH_2O		12.75
		Electric Motor - kW		15.00
Heating Equipment	Double Water Heat Exchanger	Top Exchanger	Heat Transfer Area - m^2	3.37
			Hydraulic Resistance - mH_2O	3.21 - through tubes section
		Bottom Exchanger	Heat Transfer Area - m^2	10.22
			Hydraulic Resistance - mH_2O	2.79 - on shell side
	Gas - Fired Process Boilers	Nominal Burner Rating for each boiler - kW		500
		Heating Efficiency of each boiler - kW		400 (ie 80% of total rating)
		Water Flow Rate from each boiler - 10^3.m/s		8.66
		Hydraulic Resistance of each boiler - mH_2O		0.26
	Steam top - up supply	Steam Pressure - psig		80.0
		Corresponding Temperature - °C		162.0

Table 4.1 Summary of the design specifications of all the peripheral equipment.

4.2.1 Air Supply

Unsaturated ambient air, outside the pilot plant, is drawn throught a protective grill, at floor level, into the test plant system. On route to the inlet of the fan, air is passed through a silencer, to reduce excessive noise levels, and a vane control valve, used to preset the superficial column velocity. The air is fed to the inlet of the air-water simulator via a rotary impeller blade unit, driven by an electric motor and fan belt system, and a short section of rectangular ducting. This contains an array of fifteen pitot tube pressure sensors which are linked to an air flow meter. The air, on passing through the liquid cross flow on the test tray becomes saturated and leaves the simulator column through the top exhaust duct, positioned approximately 8 m above ground level. Excess water is removed from the exiting air stream, using a demister, prior to being vented from the pilot plant to the atmosphere.

4.2.2 Water Supply

The water circuit consists of two water storage tanks, a double heat exchanger, a main line centrifugal pump, and a grey PVC pipe network. The PVC pipe is of a particular grade such that it could withstand high water temperatures of upto 75°C when used in the heat transfer experiments. For the direct-observation experiments, cold water is pumped, from the sump tanks through the heat exchanger and into the water bypass circuit, using the 15 kW centrifugal pump, from which it is returned to the sump tanks. Once a uniform flow of water has been achieved in the circuit, the desired water flow rate is preset using one of two flow meters, according to whether a high or low water loading is required in the column. Water is subsequently delivered to the inlet downcomer of the simulator, directly, from which it is discharged onto the test tray where it is contacted with vertically rising air. The aerated water is removed from the column by flowing over the outlet weir and into the outlet downcomer, from where it is discharged to the sump tanks through an exit-return pipe.

The same principle was applied to the heat transfer experiments by water-cooling, with the exception that water is heated in two sections of a double heat exchanger prior to delivery to the simulator. In the first exchanger, the water supply is preheated by hot water delivered from the process boilers. Water is immediately transferred to the second heat exchanger where is undergoes additional heating by condensing steam from the departmental utilities generator. The warm water on leaving the heat exchanger, is subsequently delivered to one of two flow meters and undergoes the same process as that described above. A water top-up line supplied fresh water to the sump tanks in order to replenish water lost through evaporation in the simulator column.

4.2.3 Heating Supply

The heat transfer process by water-cooling, involves the removal of heat from water in the main water circuit. Under steady state conditions, this must be equivalent to the heat input supplied from the hot water closed-loop cycle. Since the experimental investigations, involve the use of various air and water throughputs, ranging from very low to very high flow rates, the heating duty was designed to be variable. Hence the heat load would vary from a small temperature drop across the tray, with a large water flow rate, to a large temperature drop across the tray, with a low water flow rate, for a given air throughput.

From the work of Ani (1988) and Hine (1990), it was shown that the heat removed from

the water on the tray, for any given air flow rate, was greatest at high weir loads. The heat capacity required for a maximum water loading on the 2.44 m diameter column was, therefore, calculated to be 1.2 MW. Thus a flexible heat source of two 0.50 MW gas fired process boilers and the steam top-up supply, were used to supply the simulator column with the required heat load.

Gas Fired Process Boilers

In all heat transfer experiments, the two gas fired boilers provided the primary source of heat to the water flow prior to entering the column. Hot water circulating in a closed loop cycle between the boilers and the bottom water-water heat exchanger preheats water in the main circuit before being delivered to the top steam-water exchanger. One or both process boilers can be operated on line according to the heating duty required for water-cooling. Flue gases, produced from the process boilers, are diluted with fresh, ambient air, using a flue pipe and extractor fan system, and discharged to the atmosphere from the test plant at a height of 8 metres above ground level.

Steam Supply

Steam, at a pressure of 80 psig, is delivered to the top steam-water section of the double heat exchanger from the utilities generator through a 100 mm I.D. lagged steam line. A condensate line from the exchanger returns condensed steam for recycle in the generator. The purpose of the steam is to provide a high grade top-up heat source in order to obtain a rapid but efficient fine tuning of the water inlet temperature to the test tray. All the steam supply could be used if the maximum heat load is required. Steam injection into the steam-water stage of the heat exchanger is controlled using a perforated copper tube spring valve of length 0.5 m and diameter 25.4×10^{-3} m.

Double Heat Exchanger

The function of the heat exchanger is to transfer heat from the process boilers and the steam line to the main water circuit prior to entering the simulator. When pumped through the bottom water-water heat exchanger stage, the water is heated by a counter current flow of hot water supplied from the process boilers in the closed loop cycle. Since the primary heating load is produced in the process boilers, the heat transfer area in the water-water exchanger is much greater than that in the steam-water exchanger.

When the main water flow is discharged to the top steam-water exchanger, further heating takes place using condensed steam from the utilities generator.

4.3 The 2.44 m Diameter Simulator Column

The air-water simulator column comprises of three principle units: a 3.05 m diameter air inlet and distribution shell, the middle 2.44 m diameter tray column shell, and the top air exhaust ducting system. A schematic diagram of the simulator column is presented in Figure 4.2.

4.3.1 Air Distribution Shell

Air, on leaving the air fan and flow meter is passed through the rectangular ducting and enters the inlet of the distribution shell tangentially. From the work of Ali (1984), it was shown that for an inlet tangential feed, a system of internal cross and radial baffles, in an internal cylinder, minimised high velocity swirling and large pressure differentials, thus producing a more uniform gas distribution with negligible pressure drop. Hence this gas distributor system was incorporated into the distribution shell. The tangential air feed is forced to swirl inside an annulus, between the outer and inner column shell. The swirling effect is eliminated by a system of thirty two radial baffles which produces a downward flow of air to the bottom of the shell. On discharge from the bottom of the annulus, the air rises through the internal cylinder chamber where four large cross baffles remove any residual swirling. A schematic diagram of the tangential air inlet and radial baffle system is presented in Figure 4.3.

As will be described in Chapter 6, the original air riser (chimney) distributor plate, situated immediately above the cross baffles and annulus was replaced with a 1.80 mm hole diameter perforated tray. This improved the gas flow pattern in the region between the distributor plate and the test tray.

The whole gas distribution system ideally, works on a dry basis in order to prevent the accumulation of moisture by the rising air, and thus change its properties. Hence four drainage pipes were installed in each quadrant of the perforated distributor tray such that any weeped liquid was collected and discharged from the column.

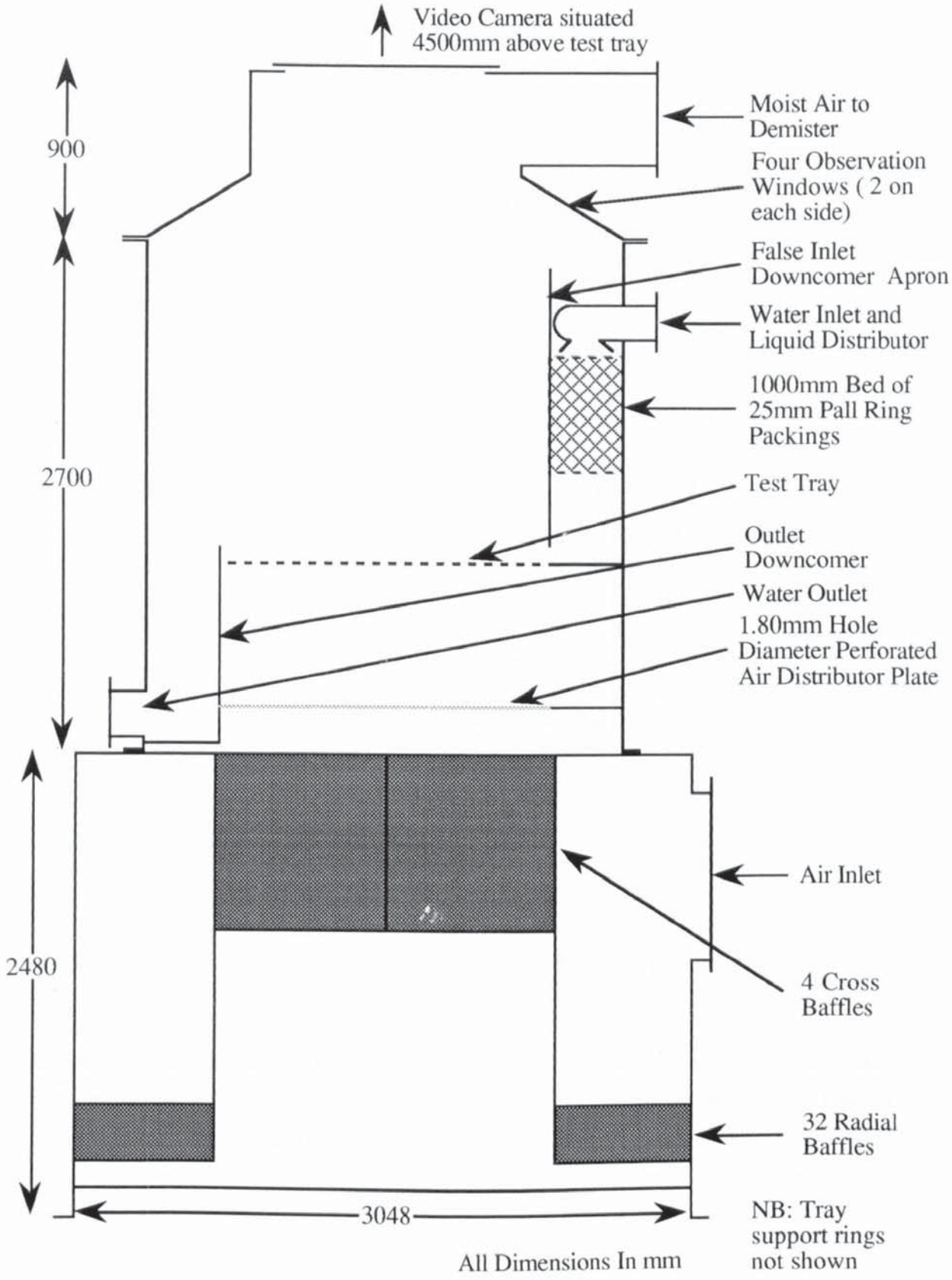

Figure 4.2 Schematic diagram of the 2.44m diameter air - water distillation simulator with modified air distributor.

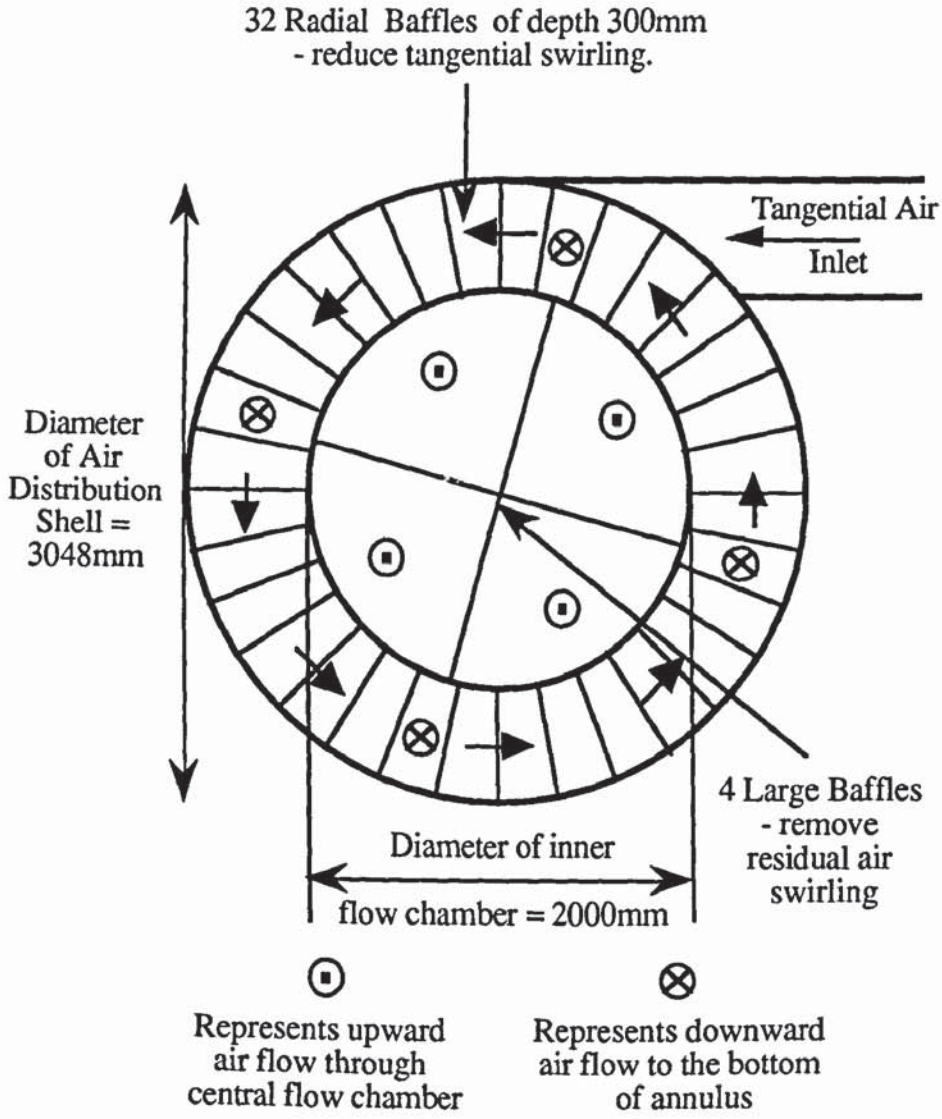

Figure 4.3 Schematic diagram of the tangential air inlet and gas distributor baffle system.

Note that in Figures 4.2 and 4.3, the distance between the inner and outer cylinder shells, or annulus, of the air distribution unit is 0.622 m, which also corresponds to the lengths of the thirty two radial baffles inside the annulus. In addition, the movement of tangential air flow in the annulus is in the anti-clockwise direction prior to entering the internal flow cylinder.

Figure 4.4 is an overhead photograph of the new small hole air distributor tray, situated 850 mm below the test tray support ring and lattice beam support frame work in the tray column shell.

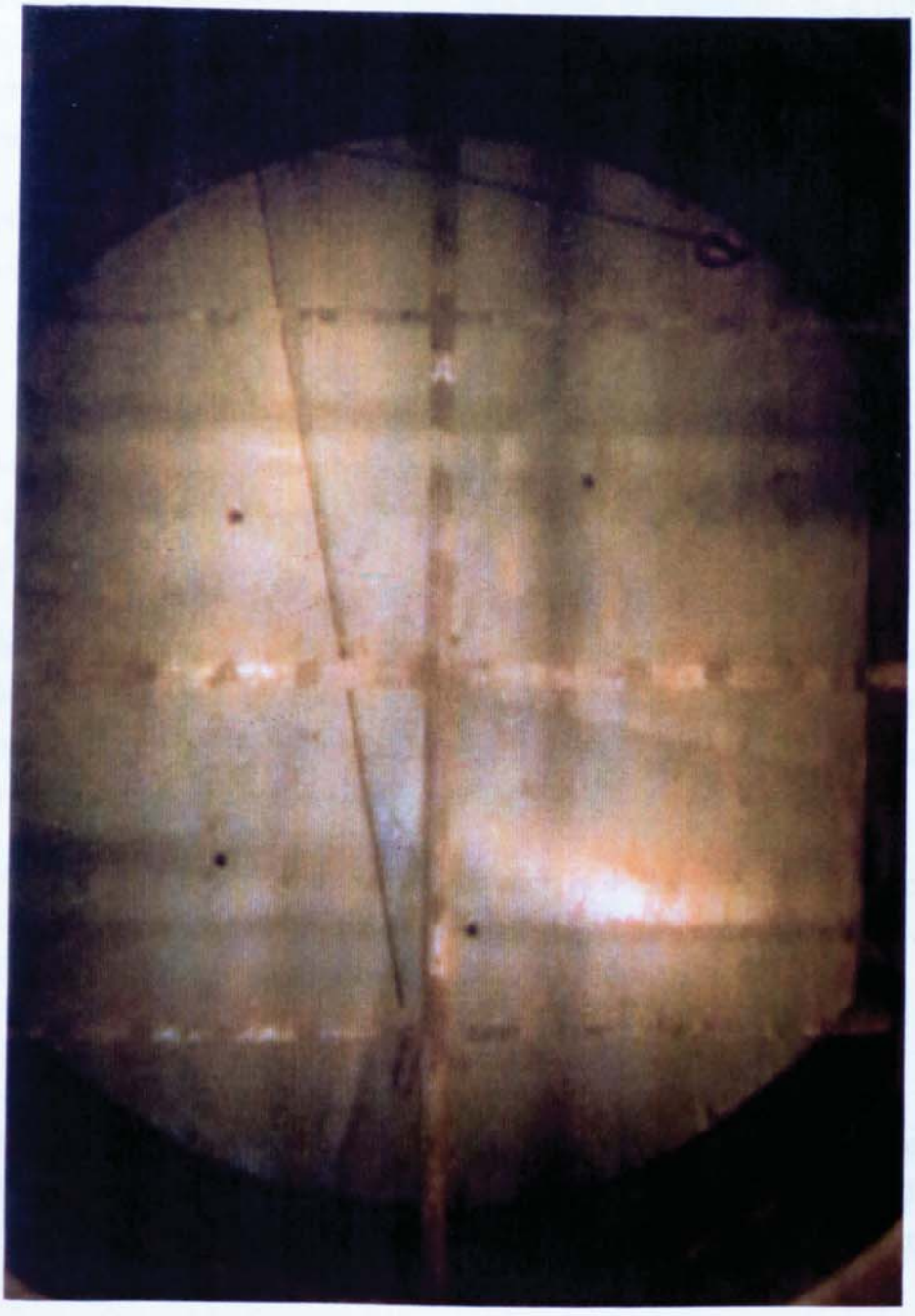

Figure 4.4 Overhead photograph of the 1.80 mm hole diameter air distributor plate.

4.3.2 Tray Column Shell

The test tray with support framework and downcomers are contained in the middle column shell which is situated directly on top of the air distribution shell. Rising air, from the gas distributor, enters the test tray which is supported on a lattice beam framework, situated 850 mm above the distributor plate. The air, on passing through the liquid cross flow on the test tray, becomes saturated and enters the exhaust ducting system where it is subsequently vented to the atmosphere.

The water distribution in the tray column shell consists of the water inlet and a sparge pipe, from which water is discharged onto a 1.0 m packed bed of 25 mm Pall Rings in the inlet downcomer. The packing is held at a clearance height of 600 mm above the under downflow plate. This method, developed by Enjugu (1986), is used to ensure a uniform distribution of water across the inlet downcomer before entering the test tray. The water on crossing the active bubbling area of the test tray is contacted with a cross flow of air before flowing over the outlet weir and leaving the outlet downcomer through an exit pipe.

At the bottom of the inlet downcomer apron, is a moveable aluminium face plate, in which the inlet gap clearance can be set, using PVC spacers, at heights of between 10 and 50mm. The outlet weir height can be varied between heights of 0 and 50mm using specially made angled aluminium strips.

The column shell is fabricated from aluminium sheet of thickness 6.35 mm and contains a number of manway windows for direct-observation as well as easy access for changing tray configurations inside the column.

4.3.3 Air Exhaust Ducting System

At the top of the column, there is a reducing section which links the tray column shell to the exhaust ducting system. This rectangular ducting section removes saturated air from the column and is discharged to the atmosphere. The reducing section consists of four windows for direct-observation of liquid flow patterns.

A video camera, supported on a platform 4.5 m above the test tray, permits flow patterns to be recorded or displayed on a monitor at ground level.

4.3.4 Test Trays

The design specifications of the test trays used in the research programme are presented in Table 4.2. A common factor of both trays is that the perforations, of diameter 6.35 mm, are drilled on a triangular pitch with sharp-edges in accordance with industrial practice. The difference between the trays is that the first tray consists of four aluminium quadrant sheets, which are pinned down onto the lattice beam support framework and secured with steel strips; whilst the second tray is a 304 stainless steel integral beam tray, details of which are given in Section 4.6.3.

4.4 Measurement of Operating and System Variables

The important variables used in the direct-observation, heat transfer and measurement of liquid head profile experiments can be separated into two categories. The air and water flow rates can be classified as the operating variables while air enthalpy, air humidity and water temperature can be categorised as system variables. The assumption was made that other physical properties of the air-water system, such as density and viscosity did not undergo significant changes for all the experimental operating conditions used in the research programme.

4.4.1 Maximum Air and Water Flow Rate Specifications

The air and water flow rate specifications required for delivery to the simulator by the flow instruments, were obtained from a tray loading diagram similar to that shown in Figure 2.1 of Chapter 2, in which capacity factor, based on the superficial vapour velocity, is plotted against weir load. This diagram contains a jet flooding curve and a weep limit for a 12.5 mm hole tray, set at a tray spacing of 600 mm and free area 8.0 %, which indicates the range of operation between the maximum and minimum throughputs. The calculation of the maximum air and water flow rates was based on the operating condition of 80% of total flooding from which data was extracted and substituted into the appropiate equations (see below) in order to compute the maximum flow rate specifications.

Design Specification of Test Trays		Perforated Metal Sheet Tray	Perforated Integral Beam Tray
General Information on the two trays	Tray Material	Alumnium	304 Stainless Steel
	Total Tray Diameter (mm)	2430	2420
	Weir Length (mm)	1500	1500
	W / D ratio	0.615	0.615
	Support Ring Dimensions (mm)	50 x 50 x 6	50 x 50 x 6
	Flow Path Length (mm)	1925	1925
Dimensions of Aluminium Tray Units			
Two tray quadrant units at inlet	Length of longest side (mm)	1215	
	Length of shortest side (mm)	745	
	Length normal to the weirs (mm)	975	
Two tray quadrant units at outlet	Length of longest side (mm)	1215	
	Length of shortest side (mm)	745	
	Length normal to the weirs (mm)	950	
Dimensions of Integral Beam Tray Units			
Two straight edge integral beam units	Length (normal to weirs) (mm)	1925	
	Width (parallel to weirs) (mm)	488 (includes tray deck + joggle)	
	Integral beam and joggle (mm)	1880 x 100 and 1880 x 46	
Two curved edge integral beam units	Length (normal to weirs) (mm)	1925	
	Maximum width (mm)	472	
	Integral beam and joggle (mm)	1880 x 100 and 1880 x 46	
Three central integral beam units	Length (normal to weirs) (mm)	662.5 (includes tray deck + joggle)	
	Width (parallel to weirs) (mm)	500	
	Manway length and width (mm)	Length: 600 Width: 500	
Tray Perforations	Hole Diameter (mm)	6.35	6.35
	Total Number of Holes	13230	11228
	Tray Thickness (mm)	2.00	2.00
	Edge of Hole	Sharp	Sharp
	Pitch of Holes	Triangular	Triangular
	Hole Pitch (mm)	19.0	18.26
	Hole Line Spacing (mm)	16.45	15.82
Downcomer Dimensions and Tray Areas	UDF Plate Length (mm)	1475	1475
	UDF Plate Chord Length (mm)	230	225
	Inlet Downcomer Length (mm)	1545	1015
	Inlet Downcomer Width (mm)	1500	1500
	Inlet Gap Heights (mm)	10,20 and 50	10,20 and 50
	Outlet Weir Heights (mm)	0,10,20 and 50	0,10,20 and 50
	Downcomer Area (mm^2)	2.43×10^5	2.43×10^5
	Active Area (mm^2)	4.189×10^6	4.189×10^6
	Total Hole Area (mm^2)	4.19×10^5	4.19×10^5
	Fractional Free Area (%)	10.00	10.00
	Area of One Hole (mm^2)	31.67	31.67

Table 4.2 Summary of tray specifications including the downcomers.

From the 80% flooding curve, the maximum vapour load factor value is 0.12 ms^{-1}. When substituted into the capacity factor based on vapour load equation,

$$Cf = \frac{Q_V}{A_b}\sqrt{\frac{\rho_V}{\rho_L - \rho_V}} \qquad (4.1)$$

and given that A_b=4.189 m^2, ρ_L =1000 kg/m^3, and ρ_V =1.22 kg/m^3, the maximum air flowrate, $Q_{V(max)}$, was calculated to be 14.38 m^3/s.

The optimum water flow rate of 0.045 m^3/s, was based on the maximum weir load value, (Q_L/W), of 0.03 m^3/m s, and by using the relation,

$$Q_L = \left[\frac{Q_L}{W}\right]W \qquad (4.2)$$

where W = 1.50 m.

In addition to the maximum air flow rate to be delivered by the air fan, the total pressure head resistance specification against the direction of flow, (including for the situation where two trays are used in the column), was calculated to be 0.51 m (see Table 4.1). This was estimated by the summation of all the individual pressure resistances around the system, and expressed as the total wet tray pressure drop since this parameter was the main contributor to the pressure head resistance. Thus,

$$h_{WT} = h_{DT} + h_{cl} + h_R \qquad (4.3)$$

where: h_{DT} is the dry tray pressure drop which is the pressure resistance caused by the passage of air through the perforated tray.

h_{cl} is the height of clear liquid defined as the resistance on the tray caused by the froth height, expressed in terms of clear liquid.

h_R is the residual pressure resistance caused by the gas-liquid momentum transfer processes.

A complete description of how the system pressure drop was calculated, is given by Hine, (1990).

4.4.2 Measurement Specifications of the Instrumentation by Error Analysis

The objective of this task is to determine the accuracy of a given experimental quantity by examining the range of error permitted for each of the measured operating and system variables required to calculate the value of this quantity. If, on the one hand, a large error specification of the measured variables associated with the experimental quantity was permitted, this would seriously undermine the value of this quantity when used in results for publication. On the other hand, a very low error specification of the measured variables, such that the accuracy of the experimental quantity was very high, would prove counter productive owing to the high costs of purchasing the appropriate instrumentation.

Hence a compromise must be achieved in order to obtain a satisfactory balance between the two extreme situations. It is important to note, however, that for a given quantity, there will always be an associated error in the measured variables caused by either an insufficient calibration scale of the instrumentation, or a lack of confidence in the calculated quantity.

The objective, outlined above, was thus achieved by Hine (1990) in which an error analysis was carried out whereby the selected experimental quantity was Murphree tray efficiency. This is calculated from air enthalpy driving forces which are obtained from temperature measurements during the heat transfer experiments by water-cooling. The accuracy of the tray efficiency was determined by the error range permitted during the measurement of the operating and system variables such that suitable instrumentation could be incorporated into the test facility.

The analysis was based upon the "Principle of Superposition of Errors" in which the error associated with the calculated tray efficiency is caused by the cumulative effect of the errors for each of the operating variables, i.e., air and water mass flow rates, and the system variables, i.e., T_{in}, T_{out}, T_{db}, and T_{wb}.

The magnitude of the error range for tray efficiency, obtained by iterative calculation using a consecutive set of error values for each measured variable, was greatest for the system variables (i.e., air and water temperatures) and least for the operating variables (i.e., air and water flow rates). Thus from the error range of the calculated tray efficiency together with the known errors for each variable, which are summarised in Table 4.3, the following error specifications for the operating and system variables were selected:

Air Flow Rate	2.0%	Air Temperatures	0.5 °C
Liquid Flow Rate	0.5%	Water Temperatures	0.02 °C

These permitted specifications yielded a Murphree tray efficiency that was within an error range of 2.1%. This was deemed to be acceptable considering the scale of the apparatus being used. The above procedures are based on the condition that measurements were made at steady state. Thus variations in any of the measured system and operating variables with time, would have to be accounted for in the final error analyses.

Measured Variable	Error	Error	Error	Error
Air Flow Rate	4.0%	2.0%	1.0%	1.0%
Water Flow Rate	4.0%	2.0%	1.0%	0.5%
Inlet and Outlet Water Temperatures	0.1°C	0.05°C	0.02°C	0.02°C
Dry and Wet Bulb Temperatures of Inlet Air	1.0°C	1.0°C	0.5°C	0.5°C
Calculated Murphree Tray Efficiency - 0.867 or 86.7%	± 0.0573 or ± 6.6%	± 0.0328 or ± 3.8%	± 0.0161 or ± 1.9%	± 0.0142 or ± 1.6%

Table 4.3 Accuracy of Murphree tray efficiency with associated errors of the measured variables.

With the minimum error specification for each variable established, and the maximum air and water flowrates known, a description of the flow measurement instruments used is presented below.

4.4.3 Measurement of Air Flow Rates

The air flow meter is directly linked to a high and low pressure tapping on the rectangular section of ducting at the air inlet to the simulator column. The device measures the differential pressure produced from an integrated network of fifteen impact and static pitot pressure sensors located in the ducting. According to the Bernoulli principle, a differential pressure, proportional to flow, is generated across the uniformily distributed network of pressure sensors, spread over the whole cross section of ducting. Each pressure sensor is of equal area, and are contained within an integrated network, in order to obtain an average differential pressure. The use of shrouds around the pressure sensors and an array of honeycomb flow straighteners upstream from the pitot sensors, serve to minimise the effects of air flow non-uniformities. The pressure sensors, required

for the full air flow operating range, was designed and purchased from Tekflo Limited, who supplied the flow grid sensors and a calibration certificate to meet the desired flow rate specifications. The differential pressure range of 3.19 up to 57.92 mm of manometric fluid is measured using a mechanical micromanometer (purchased from Perflow Instruments) with an accuracy of $\pm$ 0.005 mm of manometric fluid. The differential pressure range corresponds to superficial air (empty column) velocities of between 0.70 and 3.00 ms^{-1}.

4.4.4 Measurement of Water Flow Rates

Since a wide range of water flow rates are used in the experiments, two flow meters were incorporated into the water flow circuit. An orifice plate rotameter is used for low water loadings, of upto 0.009 m^3/s (32.4 m^3/h), and is controlled using a mechanical gate valve. The error specification for this device was approximately 2.0%. For high water loadings, in the range 0.009 - 0.090m^3/s (32.4 - 324 m^3/h), an electromagnetic flow meter, supplied from Combustion Engineering together with a calibration certifcate to meet the required water flow rate specifcation and with an accuracy of less than 0.5 %, is used. This 10 cm unit contains no moving parts, thus creating no disturbance to the liquid flow. The flow meter is a compact, volumetric liquid flow rate device in which a transducing method is employed, such that the conduction properties of the liquid are used to produce an induced voltage on passing through a magnetic field. The amplitude of the generated voltage is directly proportional to the average flow velocity of the liquid. The output of the water flow rates was calibrated in milliamps, and for a given flow rate, the corresponding current output is shown on a digital display unit located above the electromagnetic flow meter.

4.4.5 Measurement of Temperature

Humidity Detector

In order to measure the moisture content of the air inlet to the tray column, a hygrometer, incorporating a moisture sensitive silicon chip detector is used. The precalibrated hygrometer (manufactured by Moisture Control and Measurement Ltd.) operates on the principle where a change in the water vapour pressure of the atmosphere surrounding the silicon chip detector, results in a variation of the number of water molecules suspended in the pores of the detector. This change is converted into an analogue signal which is translated into the wet bulb temperature of the air sample by means of a supplied calibration chart by the manufacturers. A flow rate of 0.5 lit/min of air is required to

operate the hygrometer accurately and the error specification of the wet bulb temperature values generated is 0.5°C.

Temperature Probes

To obtain accurate water temperature measurements on the test tray, platinum resistance thermometers interfaced with a data logger device are employed. A full description of the technique used to measure water temperature are detailed in Chapter 5.

4.5 Modification of the Air Distribution System

4.5.1 Air Riser (Chimney) Distributor

As will be shown in Chapter 6, the gas flow, from the original air (chimney) distributor plate, has a significant effect on changing the liquid flow pattern. The distributor plate consists of a 2.0 m diameter grey PVC circular base which consists of 130 riser tubes arranged in a radial format. An overhead schematic diagram of the chimney distributor plate is presented in Figure 4.5. A side view of the chimney distributor plate including the dimensions is presented in Figure 4.6 while a photograph of the chimney tray is shown in Figure 4.7.

One advantage of the chimney distributor plate was that any weeped liquid from the test tray was collected on the PVC base and discharged from the simulator column using four drainage pipes inserted onto the base plate. (The brass tappings of each drainage pipe were attached to the distributor base such that they were flushed level with the plate surface.) In addition, a perimeter wall, of height 38 mm around the distributor plate prevented any weeped liquid from escaping onto the annulus section (see Figure 4.6).

However, as will be shown later, a non-uniform gas flow pattern was found in the middle of the tray column shell between the distributor plate and the test tray, with very little gas flow at the sides near the column wall.

4.5.2 Modifications and Improvements to the Gas Distribution.

To solve the problem of the non-uniform flow of gas in the inter-tray region, a gas distributor needed to be designed in order to provide a greater flow of air above the annulus near the column wall. One method would be to install a 2.44 m diameter packed bed of Pall Rings, similar to the liquid distribution system.

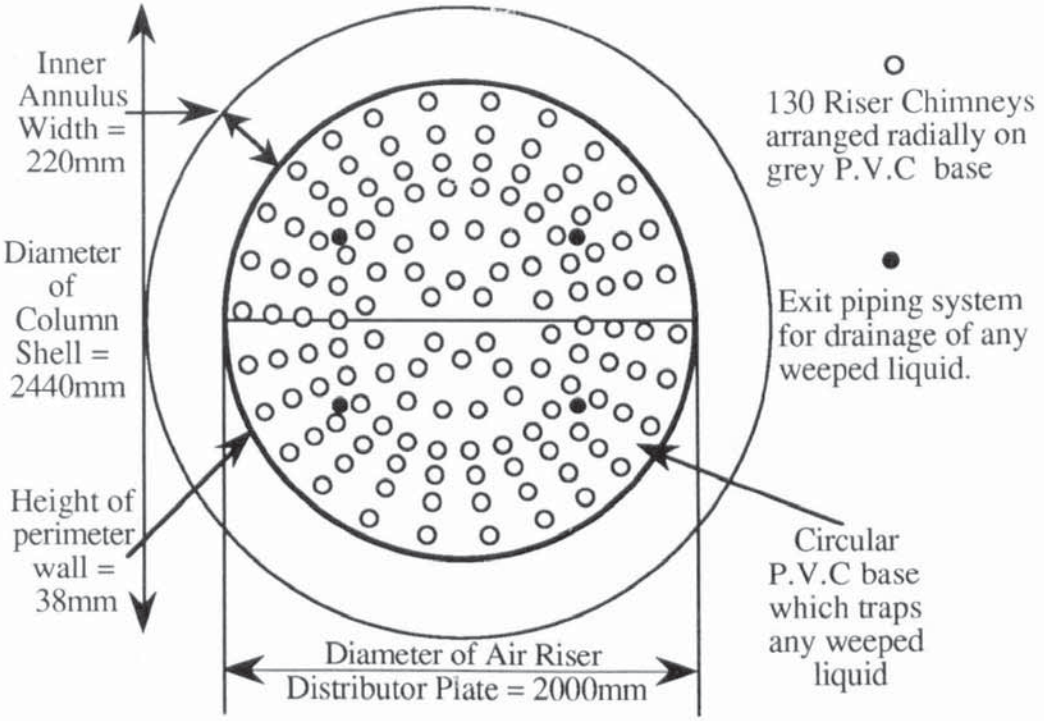

Figure 4.5 An overhead view of the air riser (chimney) distributor.

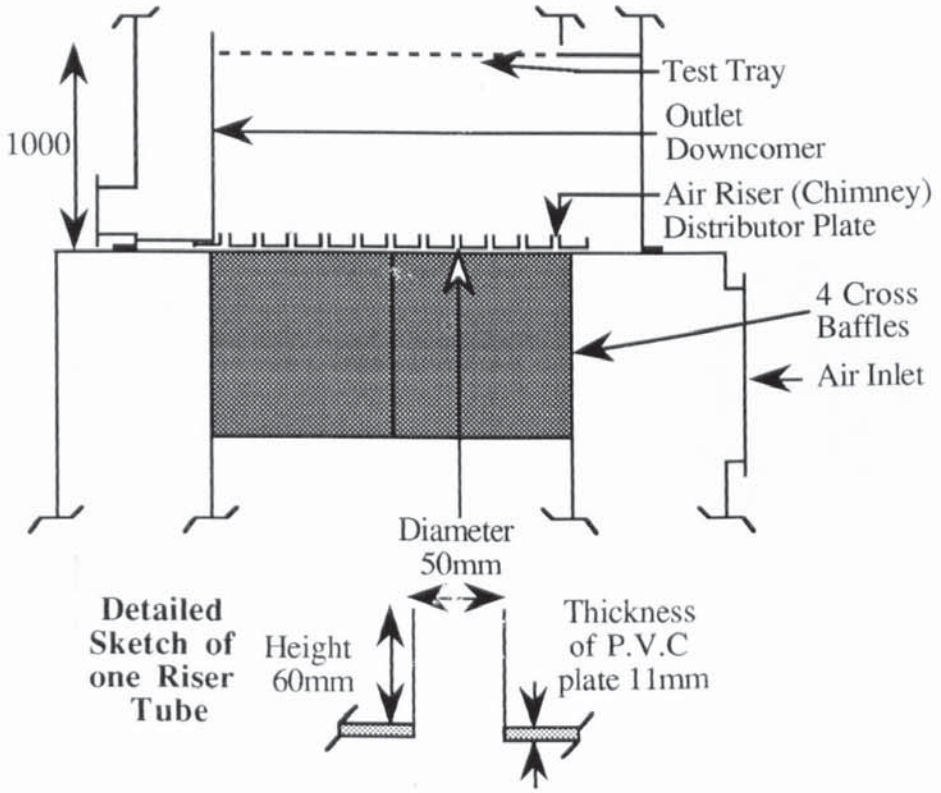

Figure 4.6 Schematic diagram of original distributor configuration in the column.

Figure 4.7 Photograph, from a side view, of the air riser (chimney) distributor plate.

This, however, could have led to a number of difficulties. For example, a large diameter shallow packed bed would be incapable of separating any weeped liquid from the rising air stream, thus changing its properties; increase the pressure drop across the gas distribution shell; prove difficult to install in such a short inter tray spacing; and the packings themselves may produce a greater non-uniform flow of gas (see Ali, 1984).

From the work of Enjugu (1986) and Ani (1988), the gas distribution system, in the 1.22 m diameter simulator column, consisted of a 1.0 m packed bed, to remove gas swirling from an inlet tangential air feed, and two perforated trays to produce a more uniform flow of gas. When a tangential air inlet feed was used in the same apparatus, Porter and Lan (1991) showed that a small hole high free area perforated tray can minimise the effect of gas driven liquid circulation on a test tray placed directly above. That is, when the tangential air flow was forced through two 1.80 mm hole perforated trays without downcomers and at a tray spacing of 600 mm, no gas or liquid rotations were observed on the top tray.

However it was difficult to design a distributor such that the effect of the gas flow on the liquid flow, on a 2.44 m diameter test tray, was shown to be negligible. Thus the following approach was pursued in order to determine whether a particular distributor design was successful in producing a negligble gas flow effect on the liquid flow pattern. For a particular distributor, the gas distribution was tested by blowing air through a non-crossflow pool of liquid, fixed by using a large outlet weir on the test tray, and observing whether any gas influenced liquid flow patterns were produced, i.e., circulating liquid. This technique was repeated for each modification of the gas distributor until the effect of the gas flow on changing the liquid flow was shown to be negligible. The most successful gas distributor was a 10 % free area 1.80 mm hole diameter perforated tray, of diameter 2.44 m. Hence, this small hole perforated plate was installed on a 50 X 50 X 6 mm aluminium support ring (see Figure 4.4). The simple shape of the perforated plate, and its relative cheapness, made this the quickest and most feasible option.

The support ring was bolted to the column wall 150 mm above the annulus and the four large cross baffles so as to allow the air to flow above the annulus region. Since the material of the perforated plate was aluminium and of a very small thickness, the plate sections were divided into four quadrants and mounted onto eight aluminium T - section radial support beams. The dimensions of the support beam framework were the same as those for the tray support ring. The tray was firmly secured to the support beam framework using stainless steel self tapping pins. A thin aluminium sheet was used to

cover the area of the perforated tray directly beneath the under down flow plate of the inlet downcomer to the test tray.

Thus the active tray area of the perforated gas distributor was identical to the bubbling area of the test tray. By using small diameter perforations, it was assumed that the rising air stream through the distributor plate would attain a more vertical velocity component compared to that of a larger hole tray. This is dealt with in more detail in Chapter 7.

4.6 Modification of the Equipment for Experiments on Two Trays

Once it had been established that the horizontal gas flow, beneath a single test tray, can sometimes have a significant effect on the liquid flow pattern, it was decided to investigate whether gas flow patterns emerging from the flowing liquid on the single tray had a significant effect on changing the liquid flow pattern on a second tray placed directly above. Hence the test facility was modified to support two countercurrent sieve trays such that one was placed directly above the other. The objective was to study whether the gas flow pattern between the two perforated trays had a significant effect on changing the liquid flow pattern on the top tray, beginning with a tray spacing of 300 mm. With the exception of cryogenic distillation, in which a tray spacing of approximately 150 mm is used, this is the lowest tray spacing used in practical distillation. Further details of the two tray experiments are discussed in Chapter 10.

The revamp of the simulator included the modification of the water circuit; the installation of a new false inlet downcomer apron and support ring; the insertion of two new observation windows, in the spacing between trays; and the manufacture and installation of a new 6.35 mm hole sieve tray. A concise description of each modification is presented in the following subsections.

The two tray simulator column is presented in a schematic diagram in Figure 4.8 and shown in a photograph in Figure 4.9.

The photograph shows the bottom air distribution shell and tangential air inlet duct; the middle tray column shell, incorporating the two test trays and downcomers; the air exhaust ducting system; and two support platforms to permit easy access to manway windows located on the column wall, both above and below the test trays. In addition, two sets of clear PVC tubing can be seen which connect the pressure tappings, located at

various positions on the two trays, to the appropiate manometers mounted on wooden support boards outside the simulator.

4.6.1 Modification of the Liquid Distribution System

To maintain the present liquid discharge system, in which water is removed from the outlet downcomer to the water sump tanks, it was decided to install the new water inlet pipe and downcomer apron directly opposite the existing set-up. Hence, the grey PVC pipe network above the water flow meters was extended, and the flanged section attached to the new PVC water inlet using six heavy duty mild steel bolts. The water inlet unit itself was plastic welded onto a large PVC gasket which was bolted to the column wall. Rubber gaskets were incorporated into the water inlet pipe system in order to prevent any water leakages.

A flexible approach in the design of the new water circuit was adopted by incorporating a T-piece and butterfly valve system such that the simulator could revert back to a one test tray column when required.

Water is fed to the new inlet downcomer using the successful technique of a sparge pipe and a 0.50 m packed bed of 25 mm Pall Rings. The packed bed is supported at a clearance height of 350 mm above the under down flow plate using an arc section of 10% free area perforated plate. A new outlet downcomer apron to the top tray, associated with an appropriate moveable face plate system, to change the inlet gap height, was bolted onto two modified bolting bars welded to the column wall.

4.6.2 Modification of the Tray Column Shell

To permit the observation of liquid flow patterns on the bottom test tray, two new clear styrene windows were installed onto the column wall. The first was incorporated at the side of the column wall in between the two existing larger windows, while the second window was incorporated into the column wall immediately above the outlet downcomer to the bottom tray. This permitted either the direct-observation of liquid flow over the outlet weir, or the mounting of an external floodlight on a support bracket so as to illuminate the intertray region and biphase flow across the bottom tray.

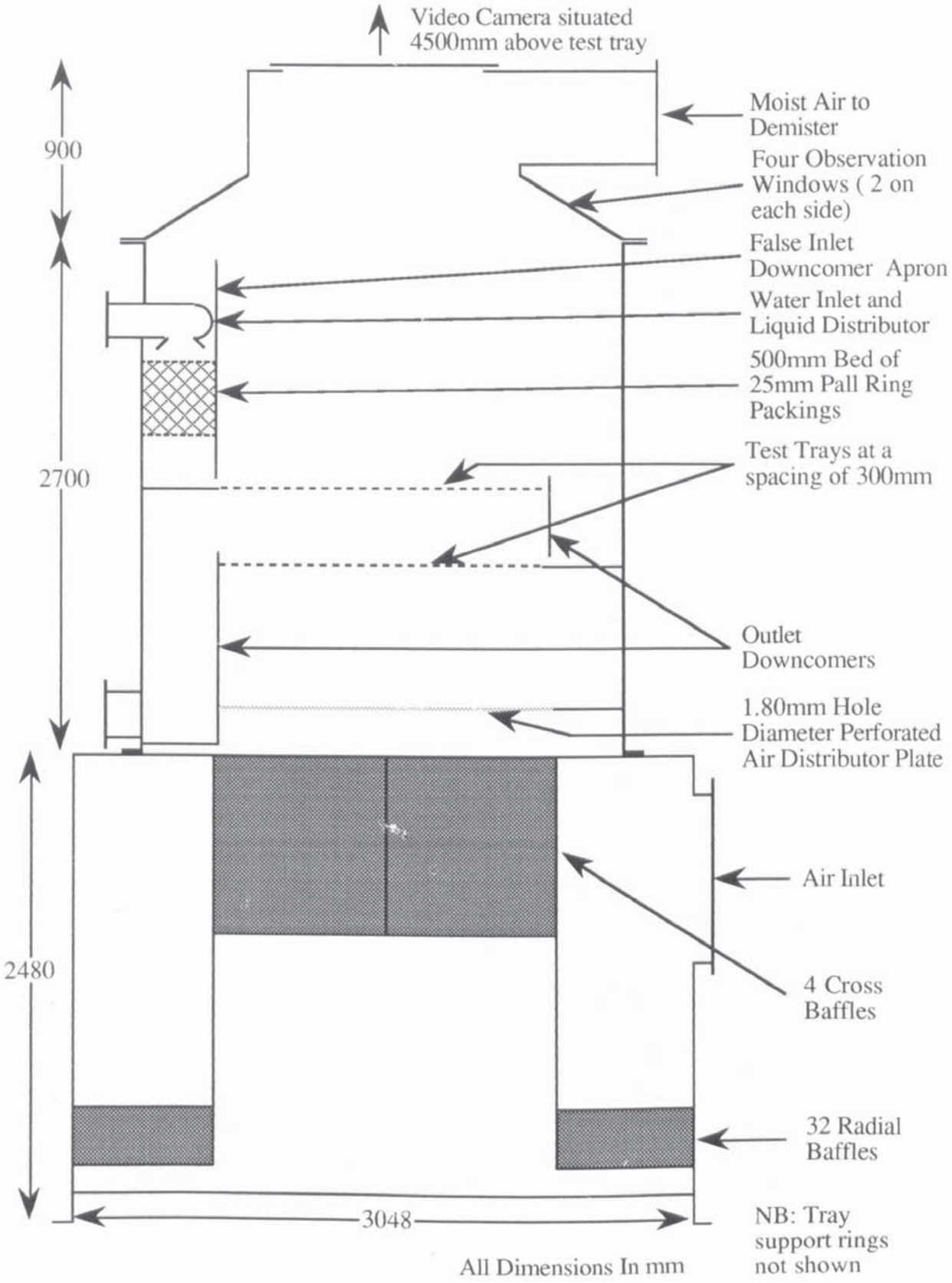

Figure 4.8 Schematic diagram of the revamped two tray air - water simulator.

Figure 4.9 Photograph of the revamped two tray air-water simulator.

The manway window above the two test trays was modified by incorporating a clear flexible styrene window such that it is flushed level with the curvature of the column wall. This was achieved by bolting aluminium strip sections internally onto the column wall, such that there was sufficient overlap of the metal strips into the window space for the styrene sheet to be bolted on. The reason for incorporating a new manway window onto the column wall, was that the air flow above the froth on the new top tray, and the liquid flow itself, would have been non-symmetrical. This may be caused by the open space formed by the manway window which extends outwards from the column wall.

In between the two test trays, provision was made for inserting thirty two lengths of clear PVC tubing into the column, in order to link the pressure tappings, spread across the new test tray, with manometers mounted onto a wooden platform. (Further details of using manometers to measure the clear liquid height, can be found in Chapter 5).

Hence the manometer tubing was distributed radially at equally spaced drilled holes around the circumference of the tray column shell, with all tubes being collected at one point, and connected to the appropriate manometers. This approach was adopted in order to minimise the amount of obstruction, caused by the experimental hardware, to the biphase flow on the bottom tray and to the air flow passing through to the top tray.

4.6.2 Installation of Two Test Trays

The two tray test system consists of aluminium perforated sheets installed on the present lattice beam support work to form the bottom tray, and a second test tray placed on a support framework situated 300 mm above the aluminium tray. To install the second test tray, two options were considered. The first was to install a lattice beam framework and alumnium tray, identical to that of the single test tray. The second was to install a variable support ring mechanism, such that any desired tray spacing, of up to 600 mm, could be set onto which a sieve tray, typical of that used in practice would be placed.

Most of the sieve trays found in practical distillation are integral beam trays. These consist of perforated horizontal sheets with indented narrow sections of metal strip, known as joggles, that run perpendicular to the tray downcomers. At the edge of the joggle section is a vertical metal plane which forms the integral beam part of the tray. The purpose of the joggle units, which incorporate regularly spaced welded steel pins, is to support the next perforated tray such that it is flushed level with the preceding tray. One advantage of the integral beam tray is that it is self supporting such that each tray is supported on the joggle and integral beam system. The material type used to fabricate

these trays is usually stainless steel. A schematic diagram of this type of tray is presented in Figure 4.10.

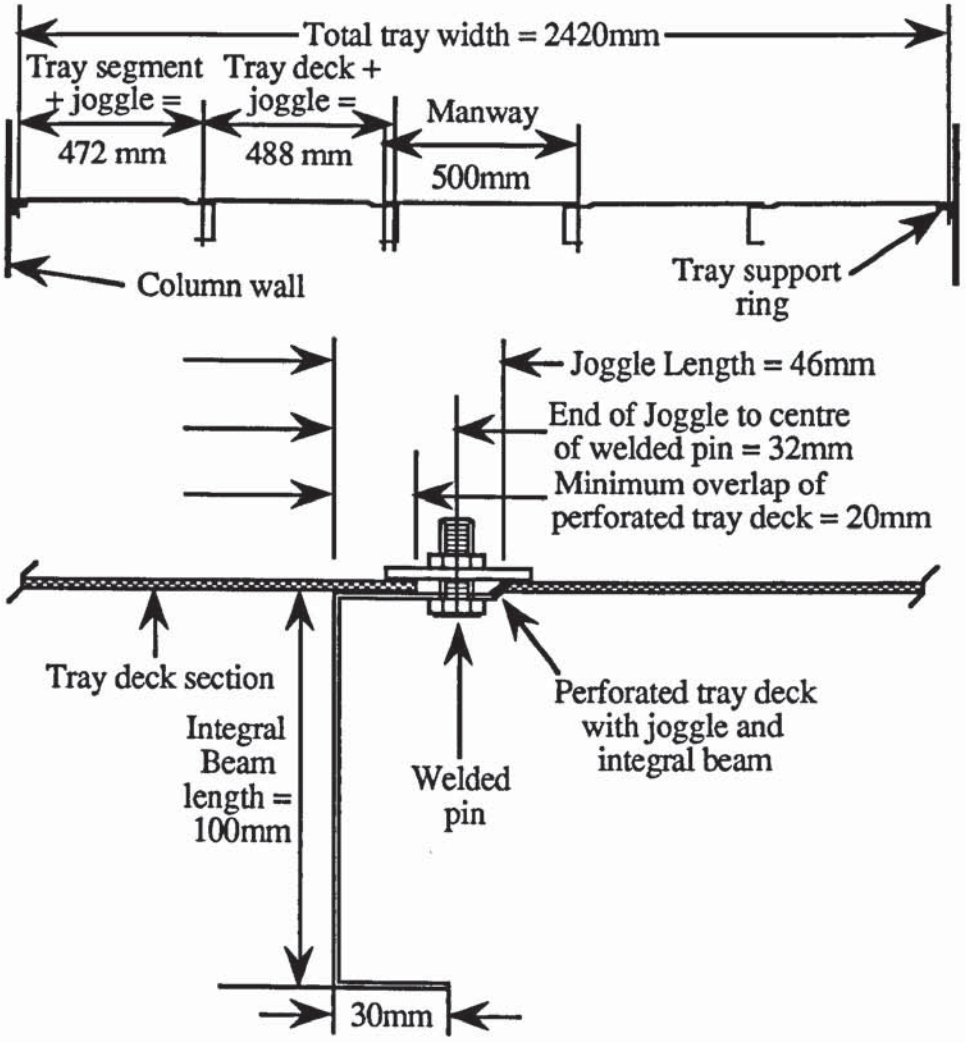

Figure 4.10 Horizontal view of the integral beam sieve tray installed in the simulator associated with a detailed sketch of the integral beam structure.

Hence, it was decided to carry out the second option since the design and manufacture of the integral beam sieve tray could run concurrently with the installation of the tray support ring. The specifications for the manufacture of the integral beam tray, such as tray diameter, hole diameter, hole pitch, percent free area and material type for fabrication, were forwarded to the tray manufacturers Distillation Technology International Limited. The support ring was to be supported on a system of steel rods and set at a distance of 300 mm above the bottom tray using spacers.

The installation of the support ring was as follows. An angled aluminium ring, similar to

that used in the installation of the perforated gas distributor tray, was fitted inside the tray column shell using eight equally spaced, partially threaded, stainless steel rods, of diameter 12.7 mm. Each rod was placed into position by bolting the appropriate threaded sections onto the two existing tray support rings set apart at a distance of 600 mm.

The stainless steel spacers, of diameter 25 mm, were cut into equal lengths and inserted onto the rods above and below the new support ring. By means of a large spirit level, mounted onto a cross section of metal beam, of length 2.4 m, the support ring was set level at a height of 300 mm above the bottom tray. This was achieved by raising or lowering each spacer below the ring by means of adjusting the nut and washer system, on the threaded rods, with a spanner. Once set at the desired height, the tray support ring was secured by lowering the upper spacers, using the same method for setting the ring at the correct height.

Since there were no tray support rings welded in the region for the new siting of the inlet downcomer and under downflow plate, the support ring was bolted onto the column wall using stainless steel long set pins.

The integral beam sieve tray was fabricated from 304 stainless steel and consisted of two tray deck segments, for the sides near the column wall; five tray deck sections, including the manway, installed in the horizontal plane between the inlet and outlet downcomers; and the under downflow plate. In addition, three outlet weir strips, of height 10, 20, and 50 mm, including the appropriate seal plates, as well as the tray edge clamps and manway beam clamps, were also supplied. A mock set up of the integral beam tray on the support ring, prior to installation in the column, is presented as a photograph in Figure 4.11. Figure 4.12 shows a more detailed photograph of a tray deck with joggle and integral beam system. As can be seen from the above photographs, the inclusion of a manway at the centre of the tray, permitted easy access to the bottom tray in order to change the inlet gap / outlet weir configurations when required.

Once the integral beam tray was installed onto the tray support ring, using tray edge clamps, the revamp of the column to a two tray test facility was complete. Preliminary testing of the air and water circuits on the two trays showed no leakages. Thus the new two tray configuration was ready for experimental investigations by adopting the research programme used for the single tray.

Details of experimental methods and the processing of results are contained in the next chapter.

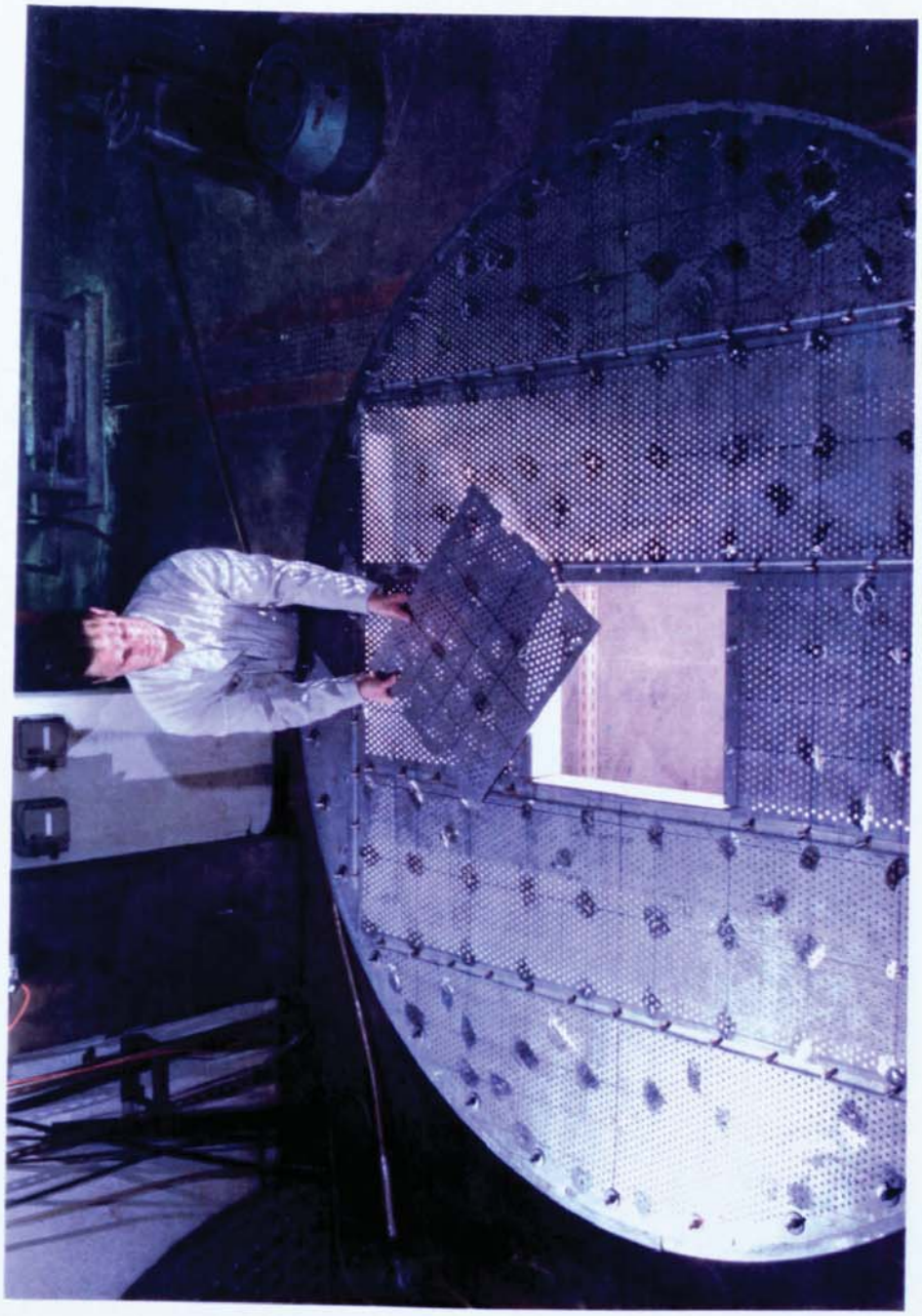

Figure 4.11 Overhead photograph of the 2.44m diameter integral beam sieve tray.

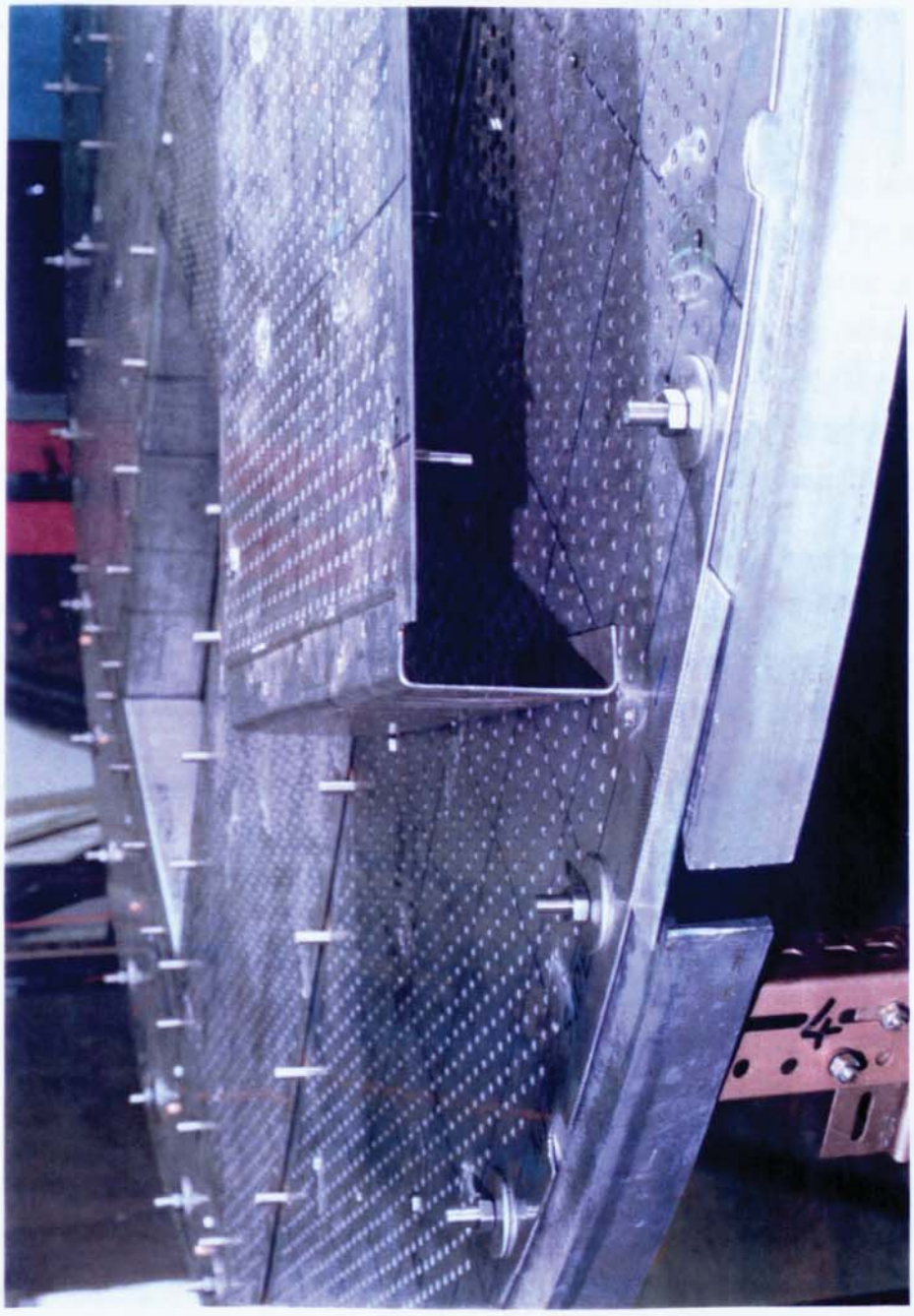

Figure 4.12 Photograph of a perforated tray section containing a joggle and integral beam.

CHAPTER 5

EXPERIMENTAL METHODS AND PROCESSING OF RESULTS

5.1 Introduction

The 2.44 m diameter air-water distillation simulator is a unique and flexible test facility for the investigation of two phase flow patterns on commercial scale trays. The apparatus incorporates three sensitive experimental techniques designed to give a greater understanding of flow pattern behaviour when air is forced through water flowing across the test tray. The techniques include direct-observation experiments using flow pointers, the study of biphase flow pattern effects on mass transfer by the cooling of hot water flowing over the tray, and the effect of liquid head variation on the biphase flow pattern.

In this chapter each experimental technique is described in detail, followed by a summary on how to interpret the flow pattern results. It is these results that will provide a major contribution in the development of the new theory on open channel two phase flow as well as providing guidance in the scientific approach required for tray design.

This section is concluded with a summary on the safe operation of the test facility.

5.2 Direct-Observation Experiments

In order to obtain the direction of flow at many positions on the tray in a particular flow regime, a simple and cost effective method of using directional flow pointers (Hine, 1990) was developed. The main advantage of flow pointers over the monitoring of a coloured dye in a flow of aerated liquid is that a dye suffers from localised mixing within the biphase dispersion over most of the tray area. This would cause difficulties in accurately recording the movement of dye within the two phase flow pattern. A description of a directional flow pointer is presented in the next section.

5.2.1 Directional Flow Pointer

Directional flow pointers are light weight aluminium devices with a painted arrow indicator. To obtain information on the biphase flow, flow pointers are partially

submerged in the froth or spray and behave in a similar manner to that of weather vanes used to show the direction of the wind.

A flow pointer, presented in Figure 5.1, consists of a thin aluminium sheet, with a double winged arrow indicator, loosely hinged on a vertical rod. It is supported above the tray deck with a spacer so it can rotate freely and become aligned with the direction of flow. Flow pointers are observed visually from above by noting the position of the arrow indicators since each indicator represents the local biphase flow pattern within the immediate vicinity of the flow pointer. The direction of biphase flow is recorded when the flow pointer reaches steady state with the surrounding froth. The flow pointers are highly sensitive to any changes in the local biphase flow as a result of the narrow width between the support rod and the edge of the aluminium sheet.

The original flow pointer design contained a half painted arrow indicator by bending the top part of the aluminium sheet into a horizontal right-angled triangle. A disadvantage of this design is that the gas, on leaving the froth on the single arrow side of the flow pointer, encounters some resistance by the underside of the indicator. On the non-arrow indicator side, the gas, on leaving the froth, bypasses the flow pointer and causes preferential rotation of the flow pointer which may not be representative of the surrounding local biphase flow. Thus to cancel out this effect, a double arrow indicator was incorporated into the design; the overall mass of the device being maintained at a light weight so it can freely align itself with the direction of flow.

Since the wide range of operating conditions on the 6.35 mm hole tray will produce different flow regimes, two sets of flow pointers were developed (see Figure 5.1) to permit easier visual observation. The tall flow pointers are to be used in the mixed and spray regimes (large dispersion heights) while the short flow pointers are to be used in the emulsion flow regime (low dispersion height).

Flow pattern information over the whole bubbling area of the tray is achieved using thirty four flow pointers strategically placed on the tray deck. The location of flow pointers, shown in Figure 5.2, provides an even coverage on the horizontal plane between the downcomers aswell as in the segmental regions at the sides of the tray. A photograph of the flow pointer design and arrangement on the test tray is presented in Figure 5.3.

Flow patterns are monitored using an overhead video camera and by visual observation. The camera, supported 4.5 m above the test tray, permits flow patterns to be recorded, together with the flow rates and tray configuration, or displayed on a monitor at ground

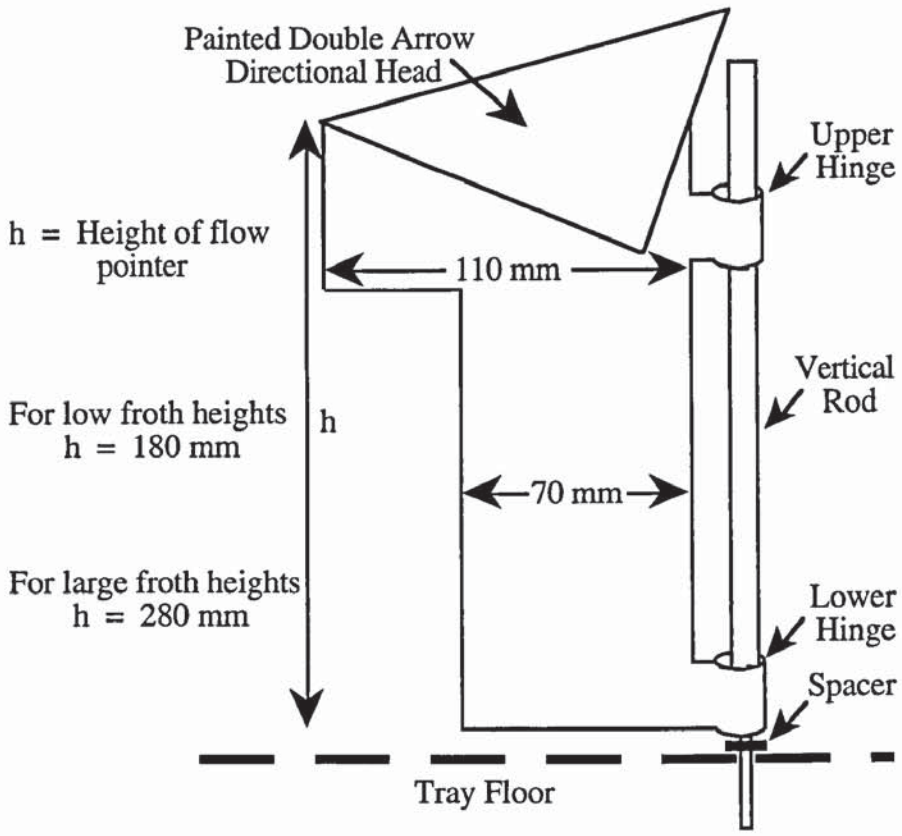

Figure 5.1 Schematic diagram of a directional flow pointer.

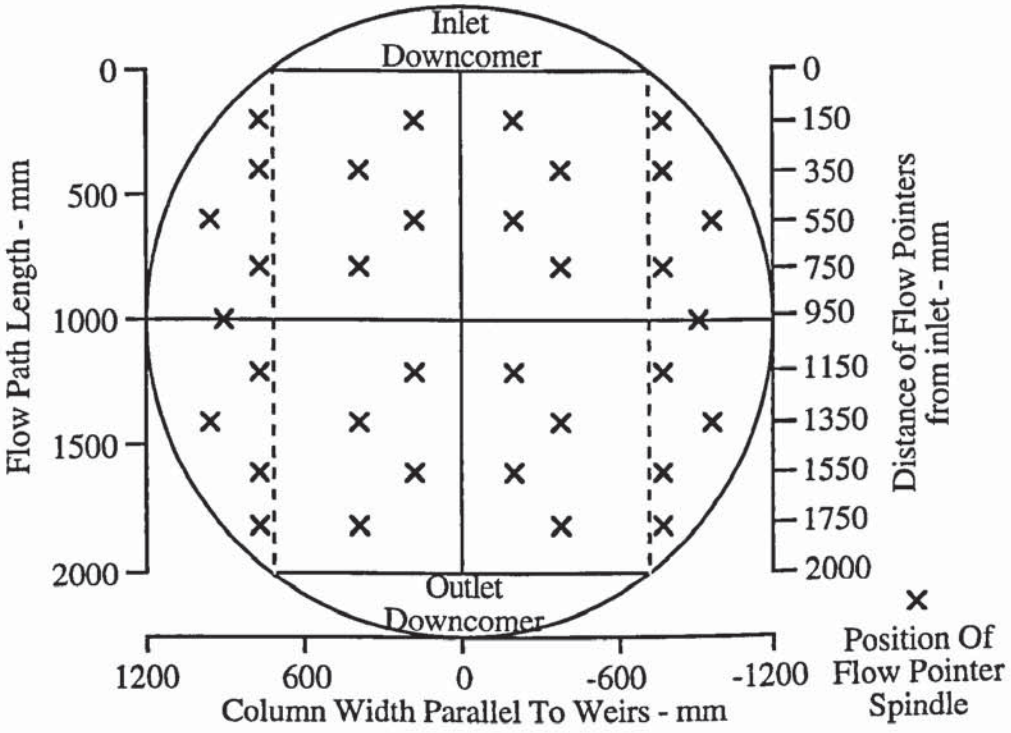

Figure 5.2 Arrangement of the directional flow pointers on the perforated test tray.

level. In addition, records of the biphase flow behaviour are made by visual observation through four large windows located on the reducing section between the exhaust ducting system and the top of the column shell. Visual records provide good backup to the video recordings since the focusing of the camera lens on the biphase flow can, in certain cases, be obscured by the large volume of tiny water droplets above the test tray.

Flow pointers reveal the direction of flow only and not the velocity of biphase flow. Nevertheless they provide reliable information about the flow patterns and, in particular, permit the observation of biphase circulation revealed by a number of rotating flow pointers on the tray segments and/or flow pointers pointing backwards towards the inlet downcomer.

In general, the direction of flow from the inlet downcomer towards the outlet downcomer is described as "**forward flow**". Flow in the opposite direction is described as "**reverse**" flow which under certain conditons may result from circulation of the liquid.

5.2.2 Interpretation of Flow Pattern Results by Direct-Observation

Three different flow patterns have been identified during experimental investigations on biphase flow patterns produced on large and small hole diameter sieve trays. These are illustrated in Figures 5.4a, 5.4b and 5.4c. Figure 5.4a shows a uniform flow pattern with forward flow produced at all points on the tray. Figure 5.4b shows a circulating flow pattern close to the tray inlet whilst Figure 5.4c reveals a circulating flow pattern close to the tray outlet.

Since a large number of direct-observation experiments are to be carried out, the biphase flow patterns produced can be identified as follows:-

Forward Flow	designation	FF	
Inlet Circulation	designation	L	and expressed as %
Outlet Circulation	designation	G	and expressed as %

Thus biphase flow pattern results can be summarised on two types of tray loading diagram. For the simple gas-liquid contacting experiments, a plot of percent of tray area occupied by circulating flow against weir load will be used. While in the experiments to simulate distillation at different operating pressures, flow pattern results will be summarised on a load factor verses weir load jet flood diagram similar to that of Figure 2.1 in Chapter 2.

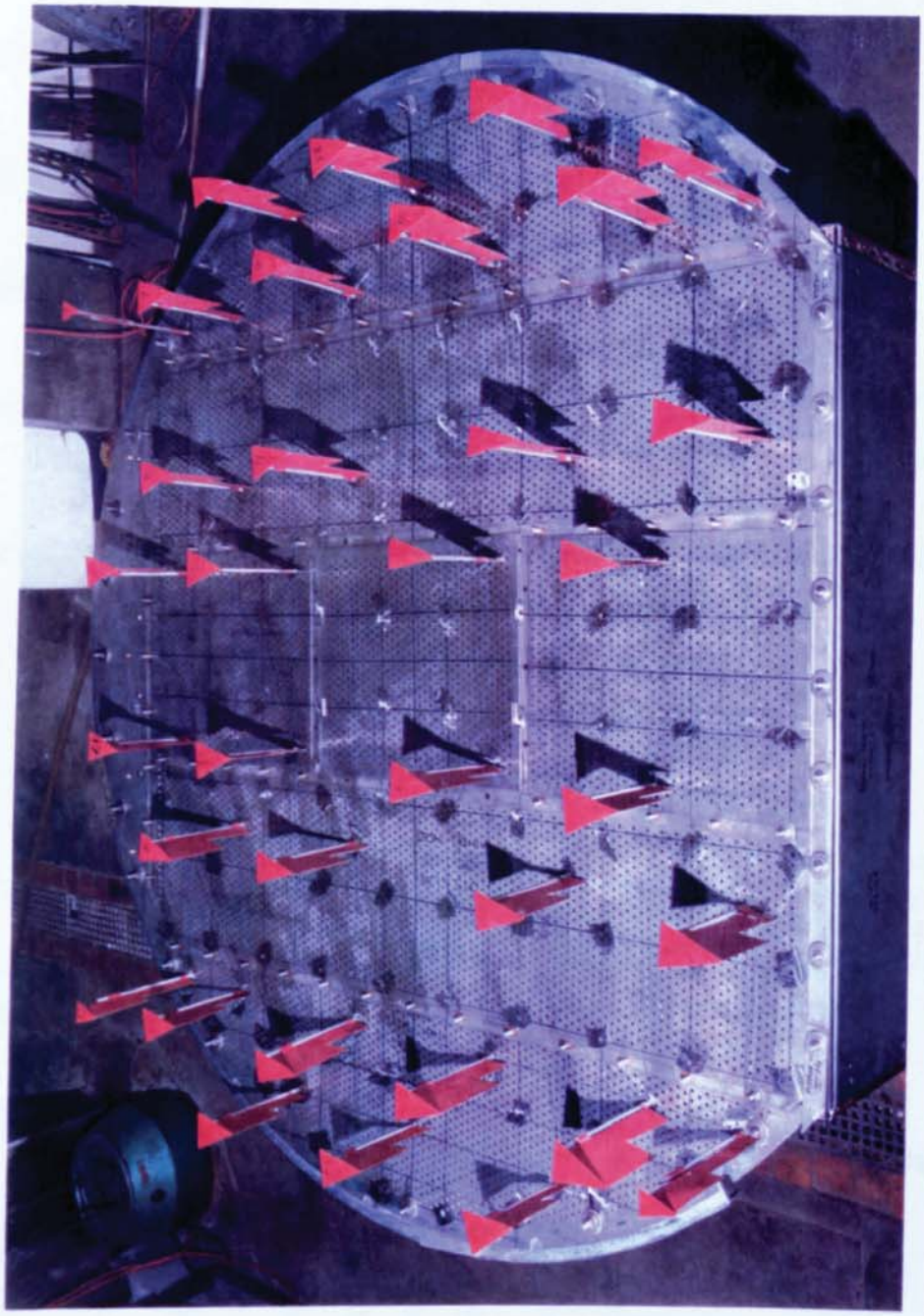

Figure 5.3 Photograph of the directional flow pointers spread over the test tray.

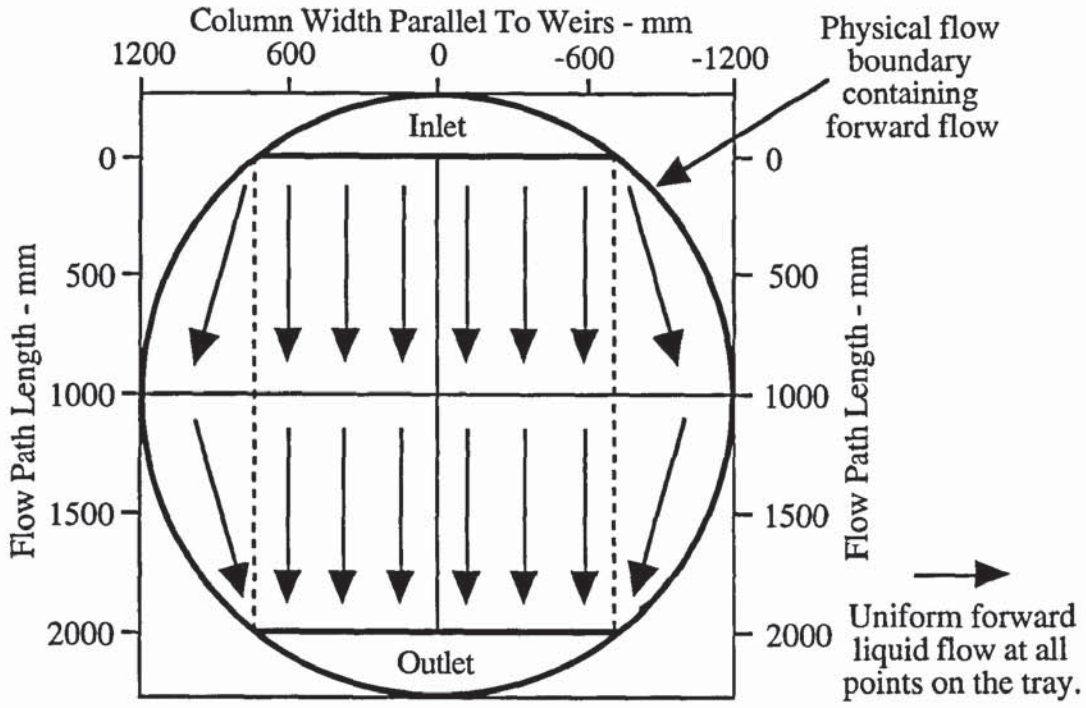

Figure 5.4a Direct-observation of the liquid flow pattern using flow pointers indicating uniform forward flow across the tray.

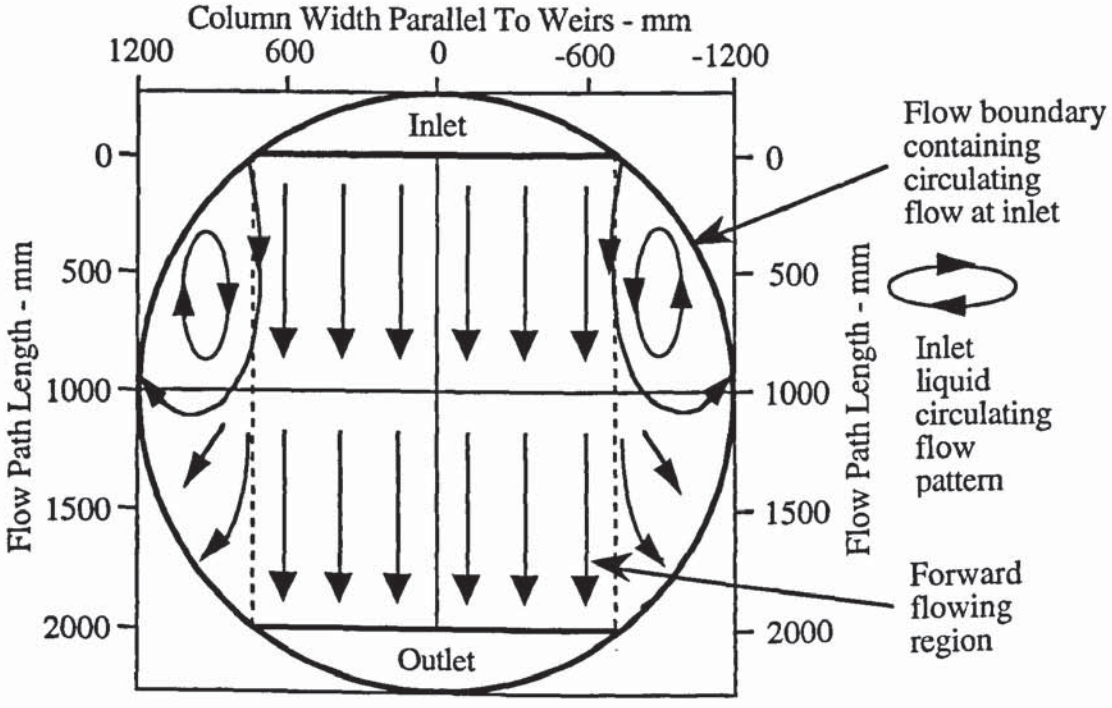

Figure 5.4b Direct-observation of the liquid flow pattern using flow pointers indicating inlet liquid circulation.

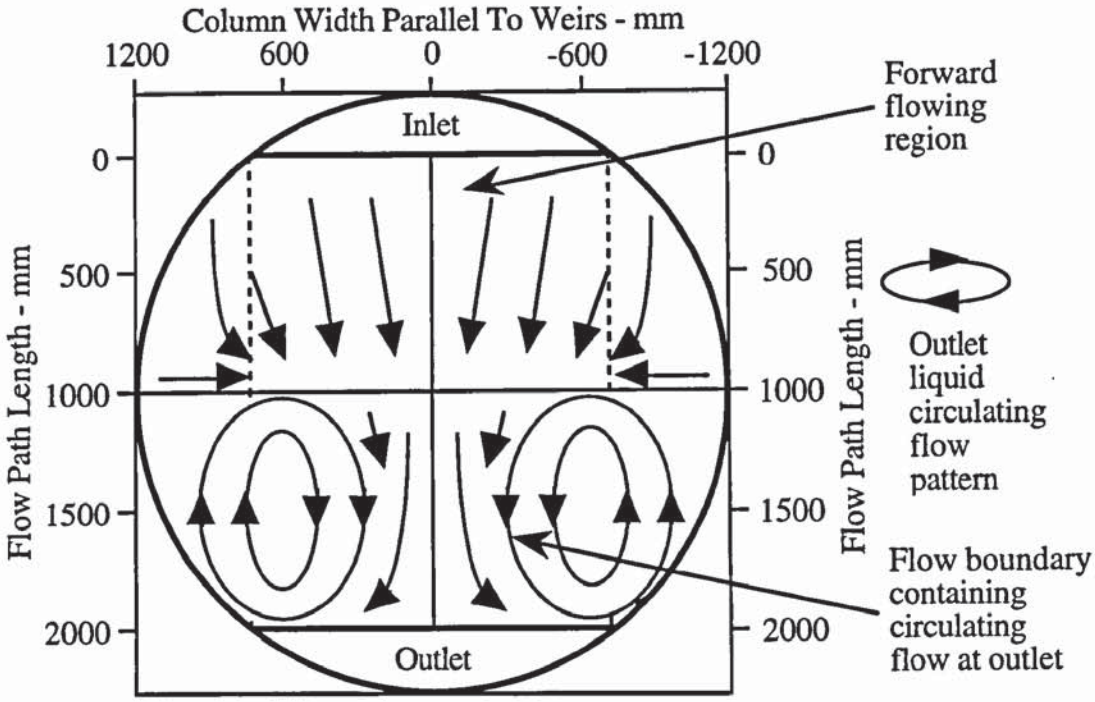

Figure 5.4c Direct-observation of the liquid flow pattern using flow pointers indicating outlet liquid circulation.

5.3 Heat Transfer Experiments by Water-Cooling

It was noted in Chapter 2 that heat transfer experiments by water-cooling involves the cooling of hot water flowing across a sieve tray by the air flow simulating the vapour. An analogy exists between mass transfer and heat transfer in which concentration profiles found in practical distillation are related to temperature profiles constructed by measurements made on a grid pattern across the tray. Temperature profiles can be interpreted in terms of enthalpy driving forces to calculate thermal point and tray efficiencies.

Before discussing the water-cooling experiment, it is necessary to review the water-cooling theory and use of the analogy between heat and mass transfer since this is the main criteria used to simulate distillation. Note that the meaning of all notation used in the development of equations in the following sections are listed at the end of the thesis.

5.3.1 Water-Cooling Theory

The theory of water-cooling considers both heat and mass transfer from the water surface when contacted with a rising stream of air. It is a well established theory used to design

cooling towers and this review seeks to relate water temperature and air enthalpy with liquid and vapour concentrations in distillation.

Use of Total Heat Theory to Explain Water-Cooling

The total heat theory (Merkel, 1925) states that evaporative cooling of hot water by cold unsaturated air results in the removal of heat from the water. Heat losses are primarily incurred by latent heat whilst a small quantity is removed as sensible heat. The loss of latent heat by water evaporation is caused by the combined transfer effects of both the water vapour and sensible heat to the rising air stream, thus inducing a cooling effect. Both the latent heat and sensible heat processes can be summarised mathematically in the general form of:

$$\begin{bmatrix}\text{Heat Transfer}\\ \text{Rate}\end{bmatrix} = \begin{bmatrix}\text{Transfer}\\ \text{Coefficient}\end{bmatrix} \times \begin{bmatrix}\text{Transfer}\\ \text{Area}\end{bmatrix} \times \begin{bmatrix}\text{Mean}\\ \text{Driving Force}\end{bmatrix} \qquad (5.1)$$

Thus to explain evaporative cooling the mean driving force for both heat transfer mechanisms is expressed as a difference of the function known as the total heat or enthalpy of the air. The definition of enthalpy for moist air includes:-

a) The sensible heat of dry air

b) The total heat associated with the water vapour which in turn consists of:

   i) The sensible heat required to change the temperature of an appropriate amount of water to that of the wet bulb temperature of the air.

   ii) The latent heat required to vapourise the water, and

   iii) The sensible heat required to change the water vapour temperature of the wet bulb to that of the air.

Clearly, the rate at which water is being cooled must equal the rate at which air is being heated. A complete mathematical derivation of the water-cooling theory is highly complex and is detailed elsewhere, (e.g., "Unit Operations of Chemical Engineering", McCabe and Smith, 1956). A description of the water-cooling process is outlined below.

The driving forces for the water-cooling process occur in a thin air film layer, which is in contact and in equilibrium with the water phase, as well as in the main bulk of the air stream. In this film layer, the temperature of the saturated air is the same as that for the water phase, and has an enthalpy H_w. The unsaturated bulk air stream has an enthalpy

H_g which is less than H_w. Thus for a given water temperature, the enthalpy driving force is $(H_w - H_g)$ which is equal to ΔH_m. Enthalpy driving forces can be determined from a driving force diagram, presented in Figure 5.5, which is a plot of air enthalpy against water temperature.

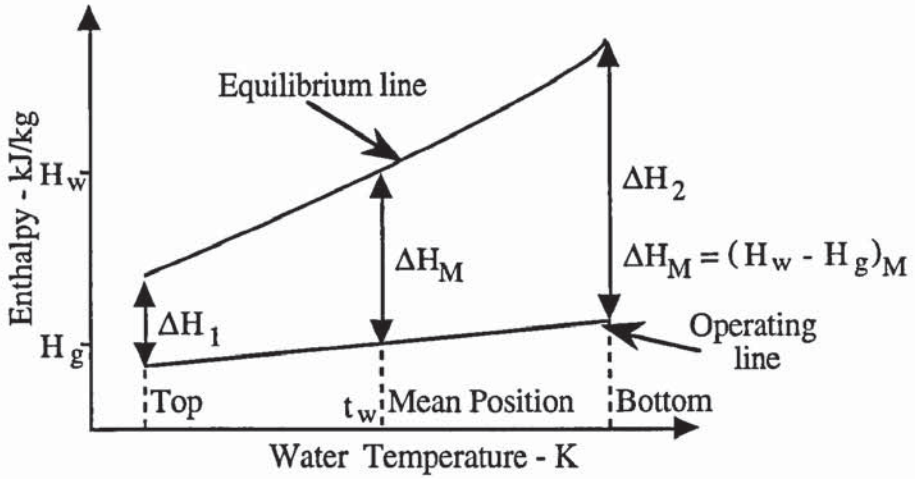

Figure 5.5 Plot of air enthalpy driving force verses water temperature diagram.

Superimposed on this diagram are the equilibrium and operating lines which show the variation in H_w and H_g with the water temperature t_w. The driving force at any temperature t_w assumes that all the resistance to mass transfer is in the vapour phase and is represented by the vertical distance between the two lines at that temperature. Figure 5.5 also shows the driving forces ΔH_2 and ΔH_1 which correspond to the inlet and outlet water temperatures, while ΔH_M represents the mean driving force at the position where the water temperature is the mean of the inlet and outlet temperatures. It is these three driving forces together with known water temperatures, the wet bulb temperature, and the water to air ratio, that are used to calculate the mean driving force for water-cooling.

Usually, the water-cooling theory is only applied to cooling towers and makes use of the parameters height of a transfer unit and the number of transfer units. The former represents the height required for the air to approach equilibrium with the water such that the air is completely saturated prior to leaving the column. The latter is a dimensionless ratio of the enthalpy transferred to, or from, the air to the mean driving force bringing about that transfer.

However the derivation of water-cooling theory used to simulate mass transfer in a trayed distillation column has yet to be developed and might occur at some stage in the future. In the mean time, an analogy between heat and mass transfer may be all that is required.

In the next section the water-cooling theory is extended to include efficiency.

Theoretical Analogy Between Heat and Mass Transfer

In the literature survey, the concept of efficiency was formulated from the basic principles used in mass transfer involving the resistance to mass transfer in the gas and liquid phases. These resistance terms are affected by the rate of gas bubbling through the liquid on a tray, the mechanism of which is explained using two concepts. These are:

a) complete mixing in the vertical direction so that point efficiency is defined as;

$$E_{OG} = N_{OG} / (1 + N_{OG}) \tag{5.2}$$

b) plug flow behaviour such that;

$$E_{OG} = 1 - e^{-N_{OG}} \tag{5.3}$$

N_{OG} is the number of overall transfer units in the gas phase and in mass transfer terms is defined as:

$$N_{OG} = K_{OG} \cdot a \cdot h_F \cdot A_F \cdot (y^* - y) \tag{5.4}$$

In heat transfer, N_{OG} is defined in terms of air humidity such that:

$$N_{OG} = K_G \cdot a \cdot h_F \cdot A_F \cdot (H^* - H) \tag{5.5}$$

By considering the "two-film addition of liquid and gas phase resistances" theory, N_{OG}, in terms of mass transfer, is expressed as:

$$N_{OG} = K_G \cdot a \cdot h_F A_F \cdot (y^* - y) = k_L \cdot a \cdot h_F A_F \cdot (x^* - x) = k_G \cdot a \cdot h_F A_F \cdot (y^* - y) \tag{5.6}$$

Thus on rearrangement of equation (5.6), the derivation of the mass transfer resistances are as follows:-

$$\frac{1}{K_G a} = \frac{1}{k_G a}\left(\frac{y^* - y}{y_i - y}\right) = \frac{1}{k_G a} + \frac{1}{k_G a}\left(\frac{y^* - y_i}{y_i - y}\right) = \frac{1}{k_G a} + \frac{1}{k_L a}\left(\frac{y^* - y_i}{x - x_i}\right)$$

$$= \frac{1}{k_G a} + \frac{m}{k_L a} \tag{5.7}$$

From the water-cooling theory used in this work, only the term $k_G a$ is utilized for the simulation of mass transfer in distillation. Equations for the heat transfer analogy are based on the assumption that the surface heat transfer coefficient within the water-air

interface and the mass transfer film coefficient are numerically equal. This assumption is expressed in terms of a Lewis number.

The Lewis number is a measure of the ratio of the diffusivity (represented by a Schmidt number, Sc) to the conductivity of the film of moist air at the interface, (represented by a Prandtl number, Pr). Hence the Lewis number is defined as:

$$Le = Sc / Pr \tag{5.8}$$

For most practical air-water applications the Lewis number, (Lewis, 1922), is assumed to be unity.

Hence expressions for liquid and gas phase resistance in heat transfer can be formulated in which heat transfer occurs in the air-water surface. Thus equation (5.6) can be rewritten in terms of a heat flux, Q, such that:

$$Q = K_T \cdot a \cdot h_F \cdot A_F \cdot (H^* - H) = h_w \cdot a \cdot h_F \cdot A_F \cdot (T - T_i) = k_T \cdot a \cdot h_F \cdot A_F \cdot (H_i - H) \tag{5.9}$$

The resistances to heat transfer can be ascertained from:

$$\frac{1}{K_T a} = \frac{1}{k_T a}\left(\frac{H^* - H}{H_i - H}\right) = \frac{1}{k_T a}\left(\frac{(H^* - H) - (H - H_i)}{(H_i - H)}\right)$$

$$= \frac{1}{k_T a}\left(\frac{H^* - H}{H_i - H} + 1\right) = \frac{1}{k_T a} + \frac{1}{h_w a}\left(\frac{H^* - H_i}{T - T_i}\right) = \frac{1}{k_G a} + \frac{m}{h_w a} \tag{5.10}$$

The method of determining $K_G a$ (mass transfer) and $K_T a$ (heat transfer) is highly complex and it is therefore sufficient to evaluate point efficiency using general equations. (See Section 5.3.5 for the calculation of thermal point and tray efficiencies based on the water temperature data collected during the water-cooling experiments described in this work).

In one sense thermal point and tray efficiencies are only defined by how we define them and have yet to be related directly to mass transfer in distillation. Thus when water-cooling is used to simulate distillation, air enthalpy and water temperature are analagous to vapour and liquid concentrations respectively. This permits the acquisition of water temperature from many positions on a tray in order to produce lines of constant temperature (isotherms) which are related to concentration profiles found in distillation. The use of water-cooling on commercial scale trays is advantageous over concentration measurements since water temperature measurements can be obtained very rapidly whereas point-to-point concentration changes are difficult to measure.

In conclusion, the review of the water-cooling theory and its application to simulate distillation demonstates that it is a powerful tool in providing much needed experimental data.

5.3.2 The Water-Cooling Experiment

During the water-cooling process, water temperature measurements are made over the tray in order to generate temperature profile isotherms. Isotherms permit interpretation of the effect of the biphase flow on mass transfer when simulating distillation. In addition the temperature isotherms can be interpreted in terms of enthalpy driving forces so as to calculate thermal point and tray efficiencies. All of these points are discussed below.

Resistance Thermometer Detectors and Data Logger System

The main criteria for the water-cooling experiment are that the water temperature measurements are made over as many points as possible, and that these measurements are made almost instantaneously. To achieve this, platinum resistance thermometers (RTDs) and a computer based data logging system are used.

Resistance thermometry is a high precision technology and is superior to thermocouple technology since RTDs require no cold junction, are less prone to noise, have a better stability and produce a high level of accuracy. In addition, resistance thermometry satisfies the error specification requirement of 0.02 ^{o}C (see Chapter 4).

The basic principle involved in RTD technology is that temperature is determined from the measurement of a comparatively small resistance across a platinum resistor. Since resistance measurements are of a high accuracy, contact resistance of the leads within the RTD becomes significant. To compensate for this, the four-lead arrangement is used in this work since it gives the most accurate measurement. Thus, for a particular temperature, the resistance is measured by applying a measuring current through two leads, while the voltage drop across the RTD is measured with a high input impedance device using the other two leads. The measurable resistance range for each RTD corresponds to a temperature range of -10 to +55 ^{o}C.

Each four-wire platinum resistor arrangement was placed inside the tip of a stainless steel probe of length 300 mm and width 3 mm. The copper lead wires, of length six metres were enclosed in an external PVC coating so as to protect the leads against any moisture. To obtain a precise temperature field over the whole tray, 118 RTD's were mounted on to the tray deck as shown in Figure 5.6.

The diagram shows that five RTDs were placed on the underdown flow plate 50 mm to the rear of the inlet downcomer, 108 were placed on a 200 mm square grid pitch across the tray, four beneath the tray, and one at the bottom of the outlet downcomer. The coordinates of the RTD probes on the tray are presented in Appendix 1.0. The significance of this arrangement will be shown later.

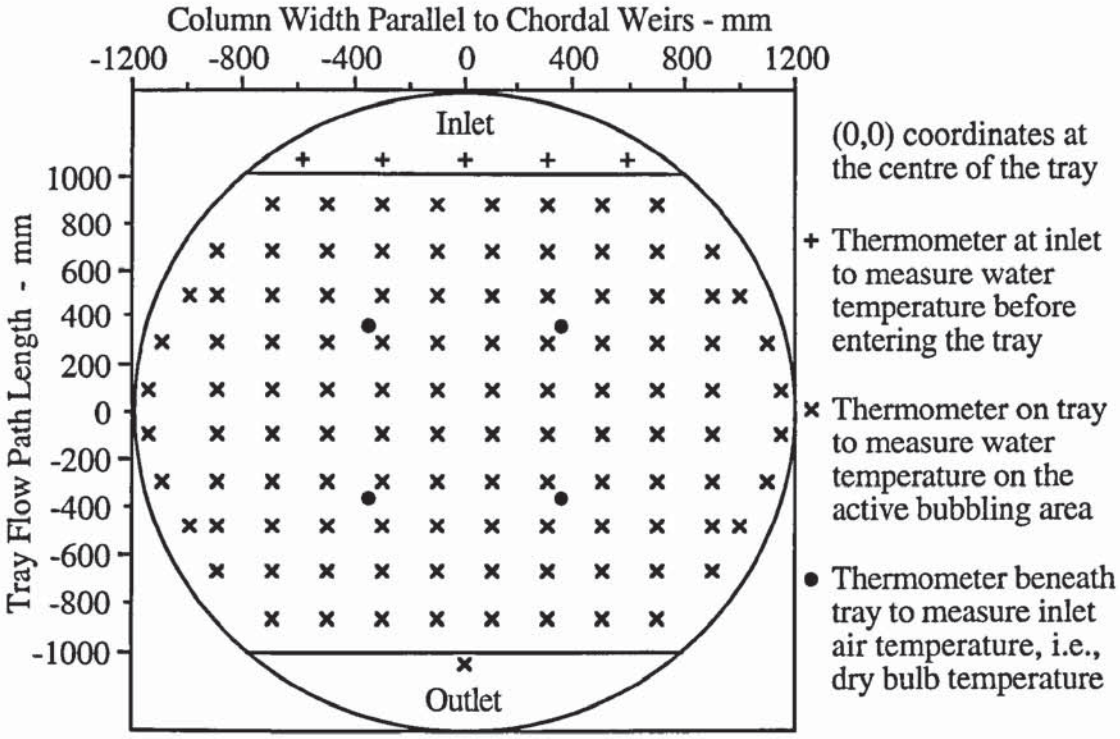

Figure 5.6 Arrangement of platinum resistance thermometers on the 6.35 mm hole tray.

With the exception of the four temperature probes beneath the tray, each RTD was mounted onto the tray deck, from beneath the tray, by means of a rubber grommet and a water shroud as shown in Figure 5.7. A photograph of the RTD and water shroud arrangement is presented in Figure 5.8. The PVC coated wires of all the RTD probes were spread out evenly beneath the tray deck, and suspended in the intertray spacing so as to prevent distortion of the rising air flow from the distributor tray to the test tray.

Water shrouds were incorporated into the RTD arrangement to prevent premature cooling of the bare probe by the rising air flow since this would have produced erroneous temperature readings. In addition the shroud permitted the capture of a water sample such that it completely surrounds the RTD tip before leaving the shroud to rejoin the biphase via four water flow outlets.

During water-cooling, "simultaneous" measurements of the tray temperature field are obtained by interfacing the 108 RTD's, attached to the tray, with a MICROLINK data

logger which in turn is linked to an on-line personal computer (model number ESP 9228) with a 130 MByte hard disk drive. The data logger unit, purchased from Biodata Ltd, consists of eighteen digital cards which comprise of one high speed clock, one analogue to digital (A-D) coverter, and sixteen RTD8H D-type connectors. Each RTD8H connector contains eight four-lead RTDs or channels.

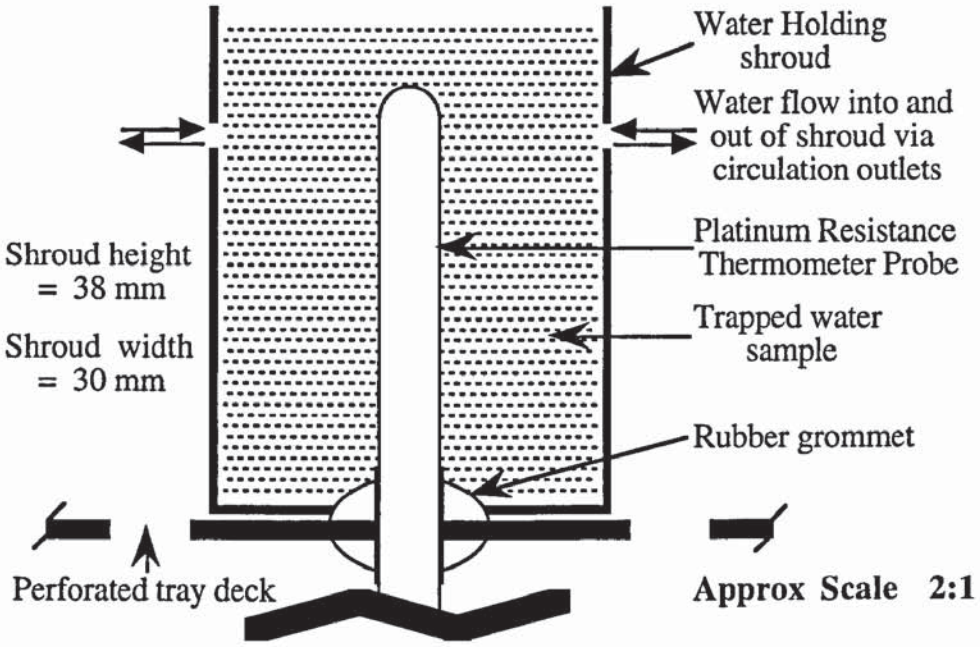

Figure 5.7 Schematic diagram of resistance thermometer and water shroud attachment to the test tray.

The high speed clock permits rapid data acquisition of water temperatures by converting the temperature from an analogue signal into a digital signal for each channel. The time delay for each analogue to digital (A-D) conversion between each channel is one millisecond which means that a complete scan of all 120 usable channels is 1.2 seconds. In the water-cooling experiments described in this work, 118 channels or RTDs are used.

The A-D convertor changes the temperature data, in the form of an analogue input signal from the RTD8H D-type connector being addressed, into a digital signal. This output signal is subsequently relayed to the on-line computer via the IEEE-488 address bus.

Computer control over the data logging system is achieved using Fortran 77 coding labelled COLTEMP.FOR. The program sends a number of parameters as input to the data logger via the IEEE-488 address bus. These include the input of the high speed clock, the range of RTD8H modules, and the calibrated temperature data file. The latter contains all the calibrated temperature data points for each RTD standardised at known

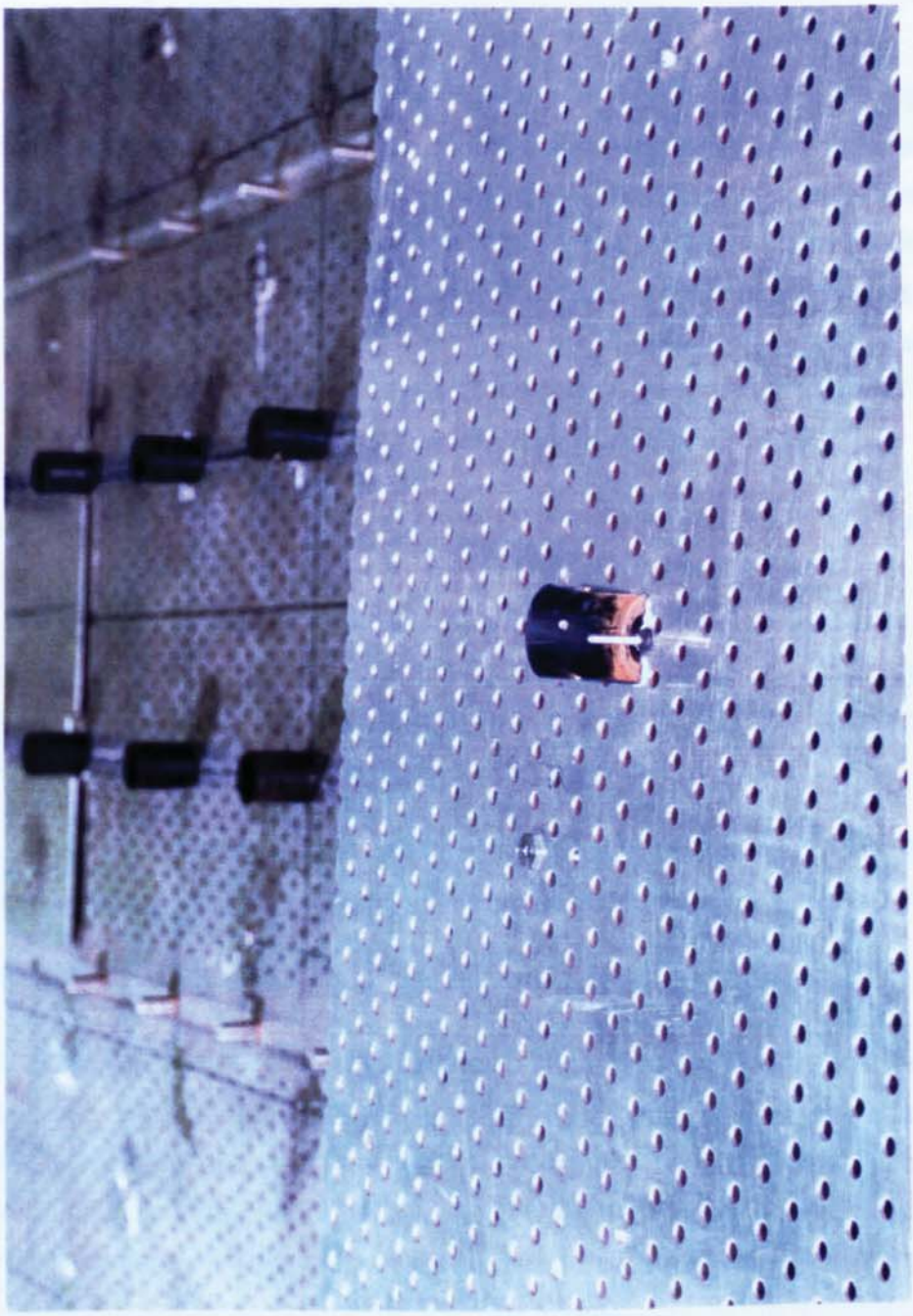

Figure 5.8 Photograph of resistance thermometer and water shroud assembly on the test tray.

temperatures. It is this data file that is used to evaluate actual temperatures from measured readings by linear interpolation between calibrated temperature points. To complete the computer based data logging system, driver software, supplied from Biodata Ltd, is used to check whether all the system components are being addressed properly. A photograph of the computer based data logging system is presented in Figure 5.9

By noting the location of the RTDs on the tray in Figure 5.6, tray temperature measurements are monitored using the COLTEMP.FOR computer program. On achieving steady state conditions, temperature data is measured and collected by scanning all of the RTDs twenty times. This data is corrected using calibration points from which data and average data are recorded on computer data files. To determine whether steady state has been achieved, one inlet and the single outlet downcomer temperature are monitored during data sampling, and if either have varied by more than 0.1 ^{o}C then the run was aborted. The run is repeated until steady state is achieved.

The average temperature data files, recorded during each successful test run, were searched for any erroneous readings in the collected data and if found, the error is displayed using a default value of 99.99. These output temperature data files contain information on the flow rates and tray configuration, followed by a display of the averaged calibrated temperature data within the physical boundary of the tray. An example of a temperature output file is presented in Figure 5.10.

Use of the raw data for the graphical presentation of temperature profiles and for the calculation of thermal efficiencies are described in the subsections 5.3.3 and 5.3.4.

5.3.3 Processing and Graphical Representation of Temperature Profiles

To present the temperature profiles graphically, two requirements must be satisfied. The first is that the raw temperature data needs to be converted into reduced temperature data so that results from different experiments can be compared on a like basis. The second requirement is that the water temperature data measured at known positions across the tray, has to be converted into intermediate temperature points, using an interpolation method, in order to generate the temperature profile graphs.

The use of reduced temperature profile diagrams provides a clear indication of the effect of the two phase flow pattern on mass transfer when simulating distillation. That is, when water flowing across the tray is cooled by air, the rate of decrease in the temperature profile corresponds to the rate of depletion of the most volatile component, mvc, from the

Figure 5.9 Photograph of the data logger and computer for rapid temperature data acquistion.

TEMPERATURE DATA INFORMATION

AIR VELOCITY (m/s)	1.500	The first three
WEIR LOAD (cm3/cm.s)	150.0	lines indicate the
DEW POINT (deg c)	5.00	flow rates
COLUMN DIAMETER (m)	2.440	These six lines
WEIR LENGTH (m)	1.500	represent information
FREE AREA (%)	10.0	on the tray geometry
OUTLET WEIR HEIGHT (m)	0.050	and configuration
INLET WEIR GAP (m)	0.050	
HOLE DIAMETER (m)	0.006	

First row = 5 inlet temperature values

10 row x 12 column matrix = 108 temperature readings over tray area

Last figure = outlet water tempertaure

Final row = four inlet air temperatures

```
                                47.50   47.70   47.52   47.73   47.73
                 42.53   44.53   47.22   47.23   47.18   46.64   44.37   42.55
         31.18   38.29   40.52   44.05   43.91   45.47   43.25   44.46   40.05   32.78
32.84    34.69   39.39   43.80   44.14   44.08   44.69   43.80   43.81   39.64   33.41   33.56
33.78    36.25   40.45   41.95   41.82   38.56   43.42   42.87   40.19   40.30   35.82   33.37
34.52    36.10   39.84   39.51   40.48   42.22   99.99   41.21   38.47   38.55   33.18   32.87
33.87    36.24   39.38   40.20   39.88   99.99   41.78   39.66   38.99   39.02   34.12   32.52
33.09    35.30   32.43   37.70   38.90   40.49   40.96   38.76   37.00   36.12   32.99   30.83
29.15    33.66   36.52   36.88   35.78   39.93   40.30   38.61   36.11   35.32   31.96   29.71
         32.67   33.13   35.26   35.93   39.06   37.80   37.01   34.91   33.31   30.92
                 31.47   33.69   36.37   37.13   37.84   36.85   33.71   31.23
                                                 36.46

           13.87    9.96    9.84    9.71
```

Figure 5.10 A representative example of collected temperature data during water-cooling.

liquid by the stripping action of the vapour, during mass transfer. In mass transfer processes such as distillation, this phenomenon is represented by a significant decrease in the concentration profile.

Processing the Raw Data

Since it was not possible to maintain the same inlet water temperature during each set of water-cooling experiments as well as the variation of the inlet air condition (i.e., dry and wet bulb temperatures), the calculation of reduced temperature points became necessary. The advantage of calculating reduced temperatures is that it permits equal comparison of results from different experiments. Reduced temperature, T_r, is calculated from:

$$T_r = \frac{T - T_{wb}}{T_{in} - T_{wb}} \qquad (5.11)$$

where T, T_{in}, and T_{wb} are the measured point water temperature, inlet water temperature, and the wet bulb temperature of the entering air respectively. It is reduced temperature data that are used to produce graphical displays of temperature profiles.

The software package used to construct these graphs is the UNIRAS suite of plotting routines. This was incorporated onto the VAX CLUSTER main frame computer such that temperature data files can be uploaded from the personal computer in order to be processed.

To produce smoothed temperature surfaces, irregularly spaced reduced temperature data points are converted into a regular grid of data points by the use of an interpolation routine. UNIRAS then fits a smooth surface curve through the measured gridded or control point values. The method of interpolating temperature data is discussed below.

Weighted Average Interpolation and Quadratic Interpolation

The two methods used to generate gridded data on a least-squares matrix, through which a smooth curve is fitted, are weighted average interpolation and quadratic interpolation.

An irregularly spaced set of data points are converted into a regular gridded set, by the selection of data points closest to a control point in four quadrants formed using a search radius for that particular control point. If a data point is found in more than one quadrant then a weighted average interpolation is performed on the data point closest to the control point, which at a distance of RAD1 units away from the grid node, is saved for the quadratic interpolation procedure. Weighted average interpolation involves the calculation

of the squared differences from the control point, or grid node, to the data points found in each quadrant. Thus:

$$D_i = \left[\frac{X_i - X_0}{DX}\right]^2 + \left[\frac{Y_i - Y_0}{DY}\right]^2 \quad \text{for } i = 1,....,N \tag{5.12}$$

where N is the number of data points; (X_0,Y_0) are the coordinates of the grid node; (X_i,Y_i) are the coordinates of the data points for i = 1,...,N; and DX and DY are the grid distances in the X and Y directions. For each grid node a weighted average value, ZEST, is computed by using:

$$ZEST_{X_0Y_0} = [\Sigma (W_i Z_i)] / [\Sigma W_i] \tag{5.13}$$

in which Z_i for i = 1, ..., N and $W_i = 1/D_i$ for i = 1, ..., N are the height values of the data points through which the surface curve is fitted.

Quadratic interpolation improves the quality of the surface fit through the data points. At each grid node the surface curves are calculated from the closest data point at a distance of RAD1 units, and at data points found RAD2 units further away from the grid node (RAD2 =1.25xRAD1). By defining Z_1 and Z_2 as the average values of data points at grid distances RAD1 and RAD2 from the grid node, then $Z_{X,Y}$, is estimated at the grid node (X,Y) from:

$$Z_{x,y}^{new} = Z_{x,y}^{old} + (Z_{int} - Z_{x,y}^{old}) \times SFACT \tag{5.14}$$

where SFACT is a factor equal to 0.15, and Z_{int} is defined as;

$$Z_{int} = \frac{RAD2^2 Z_1 - RAD1^2 Z_2}{RAD2^2 - RAD1^2} \tag{5.15}$$

The calculation of $Z_{X,Y}$ is iterated eight times for every grid point, such that slight changes in $Z_{X,Y}$ will produce a smooth surface.

The quadratic interpolation includes the effect of surface gradient in interpolating a value at the grid point. Without the quadratic interpolation the interpolated surface would have zero gradient at every grid point.

When the interpolation procedures are complete, the regular gridded data set is ready to be plotted graphically.

5.3.4 Graphical Presentation of Temperature Profiles

With all the temperature data placed on a 20x24 least-squares matrix, two and three-dimensional displays can be generated. These temperature field diagrams are presented as black and white displays, examples of which are shown in Figure 5.11. The computer coding used to perform the interpolation procedure on the raw temperature data and the generation of temperature field diagrams, (2D3DTEMP.FOR), is listed in Appendix 1.

The two-dimensional diagram is a contour map which provides a summary of isotherms showing lines of constant temperature. Temperature gradients are shown by the distance between adjacent isotherms. The isothermal contours show lines of equal temperature increments and include reduced temperature profiles in which the figures shown on each isotherm represent the reduced temperature, T_r, (see equation 5.11). The three-dimensional display shows the variation in the temperature surface across the tray area at the expense of showing no lines of equal temperature (isotherms). Again this form of diagram is a plot of reduced temperature profiles.

Note that in the two dimensional display of Figure 5.11, there is a gap between the ends of the isotherms and the tray boundary. The reason is that the UNIRAS plotting routines fitted smooth curves through defined interpolated temperature data points only. This was achieved using the GFAULT command which prevented the fitting of curves through data points on the column wall and "imaginary" data points on or outside the tray boundary that were unrepresentative of what was happening on the tray during water-cooling.

5.3.5 Determination of Thermal Efficiencies From Temperature Profiles

The cooling of hot water by rising air on an operating tray provides an analogy between heat and mass transfer. Therefore a heat balance, presented in Figure 5.12, can be constructed from which thermal point and tray efficiency calculations can be made. Fortran computer software was developed (Hine, 1990), and updated for the calculation of Murphree point and tray efficiencies.

$\overline{T_{in}}$ represents the temperature of hot water entering the test tray whereas $\overline{T_{out}}$ represents the average temperature of water leaving the tray. Air rises upto the tray with a uniform enhalpy, H_1, whilst $\overline{H_2}$ represents the enthalpy of almost saturated air leaving the froth On the basis of air enthalpy, the Murphree tray efficiency, E_{MV}, may be defined as:

$$E_{MV} = \frac{\overline{H_2} - H_1}{H^*_{Tout} - H_1} \qquad (5.16)$$

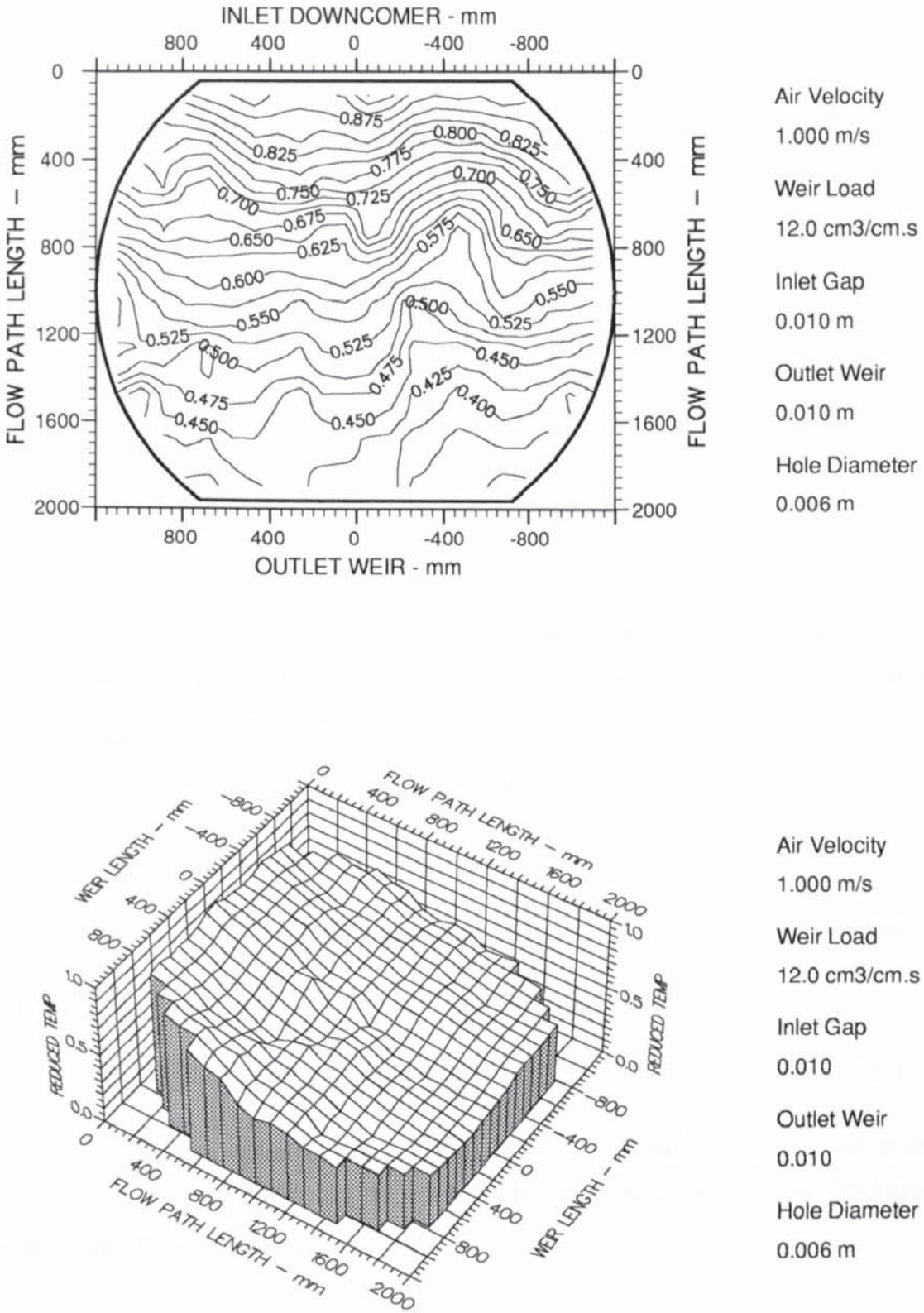

Figure 5.11 Example of a two and three dimensional temperature profile diagram

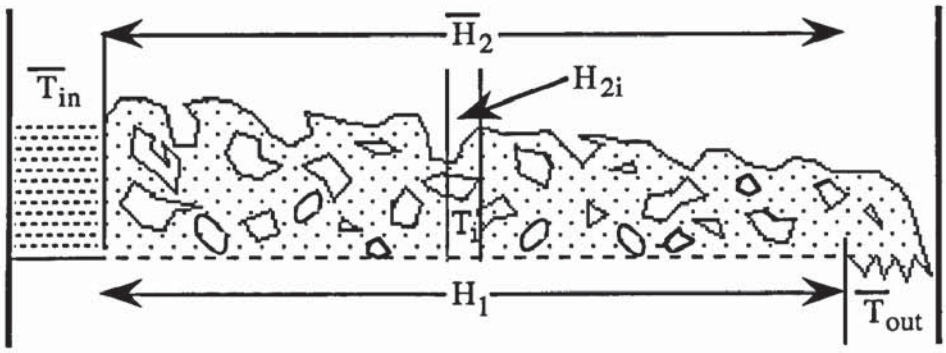

Figure 5.12 Schematic diagram of parameters used in the efficiency calculations.

where H^*_{Tout} is the enthalpy of saturated air in equilibrium with the average temperature of the water leaving the tray. Similarly the Murphree point efficiency, E_{OG}, in terms of air enthalpy at position i is defined as:

$$E_{OG} = \frac{H_{2i} - H_1}{H^*_{Ti} - H_1} \tag{5.17}$$

where T_i is the local water temperature at position i on the tray, and H^*_{Ti} is the air enthalpy in equilibrium with T_i. H_1, H^*_{Tout}, and H^*_{Ti} are obtained from psychrometric data tables. Thus H_1 is calculated from the relationship:

$$H_1 = (C_{Air} \cdot T_{db}) + H_{(T_{db}, T_{wb})}[(C_{Water} \cdot T_{db}) + H_{FG}] \tag{5.18}$$

while H^*_{Tout} is obtained using:

$$H^*_{Tout} = (C_{Air} \cdot T_{out}) + H_{Tout}[(C_{Water} \cdot T_{out}) + H_{FG}] \tag{5.19}$$

and H^*_{Ti} is calculated from:

$$H^*_{Ti} = (C_{Air} \cdot T_i) + H_{Ti}[(C_{Water} \cdot T_i) + H_{FG}] \tag{5.20}$$

During water-cooling, water temperature data acquisition is carried out at fixed air and water flowrates which permits the calculation of the overall saturated air enthalpy leaving the froth, $\overline{H_2}$, from the heat balance:

$$G \cdot (\overline{H_2} - H_1) = L \cdot Cp\,(\overline{T_{in}} - \overline{T_{out}}) \tag{5.21}$$

Substituting $(\overline{H_2} - H_1)$, from equation (5.21) into (5.16) will yield the Murphree tray

efficiency.

The determination of point efficiency, E_{OG}, is based on the assumption that it is constant at all points on the tray. This simplifies the calculation by noting that the square pitch arrangement of the resistance thermometers (Figure 5.6) justifies the assumption that each thermometer is representative of the same amount of tray area and thus of the same gas flow rate. The procedure for the calculation of E_{OG} is best explained by the following example.

Consider four equally spaced resistance thermometers a,b,c,d on a section of tray as shown in Figure 5.13.

Since the inlet air enthalpy to the tray is assumed to be uniform, the air enthalpy beneath each thermometer is H_1, while the saturated air enthalpies above the thermometers are defined as H_{2a}, H_{2b}, H_{2c}, and H_{2d}. The average saturated air enthalpy above the four thermometers is calculated from:

$$\overline{H_2} = \frac{H_{2a} + H_{2b} + H_{2c} + H_{2d}}{4} \qquad (5.22)$$

Now E_{OG} in equation (5.17) is defined in terms of air enthalpy at position i on the tray.

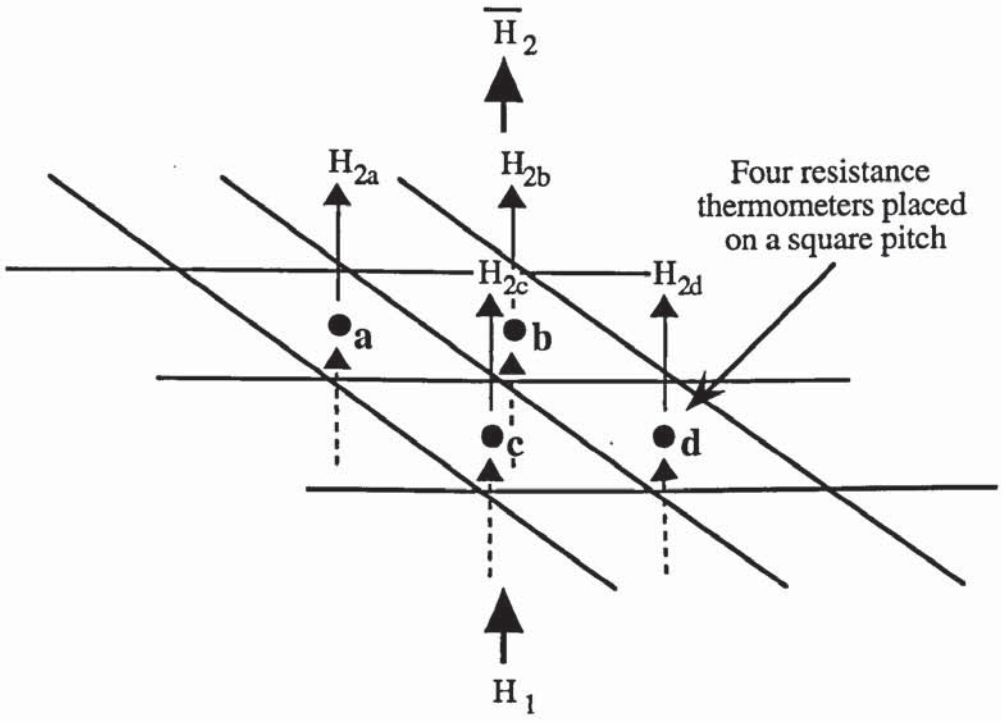

Figure 5.13 Enthalpy balance around four resistance thermometers on a small section of tray area.

Thus in this case, i is equal to a, b, c, d and therefore equation (5.17) can be rearranged in terms of the saturated air enthalpy leaving the tray to produce the following expressions:

$$H_{2a} = E_{OG}\cdot(H^{*}_{Ta} - H_1) + H_1 \qquad (5.23)$$

$$H_{2b} = E_{OG}\cdot(H^{*}_{Tb} - H_1) + H_1 \qquad (5.24)$$

$$H_{2c} = E_{OG}\cdot(H^{*}_{Tc} - H_1) + H_1 \qquad (5.25)$$

$$H_{2d} = E_{OG}\cdot(H^{*}_{Td} - H_1) + H_1 \qquad (5.26)$$

where H^{*}_{T} is the saturated air enthalpy in equilibrium with the water temperature at the four thermometer positions a,b,c,d. Since the objective is to calculate the average point efficiency, the above expressions are averaged to yield the following:

$$\frac{1}{4}\sum H_{2i} = \frac{E_{OG}}{4}\sum (H^{*}_{Ti} - H_1) + \frac{1}{4}\sum 4\,H_1 \quad \text{where i = a,b,c,d} \qquad (5.27)$$

Hence for this simple case, equation (5.27) can be rewritten in terms of mean enthalpy driving forces over the four thermometers to calculate E_{OG}, that is:

$$\overline{H_2} - H_1 = E_{OG}\cdot(\overline{H^{*}_{T}} - H_1) \qquad (5.28)$$

To calculate the average E_{OG} at the general position i on the tray, in terms of $\overline{H_2}$ and $\overline{H^{*}_{Ti}}$, it follows that:

$$\overline{H_2} = \frac{1}{n}\sum_{i=1}^{n} H_{2i} \qquad (5.29)$$

where n is the number of working resistance thermometers and H_{2i} is the saturated air enthalpy above the froth at each resistance thermometer i. Based on the procedures outlined in the above example, the average E_{OG} is calculated as follows:

By starting with

$$(H_{2i} - H_1) = E_{OG}\cdot(H^{*}_{Ti} - H_1) \qquad (5.30)$$

the left hand side may be rewritten by incorporating equation (5.29). Thus:

$$(\overline{H_2} - H_1) = \frac{1}{n}\sum_{i=1}^{n}(H_{2i} - H_1) = \frac{1}{n}\sum_{i=1}^{n}(H_{2i}) - \frac{n \cdot H_1}{n} \qquad (5.31)$$

By substitution of $(\overline{H_2} - H_1)$, from equation (5.30), equation (5.31) becomes:

$$(\overline{H_2} - H_1) = \frac{1}{n}\sum_{i=1}^{n}(H_{2i}) - \frac{n \cdot H_1}{n} = \frac{E_{OG}}{n}\left(\sum_{i=1}^{n} H^*_{Ti} - n \cdot H_1\right) \qquad (5.32)$$

Finally, by noting the overall heat balance equation, the average E_{OG} at position i is given by:

$$E_{OG} = \frac{\overline{H_2} - H_1}{\frac{1}{n}\sum_{i=1}^{n} H^*_{Ti} - H_1} = \frac{\frac{L}{G} C_p(\overline{T_{in}} - \overline{T_{out}})}{(\overline{H^*_{Ti}} - H_1)} \qquad (5.33)$$

where $\overline{H^*_{Ti}}$ is calculated from a similar expression to that of equation (5.29) and H_1 is uniform everywhere beneath the tray.

The computer coding for evaluating the thermal efficiencies is contained in Appendix 2.

5.3.6 Interpretation of Temperature Profile Results

Temperature profiles provide guidance on whether the air-water flow patterns on the tray are those likely to achieve optimum tray efficiency. If the liquid flow pattern produced a uniform liquid residence time on the tray and the air is uniformily distributed then lines of constant liquid temperature (isotherms) can be expected to be approximately straight and parallel to the inlet and outlet chordal weirs. This idealised liquid flow pattern, (Lockett, 1976), illustrated in Figure 5.14a, is expected to produce the maximum tray efficiency.

Non-uniform liquid flow is highlighted by, for example, "U-shaped" isotherms as shown in Figure 5.14b, or inverted "U-shaped" isotherms as shown in Figure 5.14c.

In general, it can be said that the coldest liquid has the greatest residence time as a result of more gas passing through it compared with that for the hotter liquid. Therefore "U-shaped" profiles (Figure 5.14b) imply either a faster moving liquid along the middle of the tray than at the sides, or more gas flow at the sides of the tray compared to that in the middle. The inverted "U- shaped" profiles (Figure 5.14c) imply either a faster moving

liquid at the sides of the tray than in the middle, or more gas flow in the middle of the tray compared to that at the sides.

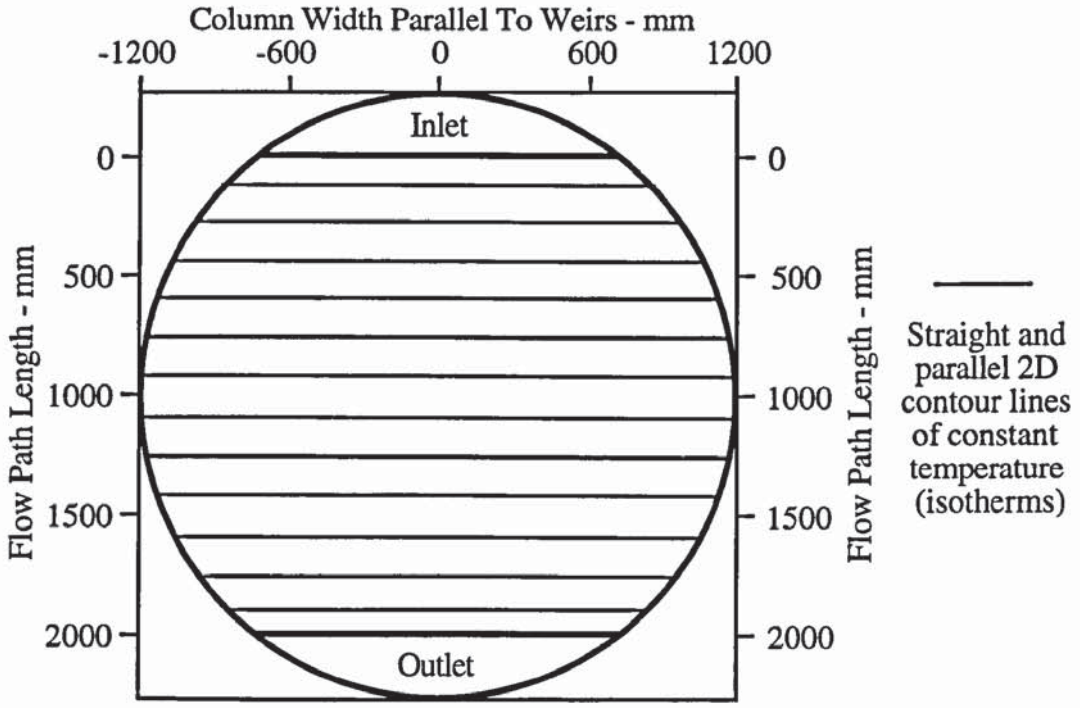

Figure 5.14a Simplified two-dimensional temperature profile diagram indicating a uniform liquid flow pattern over the tray.

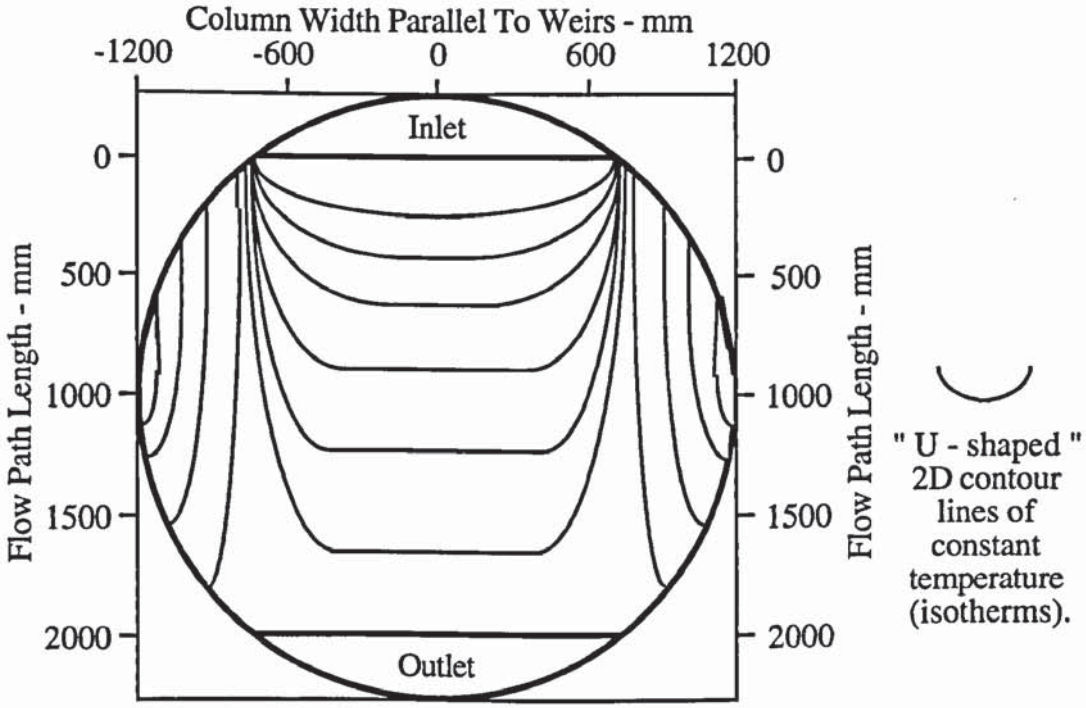

Figure 5.14b Simplified two-dimensional temperature profile diagram indicating non - uniform liquid flow across the tray, i.e., "U - shaped" isotherms.

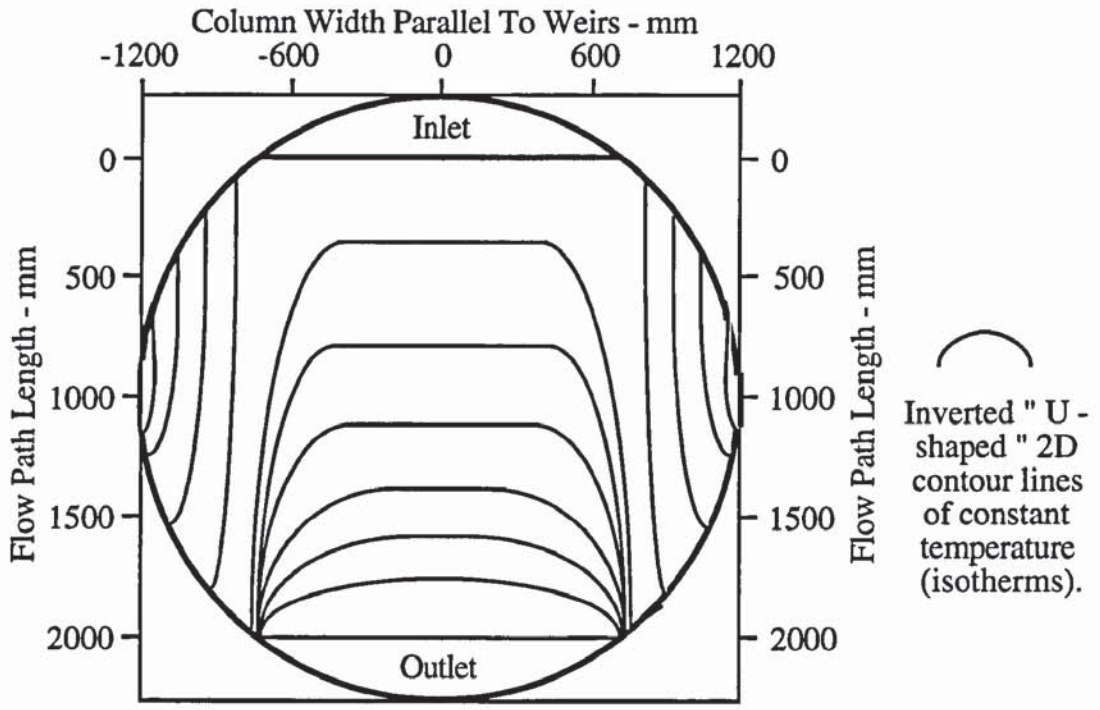

Figure 5.14c Simplified two-dimensional temperature profile diagram indicating non - uniform flow across the tray, i.e., inverted "U - shaped" isotherms.

An approximate qualitative assessment of the type of temperature profiles that will be generated during water-cooling was made as follows, such that it might be described by:

Straight or parallel isotherms	designation	P
Transverse (flat) U-shaped profiles ie a horizontal line in the middle of the "U-shape"	designation	hU shallow profiles
	designation	TU severe profiles
Distinctive or Inverted "U-shaped" profiles	designations	U and IU
Mixed or confused profiles	designation	M

This permits a summary of the temperature profiles on a tray loading diagram similar to that used for the direct-observation experiments.

5.4 Measurement of Height of Clear Liquid

Tray flow patterns are essentially controlled by three main constituents: flow direction, froth velocity and froth depth. Some progress in understanding the first two properties

has been made from the direct-observation experiments and by water-cooling described in the previous sections. However, since in many cases, non-uniform biphase flow occurs on operating trays, it is necessary to investigate the variation in froth height across the tray area under these flow conditions. Traditionally, it was assumed that a froth height gradient existed between the inlet and outlet downcomers on a tray such that the froth height is greatest at the inlet and least at the outlet.

5.4.1 Measurement Technique using Manometers

Direct measurement of the froth depth is difficult owing to the continuous movement of the froth surface. Instead the pressure drop between the tray floor, the froth or spray dispersion and the space above (which is proportional to the froth height), is evaluated by measurement of the effective froth height or height of clear liquid. Height of clear liquid is measured using a manometer which is a tube, filled with water and connected to a pressure tapping on the tray deck as shown in Figure 5.15. The definition of clear liquid height is the liquid depth on a tray when the vapour supply is stopped to eliminate foam build-up and the formation of liquid droplets above it.

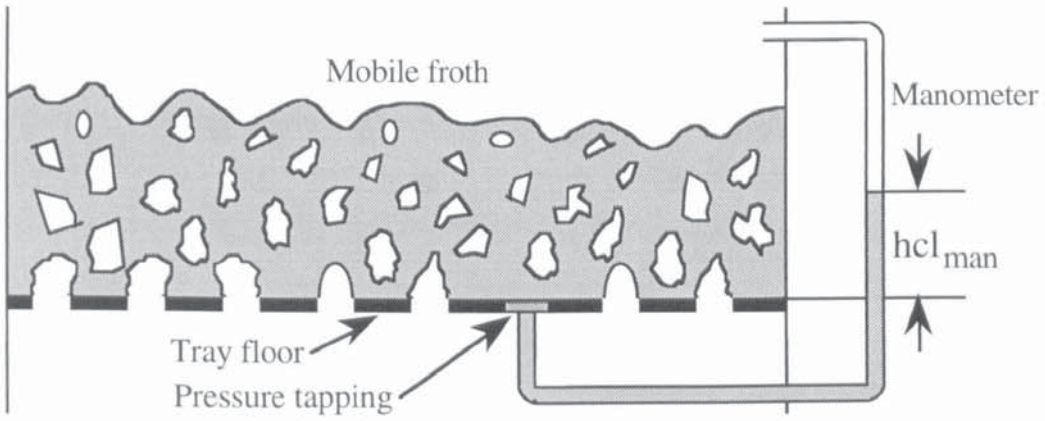

Figure 5.15 Schematic diagram of a manometer for measuring the height of clear liquid.

Capillary rise and gas momentum effects were accounted for by relating manometer readings to a datum level. Datum readings are measured directly, using calibrated manometer tubes located outside the simulator, by operating the tray with no liquid at various air flowrates. By subtracting datum values from the actual readings, obtained with a liquid head on the tray, the variation in clear liquid height is obtained. (Datum readings constitute "zero" height of clear liquid.)

5.4.2 Experimental Procedure

Height of clear liquid measurements are obtained from thirty two manometer pressure tappings spread evenly across the test tray as shown in Figure 5.16. Manometers are connected to sample points on the tray using PVC tubing which is filled with water and purged of any air bubbles trapped in the water lines using water under pressure. By setting the air and water flow rates, a time period elapses to allow for steady state conditions to occur across the tray before all the manometer liquid levels are measured. The actual readings are corrected by subtracting the datum readings in order to compute the height of clear liquid at each point on the tray.

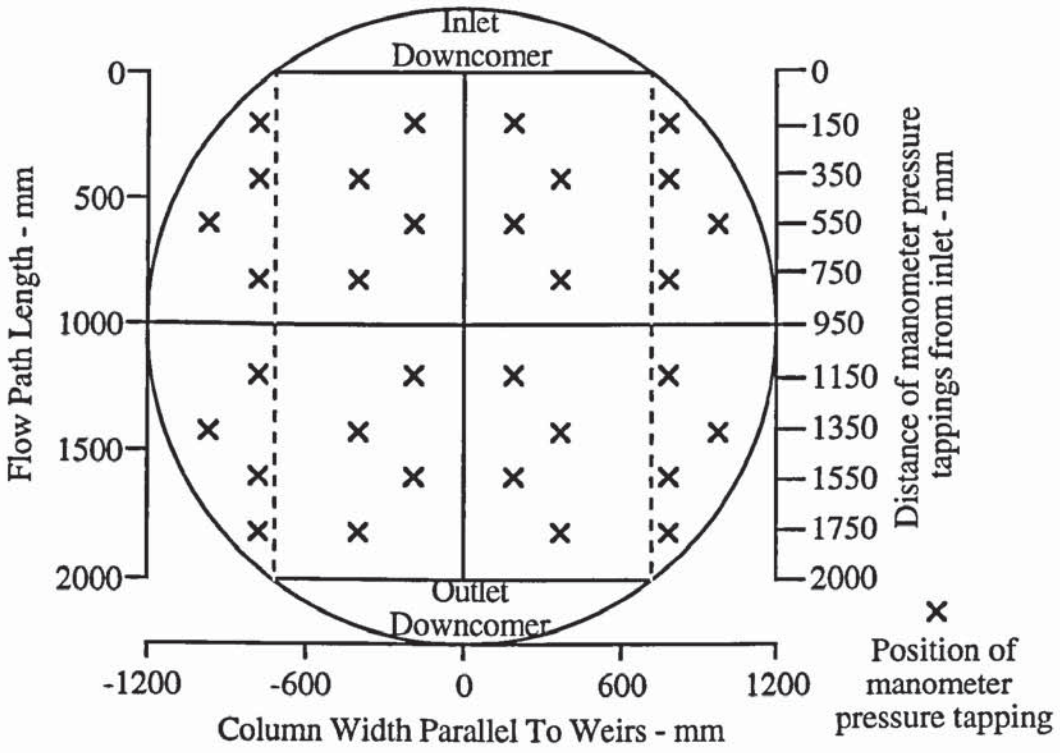

Figure 5.16 Position of manometer tappings across the test tray.

The results are computer processed in a similar manner to the three-dimensional surface temperature profile graphs to produce three-dimensional liquid surface diagrams and point height of clear liquid readings. Examples of three-dimensional height of clear liquid profile diagrams are contained in the following subsection. Figure 5.17 shows how the height of clear liquid is calculated for a given point on the tray.

The total pressure drop from below the tray to the space above the froth on the tray was measured using a U-tube manometer such that $\Delta P_{TOTAL} = P_1 - P_3$, (see Figure 5.17).

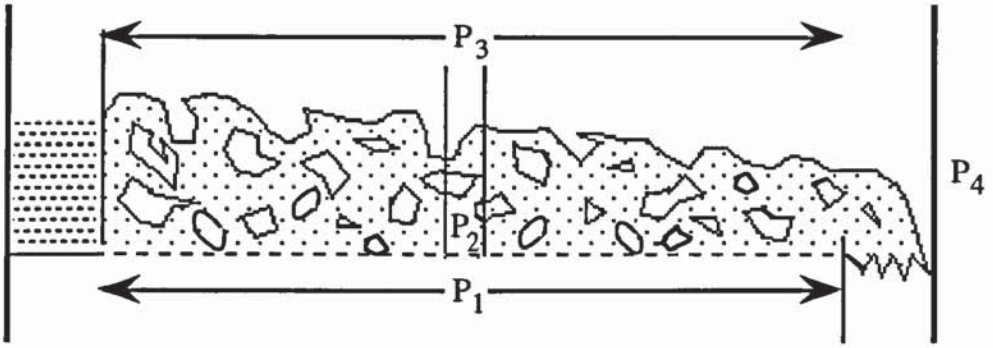

P_1 - Pressure below test tray.
P_2 - Pressure above test tray.
P_3 - Pressure above froth.
P_4 - Atmospheric pressure.

$\Delta P_{TOTAL} = P_1 - P_3$
$\Delta P_{CORR} = P_3 - P_4$
$\Delta P_{DRY} = P_1 - P_2$

Step 1: Measure the total pressure drop, $\Delta P_{TOTAL} = P_1 - P_3$

Step 2: Measure the corrected pressure drop, $\Delta P_{CORR} = P_3 - P_4$

Step 3: Measure the liquid height from manometer at point i (where i = 1 to 32), $\Delta P_{FROTH} = P_2 - P_4$

Step 4: $\Delta P_{FROTH} - \Delta P_{CORR} = (P_2 - P_4) - (P_3 - P_4) = P_2 - P_3$ = height of clear liquid at point i

Figure 5.17 A pressure diagram for the calculation of height of clear liquid.

5.4.3 Output and Interpretation of Height of Clear Liquid Results

During data processing of the raw clear liquid height measurements, thirty two sets of point height of clear liquid data are recorded onto output data files, labelled HCLOUT.DAT, and are contained within the physical boundary of the test tray. An example of point-to-point height of clear liquid results for a particular experimental run is presented in Figure 5.18. The coordinates of the manometer pressure tappings on the tray are presented in Appendix 3.0.

Since a large amount of clear liquid height measurements are to be recorded during the research programme, the liquid head profiles are identified as follows:-

A horizontal (flat) liquid head profile is designated H; an uneven liquid head profile consisting of peaks and/or troughs at the tray inlet is designated NI; and an uneven liquid head surface containing peaks and/or troughs at the tray outlet is designated NO. If the liquid head surface is uneven over the whole tray, then the N designation is used.

All of the liquid head profile results can be identified using this approach, in which they are all approximations so that in doubtful cases, the N designation is used. As with the temperature profile isotherm results, the height of clear liquid profiles can be summarised on a modified load factor verses weir load graph.

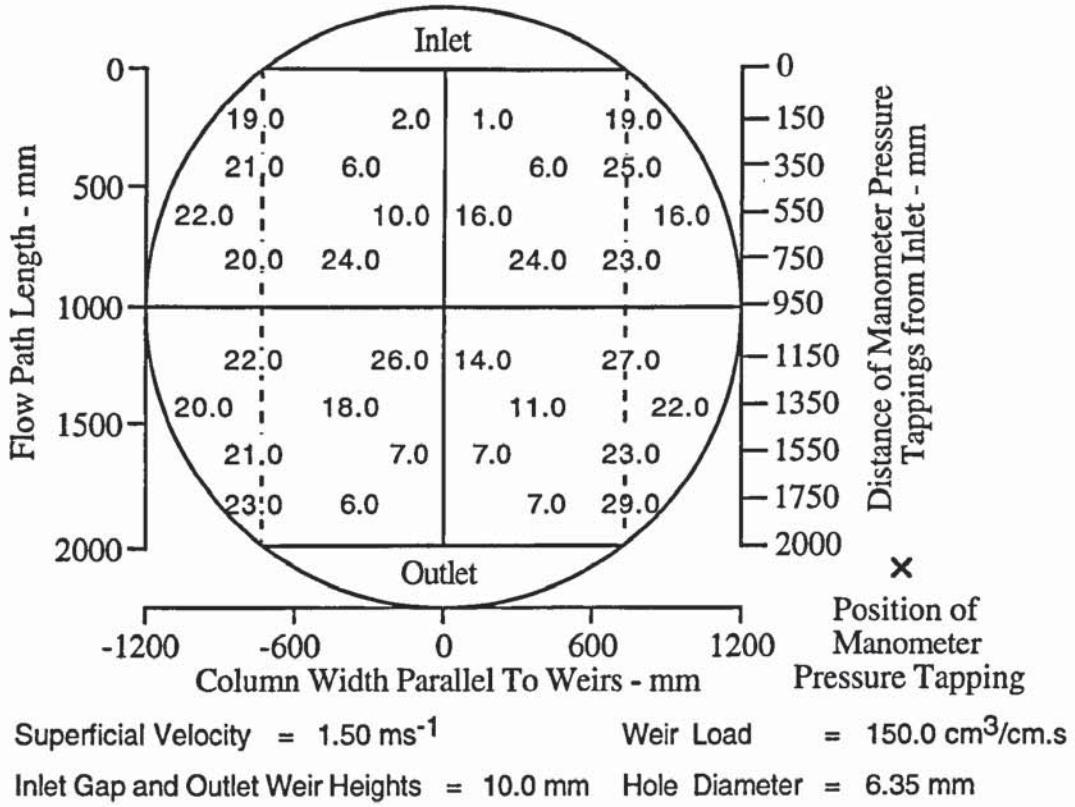

Figure 5.18 An example of point-to-point height of clear liquid results

Examples of three-dimensional height of clear liquid diagrams are shown in Figures 5.19a and 5.19b. Figure 5.19a, shows a comparatively flat liquid head profile which is likely to be associated with a uniform gas distribution. A liquid head profile with an uneven surface is presented in Figure 5.19b and is likely to be caused by a high level of turbulence over the tray area. Figure 5.19b is a classic example of a liquid head profile showing a hydraulic jump infront of the inlet downcomer such that the liquid jets onto the tray deck over a certain distance (approximately 200-300 mm) before becoming fully aerated. The uneven liquid head surface may contain a number of peaks or troughs or a combination of both across the tray. Note that the liquid head surface in Figure 5.19b corresponds to the point-to-point height of clear liquid data presented in Figure 5.18.

The computer coding that generates three-dimensional liquid head surface diagrams and the height of clear liquid output data files, (3DHCL.FOR), is listed in Appendix 3.

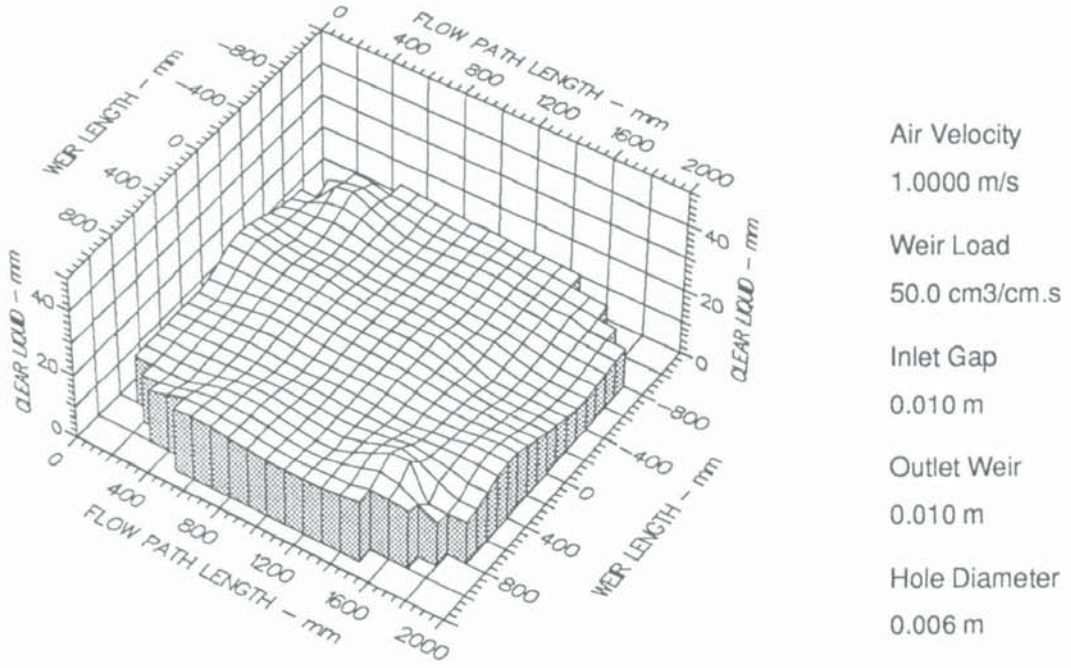

Figure 5.18a An example of a comparatively flat height of clear liquid profile

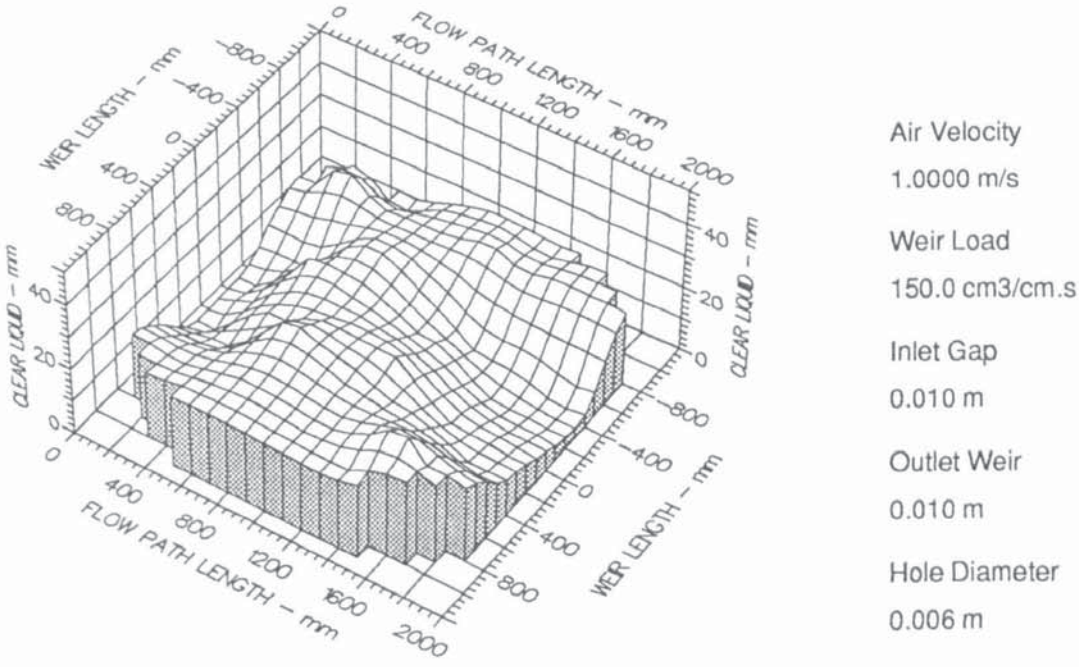

Figure 5.18b An example of a height of clear liquid profile with an uneven surface

5.5 Operation of the Air - Water Simulator

Set out below are the start-up, normal operation, and shut down procedures used for the safe operation of the distillation simulator. The steps presented are those used during the heat transfer experiments by water-cooling since it involves the use of the whole apparatus.

5.5.1 Start-Up Procedure

1. Switch on the main electricity isolator and open the manual gas valves to the gas fired process boilers.

2. Start the circulation water pump, in the primary heating circuit, and the flue dilution fan.

3. Start the main water pump, in the secondary water circuit, to circulate water through the double heat exchanger and bypass network from where it is returned to the water sump tanks.

4. Switch on the electrical supply to the gas shut-off valve.

5. Start one or both of the gas fired boilers. This is the primary heating source to the main water circuit.

6. Open the steam valve. This the secondary heating source which is used as a heat top-up supply. A spring valve is used to fine tune the inlet water temperature to the simulator prior to entering the test tray.

7. When the water, in the sump tanks, approaches 40 ^{o}C start the air fan and set the desired air flowrate using the mechanical micromanometer.

8. Once the water temperature reaches 45 ^{o}C, set the desired water flowrate to the tray simulator, then make any small adjustments to the air flowrate.

9. Adjust the steam and gas fired boiler heating flowrates, by manual control, until a steady water temperature is reached.

10. After about ten minutes of steady operation has elapsed, initiate temperature data collection. During most of the test runs, height of clear liquid measurements are recorded from the manometer pressure tappings attached to the tray.

5.5.2 Normal Operation

11. Set the new air and water flowrates and return to instruction 8.

5.5.3 Shut-Down Procedure

12. Once the last temperature data collection is complete, close the steam valve and switch off the gas fired boilers, leaving the simulator in operation.

13. Switch off all electrical equipment, apart from the two water pumps and the air fan, and close the manual gas valves.

14. When the water in the sump tanks has cooled down to a temperature of about 20 °C and both sections of the heat exchanger are cool, the water pumps can be shut down.

15. Five minutes after stopping the water pumps the air fan can be shut down.

For the direct-observation experiments, using directional flow pointers, a similar procedure to that outlined above is used with the exception of those steps used to heat the water supply to the tray simulator.

Now that the test facility, the experimental techniques, and the safe operation of the tray simulator have all been described, the investigations into two phase flow patterns on 6.35 mm hole trays are reported in the subsequent chapters.

CHAPTER 6

EFFECT OF THE GAS DISTRIBUTION ON LIQUID FLOW PATTERNS

6.1 Introduction

At this point, it is worth noting that intermediate or fairly large sized hole trays, such as 6.35 mm holes, can have a peculiar effect on two phase flow patterns in that the gas flow can sometimes change the direction of liquid flow. For instance, Porter et al., 1987, reported severely distorted liquid flow patterns, in the form of highly "U -shaped" water temperature profiles from water-cooling experiments, on a 4.5 mm hole tray, of diameter 1.22 m, compared to that obtained on 1.0 and 12.0 mm hole sieve trays at the same operating conditions. In addition the effect of the gas flow, beneath a 6.35 mm hole tray (of diameter 2.44 m), on changing the direction of liquid flow was first reported by Ayvaz (1990). In some cases, the gas forced the liquid to circulate on the tray outlet.

There was no evidence in the open literature to suggest that this phenomenon has been observed before, and as far as is known, this is the first time that these observations have been made. This raises the question of whether intermediate sized hole trays are different to small hole (1.0 mm) or large hole trays (12.5 mm), and if this is the case, under what conditions does gas-influenced liquid flow occur? With this in mind, the scope of the work, presented in this chapter, was to investigate the effects of the gas flow pattern on the liquid flow pattern and to identify those parameters which influence the flow phenomenon. As will be shown, gas-influenced liquid flow patterns were produced at high air flow - low liquid flow rates and was caused by a non-uniform gas flow above the original gas distributor tray (i.e., the chimney distributor tray).

6.2 Studies into Gas Distribution Effects on Liquid Flow Patterns

The initial investigations on the 6.35 mm hole tray were designed to confirm the observations reported by Ayvaz, and to identify those conditions which may produce gas-influenced liquid flow patterns. This involved a series of gas-liquid contacting experiments using a wide range of air flow rates and a selection of weir loads for different

combinations of inlet downcomer clearances and outlet weir heights. Details of the flowrates and the tray configurations used are presented in Table 6.1.

Experimental Investigation	Air Velocity - ms^{-1}	Weir load - $10^4.m^3/m.s$	Inlet Gap - mm	Outlet Weir - mm
	0.878	18.52		
Direct-observation	1.243	27.78	10	10
using directional	1.523	37.04	20	20
flow pointers	1.760	46.30	50	50
	1.969	55.55		
Heat transfer	1.243	27.78	10	10
by	1.523	37.04	20	20
water-cooling	1.760	46.30	50	50
	1.969	55.55		

Table 6.1 Summary of flow rates and tray configurations used in the air - water contacting experiments.

6.2.1 Programme of Experiments

The programme of experiments was as follows:-

a) The study of air-water flow patterns by direct-observation using directional flow pointers, spread over many positions on the tray, and an overhead video camera.

b) Investigations into the effects of the biphase flow pattern on mass transfer using the water-cooling technique. By measuring the water temperature at over 100 positions across the tray, temperature isotherms were produced from computer processing of the temperature data since they are analogous to concentration profiles in distillation. The interpretation of the water temperature profiles in terms of enthalpy driving forces permitted the calculation of thermal point and tray efficiencies.

In each experiment, the effect of gas distribution on the developed liquid flow pattern was monitored using a wide range of air velocities at several fixed weir loadings.

6.2.2 Investigations by Direct-Observation

When flow pointers are partially submerged in the froth or spray on the test tray, they behave in a similar fashion to weather vanes used to show the direction of the wind. Thus, for each air-water flow rate combination, the localised biphase flow at thirty four positions across the tray was recorded by noting the direction of the painted arrow

indicators. A comprehensive set of experimental data was collected by the video recording of flow patterns and by plotting the direction of flow manually using a chart similar to that presented in Figure 5.2 of Chapter 5.

The format of the results presented below show the effect of increasing air velocity, for a fixed weir loading, on the developed liquid flow pattern, as well as the progressive increase in the inlet gap-outlet weir heights from 10 mm upto 50 mm.

Results by Direct-Observation

It is important to note from these experiments that at very low flowrates, the liquid is subjected to vigorous agitation by the bubbling action of the gas, which randomises the froth elements to a certain extent. Hence the sensitivity of the flow pointers for showing the direction of flow is partially reduced which explains the asymmetric appearance of flow pointers on the tray. Nevertheless, the flow pointers will be shown to be highly sensitive to changes in the flow pattern for a wide range of flow patterns.

For all the experiments, the liquid was completely aerated over the whole tray bubbling area. Water on entering the tray, from the beneath the inlet downcomer, was vigorously agitated by the bubbling action of the air passing through the liquid and spread out so as to completely occupy those areas bounded by the changing width of the tray. That is, the biphase expanded to fill the segmental regions at the sides aswell as across the horizontal plane between the downcomers.

Flow Pattern Results at the Inlet Gap and Outlet Weir of 10 mm

The results showed forward flow on the horizontal plane of the tray between the inlet downcomer and outlet weir and a stagnant region at the sides of the tray, (see Figure 6.1a). That is, the biphase was in between slow foward flow and a reverse flow which in some circumstances can lead to circulation of the liquid.

Forward flow between the weirs was indicated by sixteen flow pointers pointing in the forward direction towards the outlet weir. A few exceptions were noted where localised biphase swirling was observed. This behaviour was mainly confined to the inlet half of the tray where the biphase was expanding to fill the tray width. At the low air velocity range of 0.878 - 1.243 ms^{-1}, for each fixed weir loading, the biphase close to the column wall towards the ends of the outlet weir, appeared to be non-moving. That is, a small area of very slow-moving reverse flow was observed, as shown by two or three flow pointers, on each side of the tray, pointing normally towards the column wall or

backwards towards the tray inlet, and occupied less than 10% of the total tray area.

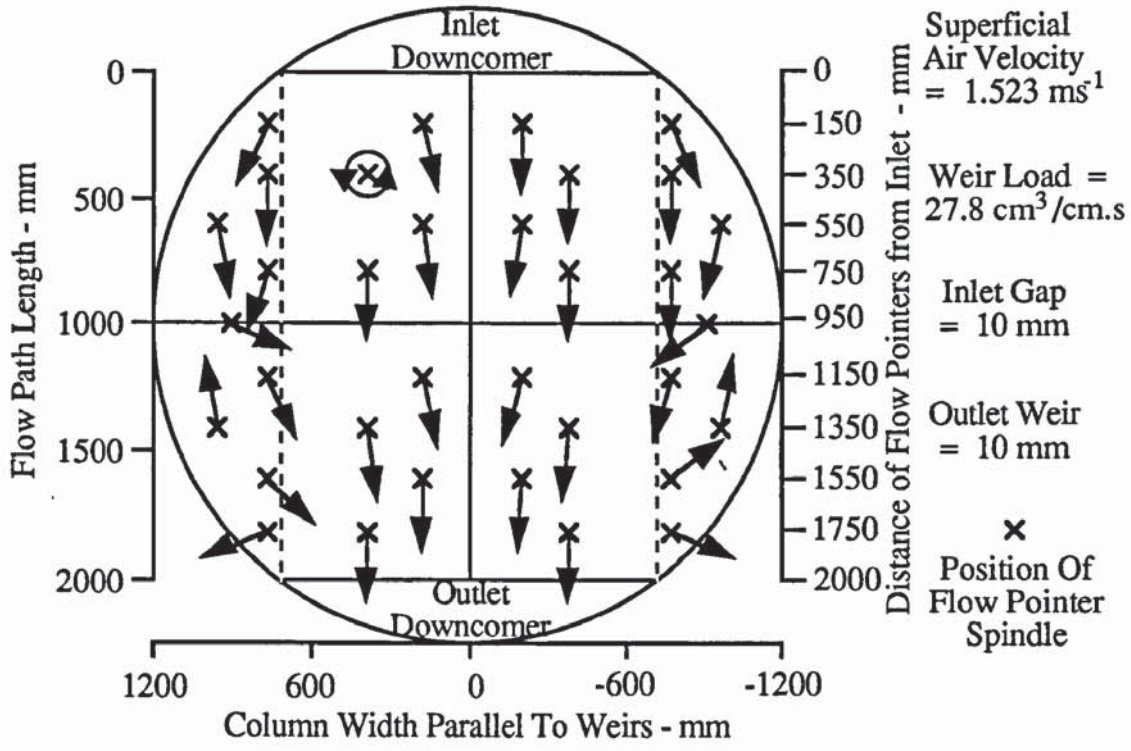

Figure 6.1a Flow pointer arrangement showing forward flow with very little reverse flow.

Although the flow pointers do not give a measure of the velocity profile for the biphase flow, it can be discerned qualitatively that a bulk velocity profile exists within the biphase forward flow. The froth was observed to be moving fastest along the centre line between the downcomers and slowest over the longer flow path at the sides of the tray. A summary of the flow pattern results, using the notation defined for different flow patterns in Chapter 5, are presented on a modified vapour load factor verses weir load diagram as shown in Figure 6.1b. The air-water flow rates and flow pattern information are presented in a matrix format. Overall, no gas distribution effects were observed on the tray liquid flow pattern.

Flow Pattern Results at the Inlet Gap and Outlet Weir of 20 mm

A change in the direction of liquid flow caused by the air flow was observed for the first time when the tray was configured with an inlet gap and outlet weir height of 20 mm. As with the above case, forward flow with an underlying bulk velocity distribution profile was produced over most of the tray inlet section for all flow rates. On the tray outlet section, however, reverse flow occupied most of the segmental regions and flowed faster

than that observed in the previous experiments.

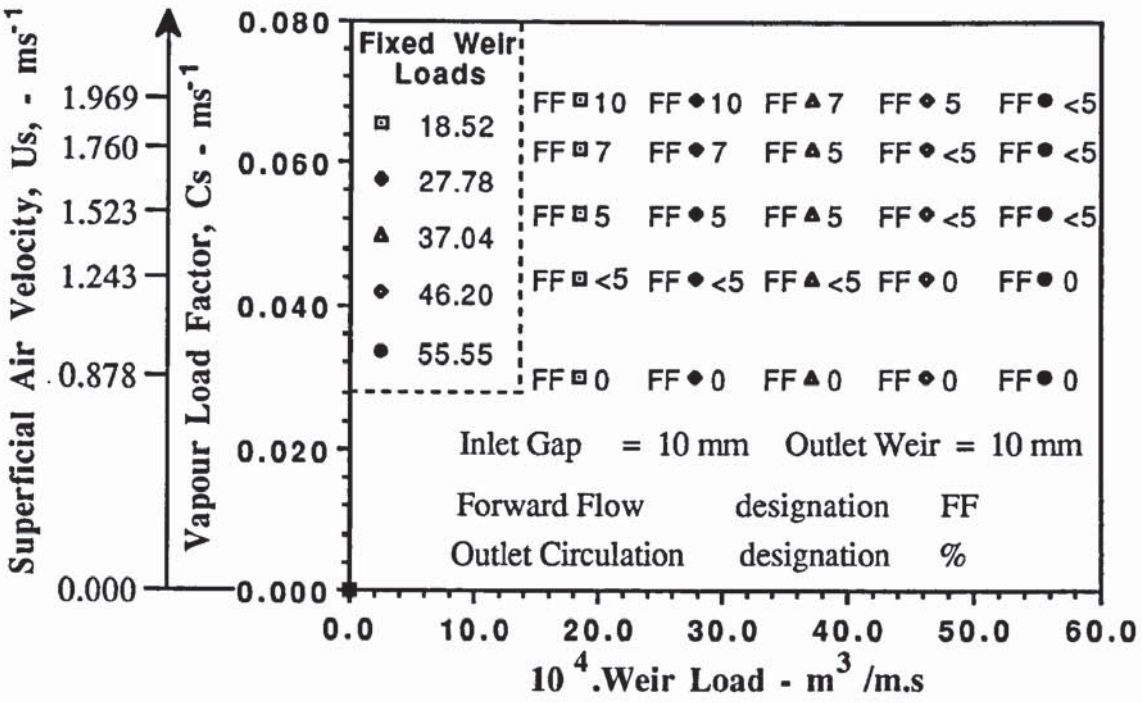

Figure 6.1b Summary of flow patterns on a load factor verses weir load diagram.

At fixed weir loadings of upto 27.78 $cm^3/cm.s$ circulating biphase flow was observed at the sides of the outlet tray section such that the froth near the ends of the outlet weir flowed backwards round the column wall towards the inlet. On encountering fresh liquid from the inlet, the froth at a distance of between 1050 and 1150 mm from the inlet was observed to perform a "U-turn" and flow forward towards the ends of the outlet weir where the rotating biphase flow started again, (see Figure 6.2a).

The velocity of circulating flow increased steadily as the superficial air velocity was increased from 1.243 ms^{-1} to 1.969 ms^{-1} and occupied between 10 to 15% of the total tray area. Outlet circulation was observed by two or three flow pointers on each side pointing backwards. In addition two flow pointers in the middle of each tray segmental region were pointing towards the tray centreline, thus indicating the rotational nature of the biphase flow.

The observation that the rate of circulation increased as the superficial air velocity was increased, for a fixed weir loading, suggests that the gas flow beneath the tray may affect the direction of liquid flow on the tray. A summary of the flow pattern results obtained for this tray configuration are presented on the modified load factor verses weir load

diagram in Figure 6.2b.

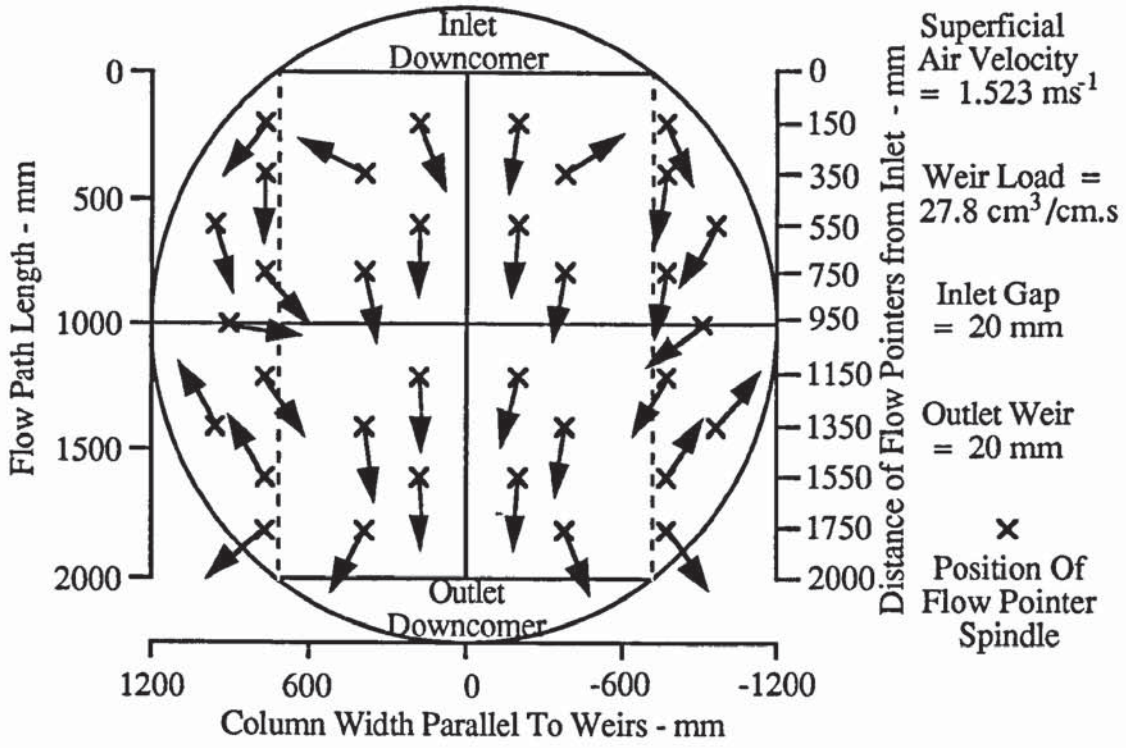

Figure 6.2a Flow pointer arrangement showing forward flow associated with 10% circulation.

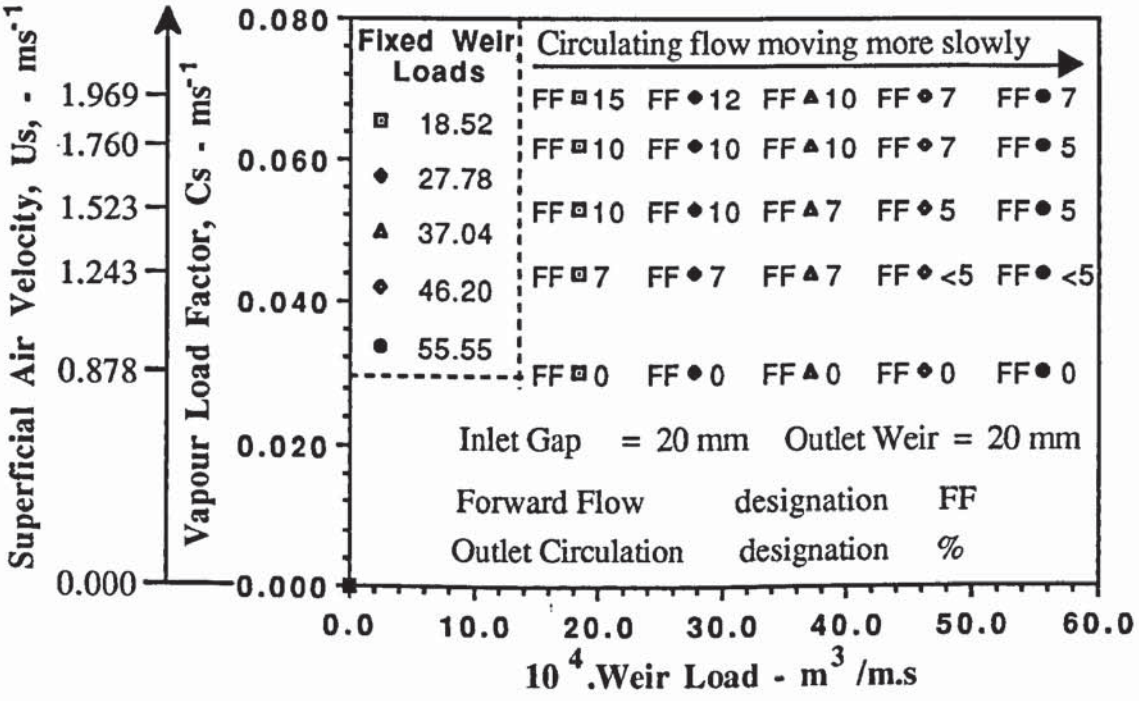

Figure 6.2b Summary of flow patterns on a load factor verses weir load diagram.

Flow Pattern Results at the Inlet Gap and Outlet Weir of 50 mm

In this set of experiments, the effect of the gas distribution on the liquid flow produced a remarkable two phase flow pattern. For a fixed low weir loading, two distinct, symmetrical circulating, biphase flow patterns on the outlet tray section were formed. This was confirmed by several flow pointers pointing sideways and backwards towards the inlet as shown in Figure 6.3a.

As the superficial velocity was increased from 0.878 ms^{-1} to 1.523 ms^{-1}, the circulating flow occupied a greater area of the tray outlet section such that liquid was forced from the tray sides towards the tray centreline. Further increases in the air velocity, enhanced the momentum and intensity of the circulating froth. This can be deduced from two continuously rotating flow pointers on each side of the tray outlet.

For several air-water flow rates, the circulating flow extended over a distance of approximately 1100 mm and was estimated visually to occupy a maximum of 30% of the total tray area. This was determined from the circulating flow occupying approximately one-fifth of the outlet tray quadrants (the area of one quadrant is equal to 25% of the total tray area) as well as approximately one third of the segments at the sides of the tray. (The total area of the tray segments, of a 60% weir to diameter ratio tray setup, has been calculated to be 30% and therefore one third of this maximum value is equal to 10%.)

The powerful circulating flow induced a narrow band of forward flow along the centre line of the tray and caused reverse liquid flow around the column wall towards the ends of the inlet downcomer. This was confirmed by two flow pointers pointing backwards at the ends of the inlet downcomer. Flow pointers pointing towards the centre line on the inlet tray section indicated the converging nature of the forward flowing froth. The fairly rapid velocity of forward flow was also noted and this may be attributed to the high velocity of circulating flow "squeezing" the froth over the outlet weir.

Although a maximum of 30% circulating froth occurred at several air-water flow rates, it was noticed that the velocity of circulating froth was less than that at weir loads above 37.04 $cm^3/cm.s$ compared to that at the lower fixed weir load settings. A summary of all the flow patterns generated for the inlet gap, outlet weir configuration of 50 mm is presented in Figure 6.3b.

From the above observations, it appears that it is possible for the gas flow to have an effect on the direction of liquid flow on a tray.

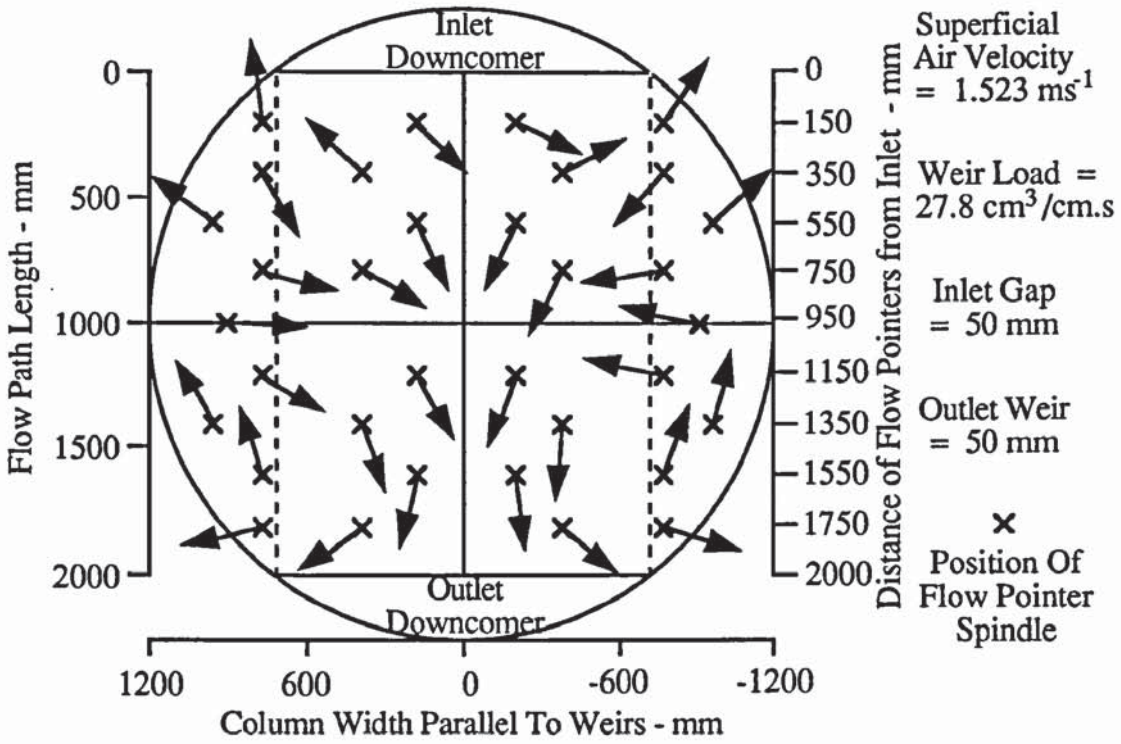

Figure 6.3a Flow pointer arrangement showing a gas-influenced circulating flow pattern occupying the maximum area of 30%.

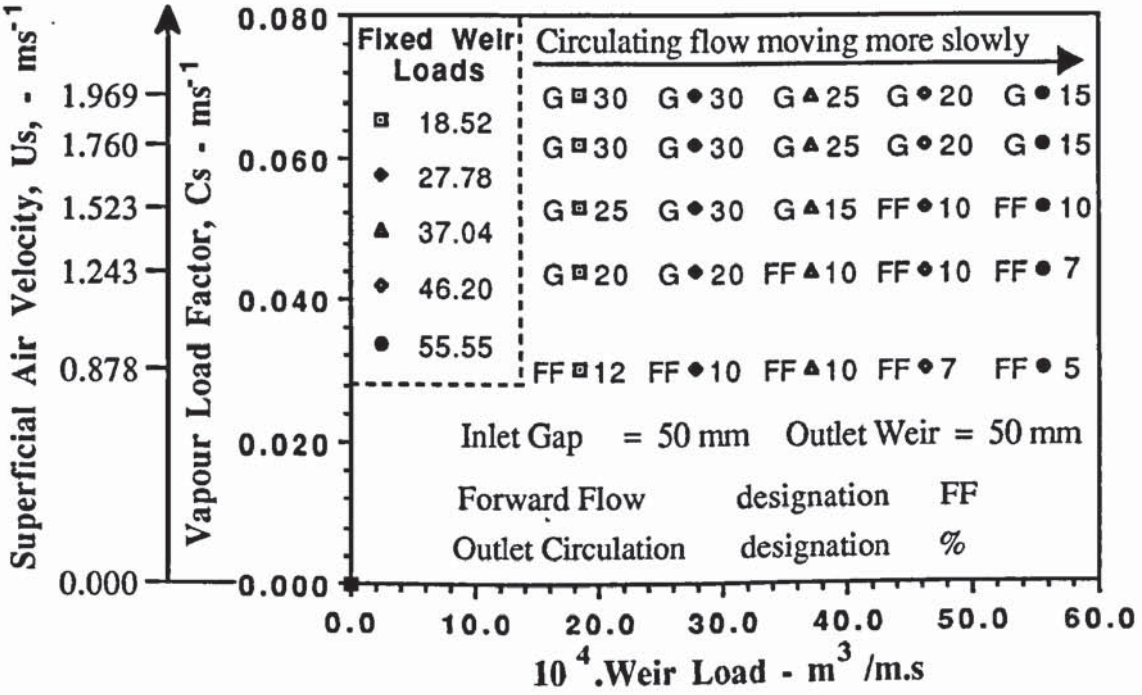

Figure 6.3b Summary of flow patterns on a load factor verses weir load diagram.

It is possible that the circulating flow may have been exacerbated by certain amount of reflection of the biphase from the relatively large outlet weir height of 50 mm. However, on repeating the above experiments using the same inlet gap height of 50 mm and reducing the outlet weir to zero so that reflection by the outlet weir was eliminated, similar but less intense gas-driven liquid circulation flow patterns were observed on the tray outlet. This suggests that a limited amount of biphase reflection contributes to the overall outlet tray circulation.

Discussion and Explanation of Results

At this stage, the gas-liquid contacting experiments have shown that the gas flow, beneath the tray, changes the liquid flow pattern. This was most severe when the inlet gap and outlet weir heights were set at 50 mm, and least severe for the inlet gap/outlet weir combination of 10 mm.

At large froth heights, the gas forced the liquid to circulate on the outlet tray section. This became larger and more powerful at high air flow rates and low weir loadings, such that, in some cases, the gas-driven liquid circulating flow forced liquid backwards towards the ends of the inlet downcomer. In contrast, a non-uniform forward flow pattern was obtained at low froth heights where the mobile froth moves faster along the middle of the tray between the downcomers compared with that at the sides of the tray.

The controlling mechanisms which may explain these observations are:

a) The gas flow pattern in the space beneath the test tray.

b) The liquid entrance velocity beneath the inlet downcomer clearance, and the froth height on the tray particularly in the outlet region.

An explanation into the cause of circulating liquid is that the gas flow circulates beneath the test tray. The column simulator was fitted with a gas distributor, (see Figure 4.6 in Chapter 4), from which the air entered the tray column shell through 130 risers, of diameter 50 mm, on a plate situated immediately above the air distribution shell. Previous work had shown that the air flow emerging from the chimney tray was essentially uniform.

However, since the diameter of the test tray is 2.44 m, and is situated 1.00 m above the distributor tray, it is possible that a circulating air flow pattern might develop between the two trays. Furthermore, it is quite possible that the air enters the tray at an angle relative

to the horizontal plane of the tray deck, and thus change the direction of liquid flow.

The experimental results show that the liquid entrance velocity to the tray, from the inlet downcomer, and froth height over the tray bubbling area, may also have important implications on gas-influenced liquid flow patterns. Thus the following hypothesis is proposed:-

On entering the tray, the inlet liquid velocity, through the large inlet downcomer clearance of 50 mm was much less than that produced from smaller inlet gap heights. Furthermore, as the liquid crossed the tray from the inlet to the outlet, the horizontal velocity of the liquid decreased until a critical point was reached where the magnitude and direction of the liquid flow changed to produce reverse flow. Factors which caused this change included the gas resistance rising through the froth, and the large froth height produced using a large outlet weir. This, in turn, produced a large liquid head across the tray which resulted in a low liquid velocity.

These effects coupled with the assumption that the gas enters the tray at an angle may have produced a reverse flow of liquid. The experimental observations show that the gas-influenced reverse flow became powerful enough to force the liquid to circulate in a closed loop on the tray outlet section with minimal replenishment of liquid from the bulk forward flow of froth.

With the tray configured at smaller inlet gap and outlet weir heights, the above mentioned effects were substantially reduced. That is, the resistance of the rising gas through the liquid was less significant owing to the faster liquid velocity from the smaller inlet downcomer clearances and the reduced gas residence time within the lower froth height.

The effect of gas-influenced and non-gas-influenced liquid flow patterns on mass transfer and tray efficiency in distillation are considered in the next section.

6.2.3 Investigation by Water-Cooling

From the above direct-observation experiments it is expected, that there will be a significant difference in distillation mass transfer between the gas-influenced and non-gas-influenced liquid flow patterns. The purpose of this section is to investigate these differences between a situation where the liquid circulates and one where it does not circulate using the water-cooling technique.

The water-cooling technique involves temperature profiling and the calculation of thermal

efficiencies, from enthalpy driving forces, for the same flow conditions used in the previous section. Complete descriptions of the water-cooling technique as well as the safe operation of the test facility are contained in Chapter 5.

The flow rate conditions and tray configurations, used in the previous section, were applied to this set of air-water contacting experiments.

To interpret the effects of gas-influenced or non-gas-influenced liquid flow patterns on the water temperature field (analogous to concentration profiles in distillation), use is made of reduced temperature profiles, so as to compare experimental results on a like basis. By definition, the water entering the tray is arbitrarily assigned a reduced temperature, T_r, of 1.0, while the water leaving the tray has a reduced temperature in between 1.0 and 0.0. In addition, the wet bulb temperature of the entering air is the minimum temperature attained by the air-water test system.

During initial water-cooling tests on the 6.35 mm hole tray, the reduced temperature profiles revealed a degree of non-symmetry on the operating tray in that the liquid tended to be colder on the right hand side. This non-symmetry may have been caused by the tray level on the right hand side being slightly lower than that on the left. Further investigation into the tray deck sheets and the lattice beam support frame on the right hand side showed that the support frame was slightly twisted and was found to be 5 mm lower than that on the left. To overcome this problem, the level of the tray deck was carefully raised by means of thin alumnium spacers, placed onto the lattice support beam framework, until the tray deck was positoned horizontally. This was determined using a large calibrated spirit level since a standard spirit level was unsuitable for the task.

During several test runs, there was some improvement in the temperature profiles on the right hand side, but despite these efforts, the reduced temperature remained slightly lower than that on the left, particularly at the lowest flow rates. This demonstrates that the water-cooling technique is sensitive to tray levelness particularly at the lowest flowrate range. Hence the temperature profiles in the following set of experiments can be interpreted by a viewing a particular temperature profile as one of a series of profiles, so that a temperature profile pattern can be seen beneath the non-symmetry.

Flow Pattern Results

In general, temperature profile results show that the longer the liquid remains on a tray, the cooler it becomes. Thus, the coldest liquid is found on tray areas where there are long liquid flow paths containing liquid which is either moving slowly forward, is stationary,

or is circulating. This corresponds to the longest liquid residence time as a result of the greater gas bypassing through the liquid in these regions compared to that on other parts of the tray. This reduces the driving force for mass transfer which yields a low tray efficiency.

A set of reduced temperature profile diagrams for each air-water flow rate combination and inlet gap/outlet weir configuration are presented in Appendix 4.0. In the following subsections, a selection of black and white temperature field diagrams are presented which show the effect of the biphase flow patterns on the temperature isotherms and the mass transfer driving forces. A review of the guidelines required to interpret the reduced temperature profiles is given in Section 5.3.6 of Chapter 5.

Discussion of Results

Temperature Profile Isotherms for the Inlet Gap and Outlet Weir Configuration of 10mm.

For all experiments, the complex gas interactions with the liquid flow on the test tray was reflected in the highly complicated displays of reduced temperature isotherms. This is in direct contrast to the staight or "U-shaped" profiles obtained in experiments where the influence of the gas flow on the liquid flow is less complex, (see Chapters 8 and 9). A summary of the temperature isotherms is presented on a modified load factor verses weir load diagram as shown in Figure 6.4.

Overall, a combination of mixed or confused isotherms and narrow elongated "U-shaped" isotherms were produced for all flow rates. Mixed isotherms consist of narrow "U-shapes", inverted "U-shapes", parallel isotherms, and straight isotherms adjacent to the tray boundary which, in many cases, "connect" to the column wall.

The temperature profiles produced during these experiments are best explained by example using the isotherm displays presented in Figures 6.5a and 6.5b.

The two dominating features of the temperature isotherms, presented in Figure 6.5a are the large, elongated "U-shaped" isotherms and two adjacent inverted "U-shaped" isotherms. The elongated "U-shaped" isotherms are situated along the centreline between the downcomers and represents warmer liquid compared to other parts of the tray. This corresponds to faster moving liquid along the middle of the tray which occupies a distance of 1400 mm from the inlet downcomer.

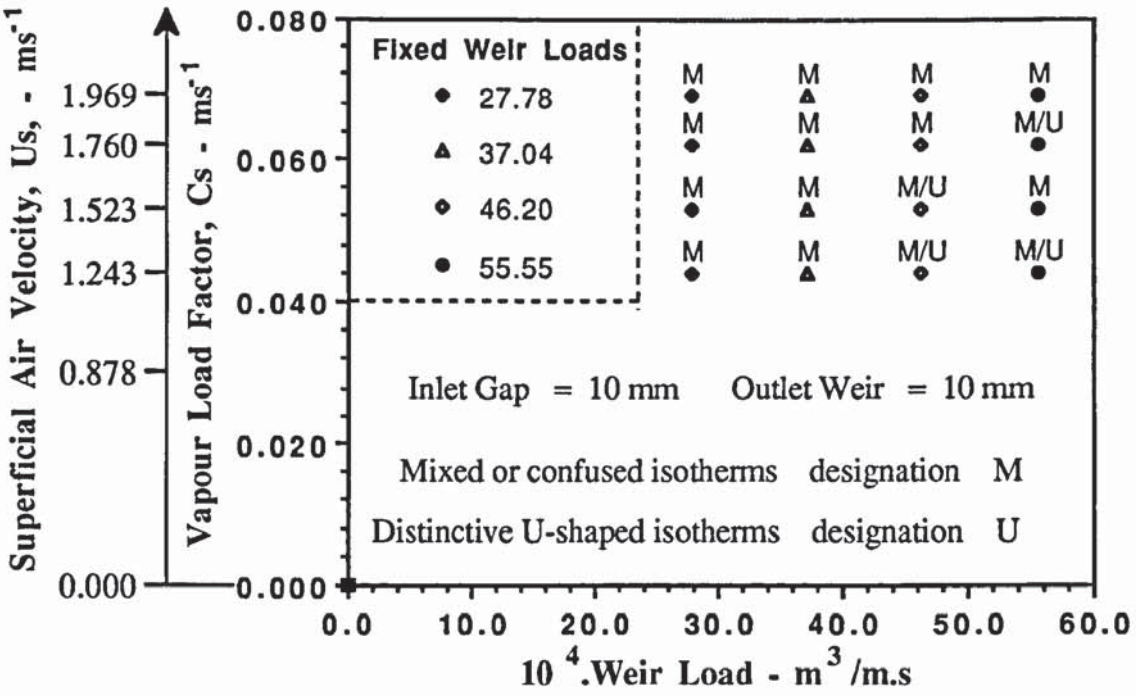

Figure 6.4 Summary of isotherm profiles on a load factor verses weir load diagram.

The two inverted "U-shaped" isotherm profiles extend from the outlet weir upstream to a distance of approximately 400 mm from the inlet downcomer. Figure 6.5a shows that the inverted "U-shaped" regions were colder than that in the central elongated "U-shape". This can be quantified from the lower reduced temperature, T_r, values ranging from 0.700 to 0.550, and the comparatively sharp increase in the temperature gradient either side of the centreline.

On the segmental regions at the sides of the tray, the "swept-back" isotherms, of reduced temperature 0.600 to 0.500, indicate colder liquid which is caused by slow forward flow over the longer liquid flow paths. The coldest liquid on the tray was on the outlet tray segments at the ends of the outlet weir and was represented by reduced temperature isotherms "linked" to the column wall. This corresponds to the stationary or slow biphase reverse flow observed in the flow pointer experiments. It is worth noting that the reduced temperature of the stagnant biphase at low air velocities (i.e., approximately 0.475) was less than the reduced temperature of liquid flow over the outlet weir which causes a reduced driving force for mass transfer. This will have an adverse effect on tray efficiency. In general, these observations were made at the low air velocity range, upto 1.523 ms^{-1} for all the fixed weir load settings.

A similar pattern of temperature isotherms were produced at the high air flow rates of upto and including 1.969 ms^{-1} (refer to Figure 6.5b), with the exception of the following:-

a) The size of the elongated "U-shapes" and adjacent inverted "U-shapes", in front of the inlet downcomer had decreased.

b) The number of mixed or confused isotherms, of reduced temperature 0.725 to 0.600 on parts of the horizontal plane between the downcomers, in addition to the tray segments, revealed colder slower moving liquid. This suggests a non-uniform flow of liquid across the tray.

c) As in the previous case, the stagnant or reverse biphase flow at the ends of the outlet weir corresponds to the coldest liquid on the tray, (i.e., the reduced temperature T_r is equal to 0.400).

Overall, temperature profiling is a sensitive method of detecting the effects of flow patterns on mass transfer.

Temperature Profile Isotherms for the Inlet Gap and Outlet Weir Configuration of 20 mm

The results of the water-cooling experiments on the test tray configured with an inlet gap and outlet weir height of 20 mm, are very similar to those obtained in the previous section. A summary of the reduced temperature profile isotherms, presented in Figure 6.6, show that for most air-water flow rates, there was a combination of large elongated "U-shaped" isotherms and confused isotherms.

The temperature profiles are similar to that produced at the inlet gap and outlet weir heights of 10 mm, except for the following.

The narrow elongated "U-shaped" profiles, in Figure 6.7a, consist of more tightly packed reduced temperature isotherms and extend over a distance of 1600 mm from the inlet downcomer . In addition, a high density of isotherms, which extend from the inlet tray segments towards the centre of the outlet weir, are approximately straight and parallel to the tray boundaries on the outlet tray section. These regions correspond to colder liquid which in turn represents slower forward flow across the tray.

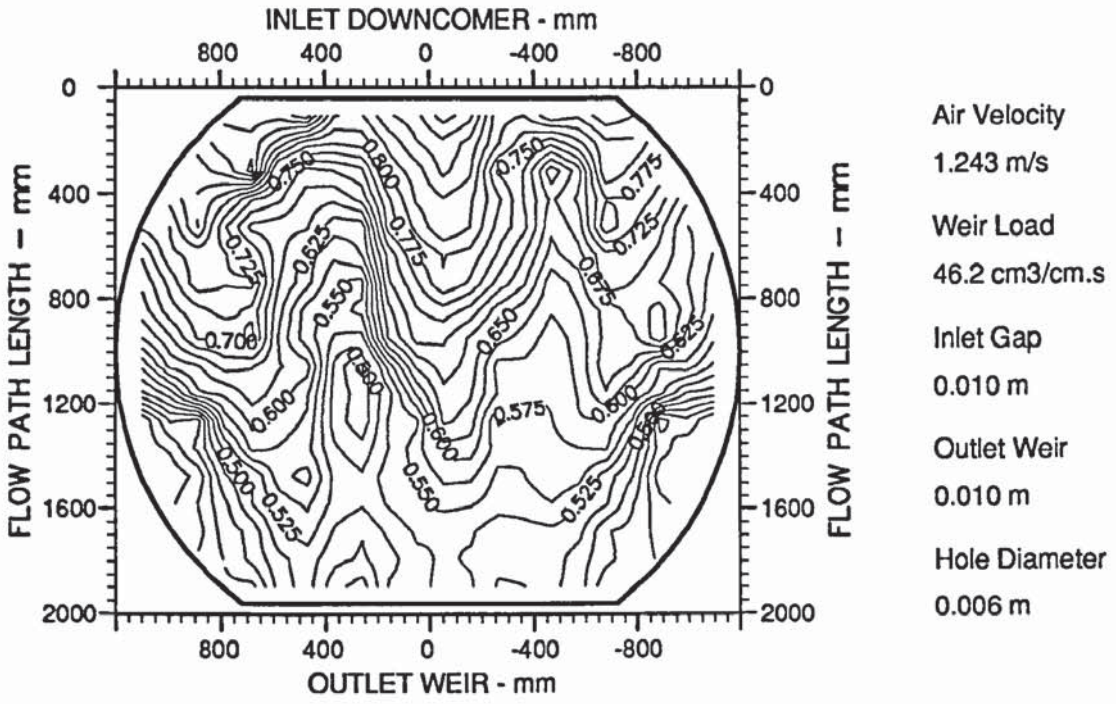

Figure 6.5a Two dimensional reduced temperature profile diagrams at the low air flow rate range which shows mixed or confused isotherms (designation M).

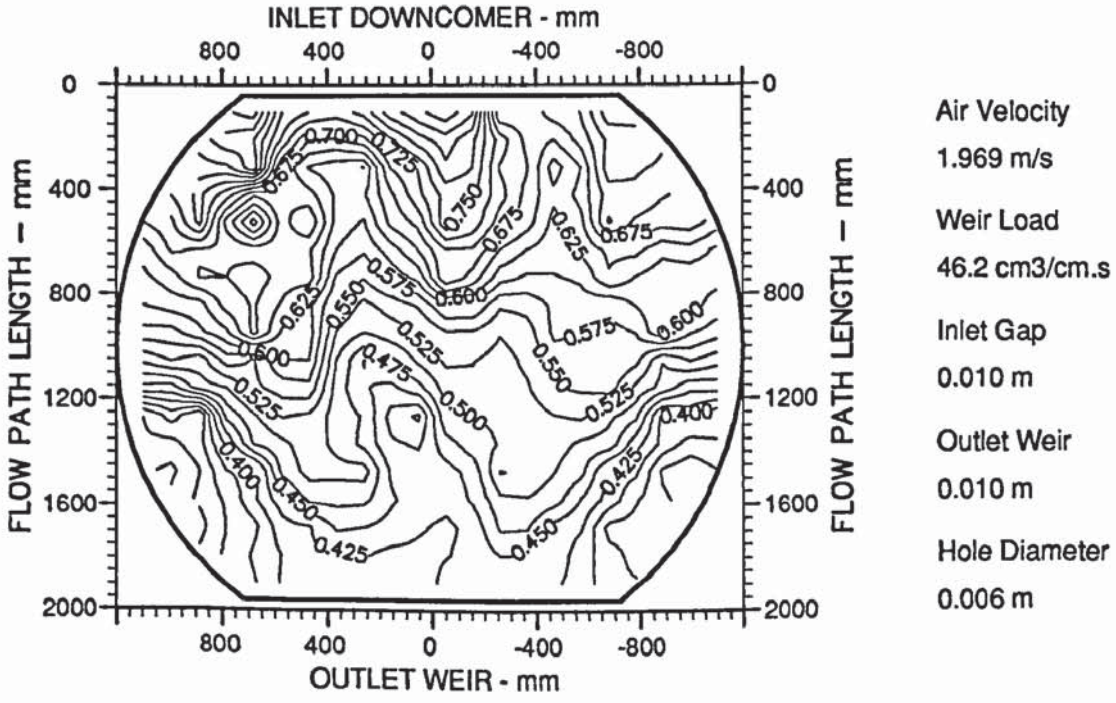

Figure 6.5b Two dimensional reduced temperature profile diagrams at the high air flow rate range which shows mixed or confused isotherms (designation M).

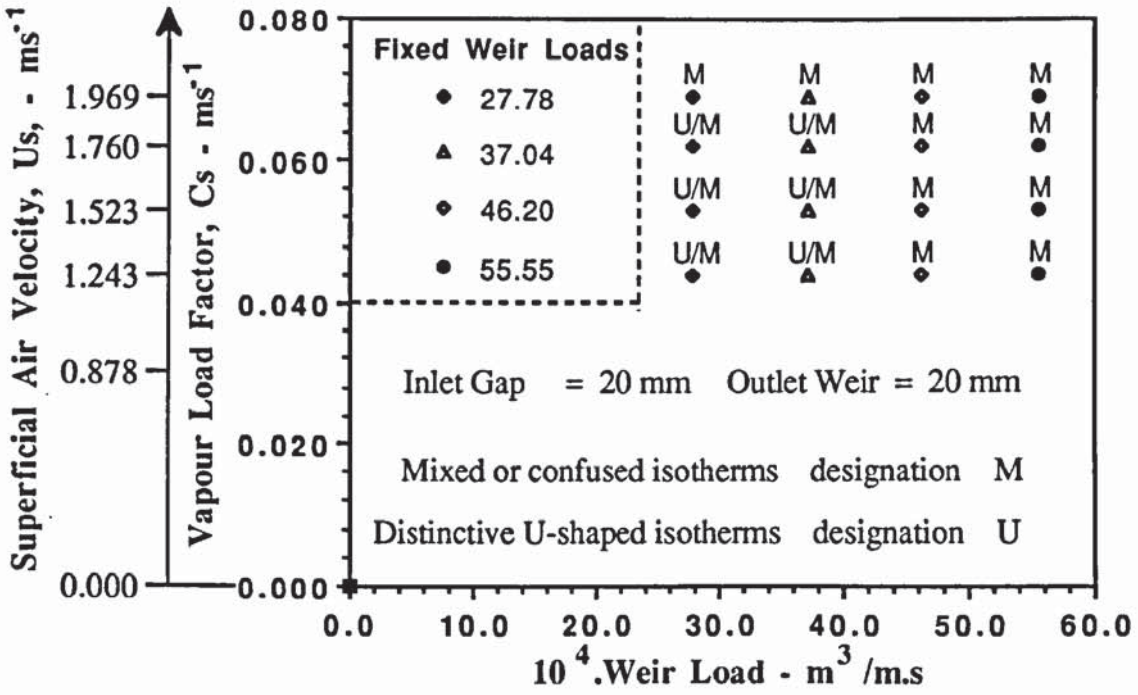

Figure 6.6 Summary of isotherm profiles on a load factor verses weir load diagram.

The coldest liquid regions were found on the outlet tray segments towards the ends of the outlet weir. These closed looped isotherms, of reduced temperature 0.250 (see Figure 6.7a), correspond to gas-influenced liquid circulation, which, in several cases, occupied 10% but not more than 15% of the tray area. Circulating flow has a longer liquid residence time on the tray which, in turn, has an adverse effect on mass transfer and tray efficiency. These observations were made over a wide range of air flow rates, upto 1.760ms^{-1}, at the lowest fixed weir load loadings.

At the superficial air velocity of 1.969ms^{-1}, the gas cross flow through the horizontal liquid flow resulted in a "flattening" of reduced temperature isotherms as shown in Figure 6.7b. Hence the size of the "U-shaped" isotherms along the tray centreline had diminished such that they only extend to a distance of 850 mm from the inlet downcomer.

The majority of temperature isotherms on the outlet section, towards the outlet weir in Figure 6.7b, are approximately straight and parallel to the downcomers, whereas the isotherms "tail-off" when extended to the segmental regions at the sides of the tray. This indicated that the biphase forward flow across the longer liquid flow path on the segmental regions was slower than that in the middle of the tray.

The coldest liquid, of reduced temperature 0.225, on the outlet tray segments near the ends of the outlet weir, corresponds to gas-influenced circulation of the liquid. The

reduced temperature of the circulating froth is less than that of the liquid flow over the outlet weir (i.e., approximately 0.300), thus confirming a reduction in the driving force for mass transfer within the circulating regions. Similar observations were made at air flow rates above 1.760 ms^{-1} and at the higher fixed weir load settings.

Overall, the elongated "U-shaped" isotherms and mixed isotherms show that the direction of horizontal liquid flow across the tray is sometimes changed by the gas flow such that liquid is forced to circulate over a small area on the outlet tray section.

Temperature Profile Isotherms for the Inlet Gap and Outlet Weir Configuration of 50 mm

Gas-influenced liquid flow patterns had a substantial effect on the temperature profiles, when the inlet gap and outlet weir heights were set at 50 mm. In most experiments, the temperature isotherms were severely distorted and are summarised in Figure 6.8 below.

Since gas-driven liquid circulation was observed for most flow rates in the direct-observation experiments, the pattern of temperature isotherms produced over the whole tray are essentially the same. Hence the generated temperature isotherms can be summarised as follows:-

At the low air velocity range of upto 1.523 ms^{-1}, for a given fixed weir loading, the gas-driven liquid circulation was represented by a large number of very severe, highly packed "U-shaped" isotherms complemented by large closed looped contours.

In many cases the U-shapes occupied more than three quarters of the flow path length (i.e., approximately 1600 mm). These tightly packed elongated "U-shaped" isotherms represents warmer, faster moving liquid along the centreline of the tray. Liquid was effectively "squeezed" over the outlet weir of the tray by the two powerful gas-driven liquid circulation zones.

The closed looped isotherms represent the gas-driven liquid circulation areas which occupied most of the outlet tray section. The closed looped isotherms extend from the ends of the outlet weir to the column wall on the inlet half of the tray and represent the coldest liquid regions on the tray (T_r = 0.300 - 0.275). It is these regions that have an adverse effect on the driving force for mass transfer.

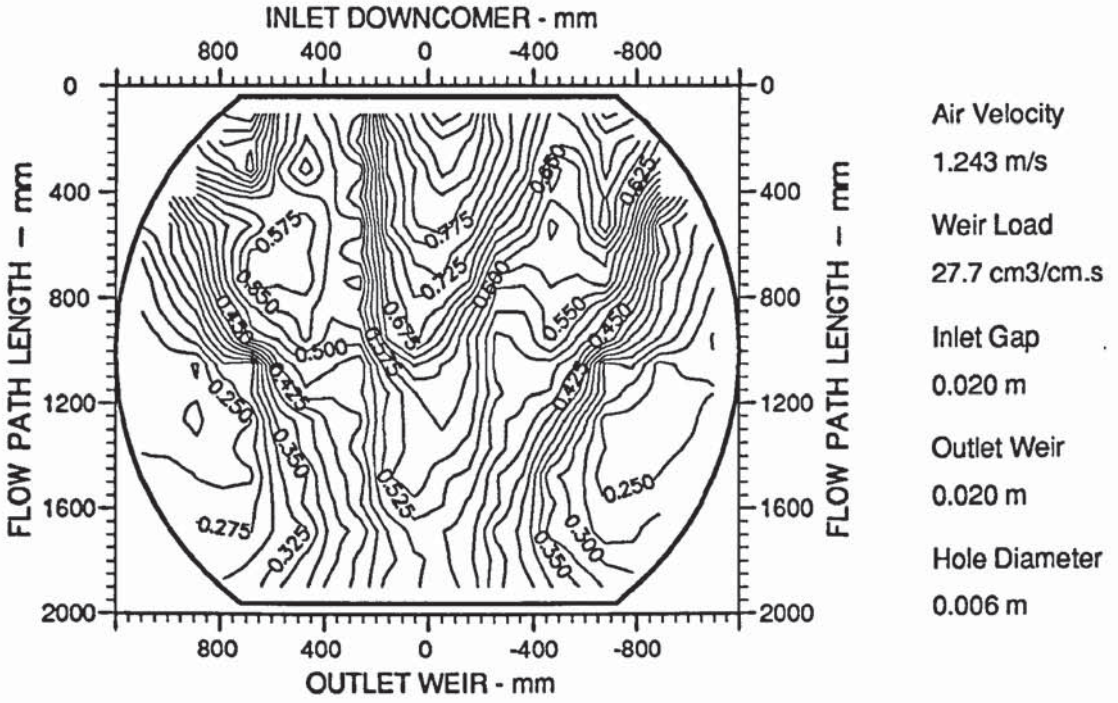

Figure 6.7a Two dimensional reduced temperature profile diagrams at the low air flowrate range which shows mixed or confused isotherms (designation U/M).

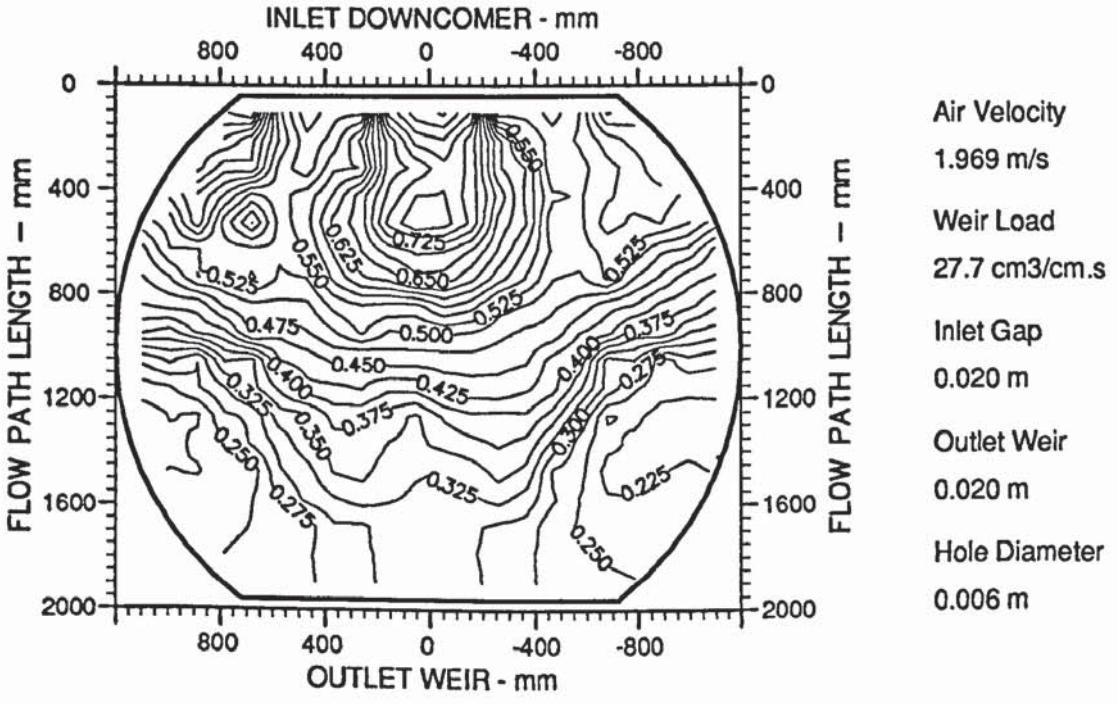

Figure 6.7b Two dimensional reduced temperature profile diagrams at the high air flowrate range which shows mixed or confused isotherms (designation M).

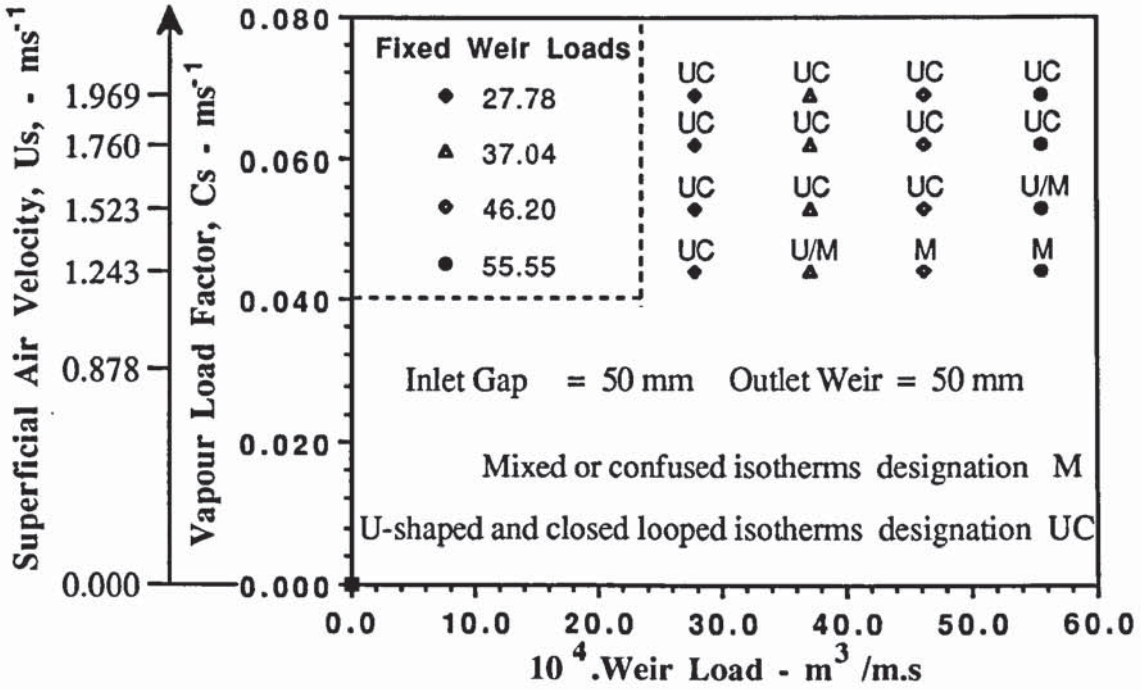

Figure 6.8 Summary of isotherm profiles on a load factor verses weir load diagram.

At the higher flow rate range, and low fixed weir loadings, the above observations are the same except that the size of the closed looped isotherms have increased such that they correspond to a maximum of 30% gas-driven liquid circulation. In addition, the large closed looped contours have "squeezed" the "U-shaped" isotherms to produce very severe elongated "U-shaped" isotherms. Examples of the above observations are presented in Figures 6.9a and 6.9b.

At the higher fixed weir load settings, the pattern of temperature isotherms changed slightly in that there was a small increase in the number of mixed temperature profiles on the tray, particularly at the low air flowrate range upto 1.523 ms^{-1}. This corresponds to the observation of forward flow associated with gas-driven liquid circulation of upto 10% on the oulet tray section.

Summary of Temperature Profile Results

The temperature profiles, obtained by water-cooling, during the gas-liquid contacting experiments , consisted of mixed or confused isotherms, large elongated "U-shaped" isotherms, and closed looped isotherms. The mixed temperature profiles, which contained normal "U-shapes", inverted "U-shapes" and isotherms parallel to the downcomers, were produced at the smaller gap and weir heights of 10 and 20 mm. The temperature profiles were severely distorted despite the better distribution of gas and its

effect on the liquid flow compared with that produced at large froth heights.

With the larger inlet gap and outlet weir configuration of 50 mm, the gas-driven liquid circulation showed up as very severe, highly packed "U-shaped" isotherms complemented with closed looped contours. In several cases where gas-driven circulation of the liquid was greater than 20%, the isotherms extended from the tray outlet to the column wall on the inlet half of the tray. The closed looped isotherms represent the coldest regions on the tray, thus reducing the driving force mechanism for mass transfer which ultimately leads to a low tray efficiency.

A discussion of the thermal efficiencies, obtained from enthalpy driving forces derived from the water temperature measurements on the tray, is presented below.

Discussion of Thermal Efficiency Results

The temperature profiles, obtained from water-cooling, are used to calculate point and tray efficiencies. The procedure for the calculation of thermal efficiencies is described in Section 5.3.5 of Chapter 5. The point efficiency, E_{OG}; tray efficiency, E_{MV}; and the ratio of E_{MV}/E_{OG} results for all the experiments are presented in Tables 6.2, 6.3 and 6.4.

The discussion presented below will compare and contrast the calculated efficiencies and assess the implications of the generated flow patterns on the efficiency results.

For normal trays, E_{OG} is calculated in terms of the number of gas phase transfer units, N_G ($= k_G'.a.t_G$), which verifies that the gas phase resistance to mass transfer may reduce efficiency. This was indeed the case for all of the experiments since the E_{OG} results showed a steady decrease as the superficial air velocity was increased for each fixed weir loading. The main reason may have been that the velocity of the air crossflow through the liquid was greater than the velocity of the horizontal liquid flow for a particular weir loading. This decreased the gas residence time within the froth dispersion, (i.e., $t_G = h_F/u_s$), which resulted in a reduced driving force for mass transfer and hence a lower point efficiency. Similar arguments apply to the E_{OG} results calculated at the higher inlet gap/outlet weir settings of 20 mm, 20mm; and 50 mm, 50 mm.

At low froth heights, the gas residence time within the froth is less than that at larger froth heights. Thus, the highest E_{OG} results were obtained at the inlet gap and outlet weir height of 50 mm (i.e., an average of 83.7%), whilst, E_{OG} results were lowest at the inlet gap and outlet weir heights of 10 and 20 mm (i.e., an average of 74.8% and 72.6% respectively).

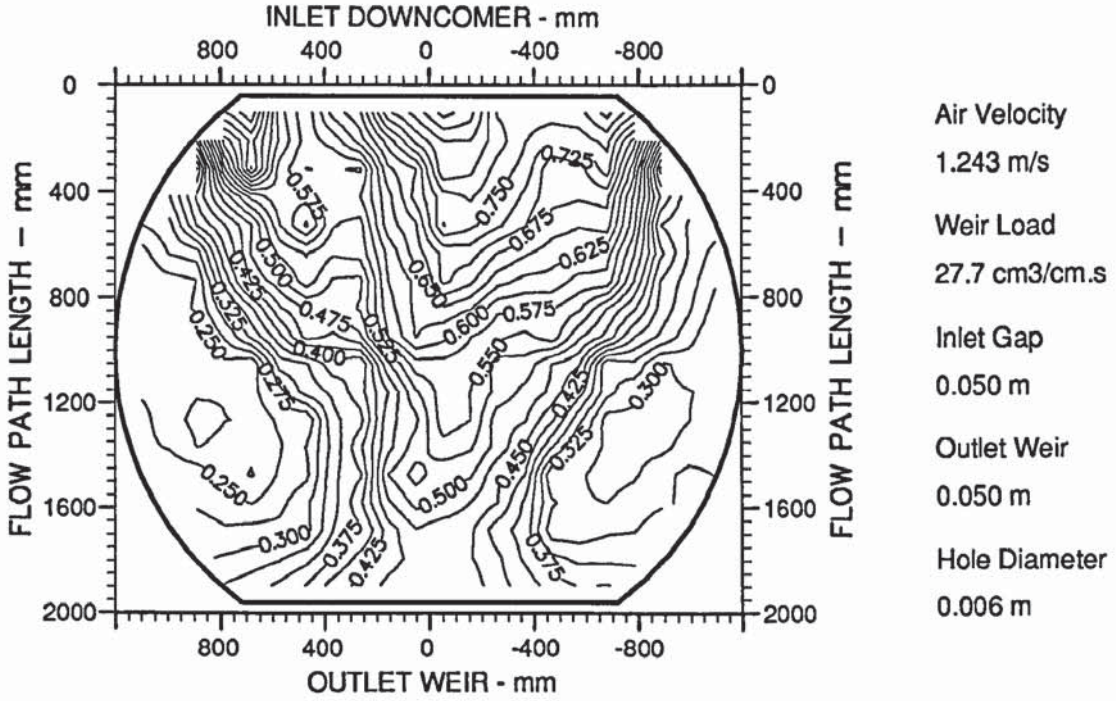

Figure 6.9a Two dimensional reduced temperature profile diagrams showing "U-shaped" and closed-looped isotherms (designation UC).

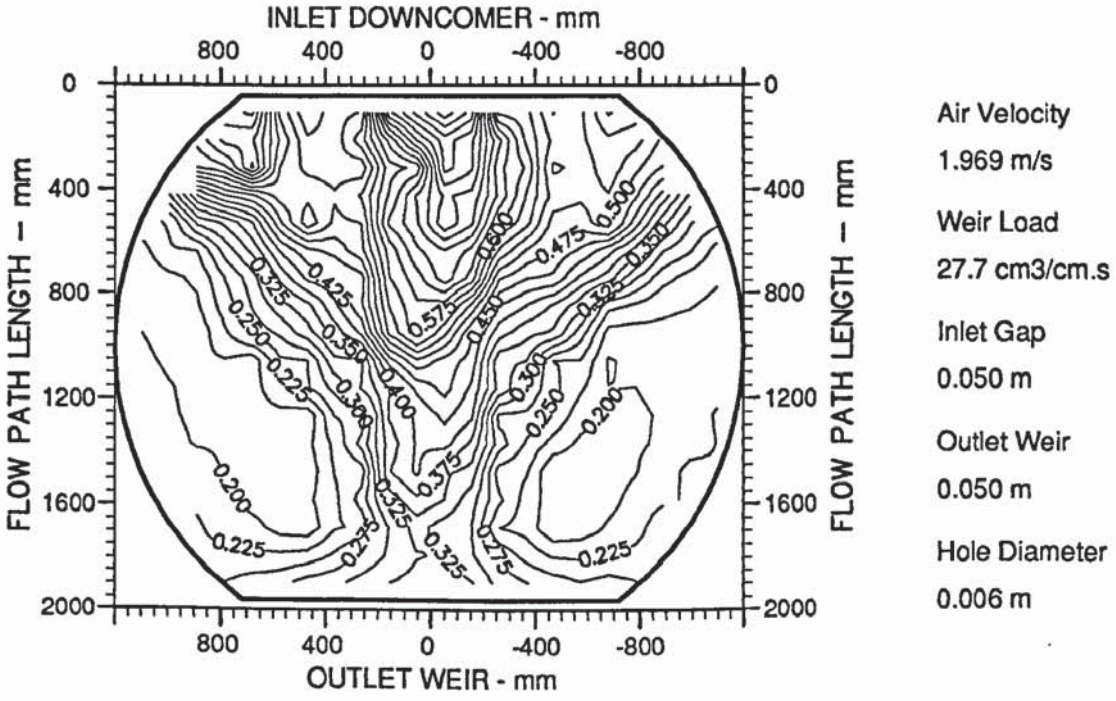

Figure 6.9b Two dimensional reduced temperature profile diagrams showing "U-shaped" and closed-looped isotherms (designation UC).

Despite the presence of gas-influenced liquid flow patterns at large froth heights, there was no severe loss in the value of the calculated point efficiencies. The reason for this was that the greater froth depth enhanced the gas-liquid contact time for mass transfer.

I.G / O.W. - mm	10,10							
10^4.Weir Load - $m^3/m.s$	27.78		37.04		46.20		55.55	
Superficial Air Velocity - ms^{-1}	Efficiency %		Efficiency %		Efficiency %		Efficiency %	
1.243	E_{OG}	70.0	E_{OG}	75.2	E_{OG}	85.9	E_{OG}	82.1
	E_{MV}	103.0	E_{MV}	106.0	E_{MV}	120.0	E_{MV}	107.0
	E_{MV}/E_{OG}	1.47	E_{MV}/E_{OG}	1.41	E_{MV}/E_{OG}	1.40	E_{MV}/E_{OG}	1.30
1.523	E_{OG}	67.4	E_{OG}	72.2	E_{OG}	73.8	E_{OG}	92.7
	E_{MV}	107.0	E_{MV}	108.0	E_{MV}	106.0	E_{MV}	127.0
	E_{MV}/E_{OG}	1.58	E_{MV}/E_{OG}	1.49	E_{MV}/E_{OG}	1.44	E_{MV}/E_{OG}	1.38
1.760	E_{OG}	68.3	E_{OG}	72.3	E_{OG}	73.3	E_{OG}	74.7
	E_{MV}	115.0	E_{MV}	111.0	E_{MV}	104.0	E_{MV}	101.0
	E_{MV}/E_{OG}	1.68	E_{MV}/E_{OG}	1.54	E_{MV}/E_{OG}	1.41	E_{MV}/E_{OG}	1.36
1.969	E_{OG}	64.9	E_{OG}	70.3	E_{OG}	74.0	E_{OG}	79.3
	E_{MV}	111.0	E_{MV}	111.0	E_{MV}	106.0	E_{MV}	112.0
	E_{MV}/E_{OG}	1.71	E_{MV}/E_{OG}	1.59	E_{MV}/E_{OG}	1.44	E_{MV}/E_{OG}	1.41

Table 6.2 Summary of measured point and tray thermal efficiencies on the 6.35mm tray using an inlet gap and outlet weir combination of 10 mm.

I.G / O.W. - mm	20,20							
10^4.Weir Load - $m^3/m.s$	27.78		37.04		46.20		55.55	
Superficial Air Velocity - ms^{-1}	Efficiency %		Efficiency %		Efficiency %		Efficiency %	
1.243	E_{OG}	76.7	E_{OG}	76.9	E_{OG}	79.3	E_{OG}	75.9
	E_{MV}	117.0	E_{MV}	93.2	E_{MV}	96.7	E_{MV}	87.0
	E_{MV}/E_{OG}	1.52	E_{MV}/E_{OG}	1.21	E_{MV}/E_{OG}	1.22	E_{MV}/E_{OG}	1.15
1.523	E_{OG}	59.8	E_{OG}	69.6	E_{OG}	76.1	E_{OG}	74.2
	E_{MV}	78.1	E_{MV}	87.1	E_{MV}	99.0	E_{MV}	90.2
	E_{MV}/E_{OG}	1.30	E_{MV}/E_{OG}	1.25	E_{MV}/E_{OG}	1.30	E_{MV}/E_{OG}	1.22
1.760	E_{OG}	70.9	E_{OG}	68.9	E_{OG}	74.3	E_{OG}	75.4
	E_{MV}	81.7	E_{MV}	94.9	E_{MV}	101.0	E_{MV}	96.3
	E_{MV}/E_{OG}	1.15	E_{MV}/E_{OG}	1.38	E_{MV}/E_{OG}	1.36	E_{MV}/E_{OG}	1.28
1.969	E_{OG}	65.7	E_{OG}	68.5	E_{OG}	73.4	E_{OG}	75.2
	E_{MV}	112.0	E_{MV}	103.0	E_{MV}	104.0	E_{MV}	102.0
	E_{MV}/E_{OG}	1.70	E_{MV}/E_{OG}	1.50	E_{MV}/E_{OG}	1.41	E_{MV}/E_{OG}	1.36

Table 6.3 Summary of measured point and tray thermal efficiencies on the 6.35mm tray using an inlet gap and outlet weir combination of 20 mm .

I.G / O.W. - mm	50,50							
10^4.Weir Load - $m^3/m.s$	27.78		37.04		46.20		55.55	
Superficial Air Velocity - ms^{-1}	Efficiency %		Efficiency %		Efficiency %		Efficiency %	
1.243	E_{OG}	80.4	E_{OG}	94.0	E_{OG}	95.3	E_{OG}	96.0
	E_{MV}	89.3	E_{MV}	109.0	E_{MV}	115.0	E_{MV}	113.0
	E_{MV}/E_{OG}	1.11	E_{MV}/E_{OG}	1.16	E_{MV}/E_{OG}	1.21	E_{MV}/E_{OG}	1.18
1.523	E_{OG}	73.8	E_{OG}	78.9	E_{OG}	88.0	E_{OG}	88.1
	E_{MV}	70.1	E_{MV}	75.5	E_{MV}	94.1	E_{MV}	94.2
	E_{MV}/E_{OG}	0.95	E_{MV}/E_{OG}	0.96	E_{MV}/E_{OG}	1.07	E_{MV}/E_{OG}	1.07
1.760	E_{OG}	71.6	E_{OG}	78.9	E_{OG}	85.1	E_{OG}	88.0
	E_{MV}	69.2	E_{MV}	80.3	E_{MV}	89.7	E_{MV}	96.8
	E_{MV}/E_{OG}	0.97	E_{MV}/E_{OG}	1.02	E_{MV}/E_{OG}	1.05	E_{MV}/E_{OG}	1.10
1.969	E_{OG}	74.0	E_{OG}	78.9	E_{OG}	81.9	E_{OG}	86.7
	E_{MV}	86.8	E_{MV}	88.3	E_{MV}	91.6	E_{MV}	99.6
	E_{MV}/E_{OG}	1.17	E_{MV}/E_{OG}	1.12	E_{MV}/E_{OG}	1.12	E_{MV}/E_{OG}	1.15

Table 6.4 Summary of measured point and tray thermal efficiencies on the 6.35mm tray using an inlet gap and outlet weir combination of 50 mm.

The tray efficiency results show that the highest values of E_{MV} are obtained at an inlet gap and outlet weir height of 10 mm, (i.e., an average of 110%), whereas E_{MV} is lowest at the inlet gap and outlet weir height of 50 mm (i.e., an average of 91.5%). This result is opposite to that found in practice and may be due to gas flow effects on the generated liquid flow patterns. That is, the effect of the gas flow on the liquid flow pattern was minimal at low froth heights compared with the gas-influenced liquid flow patterns generated at large froth heights.

It is important to note that the gas-driven liquid circulation zones on the tray have a detrimental effect on efficiency. Since liquid replenishment from the bulk biphase flow into the circulating regions is minimal, the closed area of circulating froth rapidly approaches equilibrium with the gas passing through the liquid, both with respect to concentration in distillation and temperature in water-cooling. Thus further gas bypassing through the liquid undergoes no further concentration or temperature change, which ultimately leads to a fall-off in tray efficiency.

In some cases, where there are large circulating areas, the adverse effects of no temperature (or concentration) change in the gas and liquid phases result in a decrease in tray efficiency such that it is lower than point efficiency. For example, the tray efficiency at the superficial air velocity of 1.523 ms^{-1} and fixed weir loading of 27.78 $cm^3/cm.s$ was calculated to be 70.1%, whereas the computed point efficiency was 73.8%.

The above trends in efficiency for the three tray configurations, have a significant effect on the enhancement of point efficiency ratio, E_{MV}/E_{OG}. That is, the E_{MV}/E_{OG} ratio is greatest at the inlet gap and outlet weir height of 10 mm (average calculated value of 1.48), and least at the inlet gap and outlet weir height 50 mm (averaged calculated value of 1.09).

Thus biphase flow patterns containing gas-driven circulation of the liquid, clearly have an adverse effect mass transfer and on the tray efficiency.

6.2.4 Conclusions

The air-water contacting experiments, using the direct-observation and water-cooling techniques, have shown that gas flow does have an effect on the direction of liquid flow on a 6.35 mm hole tray. These effects are favoured the most at the high-air velocity to low-liquid load flow rate range, and at large froth heights. In some cases, the gas forced the liquid to circulate on the tray outlet such that it occupied a maximum of 30% of the total tray area.

Gas-driven liquid circulation caused a number of flow pointers to rotate during the direct-observation experiments, and corresponded to the coldest liquid regions on the tray during water-cooling. Circulating flow has a longer residence time compared to other parts of the tray which reduces the driving force for mass transfer and leads to a fall-off in tray efficiency.

At low froth heights, particularly at the inlet gap and outlet weir height of 10 mm, the effect of the gas flow on the liquid flow pattern was negligible, and this was reflected in the comparatively high tray efficiency results. A comparison of the tray efficiency results for the biphase flow patterns generated at both the high and low froth heights suggests that the flow patterns are superior at low froth heights. However, even for the lowest froth heights, the mixed or confused temperature isotherms from the water-cooling experiments, show that the biphase flow pattern is non-uniform and might yet be improved upon in order to produce an optimum gas-liquid contact time for mass transfer.

Overall, these observations have not been reported previously in the open literature, and as far as is known, it is the first time that gas flow effects on changing the direction of liquid flow have been observed.

It is worth noting at this stage, that, in all of the experiments described above, the air velocity was varied over a wide range for a low fixed weir loading. If the tray was

operated at much higher weir loadings, it is possible that the effect of the gas flow on changing the direction of liquid flow so as to produce gas-driven liquid circulation may not occur? This was the subject of the work presented in the following section.

6.3 Studies into Gas Distribution Effects on Liquid Flow Patterns at Higher Weir Loadings

The aim of these experiments was to determine whether the gas flow pattern changed the direction of liquid flow at medium and high weir loadings. A wide range of air velocities were used at several fixed weir loadings during this gas-liquid contacting investigation.

6.3.1 Investigation by Direct-Observation

A complete set of biphase flow pattern results were obtained using the established technique of monitoring thirty four flow pointers, spread evenly across the tray, using the overhead video camera. Since the effect of the gas flow on changing the direction of liquid flow was most significant at large froth heights in the previous experimental investigation, the tray was configured with an inlet gap and outlet weir height of 50 mm for all the experiments. The flow rates used for this investigation are detailed in Table 6.5. Note that experiments at the superficial air velocity of 1.00 ms^{-1} were not performed in order to avoid the problem of liquid weeping.

Medium Weir Load Settings		High Weir Load Settings	
Air Velocity - ms^{-1}	Weir load - 10^4 $m^3/m.s$	Air Velocity - ms^{-1}	Weir load - 10^4 $m^3/m.s$
1.243	75.0	1.243	125.0
1.523	90.0	1.523	150.0
1.760	105.0	1.760	175.0
1.969	120.0	1.969	200.0

Table 6.5 Summary of flow rates chosen for the gas-liquid contacting experiments using medium and high weir loadings.

The format of the results presented, show the effect of increasing air velocity, for a fixed medium or high weir loading, on the developed liquid flow pattern. The results are summarised on a modified load factor verses weir load diagram and interpreted using the flow pattern notation designated in the guidelines outlined in Section 5.2.2 of Chapter 5.

6.3.2 Discussion of Flow Pattern Results

For all flow rates using medium weir loads, the biphase flow pattern consisted of a forward flow region on the horizontal plane between the downcomers and a mixture of slow forward flow, stationary liquid, and reverse flow on the tray segments.

The forward flow direction between the downcomers was revealed by all sixteen flow pointers pointing towards the outlet weir on the horizontal plane and that this flow pattern was observed for all the air and water flow rates. The biphase flow on the tray segments consisted of slow forward flow, owing to the longer liquid flow path, and a small level of circulation both at the ends of the inlet downcomer and the ends of the outlet weir, (see Figure 6.10a). Circulating flow was slow moving and occupied a negligible part of the total tray area, i.e., in most cases 5 to 7%.

A summary of the flow patterns obtained at medium weir loadings are presented on a modified vapour load factor verses weir load diagram as shown in Figure 6.10b. The results are presented in a matrix format such that for each flow rate combination, forward flow, and the percentage of tray area occupied by gas-driven liquid circulation as well as circulation at the ends of the inlet downcomer are shown.

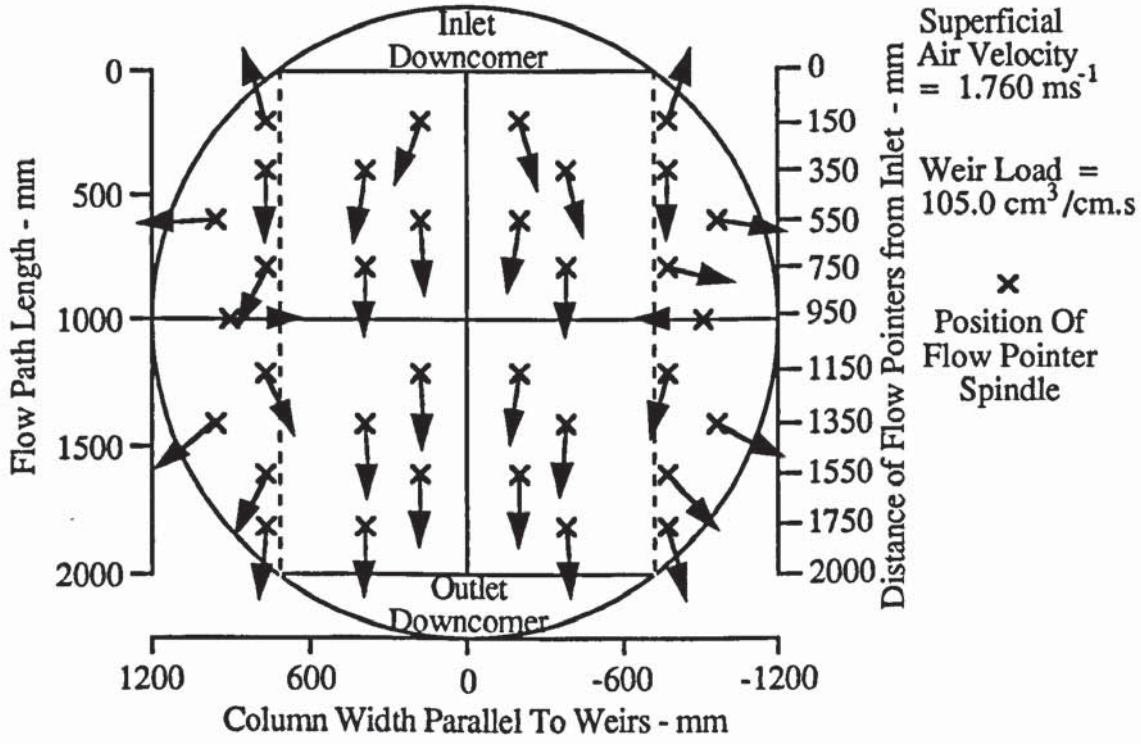

Figure 6.10a Flow pointer arrangement showing forward flow with no gas-driven circulation for the medium weir load experiments.

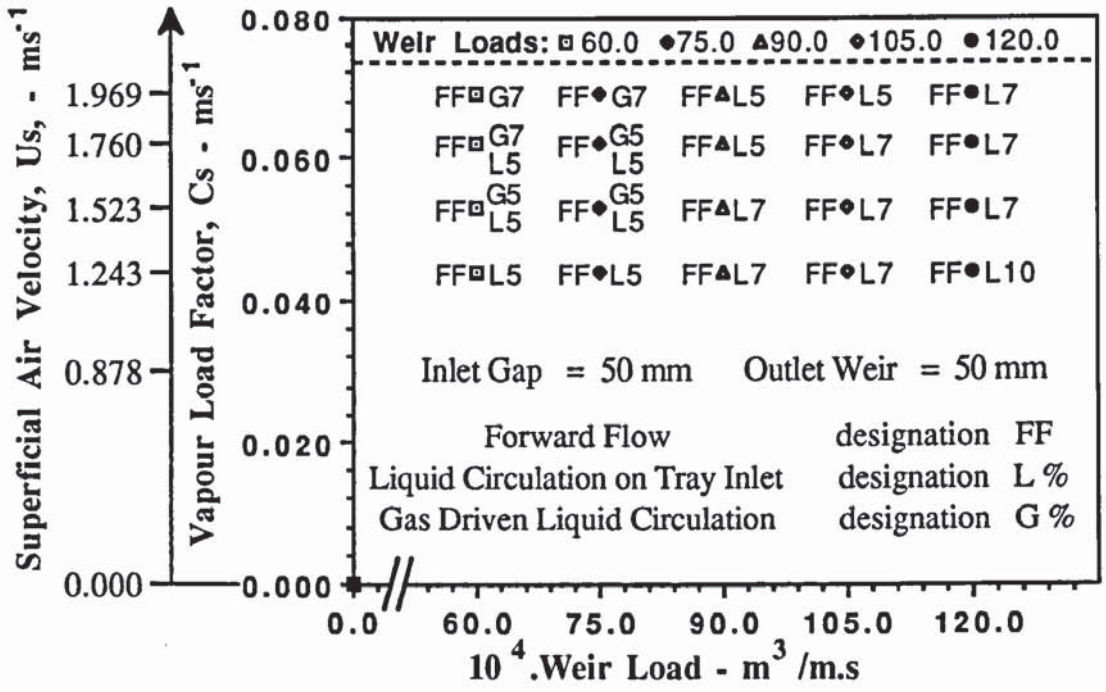

Figure 6.10b Summary of flow patterns on a load factor verses weir load diagram for the medium weir load experiments.

In the high weir load experiments, the velocity of the forward biphase flow on the horizontal plane between the downcomers was greater than that in the mixed froth regime. This was reflected in the positioning of the flow pointers in the region between the weirs, such that they were all perpendicular to the downcomers, and were all pointing towards the outlet weir.

For most flow rates, the fast forward flow between the downcomers produced a certain amount of flow separation at the ends of the inlet downcomer. This resulted in a fairly small biphase circulation which in many cases, occupied 10% but no more than 12% of the total tray area, (see Figure 6.11a).

A mixture of slow forward flow, and reverse flow towards the column wall at the ends of the outlet weir was produced on the segmental regions at the sides of the tray for most air flow rates at high fixed weir loadings. On increasing the air flow rate, the velocity of the biphase forward flow slowly decreased until it was almost stationary. At the highest weir load setting, a significant area of the tray segments was occupied by stationary biphase.

All of the flow pattern results are summarised on a modified load factor verses weir load diagram as shown in Figure 6.11b. There was no evidence of gas flow effects changing the direction of liquid flow whilst operating the tray at high weir loadings.

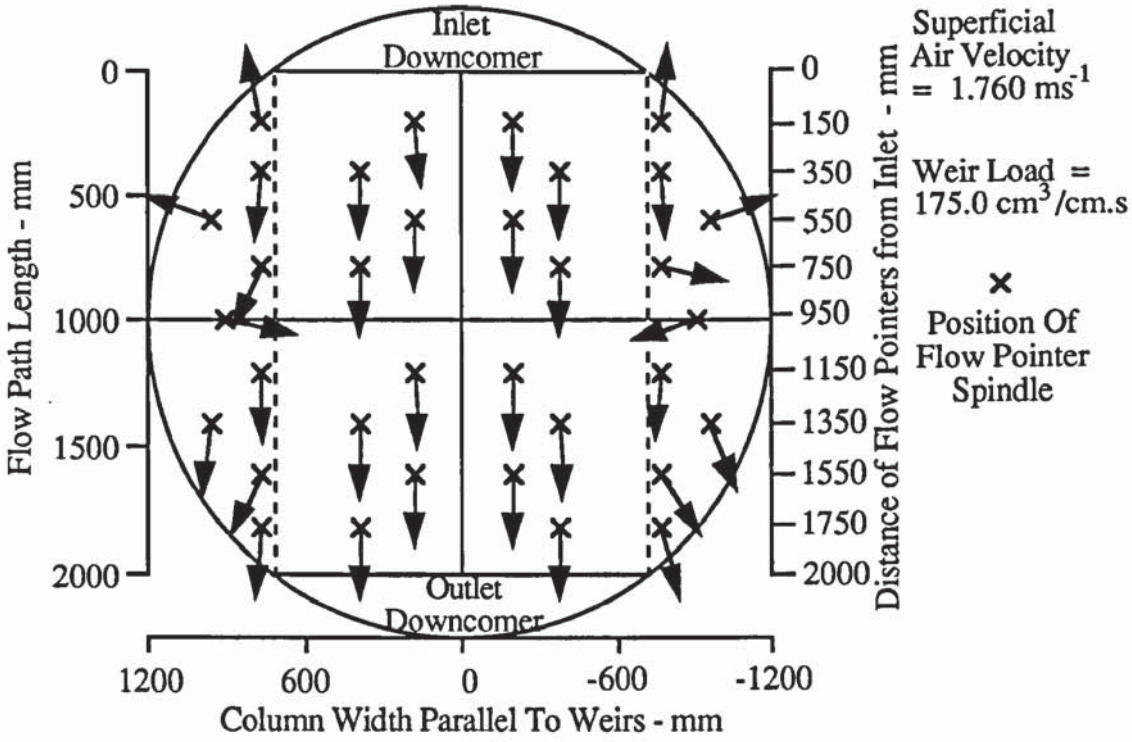

Figure 6.11a Flow pointer arrangement showing forward flow with 12% inlet liquid circulation and no gas-driven circulation for the high weir load experiments.

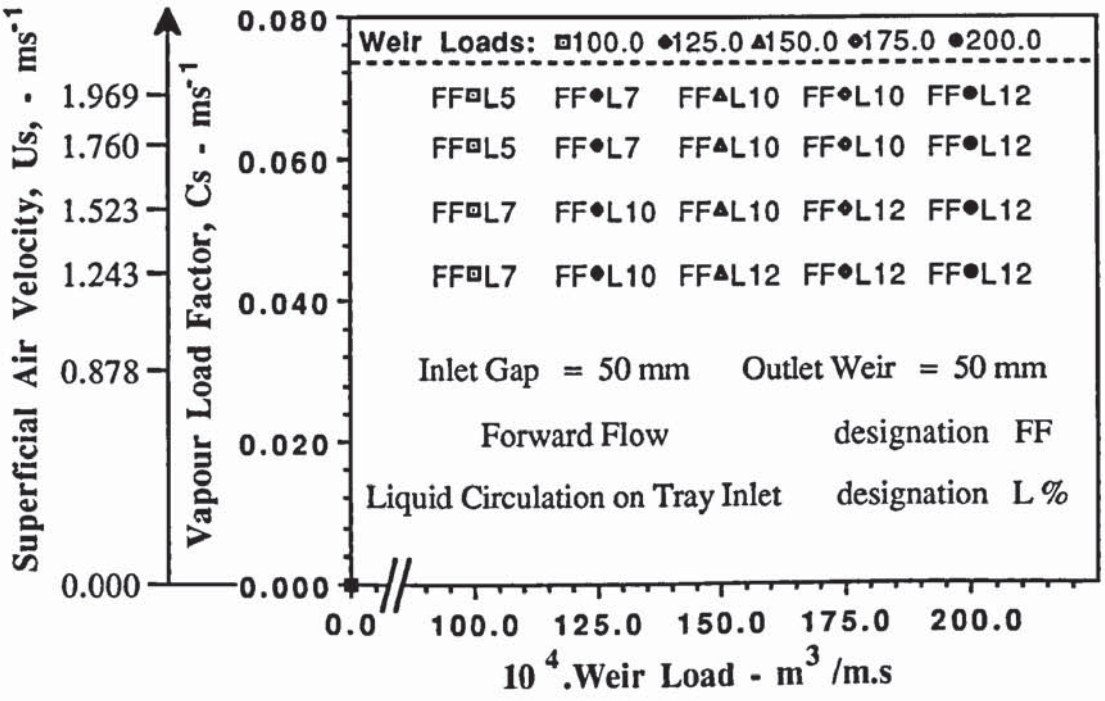

Figure 6.11b Summary of flow patterns on a load factor verses weir load diagram for the high weir load experiments.

6.3.3 Conclusions

The gas-liquid contacting experiments at the medium and high weir loadings have shown that there was very little or no gas-influenced liquid flow on the tray. Instead, forward flow associated with a small level of circulation at the ends of the inlet downcomer was observed for all flow rates. The velocity of circulating flow on the tray inlet at the sides slowly increased with increasing weir load.

From the above experimental results, it appears that gas-driven liquid circulation only occurs at high-air flow to low-liquid flow rates. An explanation into the causes of gas-driven liquid circulation was presented in Section 6.2.2 in which two suggestions were proposed. These were concerned with the velocity/momentum properties of the air passing through the froth, aswell as the possibility of gas circulation between the gas distributor and the test tray.

Hence a series of experiments were devised to investigate the gas flow pattern in the intertray spacing beneath the test tray and are described in the following section.

6.4 Investigation of Non-Uniform Gas Flow

Evidence from the air-water contacting experiments suggests that, under certain conditions, the gas flow changes the behaviour of liquid flow on the test tray as a result of a possible gas circulation beneath the tray. To confirm this, a series of air-only flow experiments were devised in which the air flow between the gas distributor tray and the test tray was monitored by direct-observation. This included the recording of red ribbon flow pointers using the overhead video camera, and the measurement of point air velocities above the gas distributor tray using a hot wire amenometer.

At this stage, it is important to recall the design and installation of the gas distributor tray into the test facility. The distributor tray consists of a 2.0 m diameter grey PVC circular base onto which 130 riser tubes were mounted in a radial format as shown in Figures 4.6 and 4.7 of Chapter 4. When incorporated into the air-water simulator, the diameter of the distributor was found to be less than the diameter of the tray column shell (i.e., 2.44 m). In addition, the distributor had only been placed across the internal cylinder flow chamber, thus leaving an unperforated horizontal surface between the perimeter wall of the distributor and the bottom of the tray column wall. This was unaccounted for in the original air distribution design and may be of importantance in the air-only flow

experiments outlined below.

6.4.1 Direct-Observation Experiments using Ribbon Flow Pointers

Air-only flow patterns were studied visually by the use of red ribbon flow pointers of length 200 mm and width 25 mm. In order to gain an even coverage of flow patterns across the whole of the distributor tray, ribbons were attached over the centre points of 58 evenly spread chimney risers by means of crosswires such that each ribbon could freely align itself with the air jet issuing from each chimney.

It was anticipated that the air jets from the outermost chimney risers may spread out towards the column wall prior to reaching the test tray. Hence a "mobile" ribbon flow pointer of length 300 mm, attached to the end of a metal rod, was placed at several positions above the horizontal annulus surface at the sides of the distributor tray.

All air flow patterns were recorded by monitoring the position of the ribbon flow pointers using an overhead video camera mounted 5.50 m above the chimney distributor. Flow patterns were recorded at the superficial air velocities of 1.00, 1.50, 2.00 and 2.50 ms^{-1}.

6.4.1 Air Flow Pattern Results

For all flow rates, the ribbon flow pointers oscillated vigorously above each of the 58 chimney risers. The ribbon flow pointers aligned themselves with the air jets issuing from each chimney such that they were positioned at an angle of less than 90^{o} relative to the horizontal plane. The angle-of-flow pointer alignment was more acute at low air flow rates compared with that observed at the high air flow rates. Overall the flow pointers indicated the presence of air jets forming diverging air cones above each of the chimney risers across the distributor plate.

When the "mobile" ribbon flow pointer was placed in between chimney risers, the ribbon, on several occasions, underwent a number of rotations thus indicating swirling eddies between the risers both in the radial and transverse directions. Continuous swirling of the air was noted when the "mobile" ribbon flow pointer was placed at several positions in the region between the outermost chimney risers and the perimeter wall.

On placing the "mobile" flow pointer at several positions above the horizontal surface of the annulus, large continuous circulating air eddies were observed. The ribbon was observed to be "following" a diverging trajectory towards the column wall before descending to the horizontal surface of the annulus. The ribbon flow pointer changed

direction again when it encountered fresh diverging air jets, from the outermost risers, and the circulation process repeated.

Circulating eddies, occupied the full width of the annulus (approximately 220 mm) and was estimated to reach heights of approximately 600 to 700 mm. (The total height of the intertray space between the distributor tray and the test tray is 1000 mm). It is worth noting that the swirling air regions lie directly below the segmental regions at the sides of the test tray and may be responsible for producing gas-driven liquid circulation.

On the distributor tray itself, diverging air jets emanated from 130 chimney risers and therefore a considerable amount of jet overlap may have occurred. This suggests that the net vertical air velocity component is greater than the horizontal velocity component which means that there is a higher air flow above the chimney distributor compared to that at the sides. However, it is not necessarily the case that the air is projected through the sieve tray perforations in the vertical direction and that it is quite possible that air streams pass through the tray holes at an angle.

On increasing the superficial air velocity from 1.00 ms^{-1} to 2.50ms^{-1}, air jets above all the chimney risers became less diverse and traversed a flow path which was closer to the vertical direction. In addition, there was a rapid increase in the swirling action of the air flow above the annulus sections. This was reflected in the increased number of complete rotations by the "mobile" ribbon flow pointer. A simplified diagram of the air-only flow pattern result is presented in Figure 6.12.

From the direct-observation results it can be concluded that the air flow in the intertray spacing is non-uniform. That is, it consists of a high air flow profile in the middle of the distributor tray associated with large circulating eddies above the annulus at the sides of the intertray spacing.

Although it has been reported that the air flow velocity is very high in the region above the distributor tray itself, it is unclear as to how uniform the air flow is above the distributor tray. Thus a second direct-observation was carried out by measuring point air velocities above the chimney risers on the distributor tray.

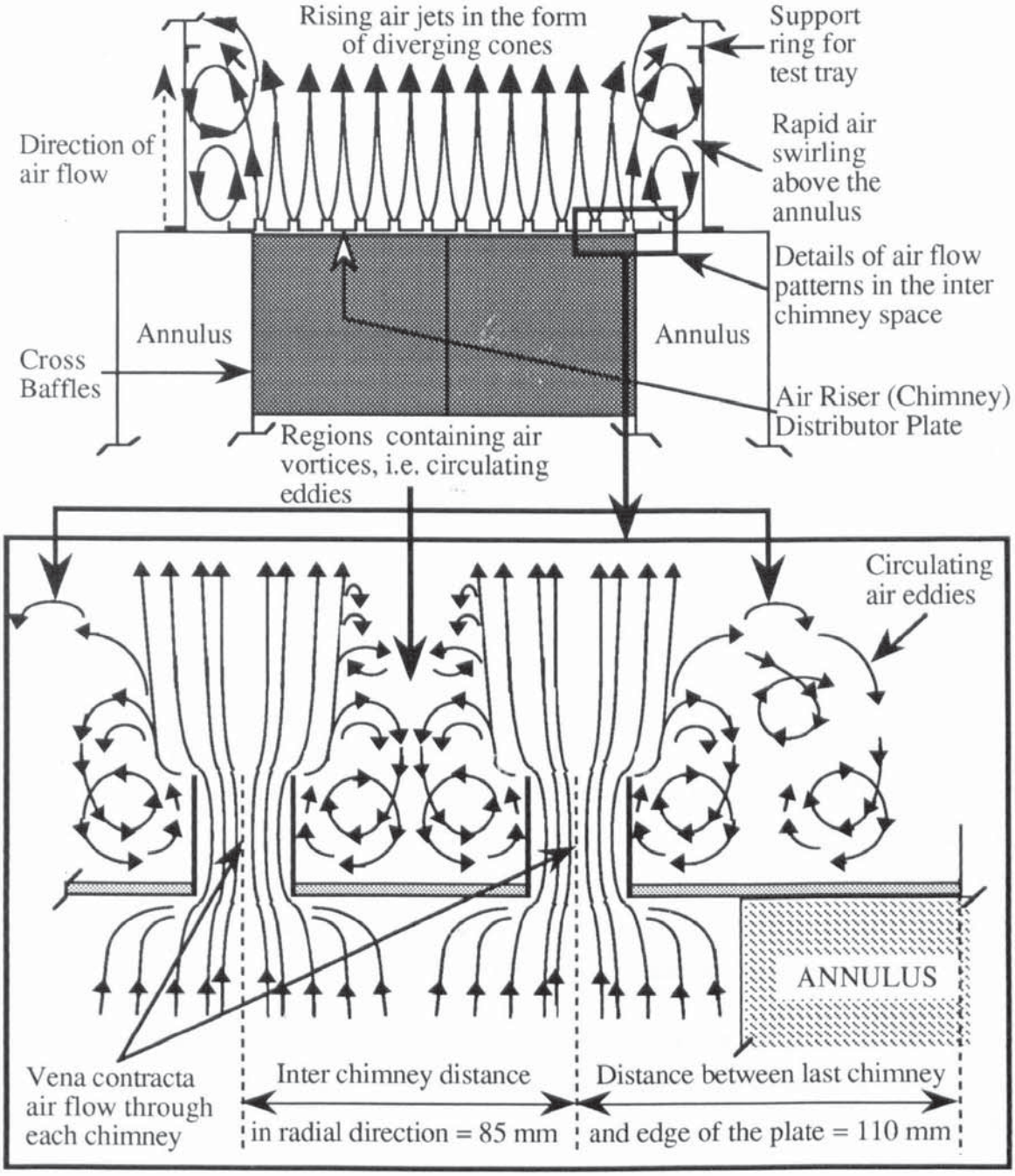

Figure 6.12 Simplified diagram of the air-only flow patterns above the chimney distributor tray.

6.4.2 Measurement of Point Air Velocity Profiles

Air velocity profiles were measured using a hot wire anemometer. The device was mounted on a small cylindrical tube of height 150 mm and internal diameter 74 mm, such that the measuring probe was positioned at the centre point of the cylinder cross-section and the point air velocity measured.

To gain an even coverage of point air velocity measurements over the whole tray, the anemometer was placed over 45 chimney risers spread evenly across the distributor. The point air velocity profiles were measured at the superficial air velocities 0.50,1.00, and 1.50 ms^{-1} only, since the point air velocities above the risers at higher superficial air velocities would have exceeded the upper limit of the anemometer measuring range.

The results are presented on a grid similar to that shown in Figure 4.6 of Chapter 4.

Air Velocity Profile Results

At the sample height of 150 mm, the point-to-point air velocity profiles indicated a relatively uniform gas distribution above the distributor tray itself at all three superficial air velocities. It was also noted that the point air velocities at the centre of the distributor tray were slightly less than those recorded on the outer regions. One reason for this is the possible interaction of the rising air streams with the centre point at which all four cross baffles meet in the internal air flow chamber. This is briefly explained below:-

The four cross baffles are held rigid at the centre of the flow chamber by means of horizontal metal disc welded to the bottom of each baffle. A fraction of the rising air is forced to flow outwards across the horizontal disc to the edges where flow separation occurs since the air can no longer maintain contact with the underside of the disc. The flow path of the air is then split into four air streams at the cross baffle centre point. Each air stream forms a boundary layer with the solid surface of the cross baffles and thus increases the effects of boundary layer, or **skin**, friction on the air stream velocity.

Immediately at the back of the horizontal disc, the separated air streams form a wake which consists of circulating eddies. These eddies are kept in motion by the shear stresses between the wake and the separated air currents which, in turn, generates heat and results in a large friction loss known as **form drag** friction.

It is the combined effects of form drag friction and skin friction that retard the air flow past the centre point of the four cross baffles, and maybe the reason for the measurement of lower point air velocities at the centre of the distributor tray.

An example of the point air velocities recorded, (which are approximately 10 x superficial air velocity), above 45 chimney risers is presented in Figure 6.13.

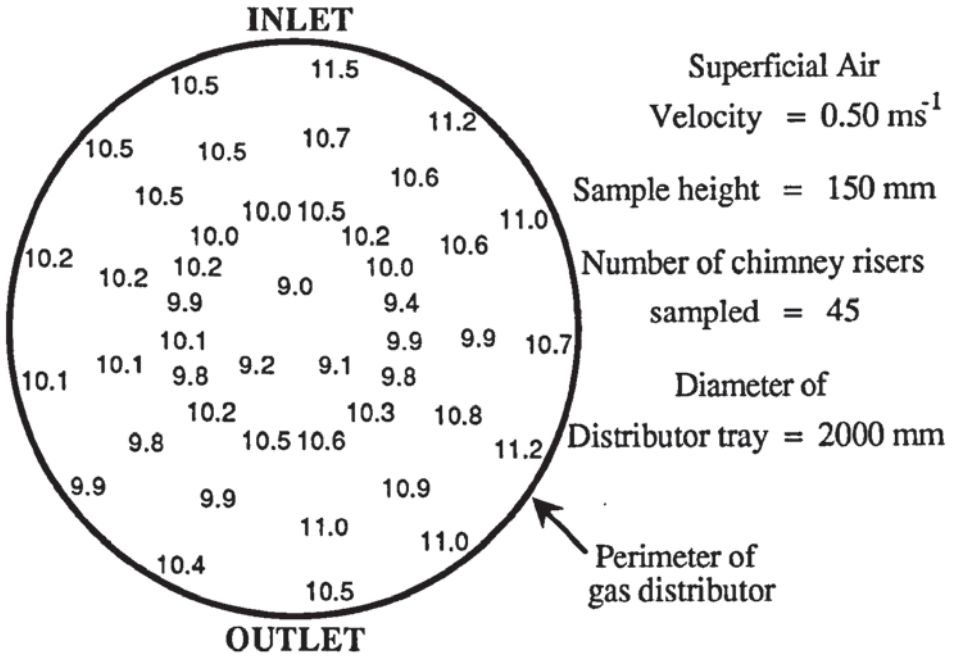

Figure 6.13 Point air velocity results superimposed on a simplified diagram of the chimney distributor tray.

6.4.3 Conclusions

The air-only flow experiments have shown that the gas flow pattern is far from ideal in the intertray region between the distributor tray and the test tray. That is, a high air flow was produced above the gas distributor tray itself in addition to large circulating eddies above the annulus at the sides of the intertray spacing. These observations show that the non-uniform air flow beneath the test tray changed the direction of liquid flow such that gas-driven liquid circulation was produced. An explanation of the non-uniform gas flow above the chimney tray is presented below.

6.4.4 Explanation of Non-Uniform Gas Flow

By reference to Figure 6.12, the velocity of air passing through the chimney tray undergoes change both in magnitude and direction as a result of frictional forces exerted by the physical nature of the distributor. If the space above and below the distributor tray are considered as large conduits and each chimney riser as small conduits, the effect of the changing cross-sectional area of each conduit, as well as frictional forces, can be explained.

When the cross-sectional area of the internal flow chamber conduit beneath the distributor tray is suddenly decreased, the air stream cannot follow the sharp edge of the chimney

adjoining the distributor base. Thus, the air stream is forced to contract by breaking contact with the wall of the flow chamber conduit or adjacent air streams, depending upon the location of the chimney riser on the distributor tray. The contracted air stream forms an air jet which flows through the short length of the chimney conduit (approximately 70 mm) before expanding into the second large conduit above the distributor tray.

This sudden expansion results in a separation of the air stream from the top of the chimney riser and enters the enlarged conduit space as a jet. The jet expands to fill the immediate vicinity above the chimney riser before encountering other expanding air jets from neighbouring chimney risers. Flow separation at the flow boundary of the expanding air jets immediately above the distributor results in the formation of air vortices or circulating eddies in between neighbouring risers both in the radial and transverse directions.

When the air flows through each riser, the minimum cross-section at which the jet changes from a contraction to an expansion is known as **vena contracta** and is depicted in some detail in Figure 6.12. The expanding air jets emanating from the outermost chimney risers, suffer most from flow separation at the physical flow boundary between the diverging air streams and the stagnant air above the annulus. The reasons for this are outlined below:-

As the cross-section of the diverging air jet increases in the direction of flow, the air velocity decreases which, in turn, causes an increase in fluid pressure according to the Bernoulli principle. The pressure build-up is most significant on an air element closest to the physical flow boundary such that at some distance along the boundary, the velocity of the air element reaches zero. At this point, known as the separation point, the air element undergoes reverse flow, whilst the velocity of air elements further away from the flow boundary maintain a forward flow path.

The results of the direct-observation experiments suggests that the extent of flow separation is so great, that the air vortices, in the form of circulating eddies expand to fill most of the space directly above the annulus. The circulating flow of air is exacerbated as the superficial air velocity is increased.

6.5 Overall Conclusions

In this chapter, the effect of the gas flow on the tray liquid flow pattern was investigated

using a wide range of flow conditions during the air-water contacting experiments. Initial gas-liquid contacting studies produced a remarkable two phase flow pattern in which the gas flow, beneath the test tray, forced the liquid to flow in the opposite direction, to that of forward flow, from the outlet downcomer to the inlet downcomer.

The observation of gas-influenced circulating flow, first reported by Ayvaz (1990), was confirmed in this study in which two large symmetrical circulating zones were produced on the tray outlet. Gas-driven circulation of the liquid was favoured only at the high-air flow to low-liquid flow operating range, and at large froth heights and not at the high-air flow to higher-weir loadings. As far as is known, this is the first time that gas-influenced liquid flow patterns have been observed on perforated trays.

Gas-driven liquid circulation showed up as the coldest liquid regions on the tray during water-cooling which corresponds to liquid having a longer residence time compared with other parts of the tray. Consequently, this led to a dramatic fall-off in tray efficiency. For instance, in some experiments where gas-driven liquid circulation was highly intense, the computed tray efficiency was less than the point efficiency.

From the air-only flow experiments, it was established that a non-uniform flow of gas in the intertray space was responsible for gas-driven liquid circulation. That is, a high air flow was produced above the chimney distributor with very little air flow near the column wall at the sides. The main reason for this was the original design of the gas distribution system in which the diameter of the chimney tray was 0.44 m less than the tray column diameter.

Measures taken to improve the gas flow pattern by distributor design are described in the next chapter.

CHAPTER 7

MODIFICATION OF THE GAS DISTRIBUTION BY DISTRIBUTOR DESIGN

7.1 Introduction

In the previous chapter, the air-only flow experiments confirmed the presence of a non-uniform flow of air in the intertray space above the gas distributor tray, and that this was the cause of gas-driven liquid circulation on the test tray. Hence the task of designing a new gas distributor so as to produce a uniform flow of air to the test tray and eliminate the effects of gas-influenced liquid flow was notoriously difficult. In this chapter, details of experiments to modify the design of the distributor are presented such that the effects of a non-uniform gas flow on the tray liquid flow pattern were removed.

It was noted that there was a very high air flow above the distributor tray itself with no air flow above the horizontal annulus surface at the sides near the column wall. Thus measures taken to rectify this, by increasing the air flow to the sides of the column were as follows:

a) Raising the air riser chimney distributor tray above the annulus.

b) Removing the chimney distributor completely from the internal cylinder flow chamber.

c) Fitting the test tray with mock integral beams, with a view to reduce any circulating tendency of the gas beneath the sieve tray, (distributor tray absent).

d) The installation of a 10% free area perforated tray, of hole diameter 1.80 mm, 150 mm above the annulus.

For each case, the gas distribution and its effect on the tray liquid flow pattern was investigated using the experimental procedures outlined below.

It will be shown, in this chapter, that the gas flow pattern was substantially improved using a 1.80 mm hole diameter, high free area perforated tray such that the effect of gas-driven liquid circulation was found to be negligible.

7.2 Programme of Experiments

The most effective method of determining whether gas flow effects change the direction of liquid flow, during each gas distributor modification, was by direct-observation of the air-water behaviour on forcing air through a fixed pool of liquid on the test tray. In addition, air-only flow patterns above each new distributor design, were studied visually using a large number of ribbon flow pointers spread evenly across the distributor tray and the annulus. Each air-only flow pattern was recorded using an overhead video camera at the superficial air velocities of 1.00, 1.50, 2.00 and 2.50 ms^{-1}.

In the non-crossflow experiments, air was blown through a fixed pool of liquid on the test tray, the volume of which was set using a large outlet weir of height 300 mm. The technique of directional flow pointers and overhead video camera was used to show whether any gas-influenced liquid flow patterns were produced, i.e., circulating liquid, after each modification of the distributor tray. Non-cross flow liquid patterns were monitored at the superficial air velocities of 1.00, 1.50, 2.00 and 2.50 ms^{-1}.

The two experimental investigations were repeated for each gas distributor modification until the effect of the gas flow on changing the direction of liquid flow was shown to be negligible.

7.3 Distributor Plate Raised above the Annulus

It has already been established that a high air flow above the chimney distributor with no air flow above the annulus at the sides, has a dramatic effect on the tray liquid flow pattern. Thus to increase the air flow to the space above the annulus, the distributor tray was raised above the internal flow chamber by 36 mm. This ensured that the same active, or free, area was maintained both through the chimney risers and the area around the perimeter of the distributor tray adjacent to the column wall. (The perimeter segments adjacent to the downcomers were blocked off using thick mild steel support beams). In addition it was envisaged that approximately the same amount of air flow would emanate from the active areas on the tray although this would be difficult to prove by accurate measurements.

The procedures for the calculation of the height at which the distributor tray was raised above the internal flow chamber and the length of the non-bubbling segments on the distributor tray are presented in Appendix 5.0.

Air-only flow patterns were studied using 58 ribbon flow pointers spread evenly across selected chimney risers on the distributor tray as well as a "portable" ribbon flow pointer. This was placed at various positions in the space above the horizontal annulus surface.

7.3.1 Effect of Distributor Modification on Air-Only Flow Patterns

The ribbon flow pointers showed that the air flow from each chimney riser produced wider diverging air jets compared with that on the original distributor tray setup. Since there were a large number of chimney risers on the distributor tray, there was a considerable amount of air jet overlap. However, the increased oscillating nature of the "mobile" ribbon flow pointer, suggests that the net airflow in the vertical direction was less intense than that with the original distributor setup and that there was a greater air flow at the sides. The air jet cones transformed into narrow high flow jets above the risers as the superficial air velocity was increased from 1.00 ms^{-1} to 2.50 ms^{-1}.

In the region above the annulus at the sides, two opposing circulations were produced by observing the rotational motion of the "mobile" ribbon flow pointer. The first circulation resulted from flow separation above the outer risers on the distributor tray and was very similar to that observed with the original distributor setup. However, the circulation size and intensity of circulation was slightly less than that with the original distribution system and was probably due to the greater flow of air to the sides.

The second air circulation was produced by the sideways air flow from the open space along the perimeter of the distributor tray. The air flowed along the horizontal plane of the annulus and upwards along the column wall. Flow separation occurred such that the air rotated round towards the perimeter wall on the distributor tray where it encountered a further horizontal flow of air along the annulus.

The circulating air was probably influenced by the physical boundaries of the horizontal annulus, the column wall, the perimeter wall of the distributor and the open gap along the perimeter of the distributor tray. This circulating flow phenomenon was observed by the clockwise rotation of the "ribbon" flow pointer.

In general, although there was a greater air flow at the sides of the column above the annulus, the gas remained non-uniform above the modified chimney tray. However, this was less intense than that obtained above the original distributor set-up.

7.3.2 Effect of Distributor Modification on the Fixed Pool Liquid Flow Patterns

The above direct-observation technique was used to study the effect of the gas flow on a fixed volume of liquid. The tray was configured with an inlet gap height of 20 mm and an outlet weir height of 300 mm. The low inlet gap was used to provide an adequate liquid seal, thus preventing the bypassing of air through the inlet downcomer, whereas the large outlet weir was used to maintain a fixed volume of liquid on the tray.

Two studies were performed for each superficial air velocity in which a fixed volume of water was fed onto the tray such that the froth height was set at approximately 20 mm and 50 mm with the aid of two flow depth indicators marked onto the outlet weir. Flow patterns were observed at the superficial air velocities of 1.00, 1.50, 2.00 and 2.50 ms^{-1}.

In general, two large elongated gas-driven liquid circulating regions were produced near the ends of the outlet weir on the outlet tray section, as shown in Figure 7.1. Circulation became larger and more powerful such that the liquid adjacent to the column walls was forced backwards towards the ends of the inlet downcomer. In addition, liquid was forced from the sides of the tray towards the middle of the tray.

The biphase underwent reverse flow on the horizontal plane in front of the inlet downcomer from the ends of the inlet downcomer towards the centreline. As the superficial air velocity was increased, the reverse flow fragmented into small zones of swirling froth on the tray inlet.

There was very little difference in the gas-influenced liquid flow patterns at the two different dispersion heights, except that the size of the circulating froth was smaller at the froth height of approximately 50 mm, particularly on the inlet tray section.

In conclusion, the above observations have shown the continued presence of gas-influenced circulating liquid both on the inlet and outlet tray sections which increased in size and intensity as the superficial air velocity was increased.

7.4 Distributor Tray Removed From the Column

By removing the chimney distributor tray completely from the air-water simulator, it was envisaged that a greater air flow from internal flow chamber would spread out to the column wall and completely fill the cross-sectional area at the level of the test tray.

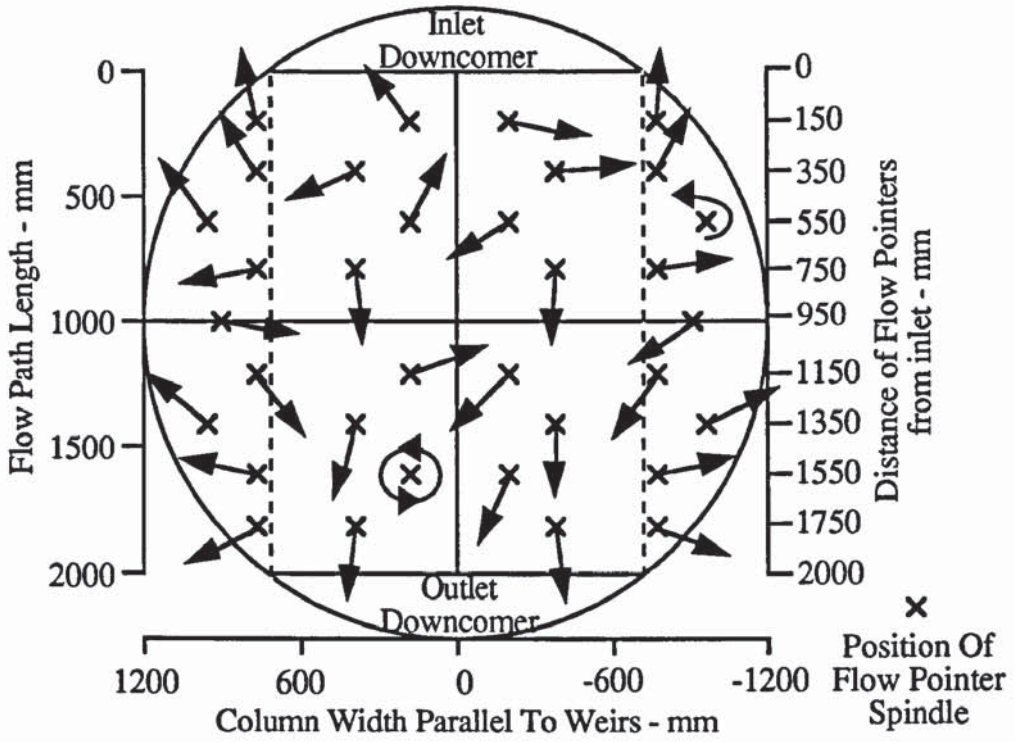

Figure 7.1 Example of gas-driven liquid circulation over most of the tray during the non-crossflow experiments with the distributor tray raised 36 mm above the annulus.

The two direct-observation techniques described above were applied to this gas distribution system, to determine whether the gas was non-uniform and does it have an adverse effect on the tray liquid flow pattern.

7.4.1 Effect of Distributor Modification on Air-Only Flow Patterns

The air-only flow patterns above the internal flow chamber and the annulus were monitored using the ribbon flow pointer technique described in the previous section. The nature of the air flow from the internal flow chamber was similar to that produced from a single chimney riser on the original distributor tray. That is, the air flow expanded to form a diverging air jet or cone and air elements within the rising jet near to the annulus region spread out towards the column wall. This was confirmed by the gentle oscillation of the ribbon flow pointer in the vertical plane which suggests that the velocity of the air jet was less than that produced from the previous gas distribution systems.

In the region above the annulus, the ribbon underwent several complete rotations, thus indicating the presence of large circulating eddies and were similar to those shown above the annulus in Figure 6.12 of Chapter 6. The circulating flow reached heights of upto 600 mm above the annulus particularly at the higher superficial air velocities. The air-only flow patterns produced can be explained as follows:-

As the rising air stream enters the tray column shell space from the internal flow chamber, the sudden enlargement of the cross-sectional area results in flow separation of the air. That is, circulating eddies were produced as a result of a change in the magnitude and direction of the air velocity at the physical flow boundary of the diverging air streams. Air streams further away from the flow boundary expand to fill the entire cross-section of the tray column shell.

Overall, the direct-observation experiments have shown the continued presence of non-uniform gas flow despite the greater flow of air to the column wall. Thus, it seems reasonable to assume that the diverging air flow from the internal flow chamber may not have expanded fully to completely occupy the cross-section of the tray column by the time it reaches the test tray. Consequently, the tray liquid flow patterns suffers from the circulating eddies produced above the annulus.

7.4.2 Effect of Distributor Modification on the Fixed Pool Liquid Flow Patterns

The fixed pool liquid flow patterns, observed using the flow pointer technique, were dominated by two very large and powerful symmetrical gas-driven liquid circulation flow patterns, as shown in Figure 7.2. As the superficial air velocity was increased, circulating flow on the tray outlet spread out to occupy a substantial area both on the tray segments and on the horizontal plane between the weirs.

Gas-driven liquid circulation forced liquid to flow backwards towards the ends of the inlet downcomer as well as forcing liquid to converge towards the tray centreline in front of the inlet downcomer. Circulating flow was much larger and more powerful than that produced using the previous gas distribution system. In addition, the same fixed pool flow pattern was observed at both the large and small dispersion heights, thus showing that the dispersion height had little effect on the gas-driven liquid circulation.

On the whole, it can be concluded that the non-cross flow experiments have showed the continued presence of gas-driven circulating liquid flow on both the inlet and outlet tray sections. It is also worth noting that circulation was greater than that using the previous gas distribution system, and showed that the flow of air without the chimney distributor tray was far from ideal. However, the gas flow pattern was slightly better than that produced from the original gas distributor set up.

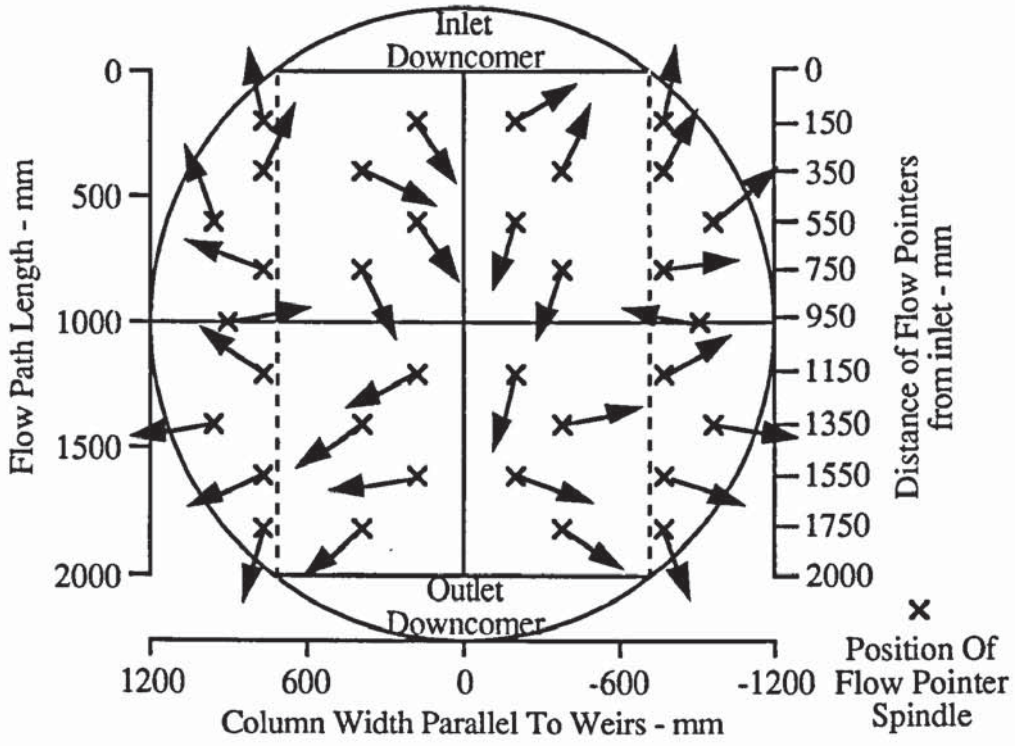

Figure 7.2 Example of gas-driven liquid circulation over most of the tray during the non-crossflow experiments (gas distributor tray absent).

7.5 Test Tray Fitted with Mock Integral Beams (Distributor Tray Absent)

Although there was a substantial non-uniform flow of gas using no distributor tray, it was found that there was a greater flow of air to the sides above the annulus compared with the previous gas distribution systems. Hence an attempt was made to control the diverging air flow and circulating eddies by "straightening-up" the air flow by means of flow control baffles. That is, mock integral beams made from aluminium sheets, were installed on the bottom of the test tray so as to reduce the horizontal velocity component of the diverging air jet and decrease the size of circulating eddies due to flow separation.

The arrangement of the mock integral beams was similar to that presented in Figure 4.11 in Chapter 4. Note that the integral beam depth was extended from 100 mm (used normally in many trayed columns) to 150 mm with a view to being more effective in reducing large swirling zones.

The air-only and liquid cross flow experiments were carried out, using the appropriate direct-observation techniques to investigate the effects of the mock integral beams on the

gas flow pattern.

7.5.1 Effect of Mock Integral Beams on Air-Only Flow Patterns

Observation of the "mobile" ribbon flow pointer in the region below the mock integral beams showed a steady moving diverging flow of air associated with circulating eddies above the annulus. On placing the ribbon in between each of the mock integral beams, the fairly rapid oscillating nature of the ribbon flow pointer indicated that the interaction of the air with the integral beams may have increased the level of air turbulence. That is, the mock integral beams may have split the horizontal component of the air flow into smaller horizontal air flows associated with small circulating eddies.

The ribbon flow pointer immediately below the test tray at the sides indicated the presence of smaller but fairly rapid circulating eddies. Overall, it appears that the integral beams failed to "straighten" the air flow through the test tray. Instead the integral beams fragmented the air stream into smaller streams of non-uniform air flow.

7.5.2 Effect of Mock Integral Beams on the Fixed Pool Liquid Flow Patterns

The gas-influenced liquid flow was identical to that described in the corresponding experiment, in Section 7.4. Thus, it appears that the mock integral beams had little effect on decreasing the maldistributed air flow, beneath the tray, when forced through the fixed volume of liquid on the test tray.

7.6 Installation of a Perforated Distributor Tray above the Annulus

So far, the gas distribution systems have produced diverging air jets associated with large circulating eddies above the annulus. The main reason for this is the sudden enlargement of cross sectional area from the smaller internal flow chamber to the larger tray column shell. This has a substantial effect on flow separation leading to the production of circulating eddies. Thus, a distributor tray was required such that it completely filled the cross section of the tray column shell and that it should be placed at a sufficent distance above the annulus. It was envisaged that such a distribution system would provide a steady flow of air upto the column wall above the annulus and that it would reduce flow separation and associated circulating eddies at the sides of the column.

The task of finding a suitable distributor tray to meet these requirements was a formidable one. However, Porter and Lan (1991) showed that, in a 1.22 m diameter air-water simulator, a small hole high free area perforated distributor tray can minimise the effect of gas-driven liquid circulation on a test tray placed directly above. That is, when a tangential air flow was forced through two 1.80 mm hole trays without downcomers and at a tray spacing of 600 mm, no gas or liquid rotations were observed on the top tray.

Thus it was decided to install a 10% free area, 1.80 mm hole perforated tray over the cross section of the tray column shell at a height of 150 mm above the annulus to permit enough air to flow to the sides of the column. It seemed reasonable to assume that the huge number of small perforations would produce very narrow jets over most of the tray area, and prevent the formation of large circulating eddies in the region above the annulus.

7.6.1 Effect of Distributor Modification on Air-Only Flow Patterns

Air-only flow patterns were studied by the direct-observation of the "mobile" ribbon flow pointer and by point air velocity measurements at 32 evenly spread positions above the distributor using the anemometer method described in Section 6.4.2 of Chapter 6.

Overall, the flow pattern consisted of a large number of air jets above the small perforations across most of the tray area including the regions above the annulus. The expanding nature of the air increased the number of overlapping air jets which has the effect of increasing the vertical air velocity component over most of the tray area.

Although circulating air eddies were observed close to the column walls and the outlet downcomer apron, they occupied a much smaller area than that observed with the previous air distribution systems. This suggests that the air flow pattern had improved considerably in the intertray spacing compared with that produced from the original chimney tray set-up.

The variation in point-to-point air velocity measurements were comparatively small at the low air velocity flow rates, but increased steadily at superficial air velocities above 2.00 ms^{-1}. Given that the sample height above the 32 measurement points was 0.233 m, it is possible that the amemometer was detecting a range of point air velocities caused by jet overlap or the formation of small circulating eddies. The air flow pattern needs to be investigated further by measuring point air velocities at various heights above the new distributor using more accurate techniques such as Laser Doppler Anemometry (LDA).

Nevertheless, the point air velocities show that there were no large differences between

that obtained in the middle of the distributor tray compared with those measured at the sides. This suggests that there was a greater air flow at the sides above the annulus. An example of a comparatively small point-to-point air velocity variation is presented in Figure 7.3a, with the corresponding three-dimensional response curve, generated using the UNIRAS suite of plotting routines, shown in Figure 7.3b. All of the point-to-point air velocity results and the corresponding response curves are presented in Appendix 6.0.

From the air-only flow experiments, it can be concluded that the air flow above the small hole, high free area, distributor tray had improved considerably compared with the previous distribution system. One reason for the improvement was that the tray thickness is approximately equal to the diameter of the small perforations, thus producing square orifices in the cross section. It seems reasonable to assume, therefore, that this would minimise the horizontal velocity component of the gas jet and increase the vertical velocity component of the gas above the distributor tray. Since there are so many small perforations in which this flow phenomenon may occur, the tendency to produce large circulating eddies in the intertray region had diminished and was confined to regions adjacent to the column wall.

7.6.2 Effect of the Distributor Modification on Fixed Pool Liquid Flow Patterns

Results from the non-cross flow experiments showed that there was no evidence of gas-driven liquid circulation near the ends of the outlet weir at the tray outlet. Instead, there was a relatively high level of turbulence and mixing of the liquid by the bubbling action of the gas flow at many points on the tray.

At the low superficial air velocities, an unusual flow pattern was produced in which the biphase was seen to be drifting very slowly in an anticlockwise direction on the horizontal plane between the weirs and parts of the segmental regions, (see Figure 7.4). This unexpected result may have been caused by the bubbling action of the gas jets passing through the liquid at an angle to the tray deck. However, the froth drift did not form one continuous circulation on the tray.

On increasing the superficial air velocity, the anticlockwise "froth drift" dispersed into a number of highly turbulent converging/diverging biphase flow patterns over many points on the tray. This was probably caused by increased level of mixing across the tray.

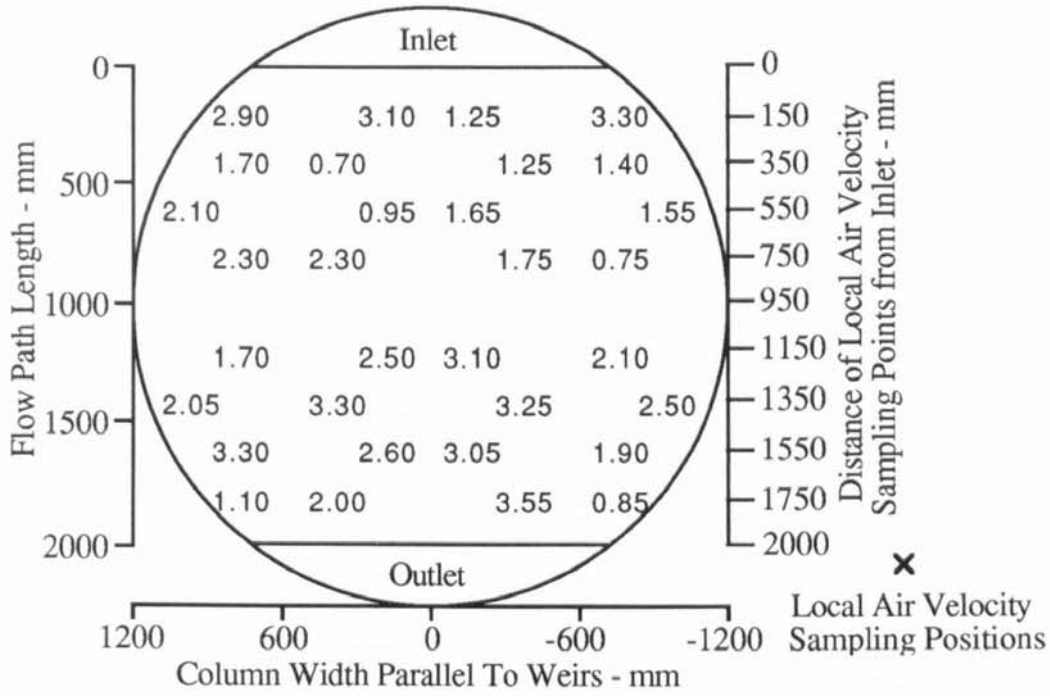

Superficial air velocity = 1.50 ms^{-1} Hole Diameter = 1.80 mm

Sample height above distributor = 0.233 m Number of points sample = 32

Figure 7.3a Measured point air velocity profiles above perforated air distributor plate at low air flowrates.

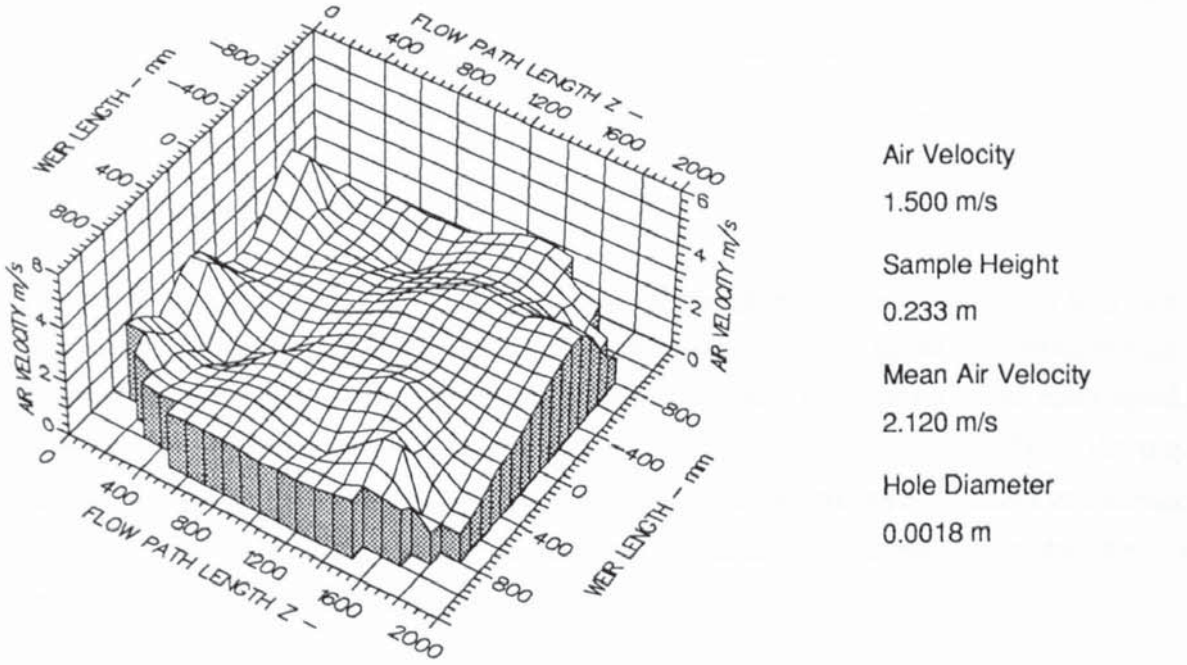

Figure 7.3b Three-dimensional response curve of a relatively small point-to-point air velocity variation.

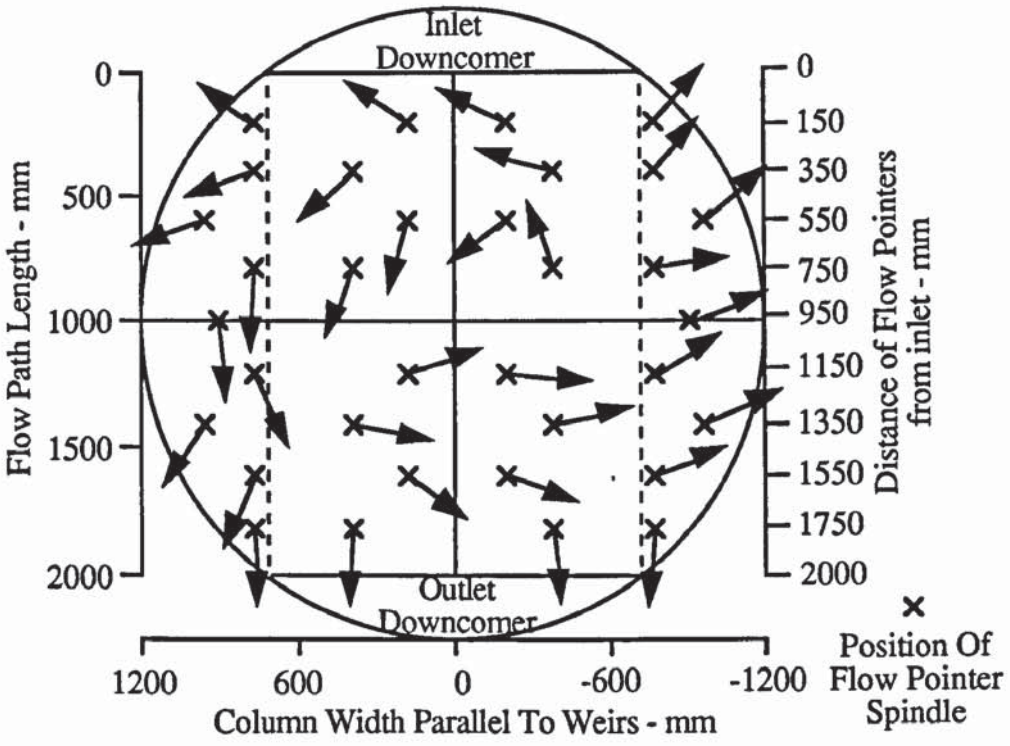

Figure 7.4 Example of negligible gas-driven liquid circulation over most of the tray during the non-crossflow experiments using a small hole distributor tray.

On the whole, the fixed pool liquid flow patterns appear to be non-uniform and may be caused by the air issuing at an angle from the tray perforations into the froth. Hence further investigations are required into the gas flow patterns above the small hole tray.

7.7 Summary

Since it was established that a non-uniform flow of gas beneath the test tray was responsible for the gas-driven liquid circulation, measures were taken to modify the gas distribution system until the effects of gas-driven liquid circulation were eliminated. Initially, the gas flow pattern consisted of a high air flow through the middle of the tray with no air flow at the sides. Hence, the gas distribution system was modified to increase the flow of air to the sides above the annulus and tested to see whether there was an improvement in the gas flow pattern within the intertray space.

Tests were carried out on three different gas distributors, and included the direct-observation of air-only flow patterns in the intertray space, and the effect of the gas flow on non-cross flow fixed liquid pool flow patterns on the test tray.

In the first two cases, a greater flow of air to the sides of the column was achieved but there was a continued presence of circulating eddies above the annulus. This was reflected in the relatively large gas-driven liquid circulations on the horizontal plane of the tray outlet in the fixed liquid pool experiments.

With the installation of a small hole, high free area perforated tray spread over the whole cross section of the tray column including the annulus, there was a significant reduction in the size of circulating eddies. This was complemented by an increase in the number of air jets over a greater area of the distributor tray. The improvement in the intertray gas flow pattern brought about the elimination of gas-driven liquid circulation on the test tray during the fixed liquid pool experiments.

In conclusion, the above experiments have shown that the most suitable gas distributor for reducing or eliminating the effects of gas-driven liquid circulation on the test tray, was the 1.80 mm hole, 10% free area perforated tray.

7.8 Overall Conclusion

The work in Chapters 6 and 7 has shown that under certain conditions, the gas flow pattern beneath the test tray, can have a significant effect on the tray liquid flow pattern and that this was a function of this particular air-water simulator design. Non-uniform gas flow effects were subsequently removed by modification of the gas distribution system.

CHAPTER 8

EFFECT OF THE GAS FLOW ON THE SEPARATION OF LIQUID FLOW

8.1 Introduction

The main theme of this chapter is to identify those two phase flow patterns on the 6.35 mm hole tray that are representative of those found in practice. It will be shown that the effect of forcing the gas through the liquid inhibited the onset of flow separation which only occurred at much higher weir loads and smaller inlet downcomer clearances compared with that obtained in the water-only experiments.

The effect of separated and non-separated biphase flow on temperature profiles and the driving force for mass transfer during water-cooling, was also investigated, as well as the liquid head variation on the tray by measurement of the height of clear liquid.

Finally, this section is completed by comparing the experimental temperature profiles with computed flow patterns generated from a turbulent two phase flow mathematical model (Yu and Zhang, 1991), for the same flow conditions. This was part of a collaborative research programme with the National Distillation Laboratory in the P.R. China headed by Professor K T Yu.

Prior to discussing the effect of the gas on the separation of liquid flow, it is worth noting the definitions of separated and non-separated flow.

8.2 Definition of Separated and Non-Separated Flow

Non-separated flow involves the movement of fluid streams in parallel straight lines at all points within a defined domain such as a pipe of constant diameter or a conduit of uniform cross section and flow depth. This type of flow exists in the form of either laminar or turbulent flow. Although the fluid flow contains a velocity distribution profile, with slower moving fluid at the sides of the domain, the net flow pattern is unidirectional, ie forward flow only.

In an expanding conduit or channel, where the physical flow boundary undergoes

continuous change, the forward velocity component of the fluid elements close to the boundary rapidly decreases. This is brought about by the increasing flow path length and a substantial pressure build-up on the fluid element closest to the boundary layer, (which is only present in turbulent flow), according to the Bernoulli principle. The effect of these two factors is such that at some point the forward velocity component reaches zero. The net effect is flow separation with the fluid stream either remaining stationary near the flow boundary, or undergoing reverse flow in which circulation may occur. Fluid streams further away from the flow boundary, continue to flow in the forward direction.

Overall, the main difference between non-separated and separated flow is that forward only flow is obtained in non-separated flow, whilst both forward and reverse flow are produced in the same domain during separated flow.

8.3 Studies into Separated and Non-Separated Air-Water Flow Patterns

To permit comparison of the air-water flow patterns generated on the 6.35 mm hole sieve tray, with water-only flow patterns, (regarded as reference flow patterns), it is necessary to review the results obtained during the water-only flow experiments, (Hine, 1990).

In both the water-only and air-water flow studies, particular attention was drawn to the direction of flow at many points across the tray. The direction of flow from the inlet downcomer towards the outlet downcomer is referred to as "**forward flow**", whereas flow in the opposite direction is described as "**reverse flow**". In some experiments, reverse flow may result in the recirculation of liquid within a specific area on the tray.

8.3.1 Review of the Water-Only Flow Pattern Results

The generated flow patterns across the unperforated tray, in the water-only experiments, showed that liquid circulation was formed at low weir loads, (of between 50 and 80 $cm^3/cm.s$), and increased rapidly with increasing weir load to reach a maximum of 30% of the tray area, (see Figure 8.1). This corresponded to a situation where the whole of the segmental regions were completely occupied with circulating liquid for a 60% weir to diameter ratio. Further increases in the weir loading merely enhanced the rotational velocity of the circulating liquid along the tray segments, and reinforced the flow separation streamlines. The inlet gap and outlet weir had little effect on the flow patterns generated.

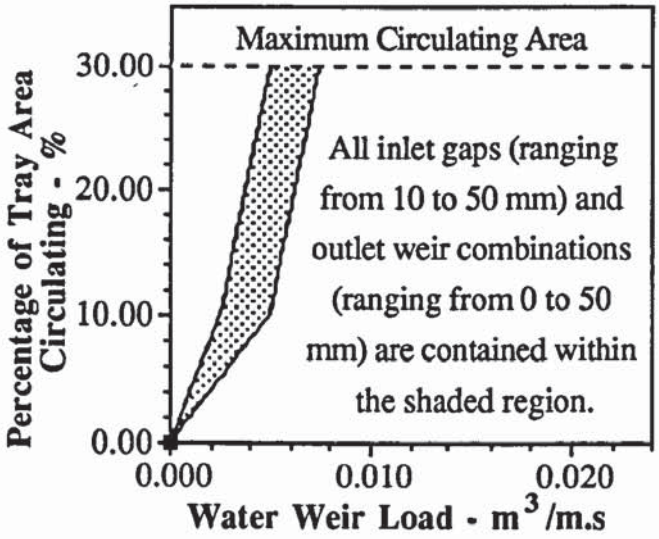

Figure 8.1 Summary of the water-only circulation flow patterns produced on the unperforated tray (Hine, 1990).

8.3.2 Programme of Experiments

The programme of experiments was in three parts:

a) Direct-observation of separated and non-separated flow patterns during the air-water contacting experiments. For each of the three combinations of inlet gap and outlet weir, (i.e., 10 mm, 10 mm; 20 mm; 20 mm; and 50 mm, 50 mm), at several fixed air velocities, the water weir load was increased and the change in the biphase flow pattern from forward flow to reverse flow recorded.

b) Investigations into the effect of separated and non-separated air-water flow patterns on mass transfer using the water-cooling technique. In these experiments, the water temperature was measured at 108 equally spaced positions on the tray, and the raw data computer processed to yield temperature profiles which are analogous to concentration profiles in distillation. By using the analogy between heat and mass transfer, the interpretation of the water temperature profiles in terms of enthalpy driving forces permitted the calculation of thermal point and tray efficiencies.

c) Investigation into the effect of separated and non-separated biphase flow patterns on the liquid head variation across the tray. This was determined by measurement of the point-to-point height of clear liquid variation on the tray using manometers, connected to thirty two pressure tappings evenly spread across the tray.

In each experiment a wide range of water weir loadings at several fixed air velocities, for

different combinations of inlet gap and outlet weir heights, were used. Details of the flow rates used and the downcomer settings for each of the three experimental investigations outlined above, are presented in Table 8.1.

Experimental Investigation	Air Velocity - ms^{-1}	Weir load - $10^4.m^3/m.s$	Inlet Gap - mm	Outlet Weir - mm
	1.00	25.0		
Direct-observation	1.25	50.0	10	10
using directional	1.50	100.0	20	20
flow pointers	2.00	150.0	50	50
	2.50	200.0		
		250.0		
Heat transfer	1.00	25.0		
by water-cooling	1.25	50.0	10	10
and	1.50	100.0	20	20
height of	2.00	150.0	50	50
clear liquid	2.50	200.0		
experiments		250.0		

Table 8.1 Summary of flow rates and downcomer settings used in the air - water contacting experiments.

8.3.3 Investigation by Direct-Observation

Direct-observation of the air-water flow patterns during the gas-liquid contacting experiments, was achieved using the established technique of directional flow pointers and overhead video camera described in Chapter 5. Flow pointers, when partially submerged in the froth or spray on the test tray, behave in a similar manner to weather vanes used to show the direction of the wind. Thus, for each air-water flow rate combination, the localised biphase flow at thirty four positions across the tray was noted by recording the direction of alignment of each painted arrow indicator.

At this stage, it should be noted that in all the experiments, the liquid was completely aerated over the whole of the tray bubbling area. Water on entering the tray formed an aerated froth, due to the bubbling action of the gas, which spread outwards so as to completely fill the tray cross section.

Another important factor is that the bubbling action of the gas through the liquid is highly chaotic and, at low liquid flow rates, tends to randomise the motion of the froth. Hence, the sensitivity of the flow pointers for showing the direction of flow is partially reduced which explains the asymmetric appearance of flow pointers on the tray. Furthermore,

when the froth appears stationary the flow pointers indicate a "direction of flow" since they have no "zero" position. One method of overcoming the problem would be to split each flow pointer into two such that the bottom half showed the movement of the liquid continuous dispersion on the tray deck, whilst the top half showed the movement of spray droplets above the froth. Nevertheless, the flow pointers prove to be highly sensitive to changes in the flow pattern for a wide range of flow rates in that they showed change from non-separated flow to separated flow.

Flow Pattern Results

An analysis of all the air-water flow patterns results showed that the passage of air through the horizontal flow of water across the tray had a significant effect on the developed flow patterns. When compared with the water-only reference flow patterns, the effect of forcing the gas through the liquid inhibited the onset of flow separation and circulating flow emanating from the ends of the inlet downcomer.

In the following subsections, it will be shown that the extent of inhibiting flow separation and the formation of circulating zones was determined by a number of factors. These include the effect of large and small froth heights, liquid entrance velocity to the tray from beneath the inlet downcomer, and an increase in the superficial air velocity.

Separated and Non-Separated Flow Patterns at Small Froth Heights

Air-water flow patterns at low froth heights were generated at the equal inlet gap and outlet weir settings of 10 mm and 20 mm. Non-separated flow patterns were produced at weir loadings of upto 50 $cm^3/cm.s$, for all air flow rates, in which forward flow was produced at most points on the tray including the segmental regions at the sides, as shown in Figure 8.2. This was reflected by most of the flow pointers facing towards the outlet weir despite their random appearance, especially on the tray inlet and at the sides.

The converging/diverging alignment of flow pointers on the tray inlet was caused by the expanding aerated liquid such that it completely filled the tray cross section. Flow pointers facing normally towards the column wall, were indicative of the sideways flow of froth from the perforated tray to the non-perforated section of the tray placed on the support ring. Another possible reason for the randomised alignment of flow pointers was that the forward flow between the downcomers was moving faster than that at the sides of the tray. Thus, the liquid flow contained a velocity distribution profile across the tray, but the flow pointers do not give a direct measure of the velocity distribution.

Overall, the gas flow prevented the onset of flow separation at the lowest weir loadings such that no circulating aerated liquid was observed. In contrast, liquid circulating regions occupied between 10 and 30% of the total tray area at the same weir loadings in the water-only flow experiments, (See Figure 8.1).

At weir loads greater than 50 $cm^3/cm.s$, flow separation was produced at the ends of the inlet downcomer such that liquid circulation was formed on the tray segments. On increasing the weir load upto a maximum, the velocity of forward flow increased. This was reflected in the "straightening-up" of the sixteen flow pointers in the region between the downcomers such that the arrow indicators were perpendicular to the weir lengths.

The faster moving forward flow across the tray was accompanied by larger and more powerful liquid circulation which occupied a greater area of the tray segments. The amount of tray area occupied by circulating flow was estimated visually in terms of the number of flow pointers affected by the rotational motion of the liquid. Although very few flow pointers were observed to be continuously rotating in the circulating liquid, there was clear evidence of flow pointers being affected by liquid circulation due to their partial "turning" behaviour, or flow pointers pointing backwards towards the inlet downcomer. A summary of the number of flow pointers which correspond to a percentage of tray area occupied by liquid circulation is presented in Table 8.2.

A maximum of 30% liquid circulation on the tray segments was produced at the highest weir loads, but the rate of formation of circulating flow was dependant upon the ease of flow separation. That is, when the tray was configured with the inlet gap and outlet weir height of 10 mm, the maximum circulating flow was achieved at the weir load of 120 $cm^3/cm.s$. Further increases in the weir load, merely reinforced the flow boundary of the circulation area, as well as increasing the rotational velocity of the circulating liquid. The intensity of liquid channelling associated with 30% circulation was the result of the high horizontal liquid velocity entering the tray from beneath the inlet gap height of 10 mm.

At the inlet gap and outlet weir height of 20 mm, however, the maximum circulating flow was achieved at the much higher weir loading of 250 $cm^3/cm.s$, as a result of the lower liquid entrance velocity from beneath the inlet downcomer. When circulating air-water flow patterns were compared with that produced during water-only flow, the effect of the gas cross flow through the liquid inhibited circulating flow, such that much higher weir loads were required to produce the same area of circulating liquid.

Percentage of Tray Area Occupied by Circulation	Number of Flow Pointers affected on each Tray Segment
5 and 7	2 completely affected, 3rd flow pointer partially affected
10	3 completely affected
12	3, 4th flow pointer partially affected
15	4, 5th flow pointer partially affected - corresponds to whole of inlet segments
17	5 completely affected
20	6 completely affected
22	6, 7th flow pointer partially affected
25	7, 8th flow pointer partially affected
30	8 to 9 completely affected - corresponds to whole of tray segments

Table 8.2 Summary of number of flow pointers used to estimate the percentage of tray area occupied by circulating flow.

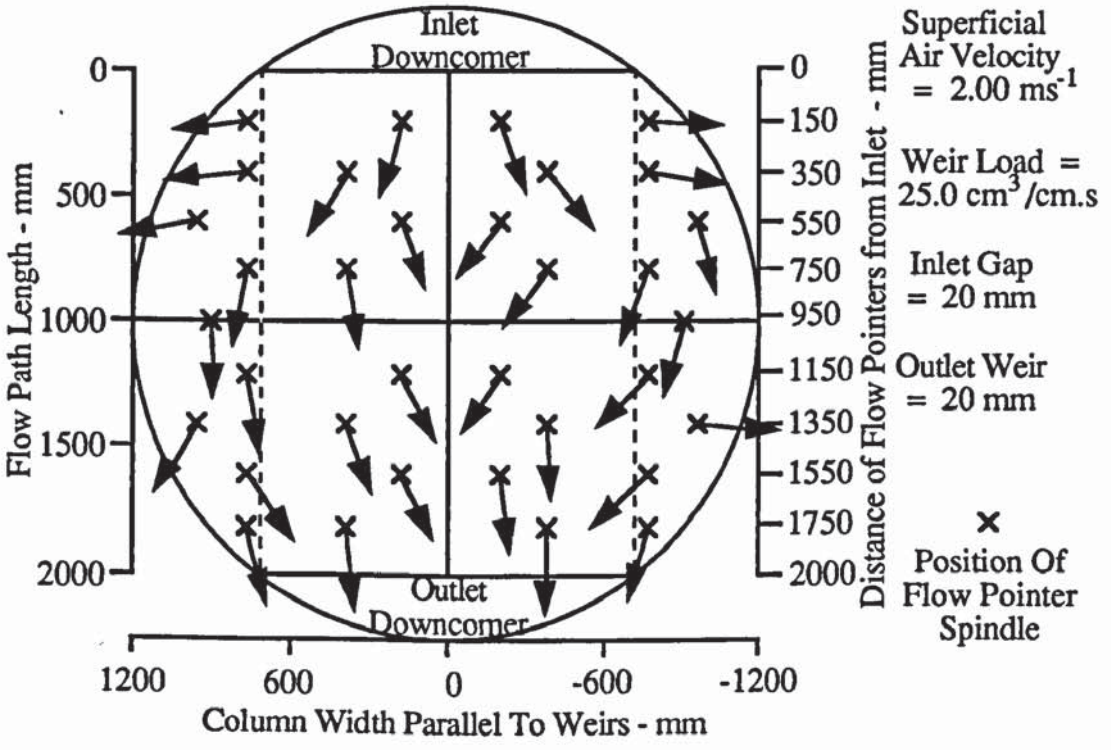

Figure 8.2 Flow pointer arrangement showing forward only flow at the inlet gap and outlet weir heights of 20 mm.

On increasing the air velocity from 1.00 ms^{-1} upto 2.50 ms^{-1}, there was a slow but steady decrease in the velocity of circulating flow and in some cases, the gas flow prevented the maximum circulation of 30%. This was especially true at the inlet gap and outlet weir heights of 20 mm. An example of liquid channelling associated with a maximum of 30% circulating flow is presented in Figure 8.3.

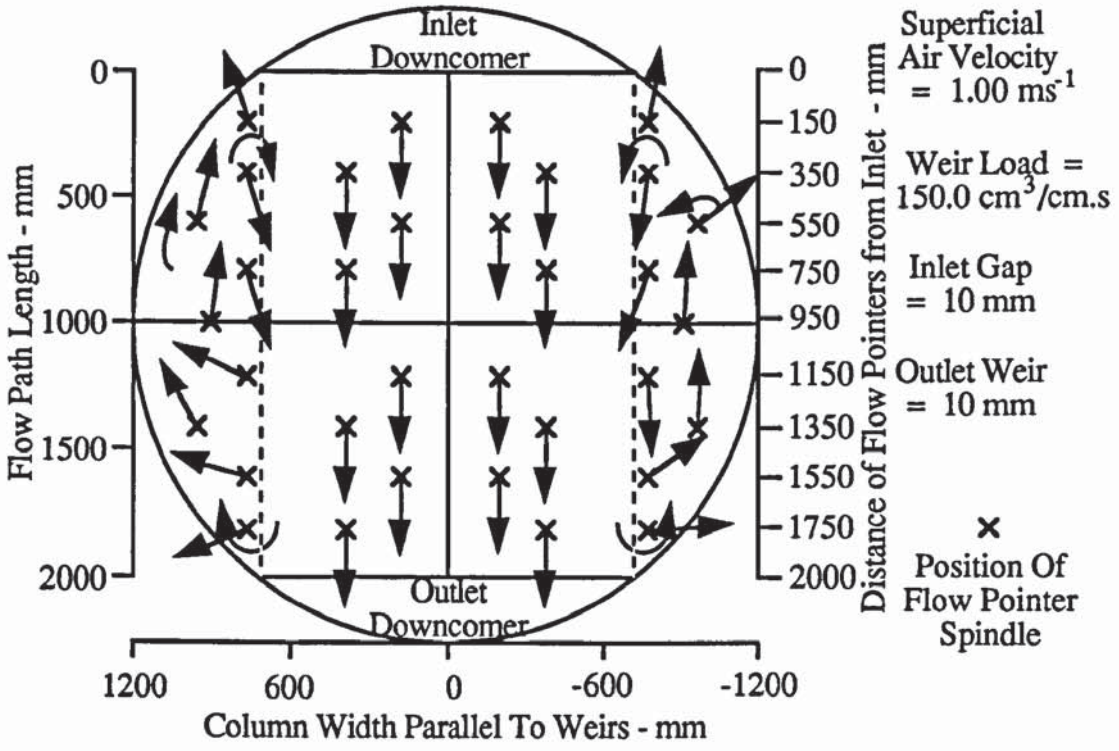

Figure 8.3 Flow pointer arrangement showing liquid channelling and a maximum of 30% circulation at the inlet gap and outlet weir heights of 10 mm.

Summaries of the flow pattern results for the two sets of inlet gap/outlet weir heights are presented on a modified vapour load factor verses weir load diagram in Figures 8.4 and 8.5, using the notation defined in Chapter 5. The air-water flow rates and flow pattern information are presented in a matrix format.

Note that in Figure 8.5, the superficial air velocity was raised from 1.00 to 1.25 ms^{-1} for weir loadings above 150 $cm^3/cm.s$ so as to eliminate the problems of liquid weeping from the test tray.

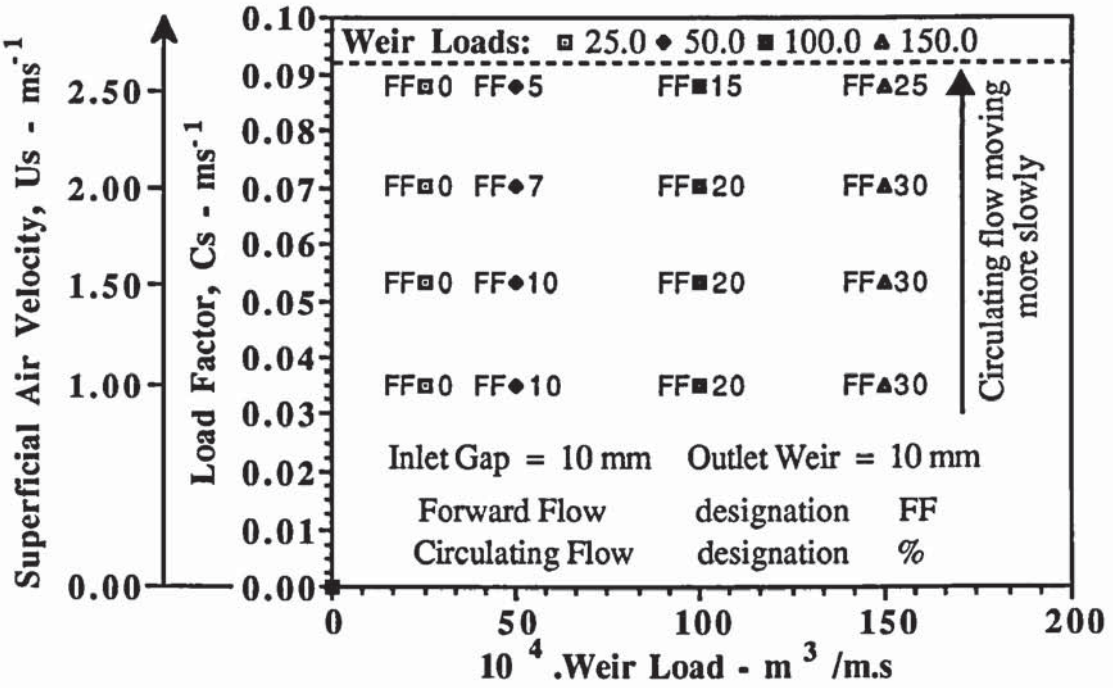

Figure 8.4 Summary of flow patterns on a load factor verses weir load diagram at the inlet gap and outlet weir height of 10 mm.

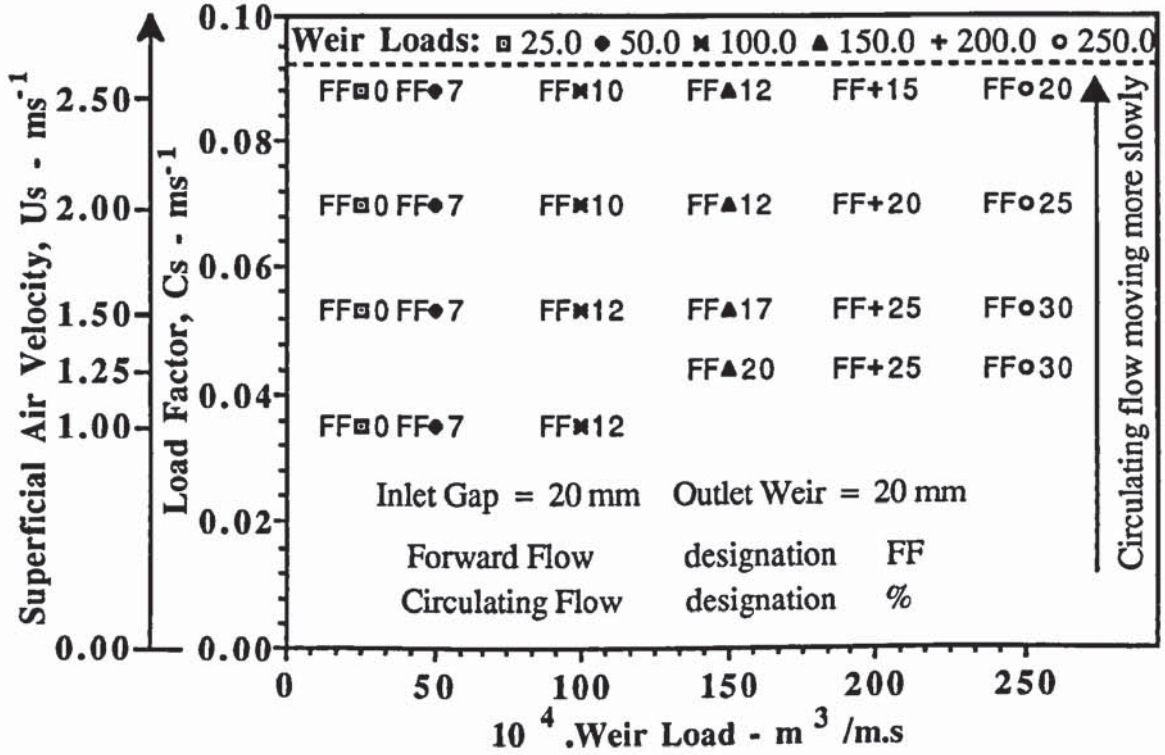

Figure 8.5 Summary of flow patterns on a load factor verses weir load diagram at the inlet gap and outlet weir height of 20 mm.

Separated and Non-Separated Flow Patterns at Large Froth Heights

The air-water flow pattern results were similar to those generated at low froth heights with a few notable exceptions. In all the experiments, the biphase dispersion appeared to be more chaotic than that observed at the lower froth heights and this was reflected in the frequent oscillating behaviour of all the flow pointers on the tray. This was caused by an increase in air-water mixing both in the horizontal and vertical directions as a result of the increased gas-liquid contact time and gas residence time within a higher depth of liquid on the test tray.

These effects in addition to the slow liquid entrance velocity from beneath the larger inlet downcomer clearance were responsible for the lower velocity of the forward flow both in the non-separated and separated air-water flow patterns. A typical example of a non-separated flow pattern, showing forward only flow is presented in Figure 8.6a.

In the experiments where flow separation occurred, the gas resistance within the slower moving higher liquid depth on the tray, compared with the previous experiments, reduced the extent of circulating flow on the tray segments even at the highest weir loads. That is, the maximum area on the tray occupied by liquid circulation was in several cases 15% but no more than 20% even when the weir load was increased to a maximum of 300 $cm^3/cm.s$, (see Figure 8.6b). Hence the gas resistance in addition to the slow liquid cross flow velocity, produced from the large inlet downcomer clearance of 50 mm, was successful in preventing 30% circulation.

All the flow patterns generated at the large froth heights are summarised on the modified vapour load factor verses weir load diagram presented in Figure 8.7. It should be noted that in order to eliminate the problems of liquid weeping from the test tray and to account for the presence of a larger liquid depth, the superficial air velocity was increased from 1.00 ms^{-1} to 1.25 ms^{-1}.

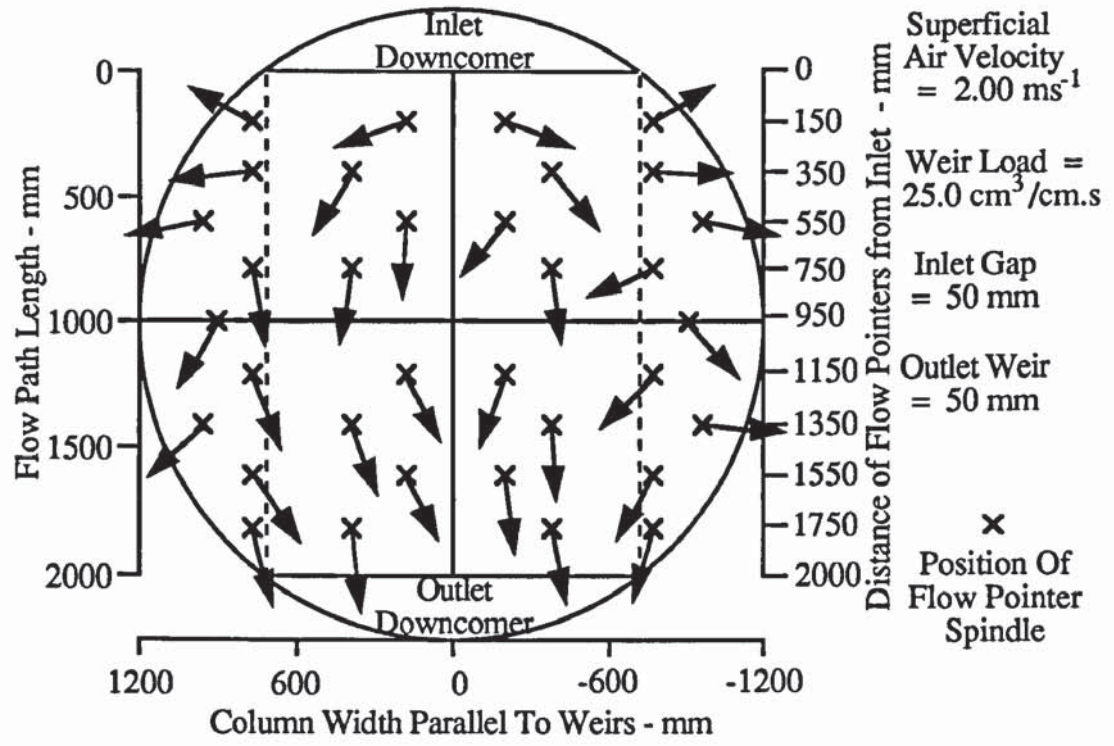

Figure 8.6a Flow pointer arrangement showing forward only flow at the inlet gap and outlet weir heights of 50 mm.

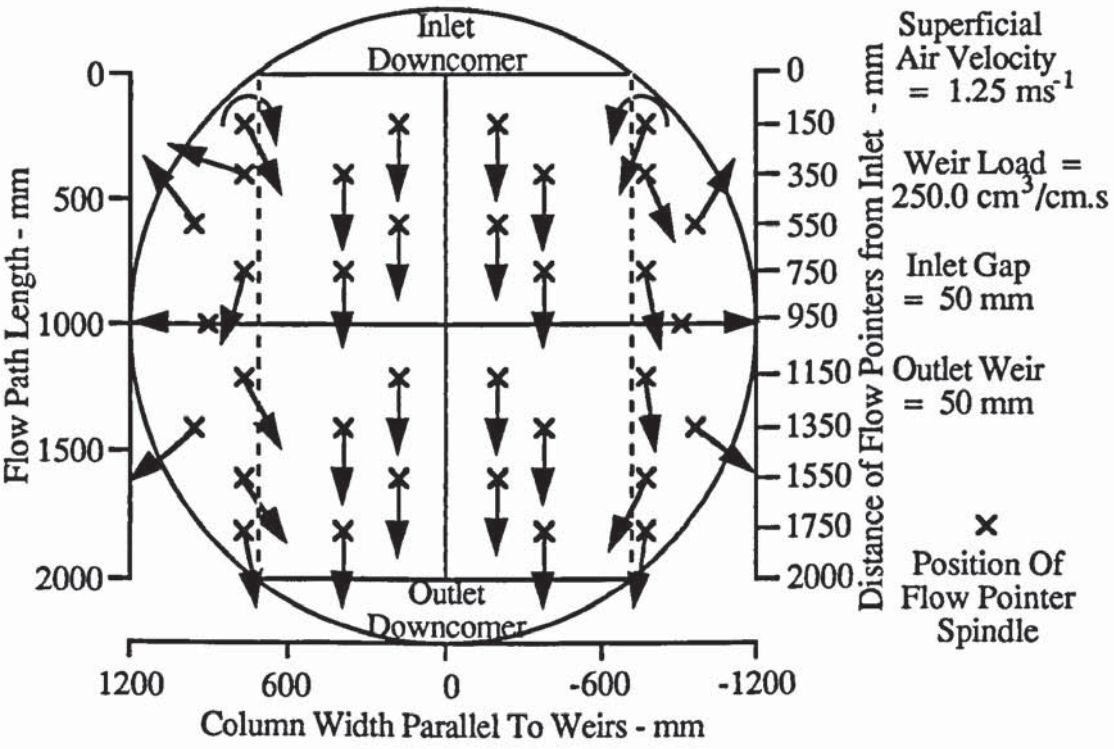

Figure 8.6b Flow pointer arrangement showing forward flow associated with 15% circulation at the inlet gap and outlet weir heights of 50 mm.

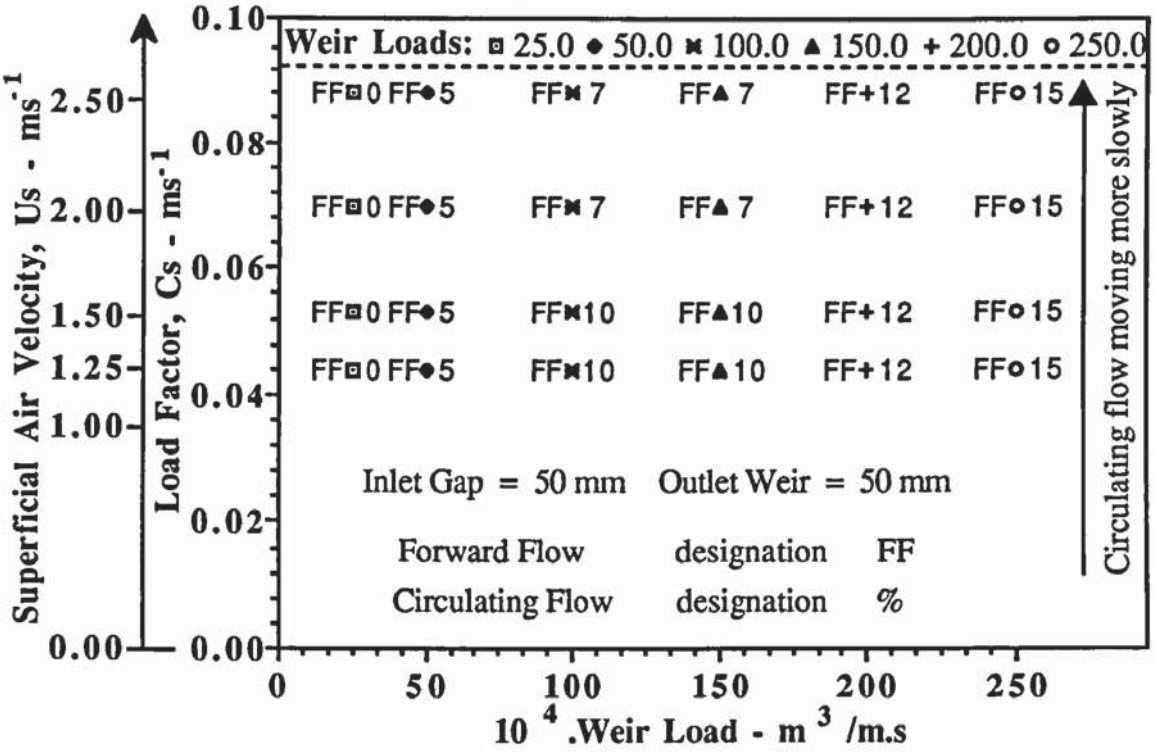

Figure 8.7 Summary of flow patterns on a load factor verses weir load diagram at the inlet gap and outlet weir height of 50 mm.

Discussion and Explanation of Results

The gas-liquid contacting experiments have shown that the passage of air through water, flowing across the perforated test tray had a significant effect on the developed flow patterns. When as a single phase, the water-only flowed across a rapidly diverging/converging open channel formed by a single pass tray, flow separation was produced at the ends of the inlet downcomer. In most cases, with the exception of very low weir loads, this resulted in the formation of circulating regions along the segments at the sides of the tray.

The effect of forcing the gas through the liquid delayed the onset of flow separation, which only occurred at much higher weir loads and high liquid inlet velocities produced from small clearance heights beneath the inlet downcomer. The rate of increase of circulating flow associated with increasing weir load, was less than that for water-only flow and showed a strong dependance on the inlet downcomer gap through which the liquid entered the tray. Hence the larger the inlet gap, the smaller the velocity of the liquid entering the tray, and the larger the weir load required to produce a given area of circulating flow.

A summary of all the flow pattern results produced at both the large and small froth

heights, were incorporated onto a graph of circulation size, expressed as a percentage of tray area, plotted against weir load and is presented in Figure 8.8.

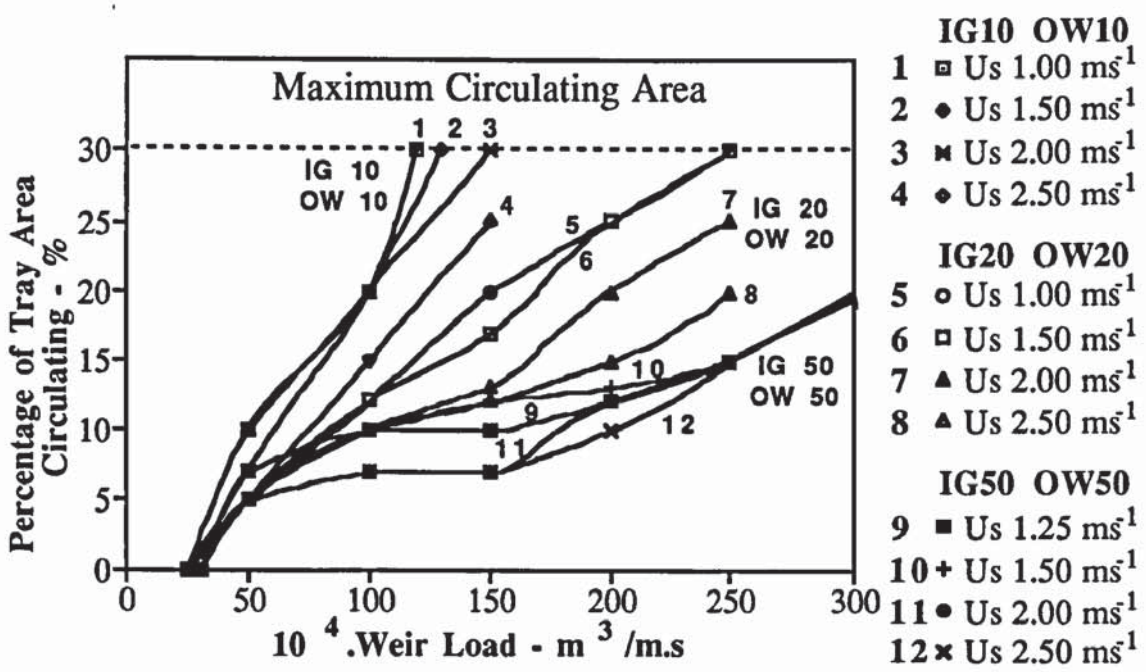

Figure 8.8 Summary of air-water circulating flow patterns on 6.35 mm tray.

Overall, the effect of increasing the froth height and the gas-liquid contacting time reduces liquid circulation and channelling.

Conclusion

The effect of forcing the gas through the liquid on a tray prevented flow separation, which only occurred at much higher weir loads and with smaller inlet downcomer clearance heights (i.e., at high liquid inlet velocities) compared with the separated water-only flow patterns.

The effects of separated and non-separated flow air-water patterns on mass transfer is presented in the next section.

8.3.4 Investigation by Water-Cooling

The water-cooling technique involves temperature profiling, to generate isothermal contour maps, and the calculation of thermal efficiencies, from enthalpy driving forces, for the same flow conditions used in the previous section. A complete description of the water-cooling technique, including the calculation of thermal efficiencies, is contained in Chapter 5.

The flow rate conditions and tray configurations used in this investigation are presented in Table 8.1.

Temperature Profile Results

All of the temperature isotherm results were compared on a like basis by using reduced temperature profiles. By definition, the water entering the tray is assigned a reduced temperature of 1.0, while the water flowing across the tray from the inlet to the outlet has a reduced temperature in between 1.0 and 0.0.

Overall, isotherms can be broadly classified as straight and parallel to the downcomers, indicative of forward only flow at all points on the tray, and "U-shapes" which correspond to forward flow with a superimposed velocity distribution profile. (That is, the liquid flows more slowly at the sides compared with that in the middle of the tray). The severity of the "U-shaped" isotherms was dependant upon the froth heights and the steady increase in the air-water flow rates.

In some of the experiments at low water flow rates, the reduced temperature profiles showed a certain level of non-symmetry on the operating tray in that the liquid tends to be colder or the isotherms are skewed towards the right hand side. Measures taken to rectify the problem have been described in Chapter 6. However, the continued presence of skewed isotherms particularly at low air and water flow rates show that the water-cooling technique is sensitive to tray out-of-levelness. Thus if a particular temperature profile is seen as one of a series of profiles, then a view beneath the non-symmetry can be obtained.

Effect of Non-Separated and Separated Flow Patterns on the Temperature Profile Results at Low Froth Heights

At the low weir loadings, for a given fixed air velocity, the reduced temperature isotherms over most of the tray were approximately straight and parallel to the downcomers. This was indicative of the non-separated flow patterns in which a calm forward flow was produced over most of the tray. Each isotherm stretched over the whole of the tray cross-section indicating the same reduced temperature of the liquid at the sides of the tray as well as in the middle. Parallel temperature profiles imply that the liquid residence time distribution would be similar, both at the sides and in the middle of the tray.

Despite the uniform distribution of reduced temperature isotherms, the liquid on the tray segments flowed over a longer liquid flow path which accounts for the slight "tailing-off"

of isotherms at the sides of the tray in some of the temperature profile results. Thus, the slower forward flow on the tray segments, particularly near the ends of the outlet weir, showed up as the coldest liquid regions. (For example, the reduced temperature, T_r, = 0.400-0.350 in Figure 8.11a).

On increasing the weir load such that flow separation occurred, forward flow, associated with the superimposed velocity distribution profile, and circulating flow showed up as "U-shaped" isotherms and contour lines adjacent to the tray perimeter. The contour lines, in many cases, "linked-up" to the column wall or formed a closed loop. One striking feature about the U-shaped profiles, is that they consist of a horizontal line parallel to the downcomers, and a "swept-back" part at the sides.

The horizontal isotherm component was approximately 1300-1400 mm in length which suggests plug flow of liquid across the horizontal plane between the downcomers. The "swept-back" part of the isotherm stretched back towards the ends of the inlet downcomer and this together with contour lines adjacent to the column wall on the tray segments, was indicative of circulating liquid. This type of U-shaped profile was designated either a shallow or a severe transverse "U-shaped" isotherm depending upon the relative steepness of the "U-shapes".

At the maximum weir loading, liquid channelling and a maximum of 30% circulation showed up as severe transverse "U-shaped" isotherms associated with tightly packed and closed looped isotherms. The coldest liquid regions, emanating from the ends of the inlet downcomer, were contained within the closed looped isotherms, (T_r = 0.625 in Figure 8.11b), and occupied most of the tray segments. The reduced temperature of circulating liquid was less than that for liquid flow over the outlet weir which causes a reduction in the driving force for mass transfer and results in a fall-off in tray efficiency.

A summary of the reduced temperature isotherms for all of the gas-liquid contacting experiments at low froth heights, are presented on a modified load factor verses weir load diagram as shown in Figures 8.9 and 8.10.

The effect of increasing the air velocity on the temperature isotherms during the flow separation experiments, was a flattening of the transverse "U-shaped" isotherms such that they became less severe. In addition, there was an increase in the number of confused isotherms particularly on the tray segments.

Overall, liquid channelling and circulating flow have a substantial effect on the reduced temperature isotherms at low froth heights.

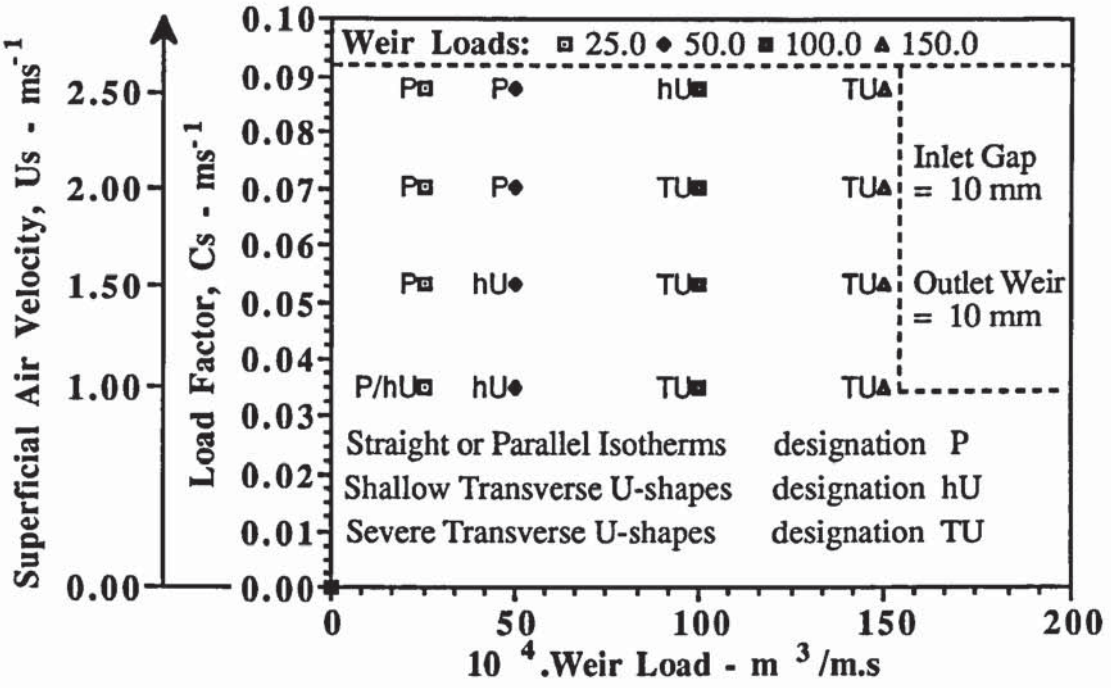

Figure 8.9 Summary of isotherm profiles on a load factor verses weir load diagram.

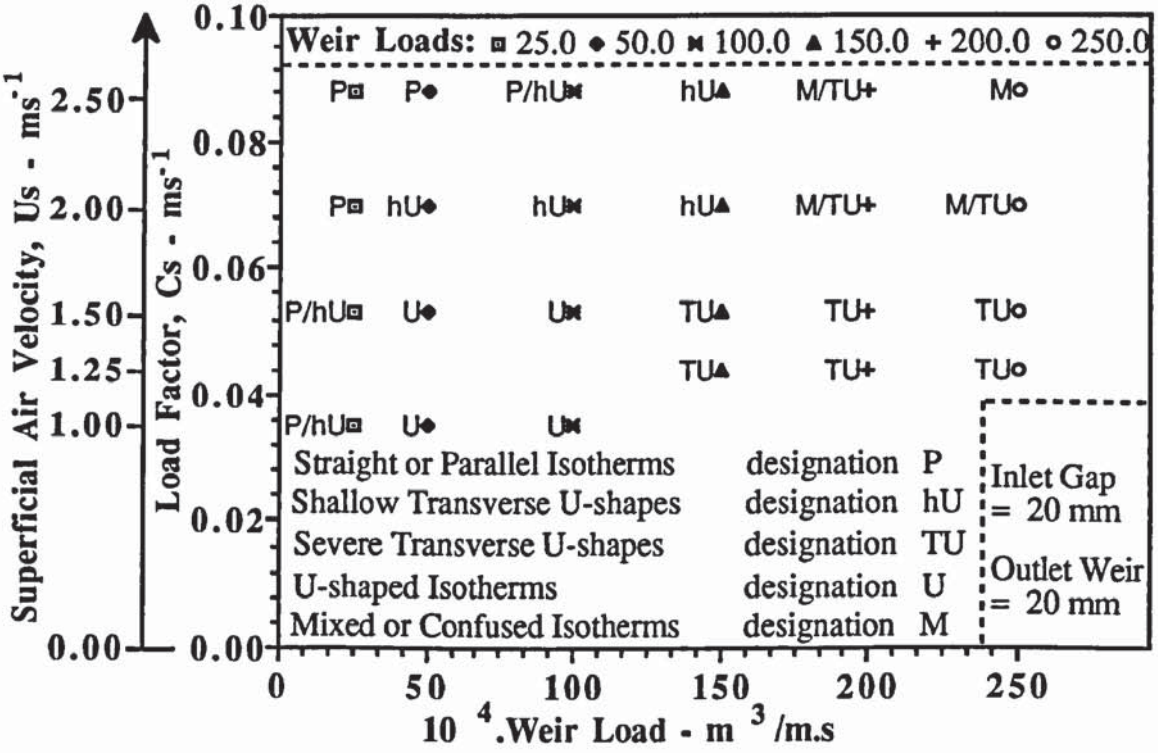

Figure 8.10 Summary of isotherm profiles on a load factor verses weir load diagram.

Examples of two-dimensional reduced temperature profiles from the non-separated flow and separated flow experiments, are presented in Figures 8.11a, 8.11b, 8.12a and 8.12b.

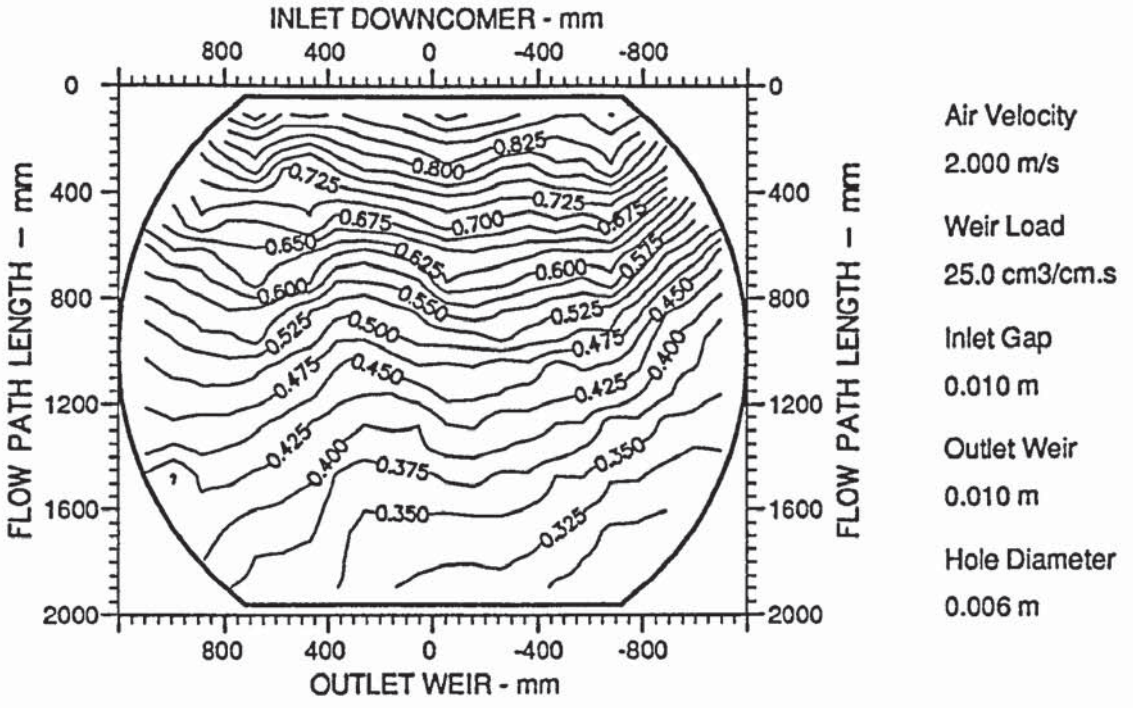

Figure 8.11a An example of a two-dimensional reduced temperature profile diagram showing straight and parallel isotherms (designation P).

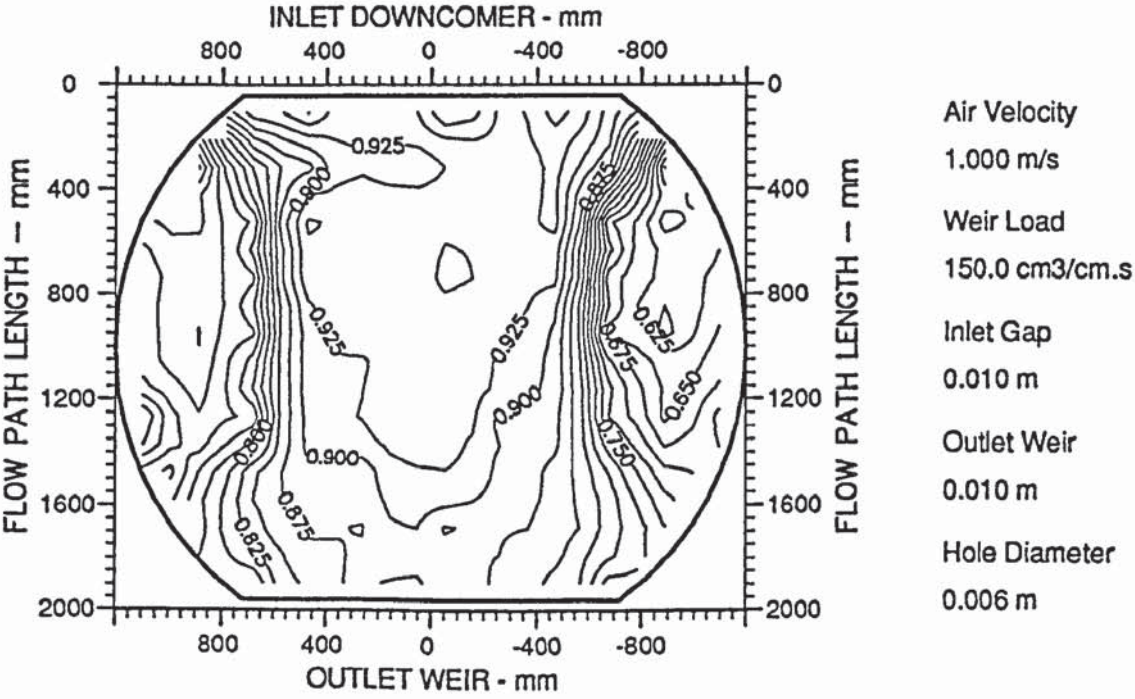

Figure 8.11b An example of a two-dimensional reduced temperature profile diagram showing severe transverse "U-shaped" isotherms (designation TU).

Effect of Non-Separated and Separated Flow Patterns on the Temperature Profile Results at Large Froth Heights

The temperature isotherm results at large froth heights are similar to those described above with a few notable exceptions. The first is that for both non-separated and separated flow, there was a greater number of mixed or confused profiles particularly at higher air velocities. These comprised mainly of "U-shapes", isotherms parallel to the downcomers, isotherms adjacent to the tray boundary, and closed looped isotherms on the tray segments.

Many of the mixed isotherms were found on the tray segments and corresponded to colder regions on the tray, indicative of slow forward flow during non-separated flow, (T_r = 0.425-0.275 in Figure 8.13a), and slow circulation during separation of flow, (T_r = 0.875-0.800 in Figure 8.13b). The increased number of mixed isotherms can be attributed to the increased level of random mixing of froth elements in all directions, and a greater gas-liquid contact time within the larger froth depth on the tray.

The second major difference in the temperature isotherm results, was that the isotherms were distinctively "U-shaped" with the leading edge located on, or close to, the tray centreline. These "U-shapes" were indicative of forward flow, with a superimposed velocity distribution profile, such that the liquid was fastest along the middle of the tray and slowest at the sides. This was shown by the alignment of flow pointers across the tray as shown in Figure 8.6b.

Flow patterns consisting of 15%, but no more than 20%, circulating liquid were reflected in the tightly packed isotherms at the ends of the inlet downcomer, and the much smaller closed looped isotherms on the tray segments. It is these regions that contain the coldest liquid and have a greater residence time as a result of more gas passing through the liquid compared with that for warmer liquid found in the middle of the tray. The reduced temperature of the circulating liquid was less than that of the liquid flow over the outlet weir, thus having an adverse effect on tray efficiency.

As with the low froth height experiments, the effect of increasing the air velocity on the temperature isotherms, resulted in a flattening of the U-shaped isotherms. In addition, there was a significant increase in the number of mixed or confused isotherms, particularly on the tray segments. This may be attributed to the higher level of turbulence and mixing of the liquid by the bubbling action of the air through the relatively large froth dispersion.

A summary of the reduced temperature isotherms generated during the large froth height experiments, is presented on a modified load factor verses weir load diagram as shown in Figure 8.12.

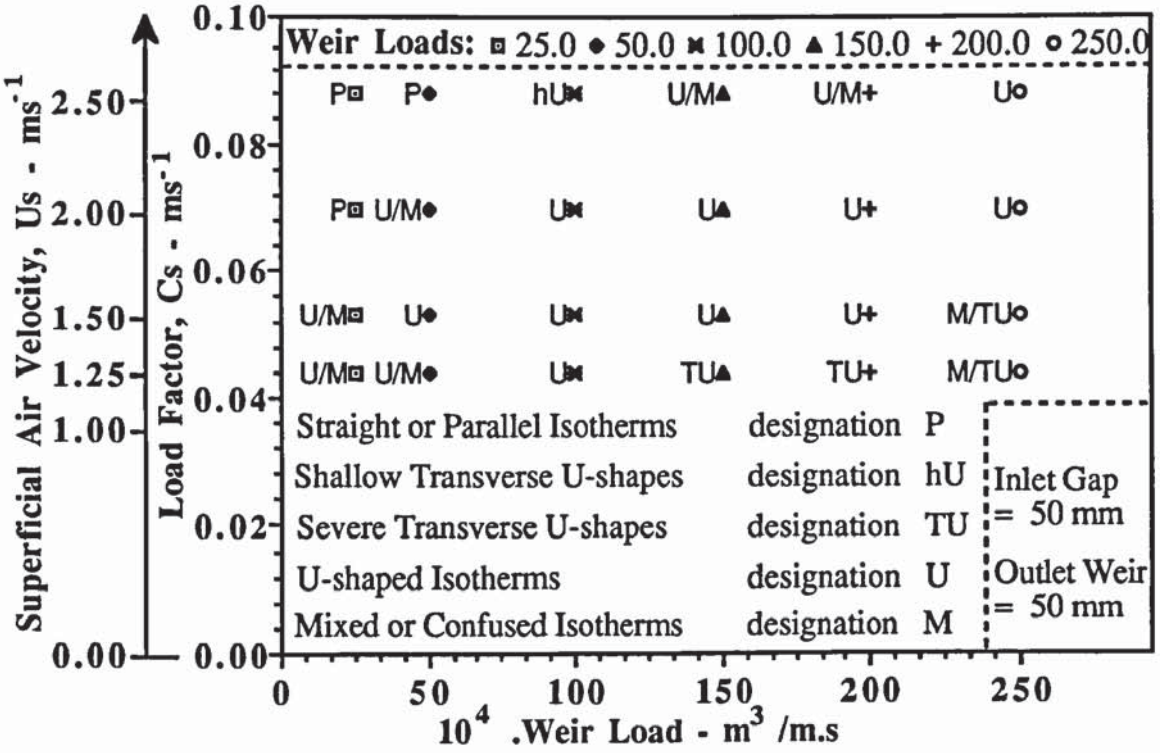

Figure 8.12 Summary of isotherm profiles on a load factor verses weir load diagram.

Overall, the effect of circulating flow on the reduced temperature isotherms was less than that encountered in the low froth height experiments. However, the increased turbulence and mixing as a result of the increased gas-liquid contacting time, and the superimposed velocity distribution on forward flow all had an effect on the reduced temperature isotherms during the large froth height experiments.

Examples of the two-dimensional reduced temperature profiles showing forward only flow and forward flow associated with 15% circulation, are presented in Figures 8.13a and 8.13b.

A complete set of two-dimensional reduced temperature isotherms generated at the equal inlet gap and outlet weir heights of 10 mm, 10 mm; 20 mm, 20 mm; and 50 mm, 50 mm are presented in Appendix 7.0.

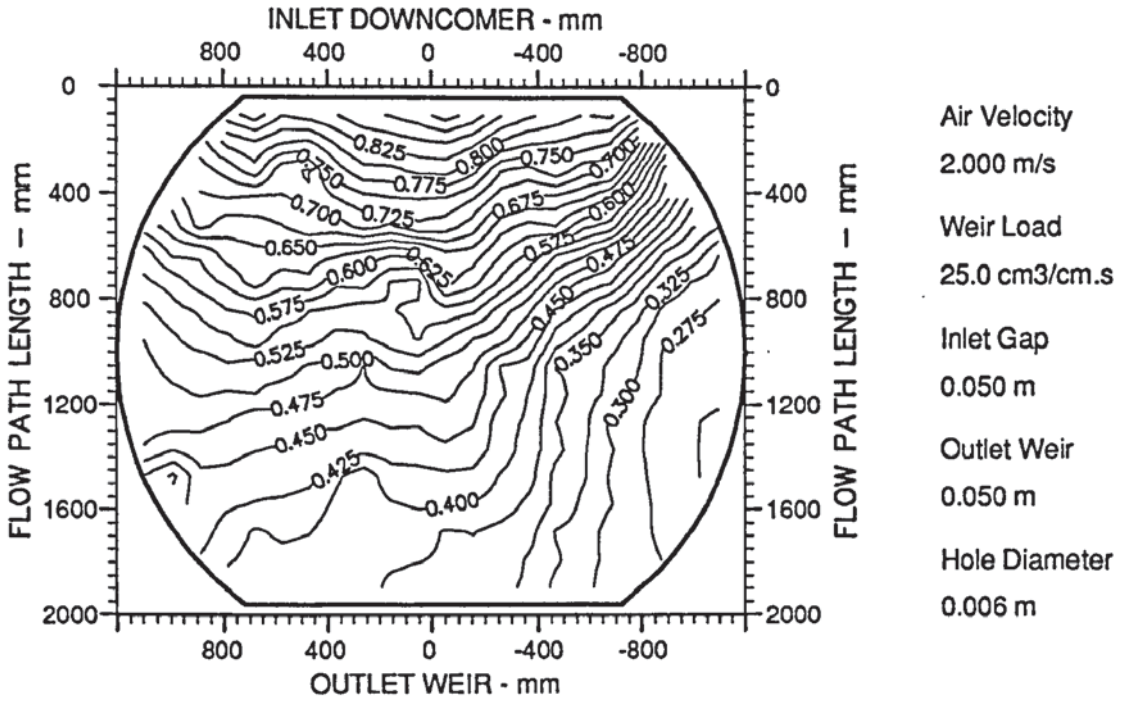

Figure 8.13a An example of a two-dimensional reduced temperature profile diagram showing straight and parallel isotherms (designation P).

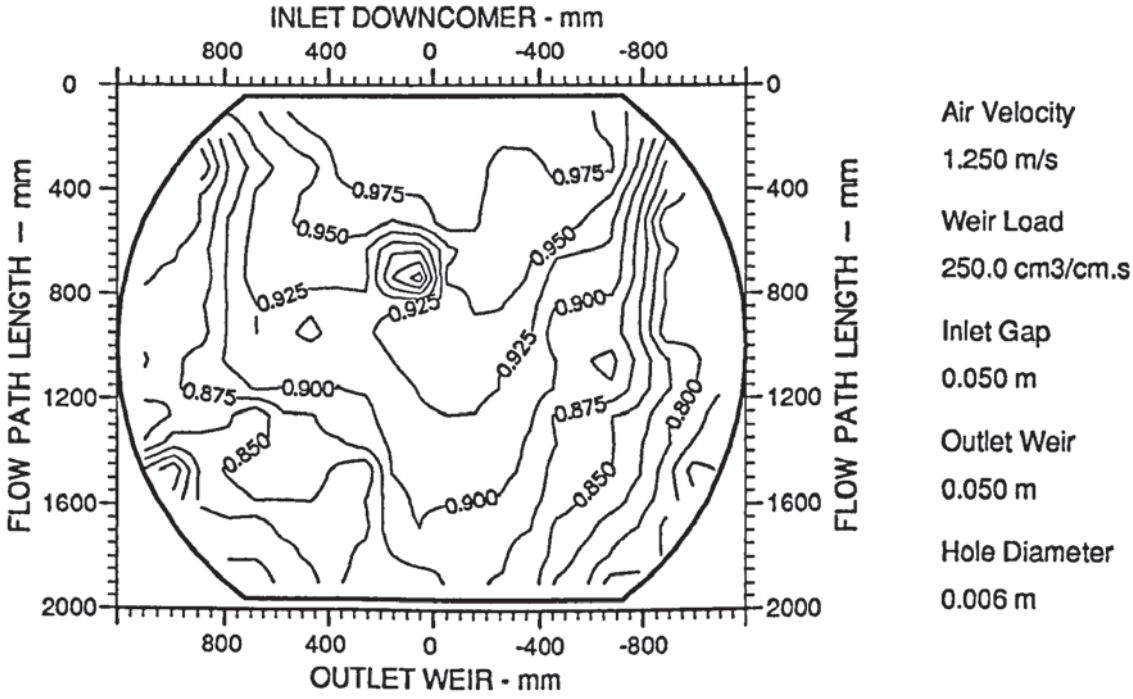

Figure 8.13b An example of a two-dimensional reduced temperature profile diagram showing transverse "U-shaped" and closed looped isotherms (designation M/TU).

Discussion of Results

In general, the temperature profiles, obtained during water-cooling, showed that the longer the liquid remained on the tray, the cooler it became. Thus colder temperatures were found on the long liquid flow path tray segments, where the liquid was either moving slowly forward or circulating. This caused a reduction in the driving force for mass transfer which ultimately leads to a low tray efficiency.

The prevention of flow separation by the gas resistance when forced through the liquid, at low weir loads, producing forward only flow, was reflected in the comparatively straight reduced temperature isotherms which ran parallel to the downcomers. At higher weir loads, where flow separation occurred, a significant proportion of the tray occupied by circulating flow showed up as "U-shaped" isotherms associated with contours lines forming a closed boundary at the sides of the tray. In the most extreme case of liquid channelling associated with a maximum circulation of 30%, the highly transverse "U-shaped" isotherms revealed a plugflow of liquid between the downcomers. The closed looped contours on the tray segments, indicated a steep temperature gradient, thus showing that the coldest liquid was near the ends of the inlet downcomer.

The "U-shaped" isotherms obtained with both forward flow and with a region of circulation at the sides of the tray are similar to the concentration profiles predicted in the stagnant regions model, (SRM), Porter et al., (1972). In this model, it was assumed, that the liquid at the sides of the tray is stagnant, i.e., in between slow forward flow and a circulating flow near the column wall. The predicted concentration profiles for various tray geometries were "U-shaped" and corresponded to a rapid depletion of the most volatile component in the stagnant zones. This is significant, particularly with large stagnant zones, because no replenishment of the most volatile component into these regions means that further passage of the vapour through the stagnant liquid undergoes no composition change. Since the duty of the tray is to change the vapour composition, this reduces tray efficiency and is discussed further in the next section.

Thermal Efficiency Results

The temperature profile results from the above experiments were used for the calculation of point and tray efficiencies. The procedure for the calculation of thermal efficiencies is described in Section 5.3.5 of Chapter 5. The point efficiency, E_{OG}; tray efficiency, E_{MV}; and the ratio of E_{MV}/E_{OG} results for all the experiments are presented in Tables 8.3, 8.4 and 8.5.

I.G./O.W. - mm	10,10							
Superficial Air Velocity - ms^{-1}	1.00		1.50		2.00		2.50	
10^4.Weir Load - $m^3/m.s$	Efficiency %		Efficiency %		Efficiency %		Efficiency %	
25.0	E_{OG}	39	E_{OG}	38	E_{OG}	43	E_{OG}	48
	E_{MV}	59	E_{MV}	60	E_{MV}	84	E_{MV}	101
	E_{MV}/E_{OG}	1.50	E_{MV}/E_{OG}	1.59	E_{MV}/E_{OG}	1.93	E_{MV}/E_{OG}	2.09
50.0	E_{OG}	66	E_{OG}	65	E_{OG}	64	E_{OG}	66
	E_{MV}	96	E_{MV}	97	E_{MV}	105	E_{MV}	121
	E_{MV}/E_{OG}	1.45	E_{MV}/E_{OG}	1.48	E_{MV}/E_{OG}	1.65	E_{MV}/E_{OG}	1.82
100.0	E_{OG}	67	E_{OG}	76	E_{OG}	69	E_{OG}	73
	E_{MV}	77	E_{MV}	90	E_{MV}	88	E_{MV}	98
	E_{MV}/E_{OG}	1.15	E_{MV}/E_{OG}	1.19	E_{MV}/E_{OG}	1.27	E_{MV}/E_{OG}	1.35
150.0	E_{OG}	54	E_{OG}	77	E_{OG}	73	E_{OG}	77
	E_{MV}	51	E_{MV}	78	E_{MV}	77	E_{MV}	96
	E_{MV}/E_{OG}	0.94	E_{MV}/E_{OG}	1.01	E_{MV}/E_{OG}	1.05	E_{MV}/E_{OG}	1.25

Table 8.3 Summary of measured point and tray thermal efficiencies on the 6.35mm tray using an inlet gap/ outlet weir combination of 10 mm.

I.G./O.W. - mm	20,20							
Superficial Air Velocity - ms^{-1}	1.00 * Us = 1.25 ms^{-1}		1.50		2.00		2.50	
10^4.Weir Load - $m^3/m.s$	Efficiency %		Efficiency %		Efficiency %		Efficiency %	
25.0	E_{OG}	52	E_{OG}	52	E_{OG}	43	E_{OG}	41
	E_{MV}	82	E_{MV}	91	E_{MV}	75	E_{MV}	72
	E_{MV}/E_{OG}	1.57	E_{MV}/E_{OG}	1.76	E_{MV}/E_{OG}	1.74	E_{MV}/E_{OG}	1.77
50.0	E_{OG}	76	E_{OG}	65	E_{OG}	65	E_{OG}	66
	E_{MV}	104	E_{MV}	92	E_{MV}	110	E_{MV}	106
	E_{MV}/E_{OG}	1.38	E_{MV}/E_{OG}	1.43	E_{MV}/E_{OG}	1.68	E_{MV}/E_{OG}	1.60
100.0	E_{OG}	62	E_{OG}	72	E_{OG}	71	E_{OG}	71
	E_{MV}	77	E_{MV}	91	E_{MV}	92	E_{MV}	93
	E_{MV}/E_{OG}	1.25	E_{MV}/E_{OG}	1.26	E_{MV}/E_{OG}	1.30	E_{MV}/E_{OG}	1.31
150.0	E_{OG}	*72	E_{OG}	74	E_{OG}	75	E_{OG}	74
	E_{MV}	82	E_{MV}	84	E_{MV}	85	E_{MV}	89
	E_{MV}/E_{OG}	1.13	E_{MV}/E_{OG}	1.14	E_{MV}/E_{OG}	1.13	E_{MV}/E_{OG}	1.21
200.0	E_{OG}	*77	E_{OG}	74	E_{OG}	77	E_{OG}	78
	E_{MV}	83	E_{MV}	77	E_{MV}	81	E_{MV}	89
	E_{MV}/E_{OG}	1.08	E_{MV}/E_{OG}	1.04	E_{MV}/E_{OG}	1.05	E_{MV}/E_{OG}	1.14
250.0	E_{OG}	*77	E_{OG}	70	E_{OG}	76	E_{OG}	81
	E_{MV}	77	E_{MV}	68	E_{MV}	75	E_{MV}	87
	E_{MV}/E_{OG}	0.99	E_{MV}/E_{OG}	0.97	E_{MV}/E_{OG}	0.99	E_{MV}/E_{OG}	1.08

Table 8.4 Summary of measured point and tray thermal efficiencies on the 6.35mm tray using an inlet gap/ outlet weir combination of 20 mm.

I.G./O.W. - mm	50,50							
Superficial Air Velocity - ms^{-1}	1.25		1.50		2.00		2.50	
10^4.Weir Load - $m^3/m.s$	Efficiency %		Efficiency %		Efficiency %		Efficiency %	
25.0	E_{OG}	53	E_{OG}	56	E_{OG}	51	E_{OG}	49
	E_{MV}	71	E_{MV}	85	E_{MV}	85	E_{MV}	91
	E_{MV}/E_{OG}	1.34	E_{MV}/E_{OG}	1.51	E_{MV}/E_{OG}	1.67	E_{MV}/E_{OG}	1.87
50.0	E_{OG}	76	E_{OG}	78	E_{OG}	70	E_{OG}	69
	E_{MV}	94	E_{MV}	105	E_{MV}	98	E_{MV}	114
	E_{MV}/E_{OG}	1.23	E_{MV}/E_{OG}	1.34	E_{MV}/E_{OG}	1.40	E_{MV}/E_{OG}	1.64
100.0	E_{OG}	85	E_{OG}	87	E_{OG}	79	E_{OG}	76
	E_{MV}	103	E_{MV}	105	E_{MV}	96	E_{MV}	102
	E_{MV}/E_{OG}	1.22	E_{MV}/E_{OG}	1.20	E_{MV}/E_{OG}	1.22	E_{MV}/E_{OG}	1.34
150.0	E_{OG}	79	E_{OG}	91	E_{OG}	81	E_{OG}	79
	E_{MV}	92	E_{MV}	102	E_{MV}	89	E_{MV}	96
	E_{MV}/E_{OG}	1.17	E_{MV}/E_{OG}	1.13	E_{MV}/E_{OG}	1.10	E_{MV}/E_{OG}	1.21
200.0	E_{OG}	80	E_{OG}	89	E_{OG}	87	E_{OG}	81
	E_{MV}	90	E_{MV}	95	E_{MV}	94	E_{MV}	93
	E_{MV}/E_{OG}	1.12	E_{MV}/E_{OG}	1.06	E_{MV}/E_{OG}	1.07	E_{MV}/E_{OG}	1.14
250.0	E_{OG}	80	E_{OG}	85	E_{OG}	87	E_{OG}	83
	E_{MV}	85	E_{MV}	88	E_{MV}	92	E_{MV}	92
	E_{MV}/E_{OG}	1.07	E_{MV}/E_{OG}	1.04	E_{MV}/E_{OG}	1.05	E_{MV}/E_{OG}	1.11

Table 8.5 Summary of measured point and tray thermal efficiencies on the 6.35mm tray using an inlet gap/ outlet weir combination of 50 mm.

Since the separation of flow was affected most by the water weir load operating variable, the E_{OG}, E_{MV}, and the ratio of E_{MV}/E_{OG} results were averaged for each superficial air velocity and plotted against the corresponding average clear liquid height readings. (See Section 8.3.5 for the measurement of clear liquid height). Graphical presentation of the efficiency results are shown in Figures 8.14, 8.15, and 8.16.

The E_{OG} results show a dramatic increase as the weir load was increased from 25.0 to 100.0 $cm^3/cm.s$, (which corresponds to a significant increase in the clear liquid height). However, a further increase in the weir load (clear liquid height) resulted in a rapid decline in the rate of increase in point efficiency and in some cases, particularly at the low froth heights, there was a slight decrease in the value of E_{OG}, (see Figure 8.14). In principle, E_{OG} is calculated independant of the flow pattern and therefore the trend in E_{OG} results may be attributed to variations in the height of clear liquid which were most significant at the highest weir loadings. That is the liquid head at the sides of the tray was much greater than that in the middle, particularly on the tray inlet. This would have reduced the gas residence time both in the fast forward liquid flow in the middle of the tray and in the slowly forward or circulating liquid flow at the sides, (see Section 8.3.5).

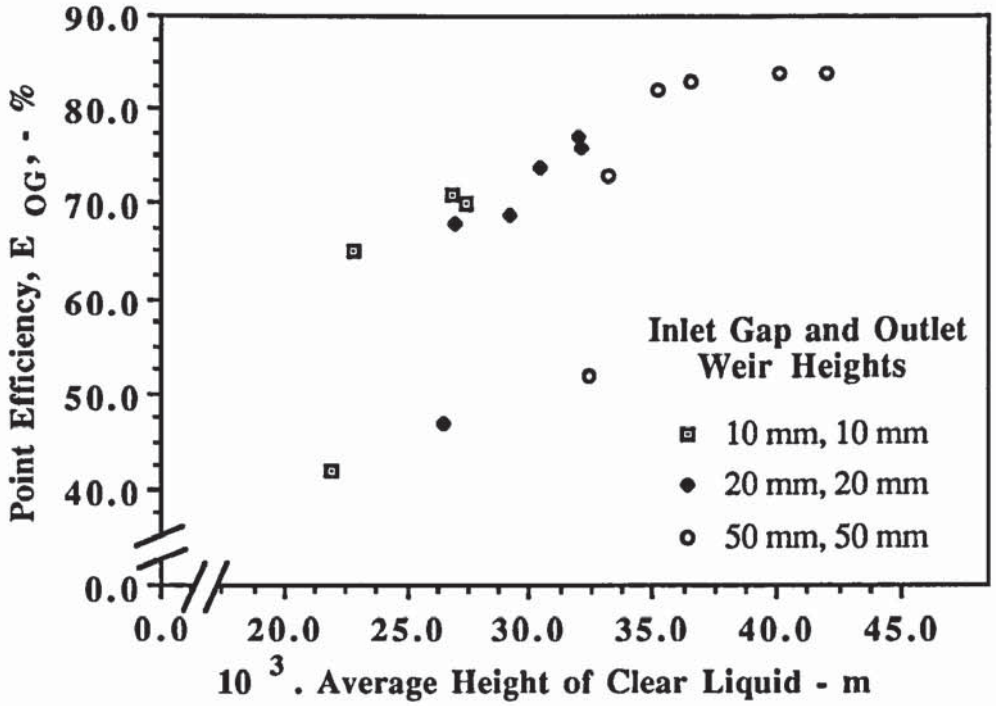

Figure 8.14 Graph of the point efficiency results plotted against average height of clear liquid.

The trend in tray efficiency, for each of the three inlet gap/outlet weir settings, showed a sharp increase to a maximum value, at a comparatively low clear liquid height, before declining steadily with increasing height of clear liquid, (see Figure 8.15). The peak in E_{MV} ocurred at the relatively low weir loading of 50.0 $cm^3/cm.s$, for each fixed air velocity. This corresponds to non-separated flow and suggests that this combination of flow rates provided the most favourable conditions for an optimal gas-liquid contacting time. The decline in E_{MV} may be attributed to a steady growth in circulating flow with increasing weir load and an increasing variation in the clear liquid height, particularly on the tray inlet (see Section 8.3.5).

This result can be explained in terms of the λ (ratio of the equilibrium line to the operating line) effect, which for an optimum design close to the reflux ratio, is near to 1.0. However in many practical situations, λ is varied over a very narrow range of between 0.7 and 1.3 despite the fact that an optimal design for vacuum distllation results in low weir loadings and high weir loadings in pressure distillation. Since the water flow rate is varied over a wide range for a fixed air flow rate, it is not possible to separate the value of λ from the air and water flowrates when using the water-cooling technique to simulate the effect of flow patterns on mass transfer. Thus at high water flowrates, the λ value is low compared to the much higher λ value at low water flowrates. It is these changes in λ that are caused solely by changes in the liquid rate to air rate ratio (L/G), since the gradient of

the saturation line, (heat transfer equivalent of the equilibrium line), remains almost constant.

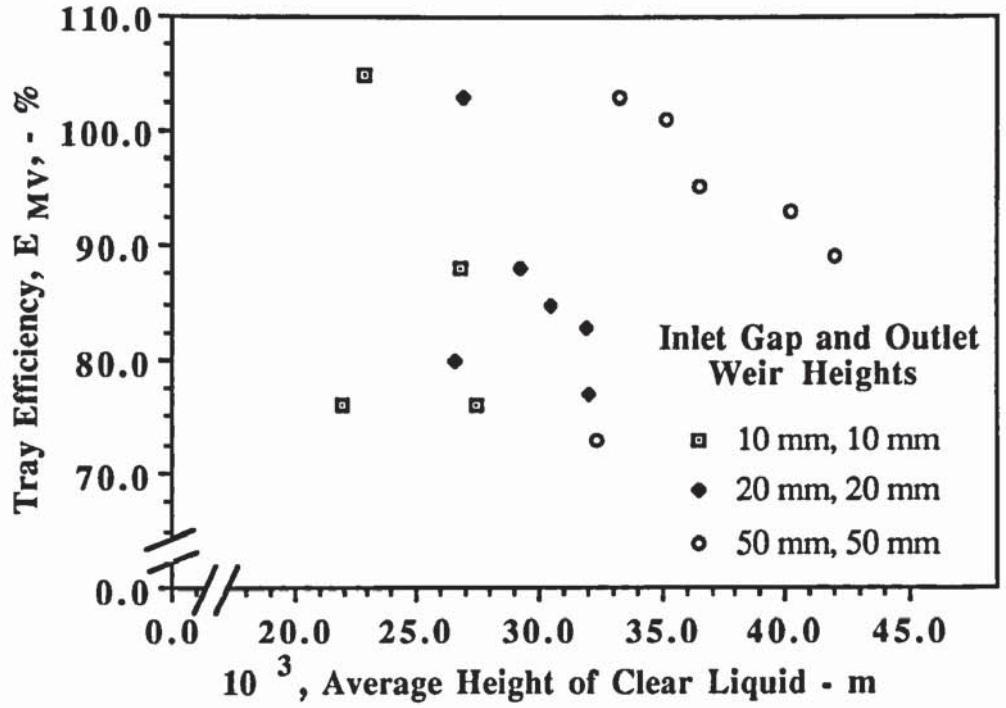

Figure 8.15 Graph of the tray efficiency results plotted against average height of clear liquid.

With this in mind, the results presented in Tables 8.3, 8.4 and 8.5, show that low E_{OG} values were obtained at very low weir loadings and at a high λ value. This implies that the relative increase from E_{OG} to E_{MV} yields a high E_{MV}/E_{OG} ratio. Increasing the weir load produces a higher average clear liquid height and an increase in E_{OG}. This has the effect of decreasing λ which, in turn, serves to maximise the value of E_{MV}. The efficiency results presented above show that a maximum E_{MV} was achieved at the weir loading of 50.0 $cm^3/cm.s$ for all inlet gap/oulet weir combinations, and corresponds to the biphase flow pattern where the transition from non-circulating to circulating flow was rapidly approached.

A steady decline in E_{MV} was obtained on increasing the weir load (refer to Figure 8.15), which means that the effects of circulating flow have 'overtaken' the effects of λ, and thus have an adverse effect on tray efficiency. In some experiments, the adverse effects of liquid channelling associated with a maximum circulation of 30 % on the calculated efficiencies were such that the tray efficiency was less than the point efficiency. For example in Table 8.3, the tray efficiency, at the weir loading of 150.0 $cm^3/cm.s$ and the

fixed superficial air velocity of 1.00 ms^{-1}, was calculated to be 51%, whereas the computed point efficiency was 54 %. This can be attributed to the large circulating zones rapidly approaching equilibrium with the gas rising through the liquid. On further passage of gas through the circulating liquid, no further temperature changes, (concentration in distillation), occur thus causing a dramatic fall-off in tray efficiency.

The above trends in efficiency, over the same L/G ratio range for the three tray configurations, have a significant effect on the enhancement of point efficiency ratio, E_{MV}/E_{OG}. That is, for both large and small froth heights, the E_{MV}/E_{OG} ratio is much larger at low weir loadings (small clear liquid heights) compared with that calculated at higher weir loadings (larger clear liquid heights), as shown in Figure 8.16. This is due to the λ effect, which is lower at low weir loadings compared with that for higher weir loads. Hence the relative increase from point efficiency to tray efficiency was found to be greater for the low weir loadings than for the higher weir loadings, and that the effect of air to water ratio change is greater than the change in point efficency.

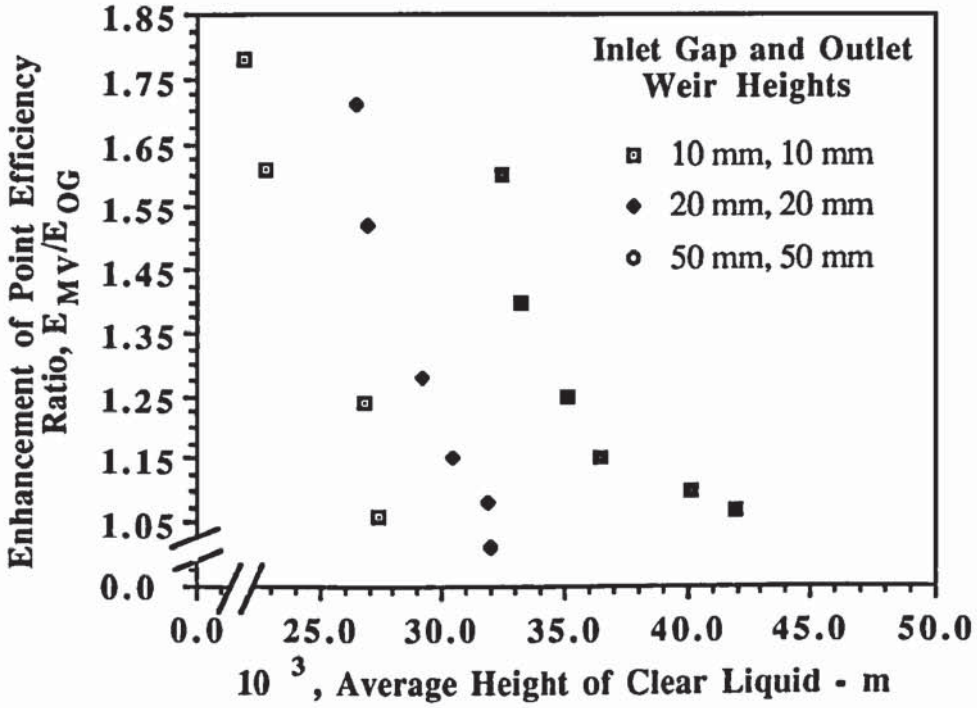

Figure 8.16 Graph of the enhancement of point efficiency results plotted against average height of clear liquid.

Discussion of Results

The results have shown that regions on the tray which have a longer liquid residence time, as a result of either slow forward flow or circulation, can have a detrimental effect

on tray efficiency. This is similar to predictions of the stagnant regions model, (SRM), Porter et al., (1972) in which the calculated concentration profiles gave a measure of the driving force for mass transfer. In this model, it was shown that as the tray diameter increased for a single pass tray, the increased size of the stagnant zones resulted in vapour bypassing with no concentration change, and ultimately caused a fall-off in efficiency. This is significant since it was predicted that in a column of single pass trays placed one above the other, this effect produces a much greater reduction in both tray and column efficiency than for a single tray (Lockett et al., 1973).

Conclusion

The effect of the gas flow on the separation of liquid flow had a substantial effect on the water temperature profiles and thermal efficiencies during water-cooling. The non-separated flow patterns, which contained slow moving liquid at the sides of the tray, produced comparatively straight and parallel isotherms, and yielded significantly high tray efficiencies. In the separation of flow, the reduced temperature isotherms were "U-shaped" with the coldest liquid representing circulating flow emanating from the ends of the inlet downcomer. These colder regions resulted in the calculation of lower tray efficiencies. The results are similar to that produced on the 1.0 mm tray, (Hine, 1990), and that predicted in the stagnant regions model (Porter et al., 1972).

8.3.5 Investigation by Liquid Head Measurements

So far progress in determining the effects of the gas flow on the separation of liquid flow have been made from the direct-observation and water-cooling experiments described above. However, these experiments provided very little information about the effect of flow separation on the froth height variation across the tray area. Thus froth height variations during the separation of flow were determined by measurement of the clear liquid height across the tray.

The height of clear liquid experiment involved the use of thirty two manometers attached to the tray deck to measure the pressure drop between the top of the tray deck, the froth dispersion and the space above the tray. The pressure drop through the froth, which is proportional to froth height, gives a measure of the height of clear liquid on the tray. For each experiment, the point values of clear liquid height were computer processed, in a similar manner to the water temperature profiles, to yield three-dimensional graphs of the liquid head profile. A complete description of the height of clear liquid experiment is presented in Chapter 5.

Height of Clear Liquid Results

From Chapter 5, the liquid head profiles were identified as follows:-

A horizontal (flat) liquid head profile was designated H; an uneven liquid head profile consisting of peaks and/or troughs at the tray inlet was designated NI; and an uneven liquid head surface containing peaks and/or troughs at the tray outlet was designated NO. In addition, if the liquid head surface is uneven over the whole tray, then the N designation was used.

Effect of Non -Separated and Separated Flow Patterns on the Height of Clear Liquid Results

On the whole, the results show that horizontal or flat profiles were produced at low weir loadings which was indicative of forward only flow in the non-separated flow patterns. As the weir load was increased such that circulating flow became the dominating flow pattern, the height of clear liquid in the divergent section of the tray in front of the inlet downcomer was much less than that on the tray segments. This was observed during the extreme case of liquid channelling associated with a maximum of 30% circulation which occurred mainly at the inlet gap and outlet weir heights of 10 mm. The height of clear liquid profiles at the equal inlet gap and outlet weir heights of 10 mm and 20 mm are summarised in Figures 8.17 and 8.18.

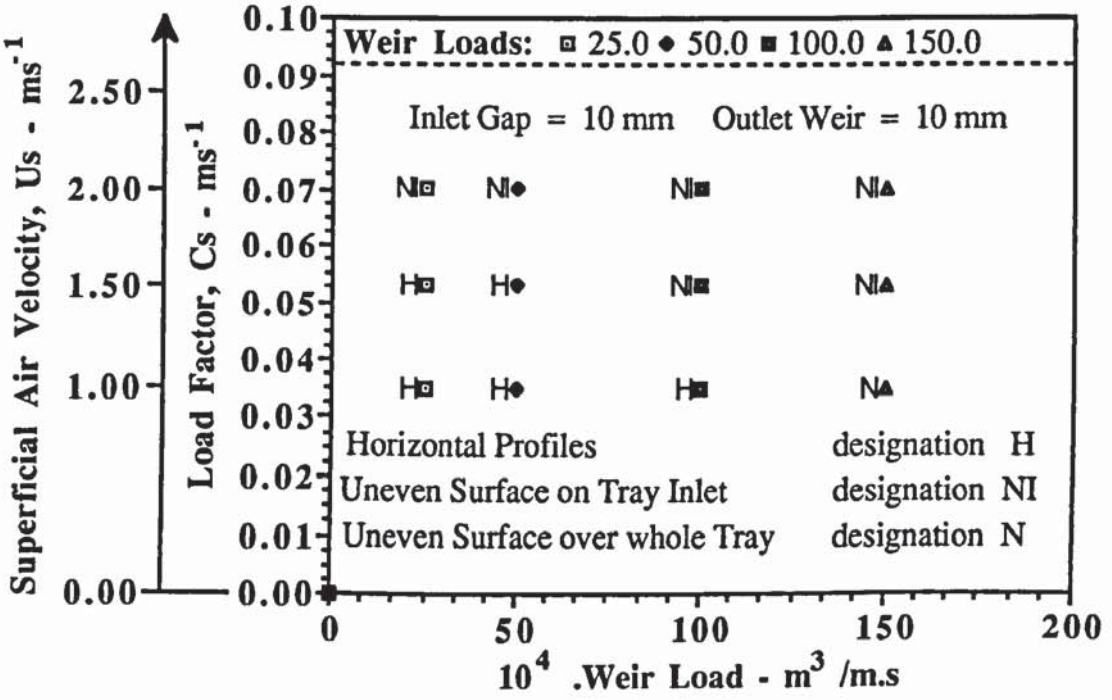

Figure 8.17 Summary of liquid head profiles on a load factor verses weir load diagram.

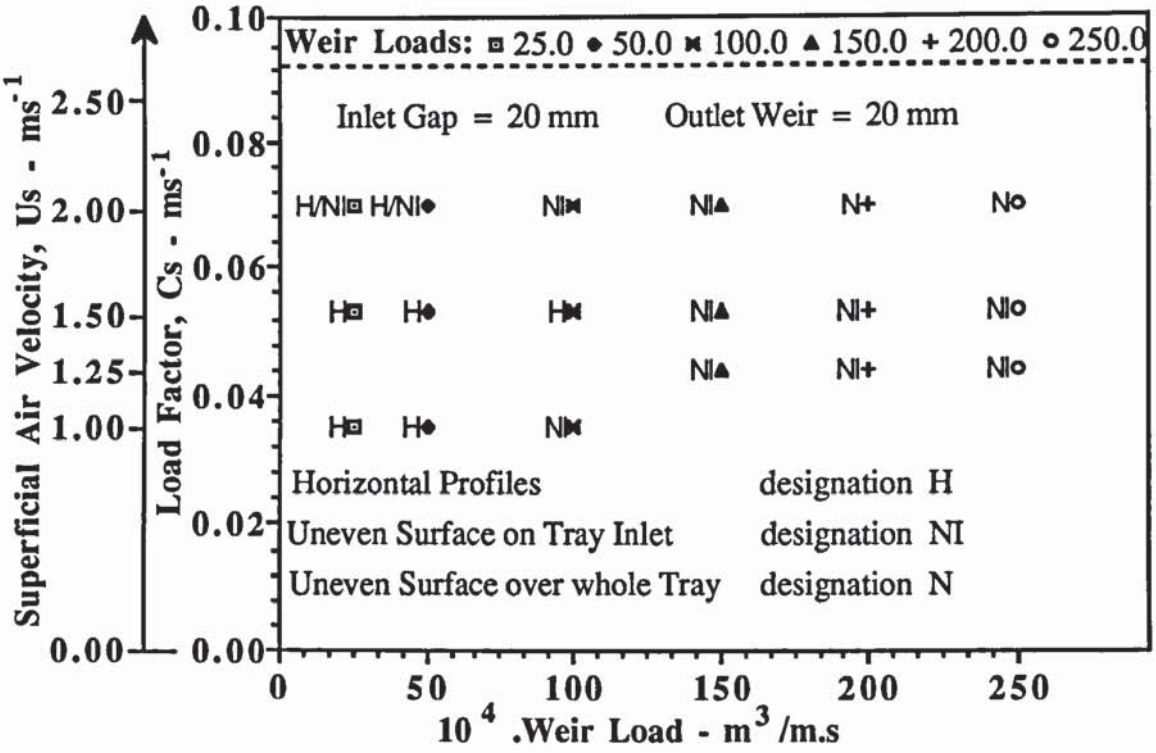

Figure 8.18 Summary of liquid head profiles on a load factor verses weir load diagram.

As the superficial air velocity was increased, the bubbling action of the gas through the liquid increased the level of turbulence and mixing. This was reflected in the more uneven liquid head surface across the tray. These observations were most significant at large froth heights.

A summary of the height of clear liquid profiles at large froth heights are summarised on the modified load factor verses weir load diagram as shown in Figure 8.19.

Note from Figures 8.17, 8.18 and 8.19, that liquid head surface profiles were not determined at the superficial air velocity of 2.50 ms^{-1} since the high gas velocity caused a venturi effect at a number of pressure tappings across the tray. That is, the gas forced the liquid out the pressure tappings thus giving erroneous clear liquid height readings that were not representative of the liquid head profile on the tray.

Examples of a horizontal liquid head surface (non-separated flow), and an uneven liquid head surface (separated flow), both at the tray inlet and outlet, for the small and large froth heights are presented in Figures 8.20a, 8.20b, 8.21a, 8.21b, 8.22a and 8.22b. The liquid head profiles for all of the experiments conducted at the inlet gap/outlet weir heights of 10 mm, 20 mm, and 50 mm, are presented in Appendix 8.0.

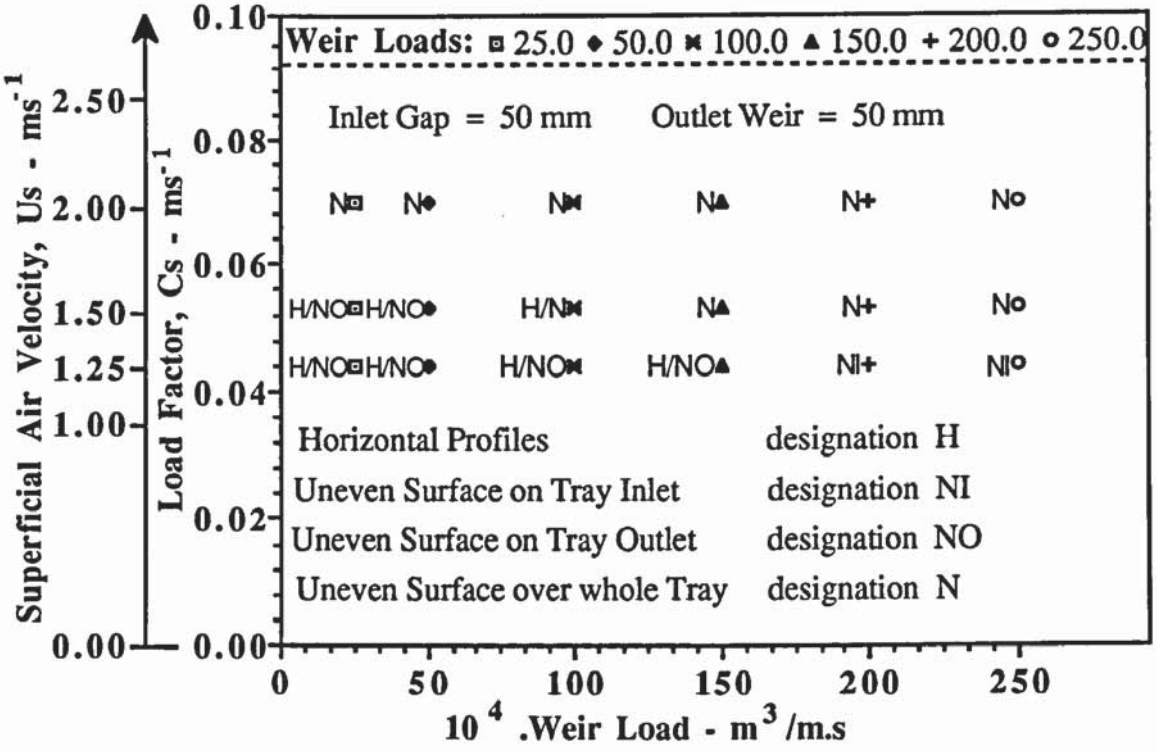

Figure 8.19 Summary of liquid head profiles on a load factor verses weir load diagram.

Conclusions

The above height of clear liquid experiments have shown that the liquid head profiles became increasingly non-uniform with increasing weir load, especially in front of the inlet downcomer. However, the low height of clear liquid associated with higher superficial air velocities, did not produce substantial differences in the liquid head surface despite the flow pointers showing slow forward flow and circulation particularly at higher weir loads. From this, it can be concluded that the height of clear liquid technique does not 'distinguish' between slow forward flow and circulation at the sides of the tray, and is not sensitive enough for highlighting small differences around circulating regions.

Despite this, the height of clear liquid profiles of slower moving or circulating liquid on the divergent tray section at the ends of the inlet downcomer, were on the whole greater than that of the faster moving liquid along the middle of the tray. This can be attributed to the sudden expansion of liquid onto the tray from the gap beneath the inlet downcomer. Nevertheless non-uniform liquid head profiles have an adverse effect on E_{OG} particularly at high weir loads (see the previous section).

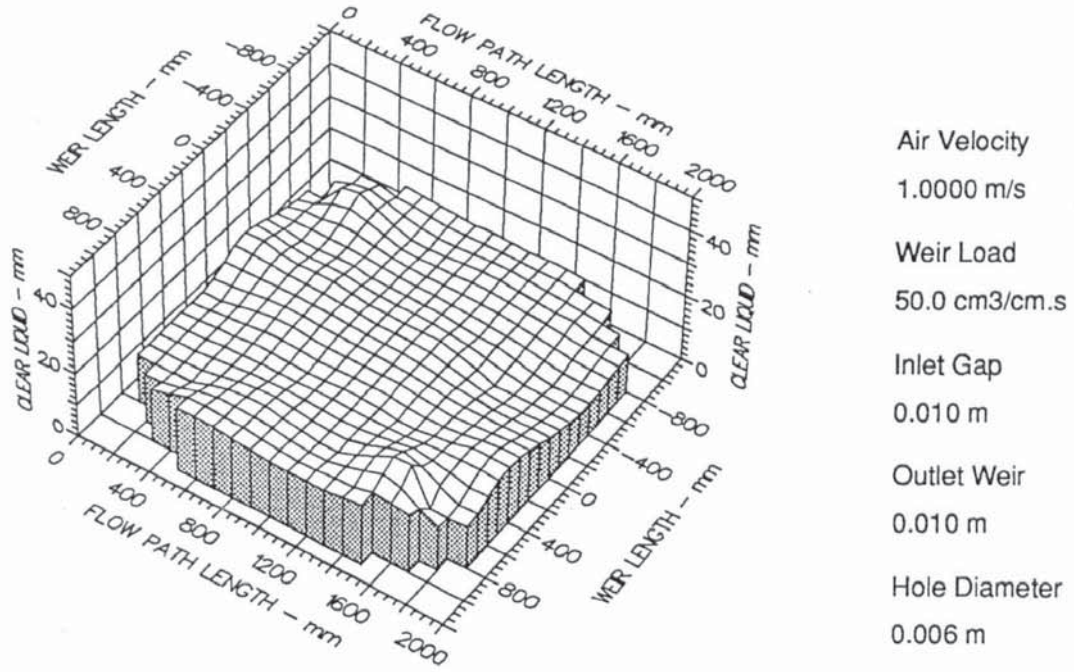

Figure 8.20a An example of a comparatively flat height of clear liquid profile (designation H).

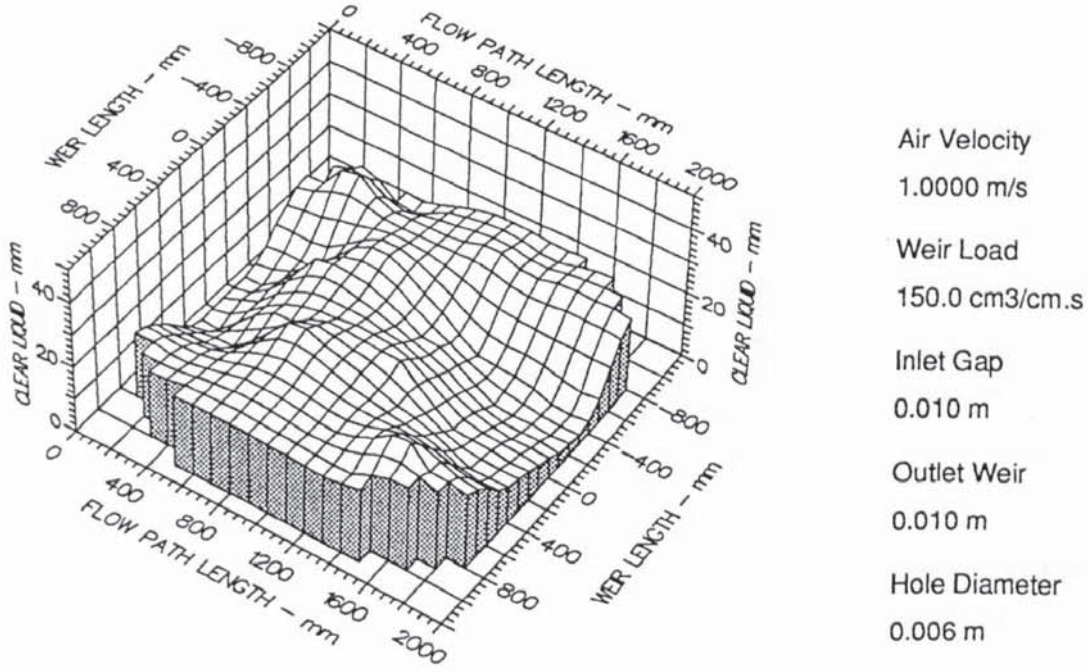

Figure 8.20b An example of a height of clear liquid profile with an uneven surface (designation N).

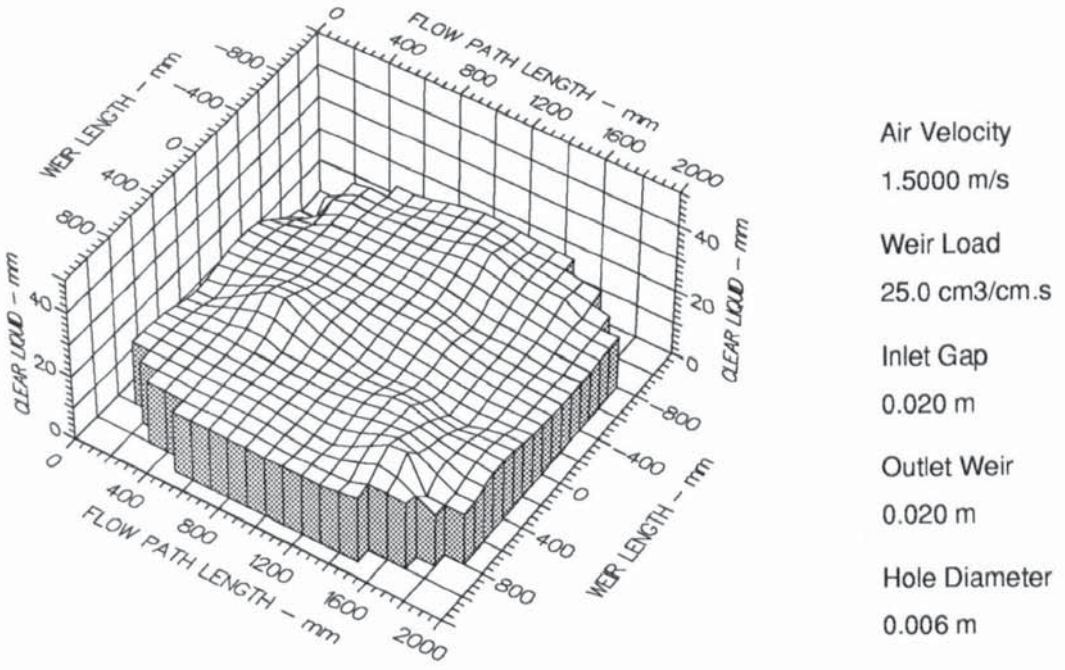

Figure 8.21a An example of a comparatively flat height of clear liquid profile (designation H).

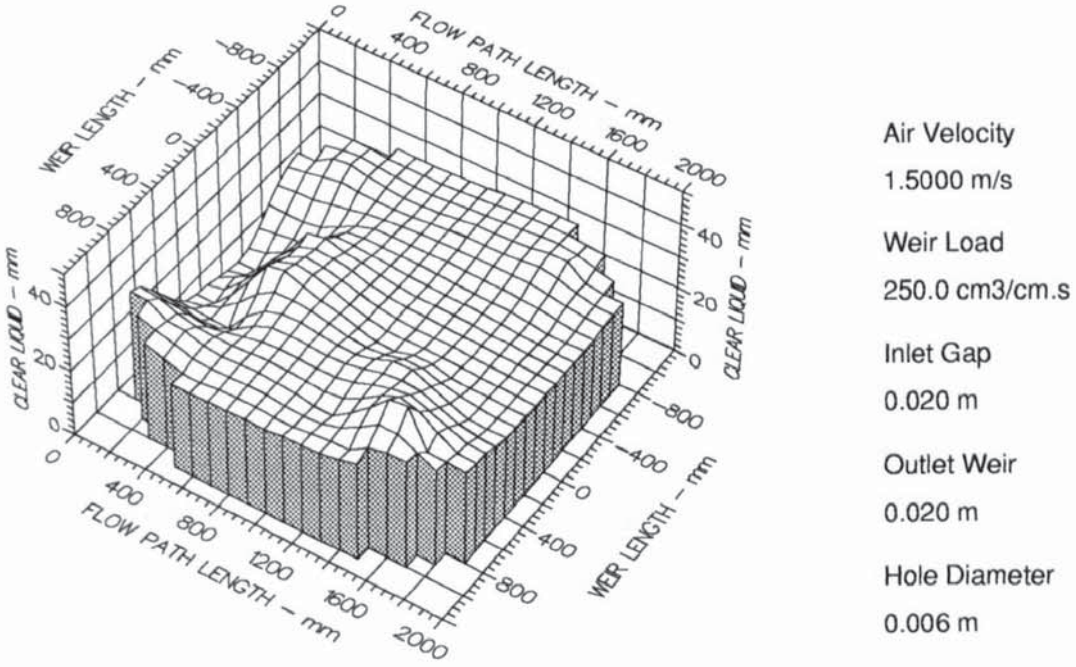

Figure 8.21b An example of a height of clear liquid profile with an uneven surface (designation NI).

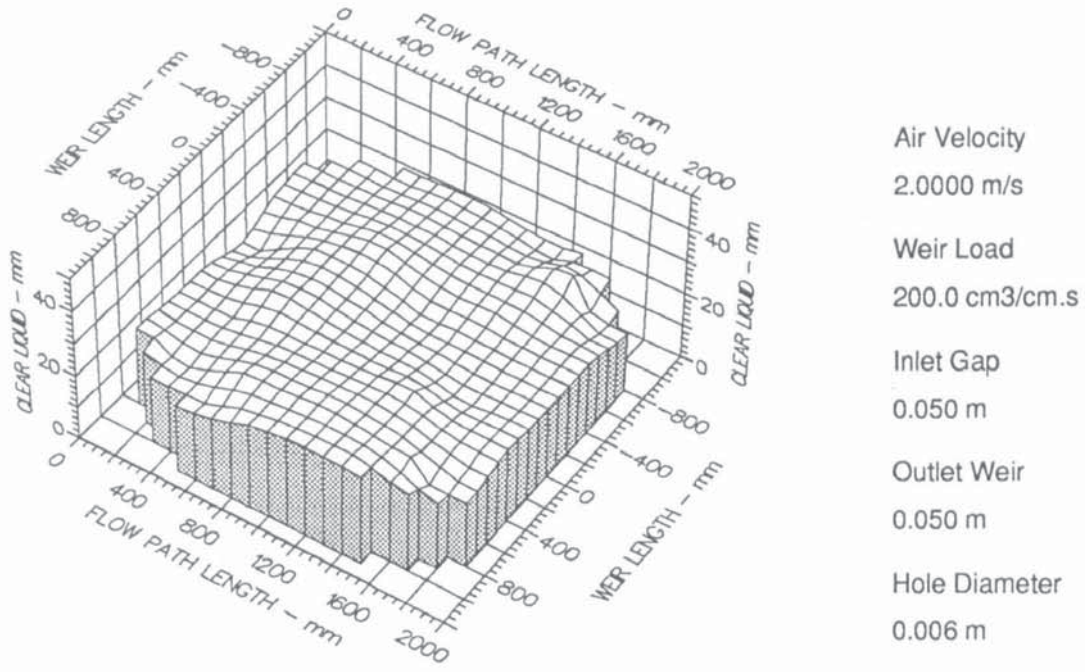

Figure 8.22a An example of a comparatively flat height of clear liquid profile (designation H/NO).

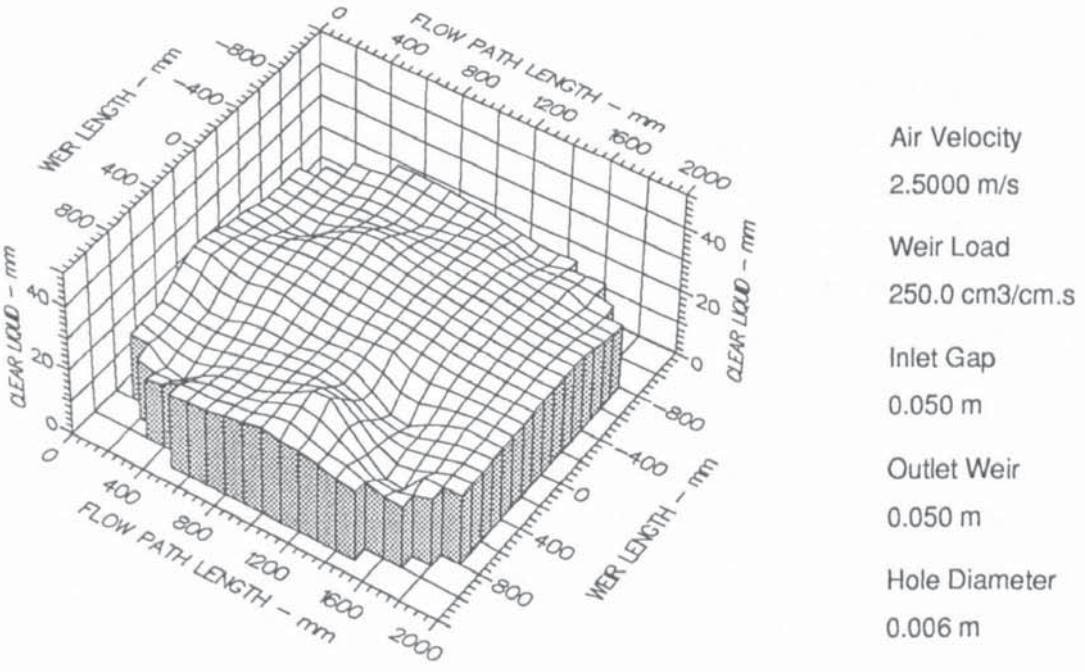

Figure 8.22b An example of a height of clear liquid profile with an uneven surface (designation N).

8.4 Computed Air-Water Flow Patterns From the Turbulent Two-Dimensional Single Phase Flow Model

In earlier chapters, it was stated that the experimental results from this work are to be incorporated into a new mathematical model of open channel two phase flow, some progress has already been made in this area. That is, as part of the collaborative research programme with the National Distillation Laboratory in P.R. China, flow conditions from the experimental work, presented in this chapter, were incorporated into a turbulent two phase flow mathematical model (Yu and Zhang, 1991). The model is based on the assumption that the gas enters the froth in a vertical direction and attains a horizontal velocity component equal to that of the liquid crossflow before leaving the froth. Thus the momentum required to accelerate the gas in the horizontal direction offers an additional resistance to the liquid flow which is much greater than the frictional drag resistance of the liquid along the tray floor. This would have a significant effect on the liquid flow pattern, and the assumption seemed reasonable for the conditions of the experiments described above. (Mathematical development of the theoretical model has been described in Chapter 2).

8.4.1 Computed Flow Pattern Results

The computed flow pattern, presented in Figure 8.23 shows the two-dimensional velocity distribution in which a number of velocity profiles represented forward flow from downcomer to downcomer, as well as reverse flow in the segmental regions at the sides. The reversed flow region in this specific case was estimated to be approximately 8.5% of the total bubbling area which is in fair agreement with the experimental result of 12% shown in Figure 8.8 for the same operating condition. However, in many cases the computed results do not show the existence of reverse flow, but instead, a region of almost zero velocity appeared adjacent to the column wall. Further details can be found elsewhere (Zhang, 1991).

Figure 8.23 also shows that in the divergent section of the tray, the liquid velocity remained uniform in the main flow region between the downcomers but diminished sharply in the segmental region, whilst in the convergent section the velocity distribution became parabolic owing to the mixing of the contracted flow of liquid from the segmental region.

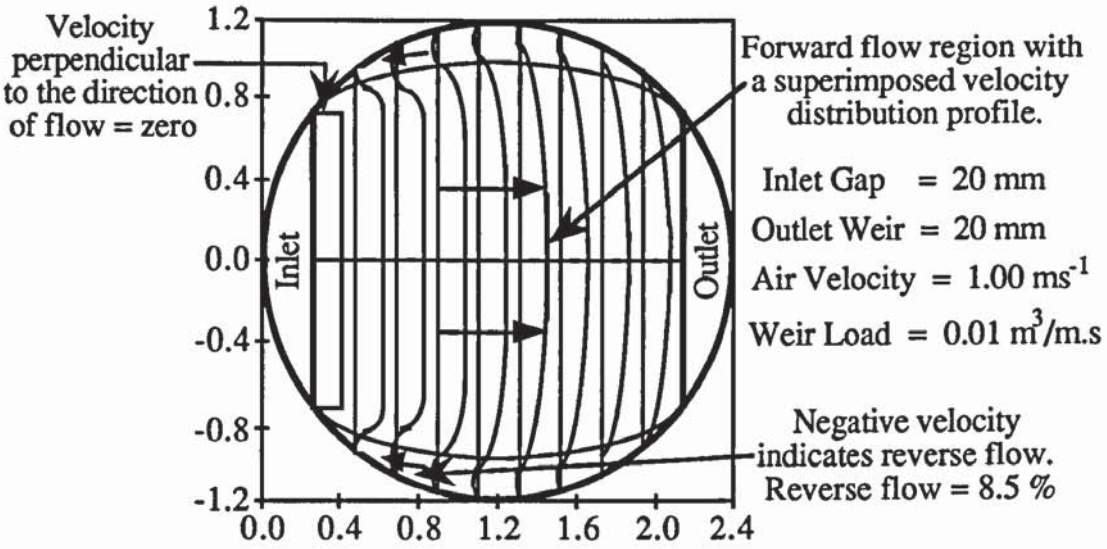

Figure 8.23 Computed velocity distribution profile showing reversed flow on the tray segments.

8.4.2 Conclusion

The computed flow pattern presented above, was obtained from a turbulent two phase flow mathematical model which incorporates the resistance to the liquid flow of the rising gas through it. In general, the computed flow patterns revealed forward flow between the downcomers with very slow or non-moving liquid at the sides of the tray. In some cases the computed flow pattern contained reverse flow near the column wall.

8.5 Overall Conclusions

It has been shown in this chapter that the passage of the gas through liquid can have a significant effect on the liquid flow pattern. When, as a single phase, the liquid flows through the divergent/convergent channel formed by a single pass tray, except for very low weir loads, the flow separates at the ends of the inlet downcomer and forms circulating regions throughout the segments at the sides of the tray. The effect of forcing the gas through the liquid inhibited flow separation which only occurred at much higher weir loads and with smaller clearance heights under the inlet downcomer (i.e., at high liquid inlet velocities).

The effect of the gas flow on the separation of liquid flow had a significant effect on both the temperature profiles, which give a measure of the driving force for mass transfer, and on the variation of the liquid head surface across the tray.

In several cases, during water-cooling, the presence of colder regions on the tray as a result of slow moving or circulating liquid, showed that these regions had a longer residence time. This reduced the driving force for mass transfer and in some cases, caused a dramatic fall-off in tray efficiency. The presence of slow moving and circulating flow in the separated flow patterns, was confirmed by the relatively large height of clear liquid measurements in these regions compared with those in the middle of the tray, particularly on the tray inlet.

The input of experimental data presented in this work, into a theoretical model for computing the liquid flow across the tray, by considering the vapour flow as a resisting force, provided a promising start at a new theoretical description of the flow phenomena. This theoretical model of turbulent two phase flow needs to be further developed since many of the computational procedures used in the calculation of flow patterns were based on single phase flow. Nevertheless, there was fair agreement between the computed flow pattern and the experimental flow pattern for the same operating conditions.

Overall, considerable progress has been made in this chapter to gain a deeper understanding of the controlling phenomena of two phase flow across sieve trays. However, this needs to be extended by considering two phase flow patterns produced under conditions where the inlet velocity of the liquid is reduced in order to decrease the liquid backup in the downcomer to levels found in practical distillation. This is the subject of the studies pursued in the next chapter.

CHAPTER 9

SIMULATION OF DISTILLATION AT DIFFERENT PRESSURES

9.1 Introduction

So far, it has been shown that the gas flow has a significant effect on preventing the onset of flow separation and circulating flow. However, this approach needs to be extended by considering the biphase flow patterns produced using conditions where the inlet velocity of the liquid is reduced in order to decrease the liquid backup in the downcomer to levels found in industrial scale practical distillation.

The objective of this chapter was to obtain a comprehensive set of flow pattern results by simulating the conditions used to operate commercial scale trayed columns under different pressures. All of the results, outlined below, can be incorporated onto operating lines, chosen to represent each simulated pressure, on a tray loading diagram. This would provide a promising start to a more scientific approach required for tray design.

From the direct-observation experiments, it will be shown that the biphase was in forward flow over most of the tray even for the conditions which simulated distillation under the conditions of atmospheric and moderate pressure. The observation of slower moving liquid at the sides, either in the form of slow forward flow or a small circulating flow, implies a longer liquid residence time compared with other parts of the tray.

This is important in interpreting temperature profile results, from water-cooling, since they give a measure of the driving force for mass transfer. Furthermore, flow patterns have an effect on the liquid head variation across the tray, which was measured in terms of the height of clear liquid.

Comparisons were then made between the efficiencies, calculated from the water temperature profile results with those obtained by air-humidification (Prado and Fair, 1990). This was followed by a comparison of the measured height of clear liquid results with those predicted by Bekassy-Molnar and Mustafa (1991), for similar operating conditions.

Finally, this chapter is completed by a comparison of the temperature profile isotherms

with the concentration profiles predicted from the stagnant regions model (Porter et al., 1972), by incorporating experimental data into the theoretical model. In addition, experimentally determined thermal efficiencies can be compared with the computed efficiencies for each simulated pressure.

Before discussing the different flow patterns generated at three simulated pressures, a brief description of the procedures used for simulating distillation at different pressures is presented below.

9.2 Simulating Distillation at Different Pressures

The capacity or maximum throughput of a distillation tray or packing, for a particular system, is often correlated against the flow parameter, X, where,

$$X_{System} = \frac{L}{V}\sqrt{\frac{\rho_V}{\rho_L}} \tag{9.1}$$

in which L and V are the total liquid and vapour mass flow rates. The flow parameter for the system at total reflux X is equal to,

$$X_{\infty\ System} = \sqrt{\frac{\rho_V}{\rho_L}} \tag{9.2}$$

For the air-water system, a mean value of the square root of the density ratio, $(\rho_V/\rho_L)^{0.5}$, is 3.51×10^{-2}. Thus the flow ratios, L/V, required to simulate distillation systems at total reflux are obtained by making

$$X_{\infty\ System} = X_{Air/Water} \tag{9.3}$$

$$\text{That is, } \left(\frac{\rho_V}{\rho_L}\right)^{0.5}_{\infty\ System} = \frac{L}{V}\left(\frac{\rho_V}{\rho_L}\right)^{0.5}_{Air/Water} \tag{9.4}$$

which, in turn, yields,

$$\left[\frac{L}{V}\right]_{Air/Water} = \frac{(\rho_V/\rho_L)^{0.5}_{\infty\ System}}{(\rho_V/\rho_L)^{0.5}_{Air/Water}} = \left(\frac{1}{0.0351}\right)_{Air/Water}\left[\frac{\rho_V}{\rho_L}\right]^{0.5}_{\infty\ System} \tag{9.5}$$

Note that the L/V ratio increases with the simulated operating pressure. That is, vacuum

distillation is a low liquid load duty and distillation under a moderate or high pressure is a high liquid load duty.

For each simulated distillation system, the L/V ratio remained constant while the air flow rate, V, was varied over a range of upto 2.5:1. The operating lines for the simulated pressure experiments were superimposed on a tray loading jet flood diagram, similar to that presented in Figure 2.1 of Chapter 2, in which the gas (or vapour) load factor, Cs, is plotted against the weir load, q/b. (The tray loading diagram may be used as a guide for the design of distillation trays at 80% flood (Porter and Jenkins, 1979), using methods which are essentially empirical).

The vapour load factor and weir load, used to plot the jet flood diagram, are defined as:-

$$\text{Load Factor: } C_S = u_{SB}\sqrt{\frac{\rho_V}{\rho_L - \rho_V}}, \quad \text{Weir Load: } \frac{q}{b} = \frac{Q_L}{W} \qquad (9.6)$$

The three L/V operating lines incorporated onto the tray loading diagram include low weir load vacuum distillation simulation on the left hand side and high weir load moderate pressure distillation on the right hand side, with the medium weir load atmospheric pressure distillation located in between the two.

9.3 Studies into Air-Water Flow Patterns at Different Simulated Pressures

The approach of comparing air-water flow patterns with water-only flow across an unperforated tray in Chapter 8 was pursued in these studies to simulate distillation, in that attention was drawn to the direction of flow at many points across the tray. Forward flow was designated to the direction of flow between the downcomers, while reverse or recirculating flow was designated to flow in the opposite direction.

9.3.1 Programme of Experiments

The programme of experiments was in three parts:

a) Direct-observation of flow patterns during the air-water contacting experiments in which distillation was simulated at three different pressures. In these experiments, flow rates were varied at a fixed ratio of liquid flow to air velocity. Three flow rate ratios were chosen to represent distillation under vacuum, at atmospheric pressure,

and at a moderate pressure (about 2 bar). The inlet gap and outlet weir height were set equal for each pressure simulation, details of which are presented in Table 9.1, and were chosen to maintain a comparatively low liquid head (backup) in the inlet downcomer, representative of industrial scale practical distillation. (That is, the downcomer backup measurements were in the range of 21.5 - 48.8 mm for vacuum distillation, 39.8 - 74.5 mm for atmospheric pressure distillation, and 48.5 - 88.3 mm for moderate pressure simulation).

b) Investigations into the effect of air-water flow patterns, generated at the three simulated pressures, on mass transfer using the water-cooling technique. In these experiments, the water temperature was measured at over 100 equally spaced positions on the tray, and the raw data computer processed to yield temperature profiles which are analogous to concentration profiles in distillation. By using the analogy between heat and mass transfer, the interpretation of the water temperature profiles in terms of enthalpy driving forces permitted the calculation of thermal point and tray efficiencies.

c) Investigation into the effect of the biphase flow patterns, for each simulated pressure, on the liquid head variation across the tray. This was determined by measurement of the height of clear liquid using manometers, connected to thirty two pressure tappings spread evenly across the tray.

For each simulation experiment, a wide range of air and water flowrates at the three flow rate ratios, for different combinations of inlet gap and outlet weir heights, were used, and are presented in Table 9.1.

Simulated Pressure					
Vacuum		Atmospheric Pressure		Moderate Pressure	
Inlet Gap = 10 mm Outlet Weir = 10 mm		Inlet Gap = 20 mm Outlet Weir = 20 mm		Inlet Gap = 50 mm Outlet Weir = 50 mm	
Air Velocity - ms^{-1}	Weir load - 10^4 $m^3/m.s$	Air Velocity - ms^{-1}	Weir load - 10^4 $m^3/m.s$	Air Velocity - ms^{-1}	Weir load - 10^4 $m^3/m.s$
1.00	12.5	1.00	60.0	1.25	100.0
1.50	18.5	1.50	90.0	1.50	150.0
2.00	25.0	2.00	120.0	2.00	200.0
2.50	31.0	2.50	150.0	2.50	250.0

Table 9.1 Summary of flow rates chosen for the simulation of distillation experiments at three different pressures.

9.3.2 Investigation by Direct-Observation

Direct-observation of the air-water flow patterns was achieved using the established technique of directional flow pointers and overhead video camera described in Chapter 5. For each simulated pressure, the localised biphase flow at thirty four positions across the tray was noted by recording the direction of alignment of each painted arrow indicator.

For all of the experiments, the liquid was completely aerated over the whole of the tray bubbling area. Water on entering the tray, from beneath the inlet downcomer, formed an aerated froth, due to the bubbling action of the gas, which spread outwards so as to completely fill the tray cross section.

Another important factor is that the gas-liquid contacting at low liquid flow rates is highly chaotic, and tends to randomise the motion of the froth elements, thus producing the spray regime. Hence, the sensitivity of the flow pointers for showing the direction of flow is partially reduced which explains the asymmetric appearance of flow pointers on the tray, and methods of overcoming the problem have been described in the previous chapter. Nevertheless, the flow pointers prove to be highly sensitive to changes in the flow pattern encountered for each simulated pressure experiment.

Flow Pattern Results

For all flow rates during the simulation of vacuum distillation the general alignment of the flow pointers torwards the outlet indicated forward only flow which was produced at all points on the tray including the segmental regions at the sides.

The converging/diverging alignment of flow pointers on the tray inlet was caused by the expanding aerated liquid such that it completely filled the tray cross section. Flow pointers facing normally towards the column wall, were indicative of the sideways flow of froth as a result of the support ring effect described in Chapter 8. The main reason for the randomised alignment of flow pointers was that the velocity of forward flow between the downcomers was greater than that at the sides of the tray as a result of the shorter flow path compared with that at the sides.

A typical example of forward only flow at all points on the tray during the simulation of vacuum distillation is presented in Figure 9.1, and is also shown in the photographs presented in Figures 9.2a and 9.2b.

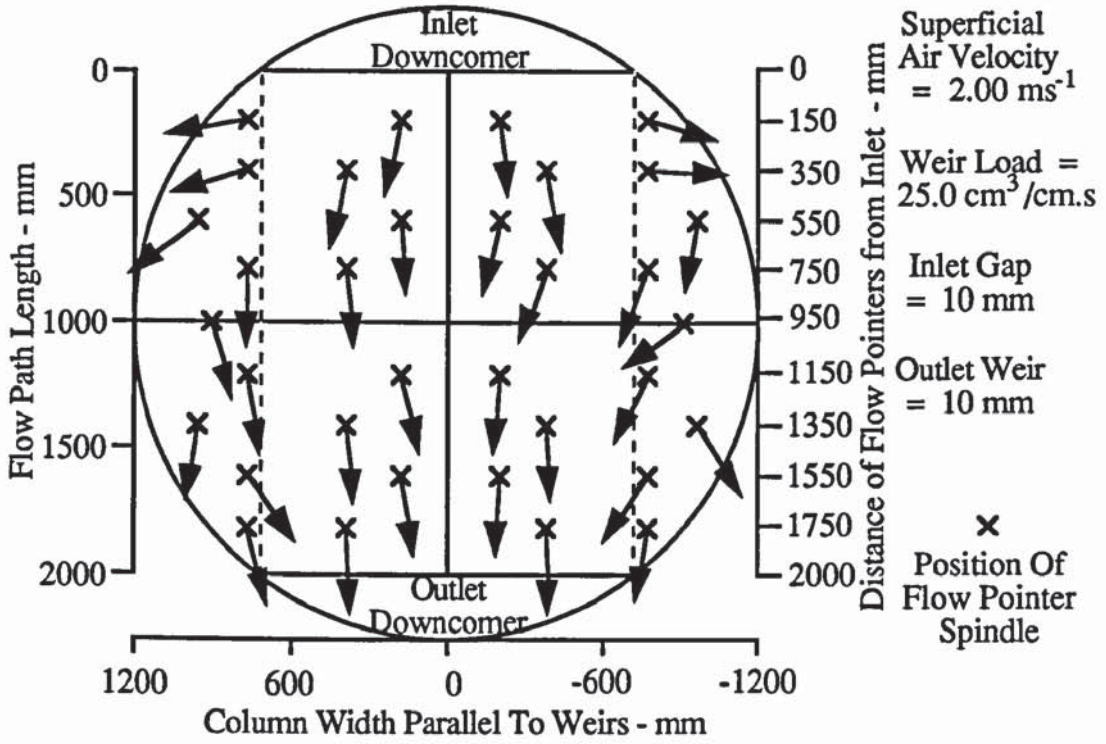

Figure 9.1 Flow pointer arrangement showing forward only flow during the simulation of vacuum distillation.

The higher weir load simulations of atmosphere and moderate pressure distillation showed forward flow along the horizontal plane between the downcomers, associated with a mixture of slow forward flow, stationary liquid and circulating flow on the tray segments. Forward flow between the downcomers was shown by all sixteen flow pointers in which the painted arrow indicators were pointing towards the outlet weir. On the tray segments, eight flow pointers (four on each side) represented slow forward flow in the regions close to the ends of the outlet weir, while two areas of stationary froth were observed approximately 1100-1300 mm downstream from the inlet downcomer. Furthermore, the first three to four flow pointers on the inlet tray segments revealed circulating flow which emanated from the ends of the inlet downcomer. For most of the simulated pressure experiments, circulating flow was relatively small and in most cases occupied 12% but no more than 15% of the total tray area.

Representative examples of the flow patterns produced during the simulation of atmospheric and moderate pressure distillation, are presented in Figures 9.2 and 9.3.

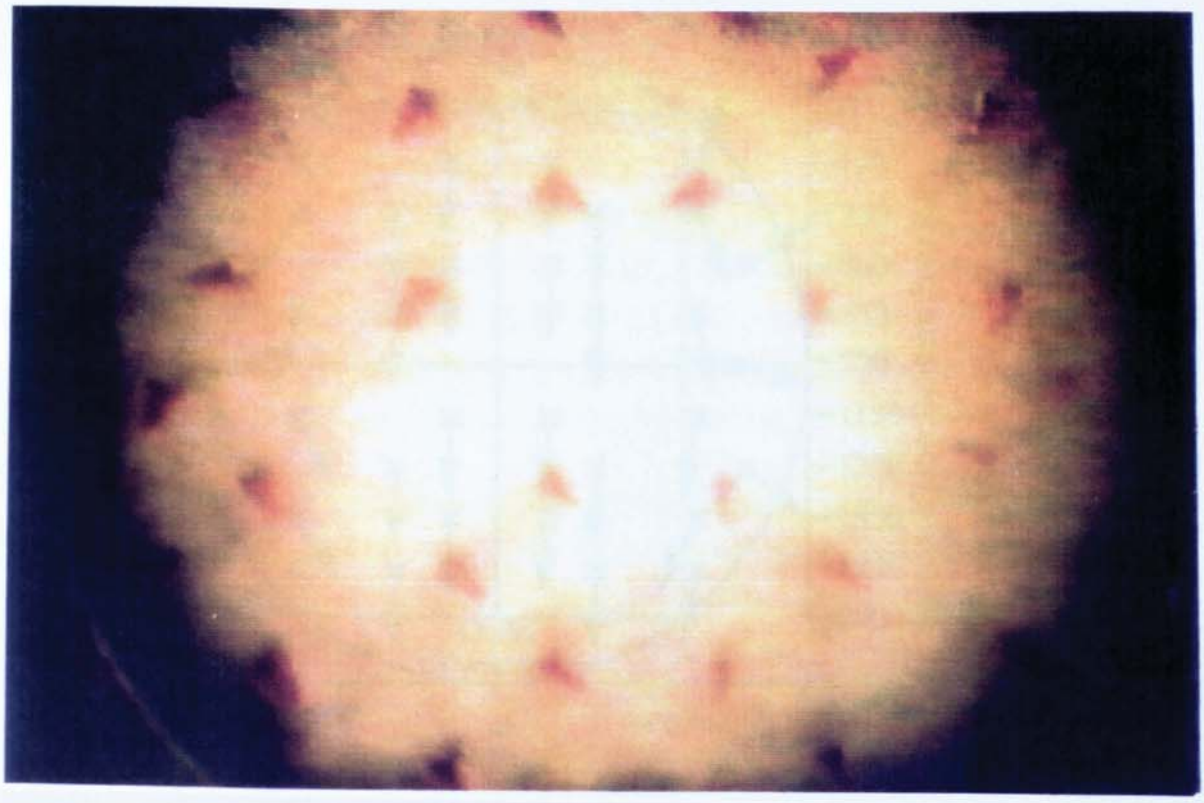

Figure 9.2a Photograph of the flow pointer arrangement showing forward only flow during the simulation of distillation under vacuum at low flowrates.

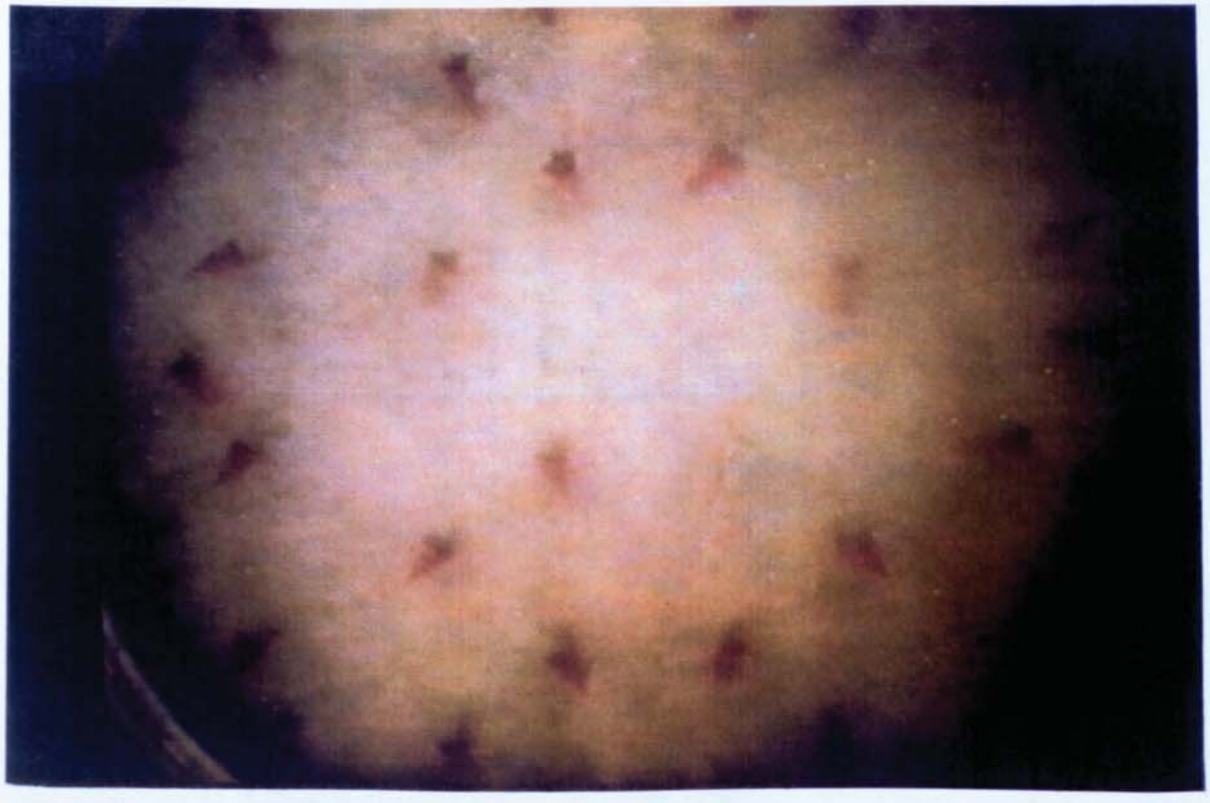

Figure 9.2b Photograph of the flow pointer arrangement showing forward only flow during the simulation of distillation under vacuum at high flowrates.

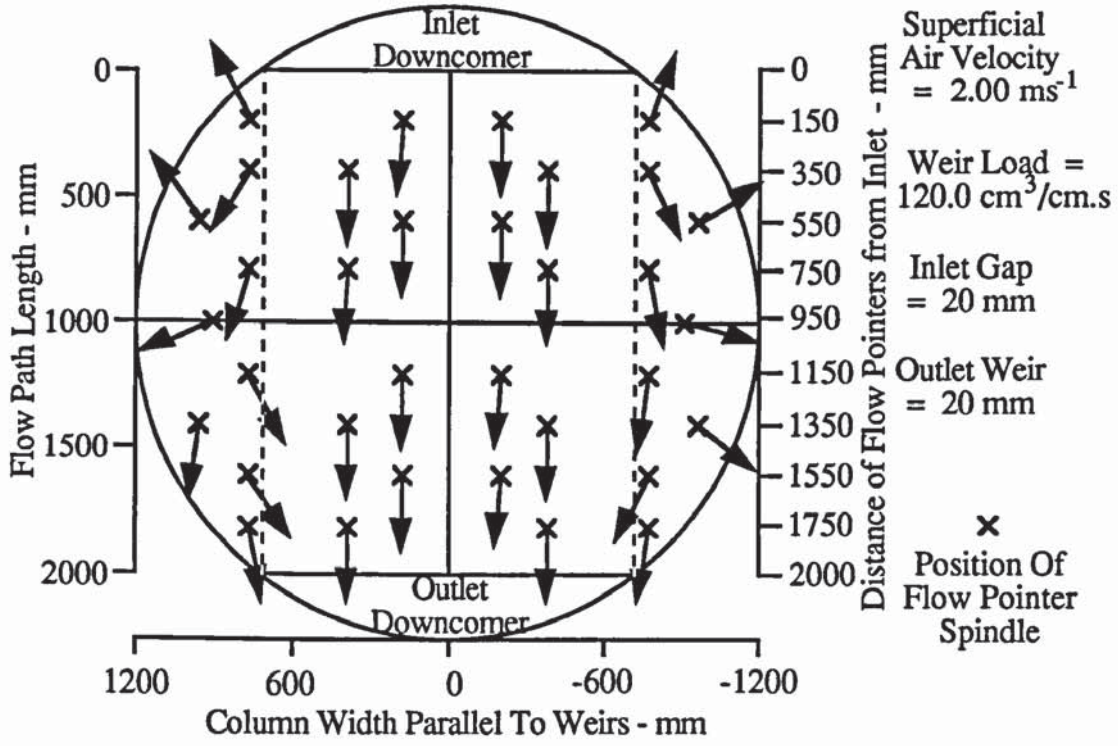

Figure 9.3 Flow pointer arrangement showing forward flow associated with 12 % circulation during the simulation of atmospheric pressure distillation.

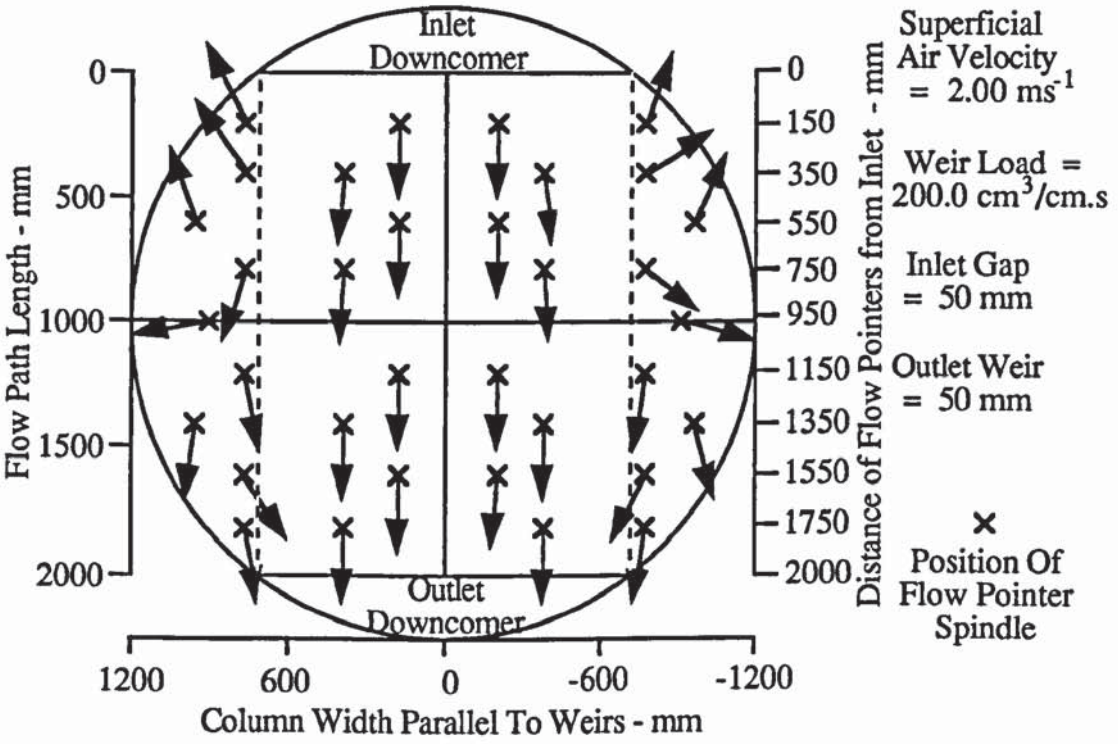

Figure 9.4 Flow pointer arrangement showing forward flow associated with 12 % circulation during the simulation of moderate pressure distillation.

Discussion of Results

The most convenient way of summarising the flow patterns, generated at the three simulated pressures, is to use a modified version of the vapour load factor verses weir load jet flood diagram. This was devised by Porter and Jenkins (1979) for a 12.5 mm hole tray, using the experimental data of Sakata andYanagi (1979). It is worth recalling that vacuum distillation systems operate in the spray regime and are found on the left hand side of the jet flood diagram, whereas higher pressure systems operate in the emulsion flow regime and are found on the right hand side.

When applied to this investigation, the incorporation of three L/V operating lines, representing each simulated pressure, for the 6.35 mm tray on the jet flood diagram may not necessarily correspond to precisely the same flow regime expected on the 12.5 mm hole tray. That is, if smaller hole trays are operated in the spray regime, this will tend to "push" the operating conditions for the tray further towards the left hand side of the jet flood diagram compared to that for the 12.5 mm hole tray. (Note it still not yet known how spray flows across perforated trays).

Hence it is possible that the flow conditions on the left hand side of the jet flood diagram may correspond to a mixture of spray and mixed froth whereas the flow conditions in the middle may correspond to a mixture of mixed froth and emulsified flow. From the direct observation experiments, however, it was found that for the flow conditions chosen to simulate vacuum distillation, the tray was operating in a coarse spray regime, whereas the mixed and emulsion flow regimes were produced during the simulation of atmospheric and moderate pressure. (Further work on the spray-to-mixed and mixed-to-emulsion flow transition on trays of various hole sizes including 6.35 mm holes is required so as to locate precisely the flow conditions required to operate a tray in the spray, mixed and emulsion flow regimes).

For this set of experiments, flow patterns are summarised on the modified vapour load factor verses weir load diagram as shown in Figure 9.5. Note that the spray-to-mixed and mixed-to-emulsion flow transition lines, based on data for a 12.5 mm tray, are included on the diagram in addition to the three L/V operating lines for each simulated pressure. On each line, are shown the percentages of tray area occupied by circulating liquid. The load factor verses weir load plot showed that in the simulation of vacuum distillation, forward flow was produced at all points on the tray with no circulation. For the simulation of atmospheric and moderate pressure distillation, the tray area occupied by circulating flow was in most cases 12% but not more than 15%.

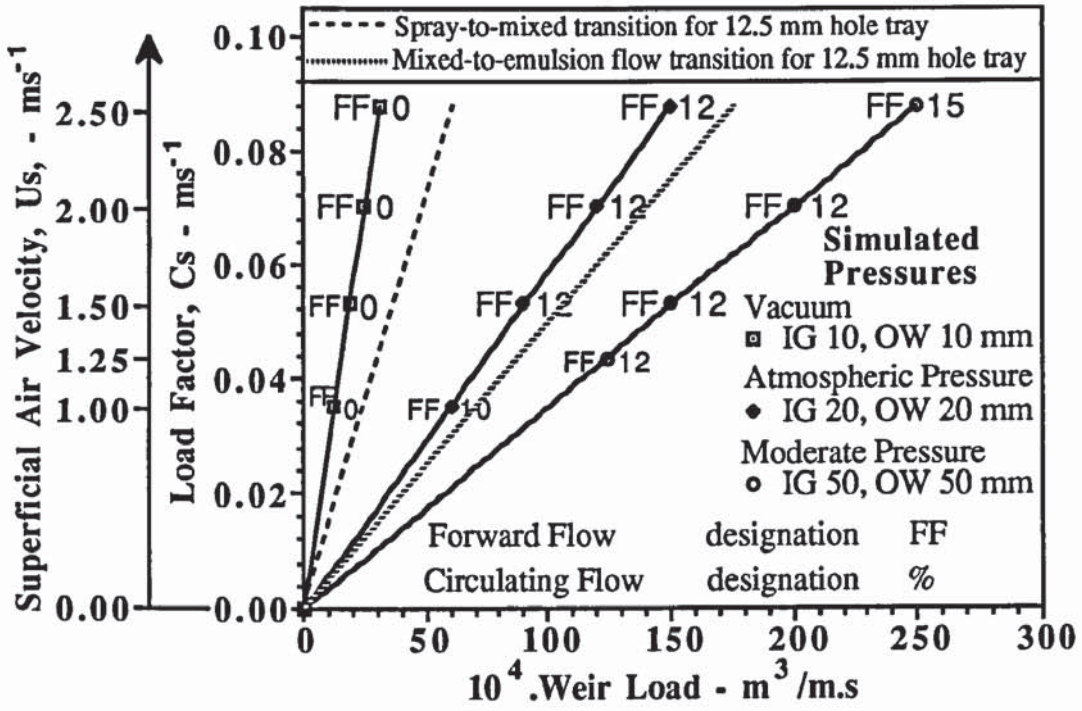

Figure 9.5 Summary of biphase flow patterns obtained in the simulation of distillation experiments at three different presssures.

Conclusions

The air-water flow patterns generated during the simulation of distillation, showed that most of the tray area was occupied by forward flow, i.e., in the direction from the inlet downcomer to the outlet weir. However, at the high weir load simulations of atmospheric and moderate pressure distillation, the velocity of flow near the column wall was less than that in the middle of the tray between the downcomers. This is important in interpreting the results of the water-cooling experiments described below.

9.3.3 Investigation by Water-Cooling

The experiments described above, were followed by the water-cooling experiments to determine the effect of the flow patterns on mass transfer. A complete description of the water-cooling technique is presented in Chapter 5.

During some of the pressure simulation experiments, particularly at low air-water flow rates, the reduced temperature profiles showed a certain level of non-symmetry on the operating tray in that the isotherms were skewed towards the right hand side. Measures taken to rectify the problem have been described in Chapter 6. However, despite the

slight improvement in levelling the tray, the continued presence of skewed isotherms show that the water-cooling technique is sensitive to tray levelness particularly at low flowrates. Hence for this work, if a particular temperature profile is seen as one of a series of profiles, then a view beneath the non-symmetry can be obtained.

Temperature Profile Results

As in the previous water-cooling experiments described in Chapters 6 and 8, all of the temperature isotherm results were compared on a like basis by using reduced temperature profiles. Overall, isotherms can be broadly classified as straight and parallel to the downcomers, indicative of forward only flow, and "U-shapes" which correspond to forward flow associated with a superimposed velocity distribution profile, thus causing a significant variation in the residence time distribution. The severity of the "U-shaped" isotherms was dependant upon the froth heights and the steady increase in the air-water flow rates during each pressure simulation.

For all flow rates in the simulation of vacuum distillation, the reduced temperature profiles were approximately straight and parallel to the downcomers, (see Figure 9.7a). Each isotherm completely occupied the width of the tray cross section thus indicating the same reduced temperature of the liquid at the sides as well as in the middle. The temperature profile results support the direct-observation of forward only flow over the whole tray area.

Parallel isotherms imply that the liquid residence time would be similar both at the sides as well as in the middle of the tray, and are similar to the concentration profiles predicted for the spray regime by Porter et al., (1977). Comparisons of experimental temperature profiles with concentration profiles, predicted from the Porter/Lockett theoretical models, are discussed further in Section 9.4.

In the medium weir load atmospheric pressure experiments, transverse "U-shaped" isotherms and contour lines adjacent to the column wall at the sides of the tray were produced as shown in Figure 9.7b. The horizontal isotherm component was parallel to the downcomers and approximately 1300 mm in length, which suggests a plugflow of liquid in the middle of the tray. The "swept-back" isotherm component extended back towards the ends of the inlet downcomer and this together with contour lines adjacent to the column wall at the sides was indicative of a low liquid velocity for either slow forward flow or circulation.

The transverse "U-shaped" isotherms were caused by slow moving liquid flow over the

longer liquid flow path at the sides of the tray, which in turn has a longer liquid residence time. At the lower flow rate range, the coldest liquid was found close to the ends of the inlet downcomer, indicative of a relatively small slow moving circulating flow. At the higher flow rate range, the coldest liquid was found close to the ends of the outlet weir as a result of slow moving liquid at the sides of the tray outlet. This seemed reasonable since the liquid velocity decreased, as a result of the gas resistance when forced through the liquid, during its journey across the long liquid flow path at the sides of the tray.

In both cases, the reduced temperature of the liquid was less than the temperature of the liquid flowing over the outlet weir, thus reducing the driving force for mass transfer which in turn causes a fall-off in tray efficiency.

The effect of increasing the air flow rate in proportion with the liquid flow rate, during the simulation of atmospheric pressure distillation was a flattening of the transverse "U-shaped" isotherms. In addition, there was a marginal increase in the number of confused isotherms, particularly at the sides of the tray.

The temperature profile results in the moderate pressure simulation experiments were similar to those yielded in the previous case, with one noticeable exception. That is, the isotherms were distinctively "U-shaped" with the leading edge located on, or close to the tray centreline as shown in Figure 9.7c. The "U-shapes" were indicative of a bulk forward flow with an underlying velocity distribution profile across the horizontal plane of the tray. In other words, the biphase forward flow moved fastest along the tray centre line and much more slowly at the sides.

Unlike the atmospheric pressure experiments, the coldest liquid regions showed up as tightly packed isotherms adjacent to the column wall on the tray outlet and corresponded to slow moving forward flow towards the ends of the outlet weir. (This occurred despite the presence of a relatively small inlet circulation). The effect became more significant at the higher flow rate range. This seemed reasonable since the velocity of the liquid flow at the sides of the tray, was reduced considerably by the gas resistance through the liquid, and by the large froth height produced using a high outlet weir.

The reduced temperature of the liquid near the ends of the outlet weir, was less than that flowing over the outlet weir in the middle of the tray, thus producing an adverse effect on mass transfer and tray efficiency.

A summary of all temperature profile results are presented in Figure 9.6 which is a modified diagram of load factor plotted against weir load for each of the simulations. In

addition, a set of all the temperature profile results, for each simulation, are shown in Appendix 9.0.

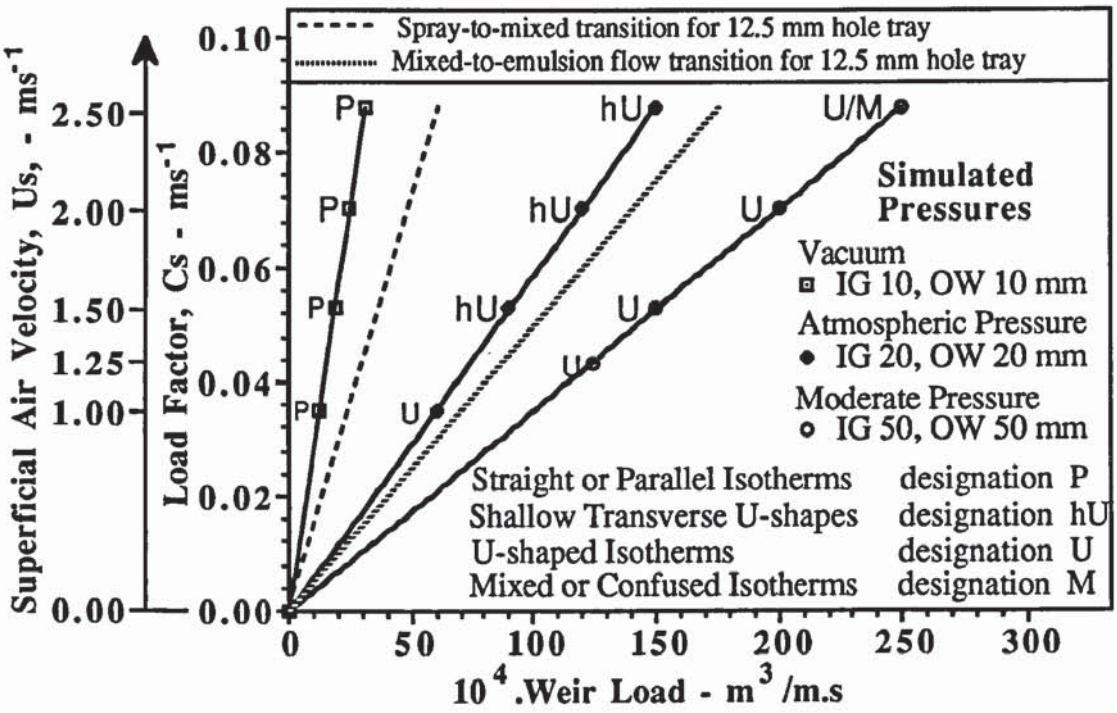

Figure 9.6 Summary of isotherm profiles on a load factor verses weir load diagram.

Discussion of Results

In general, the temperature profile results showed that the coldest regions on the tray corresponded to liquid having a longer liquid residence time. The coldest liquid was found on the long liquid flow path tray segments, where the liquid was either moving slowly forward or circulating. This caused a reduction in the driving force for mass transfer which ultimately leads to a low tray efficiency.

"U-shaped" isotherms obtained for both slowly forward moving and circulating flow, at the higher pressure simulations, are similar to the concentration profiles predicted in the stagnant regions model, (Porter et al., 1972) and is discussed further in Section 9.4. The isotherms obtained at the flow rate ratio which simulated vacuum distillation are approximately straight and parallel to the downcomers. This implies that there is very little variation in the mean residence time distribution across the tray which may have been caused by a different flow mechanism for this flowrate ratio, (high gas rate and low liquid rate). Furthermore this may be related to operating the tray in the spray regime (Porter et al., 1977; Raper et al., 1984), and is discussed further in Section 9.4.

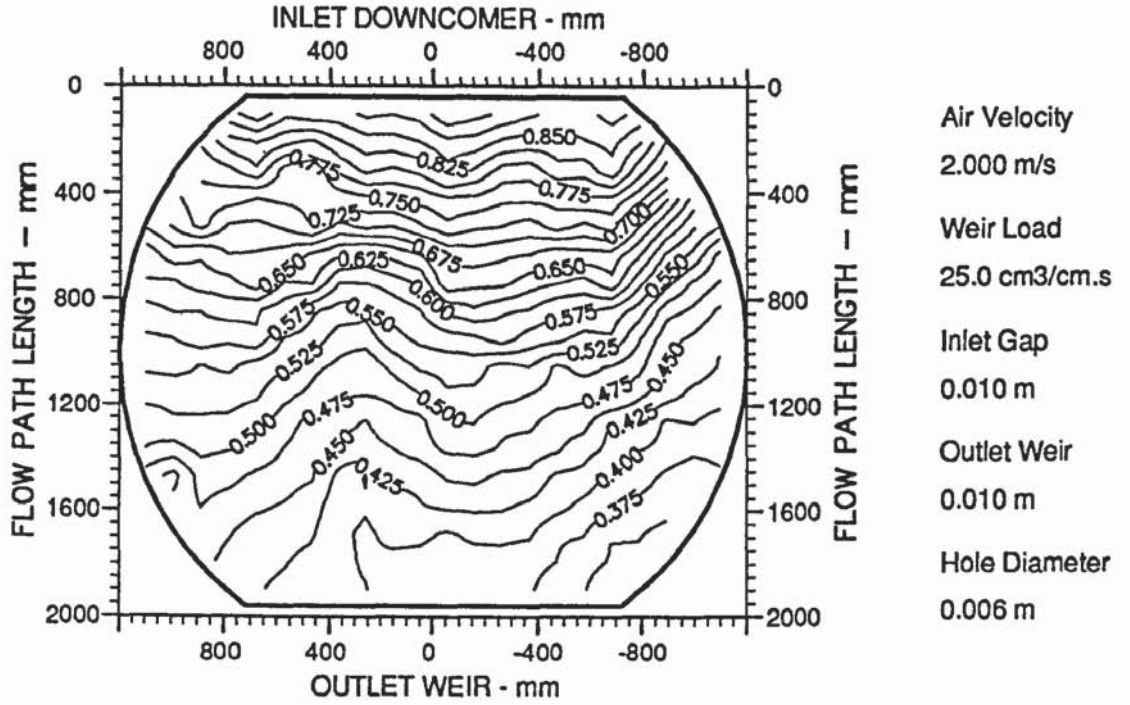

Figure 9.7a An example of a two-dimensional reduced temperature profile diagram showing parallel isotherms during vacuum simulation (designation P).

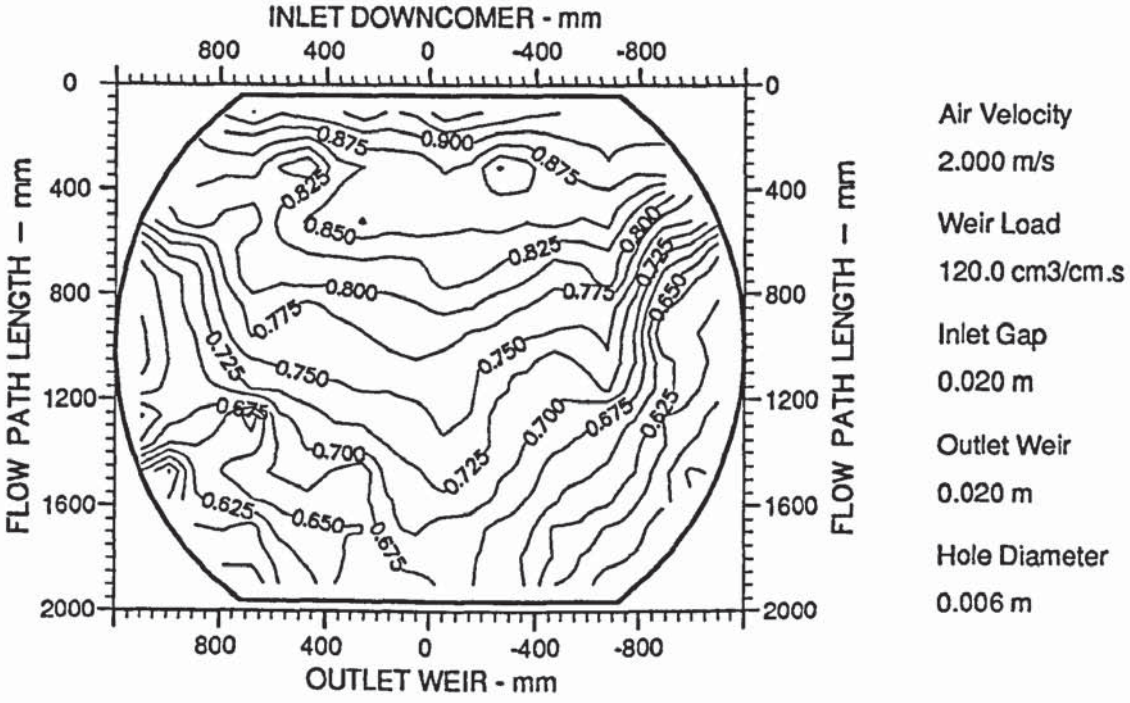

Figure 9.7b An example of a two-dimensional reduced temperature profile diagram showing "U-shaped" isotherms during atmospheric pressure simulation (designation hU).

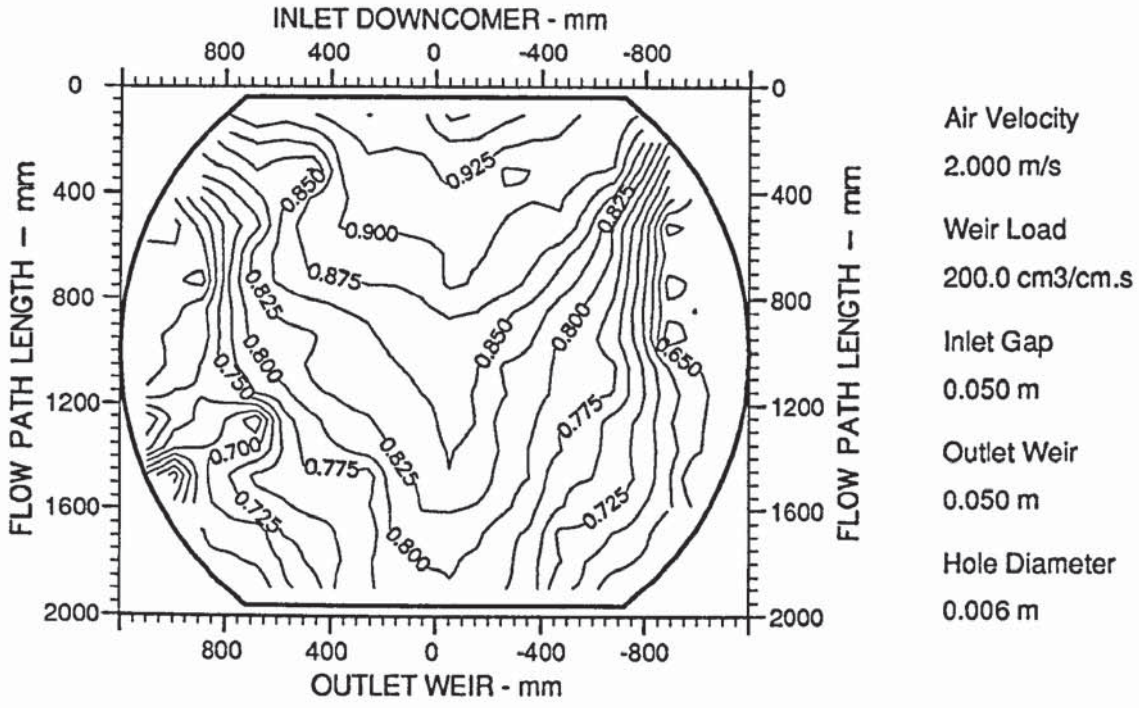

Figure 9.7c An example of a two-dimensional reduced temperature profile diagram showing "U-shaped" isotherms during moderate pressure simulation (designation U).

Thermal Efficiency Results

Point, E_{OG}, and tray efficiency, E_{MV}, results were calculated using the reduced temperature profiles from above, and are presented in Table 9.2. The changes in the point efficiency, E_{OG}, from an average of 42% for the simulation of vacuum distillation, to an average of 81.5% for atmospheric distillation and 88% for moderate pressure distillation are similar to those found in industrial scale practical distillation columns. The changes in tray efficiency, E_{MV}, from an average of 105% for atmospheric simulation to 99% for pressure simulation are opposite to that found in distillation owing to the changes in the flow rate ratio which results in changes in λ (= mG/L) and a reduction in the expected value of E_{MV}/E_{OG}.

The ratio of water rate to air rate is lower in the simulation of vacuum distillation than the ratio used to simulate pressure distillation. This means that the relative increase from point efficiency to tray efficiency is greater for the simulated vacuum distillation than for the simulated pressure distillation. This effect of air to water ratio change is greater than the change in point efficiency.

The reason why the lowest point and tray efficiencies were found in the vacuum simulation experiments, and the highest produced at the higher pressure simulation experiments, can be explained as follows. In the pressure simulation experiments, the relatively high gas residence time within the froth permitted a longer gas-liquid contact time for mass transfer, which in turn yielded the highest efficiencies. This is the expected result which is found in practice. In contrast, the low gas residence time within the small froth heights, during the simulation of vacuum distillation resulted in a reduced driving force for mass transfer thus leading to lower efficiencies.

Simulated Pressure	**Vacuum**			**Atmospheric Pressure**			**Moderate Pressure**		
IG/OW-mm	10,10			20,20			50,50		
Superficial Air Velocity - ms^{-1}	Weir Load - cm^3/cms	Efficiency - %		Weir Load - cm^3/cms	Efficiency - %		Weir Load - cm^3/cms	Efficiency - % * (Us = 1.25 ms^{-1})	
1.00	12.5	E_{OG} E_{MV} E_{MV}/E_{OG}	36 68 1.90	60.0	E_{OG} E_{MV} E_{MV}/E_{OG}	77 99 1.29	100.0	E_{OG} E_{MV} E_{MV}/E_{OG}	*88 103 1.17
1.50	18.5	E_{OG} E_{MV} E_{MV}/E_{OG}	41 75 1.83	90.0	E_{OG} E_{MV} E_{MV}/E_{OG}	86 115 1.34	150.0	E_{OG} E_{MV} E_{MV}/E_{OG}	94 106 1.13
2.00	25.0	E_{OG} E_{MV} E_{MV}/E_{OG}	45 80 1.78	120.0	E_{OG} E_{MV} E_{MV}/E_{OG}	82 105 1.28	200.0	E_{OG} E_{MV} E_{MV}/E_{OG}	87 95 1.09
2.50	31.0	E_{OG} E_{MV} E_{MV}/E_{OG}	47 93 1.95	150.0	E_{OG} E_{MV} E_{MV}/E_{OG}	81 100 1.24	250.0	E_{OG} E_{MV} E_{MV}/E_{OG}	83 92 1.11

Table 9.2 Summary of measured Point and Tray Efficiencies on the 6.35mm tray at three simulated pressures.

Discussion of Results

The results have shown that regions containing circulation and in many cases slow forward flow, have a longer liquid residence time. This in turn had an adverse effect on both point and tray efficiency, and is similar to predictions from the stagnant regions model of Porter et al., (1972) in which the calculated concentration profiles gave a measure of the driving force for mass transfer (see Section 9.4).

Comparison of Thermal Point Efficiencies with the Efficiency Results of Prado and Fair (1990)

To test the validity of the efficiencies presented in this chapter, it was decided to compare

the experimental results with those of Prado and Fair (1990). In these experiments, the air-humidification technique was used in which water flowing across a 6.35 mm hole sieve tray was evaporated into a dry air stream when forced through the liquid. Although there were slight differences in the inlet gap/outlet weir settings and the flow rates used in both the water-cooling and air-humidification experiments, the point efficiencies of Prado and Fair were compared with those obtained during the simulation of vacuum distillation.

All the operating conditions and tray geometries as well as the E_{OG} results from both sets of experiments are presented in Table 9.3.

Water-Cooling Experiments in this Study				**Prado and Fair ,1990 (Air-humidification)**			
Tray Details	2440 mm diameter sieve tray of 10 % free area			Tray Details	121 mm diameter sieve tray of 11% free area		
Simulated Pressure	Vacuum			Study ?	Simple Gas-Liquid Contacting Experiments		
I G/OW - mm	10.0,10.0			I G/OW -mm	8.0, 25.4		
Superficial Air Velocity - ms^{-1}	10^4.Weir Load $m^3/m.s$	Efficiency - %		Superficial Air Velocity - ms^{-1}	10^4.Weir Load $m^3/m.s$	Efficiency - %	
1.00	12.5	E_{OG}	36	1.50	21.0	E_{OG}	85
1.50	18.5	E_{OG}	41	1.75	21.0	E_{OG}	85
2.00	25.0	E_{OG}	45	2.00	21.0	E_{OG}	85
2.50	31.0	E_{OG}	47	2.40	21.0	E_{OG}	84

Table 9.3 Comparison of point efficiencies from this study with those of Prado and Fair (1990) on 6.35mm hole sieve trays.

In general, the point efficiencies of Prado and Fair are greater than those presented in this study, and may be due to several reasons, which are as follows:-

a) Since a small scale sieve tray was used by Prado and Fair, a splash baffle was installed at the liquid outlet to increase the liquid depth in order to simulate the conditions in large trayed columns. This may have over-compensated thus giving a larger gas-liquid contact time. In addition, since the tray was of a much smaller diameter (i.e., 121 mm) compared with that used in this work, the air-water mixture on the tray may suffer from wall effects similar to that experienced in a laboratory Oldershaw Column.

b) In order to calculate E_{OG}, from gas phase resistant mass transfer data, Prado and Fair assumed a completely mixed tray in which the liquid composition was uniform

throughout the two phase dispersion and that the gas passed through the liquid vertically in plug flow without mixing. It is possible therefore, that there may have been a small gradient in the water temperature such that the liquid on the tray was not completely mixed.

c) The water temperature during the vacuum simulation experiments was higher than that in the air-humidification experiments. That is, the difference between the average water temperature at the inlet and that leaving the tray at the outlet, was approximately 30 degrees with a view to producing a large driving force for heat transfer (analogous to mass transfer in distillation). However, the slope of the equilibrium curve, m, which corresponds to this temperature difference, may have departed from linearity on an enthalpy driving force diagram where air enthalpy is plotted against water temperature, (see Figure 5.5 in Chapter 5). In principle this may have increased any liquid film resistance to heat transfer and thus affected the calculation of E_{OG}. (Water-cooling is essentially a gas film controlled operation.)

d) Although the E_{OG} calculation procedure is independant of the flow pattern, the nature of biphase flow in these experiments may have influenced the E_{OG} results. That is, the biphase flow on the 121 mm diameter tray (Prado and Fair) was essentially unidirectional compared with that on the 2440 mm diameter tray. Although forward only flow was produced during the vacuum simulation experiments, the biphase moved faster in the middle of the tray compared with that at the sides. In some cases the biphase was almost stationary at the sides and this would have had an effect on the driving force for mass transfer.

Despite the imperfections of both experiments, it is proposed with some confidence that the calculated E_{OG} results, particularly on the commercial scale tray, reflect the current trend of efficiencies found in practice (i.e., low efficiencies during vacuum distillation and high efficiencies at higher pressure distillation). However, the results suggest that the flow pattern might be improved. It is not yet known how this can be achieved.

Conclusions

The simulation of distillation at three different pressures had a substantial effect on the water temperature profiles and thermal efficiencies during water-cooling. Although in several cases, forward flow was produced over most of the tray area, there were colder regions at the sides of the tray where the slower moving liquid has a longer residence time. These colder regions resulted in the calculation of low tray efficiencies.

A comparison of E_{OG} results, from the vacuum simulation experiments, with those of Prado and Fair (1990), were unrealistic owing to the use of a small scale test tray, and the high E_{OG} results computed are probably not typical of that found on commercial size trays. However the low E_{OG} results, from the vacuum simulation (spray regime) experiments do reflect the curent trend of efficiencies found in practice which suggests that the flow pattern might yet be improved. This will be the subject of future work.

9.3.4 Investigation by Liquid Head Measurements

Upto this point, some progress has been made in determining the air-water flow patterns generated at three simulated pressures from the direct-observation and water-cooling experiments described above. However, there was very little information to show the effect of froth height variation on the biphase flow pattern. Thus froth height variations were determined by measurement of the clear liquid height across the tray.

The height of clear liquid experiment for the three simulated pressures is the same as that described in the previous chapter. For each experimental run, the point values of clear liquid height were computer processed, using the UNIRAS suite of plotting routines, to yield three-dimensional liquid head surface profiles. A complete description of the concepts involved in determining the height of clear liquid profiles are presented in Chapter 5.

Height of Clear Liquid Results

All of the height of clear liquid results, for each simulated pressure, are presented on the load factor verses weir load diagram as shown in Figure 8.8. On the whole, the results show some changes in the liquid head surface profiles according to the flow patterns produced in each simulated pressure. However, there were no substantial differences between the liquid head surface of the slower moving or circulating liquid at the sides of the tray compared to that for the faster moving liquid in the middle. The reasons for this are described in Chapter 8.

The horizontal or flat profiles produced during the low weir load vacuum simulation experiments, were indicative of forward flow at all points on the tray. At the higher weir load pressure simulation experiments, the uneven liquid head surface was found initially on the inlet tray section, but this spread over the whole tray cross section at the higher air flow to liquid flow operating range in the moderate pressure simulation. This can be attributed to the increased level of liquid mixing and turbulence, by the bubbling action of the gas, within the large froth heights produced using an outlet weir height of 50 mm.

Note that liquid head profiles were not determined at the superficial air velocity of 2.50 ms^{-1}, for the same reasons as that outlined in Chapter 8.

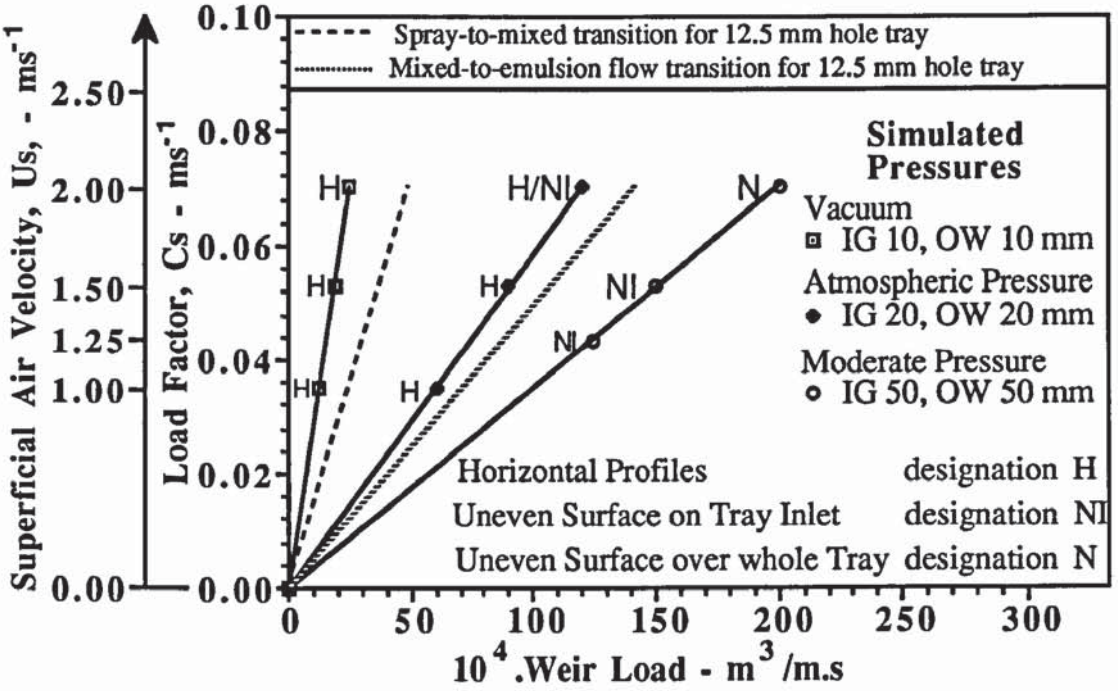

Figure 9.8 Summary of liquid head profiles on a load factor verses weir load diagram.

Examples of a horizontal liquid head surface, from the vacuum simulation experiments, and an uneven liquid head surface over all of the tray, at the higher pressure simulation experiments, are presented in Figures 8.9a and 8.9b. A complete set of all surface liquid head profiles for the simulated pressure experiments are presented in Appendix 10.0.

Comparison of Experimental Height of Clear Liquid Results with Results Predicted from Height of Clear Liquid Correlations Derived by Bekassy-Molnar (1991)

To ratify the height of clear liquid results from the pressure simulation experiments, it was decided to compare them with predicted results from correlations available in the open literature. Since the measured data were obtained when the tray was operated under different flow regimes, correlations formulated for the spray, mixed, and emulsion flow regimes were required in order to make meaningful comparisons. In a recent paper by Bekassy-Molnar and Mustafa (1991), height of clear liquid correlations for the spray, mixed, and froth regimes, based on experimental measurements made in a 400 mm diameter column, were proposed.

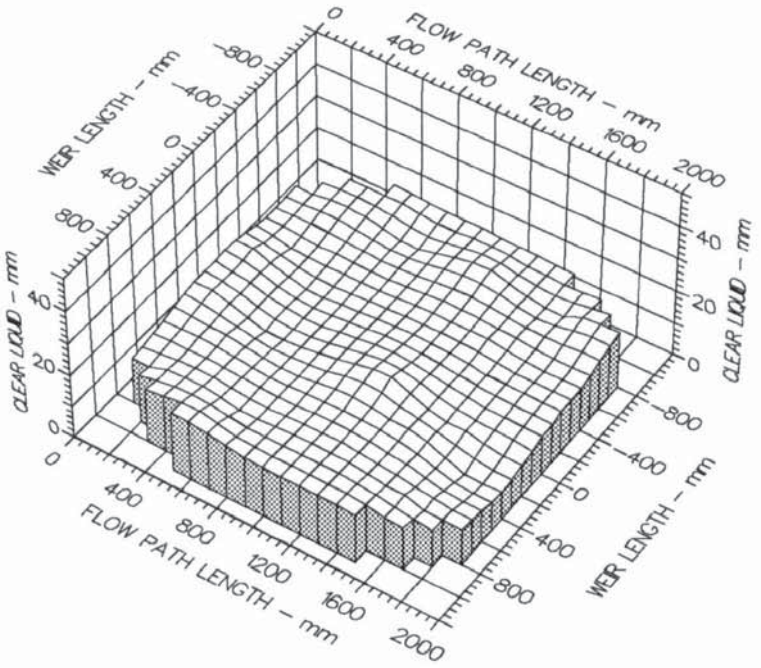

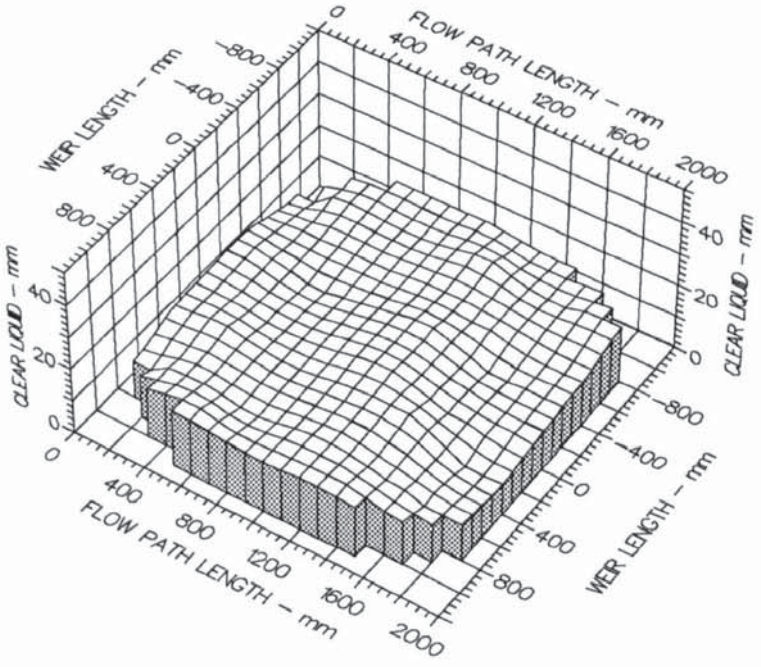

Figure 9.9a Examples of comparatively flat height of clear liquid profiles during the simulation of vacuum distillation (designation H).

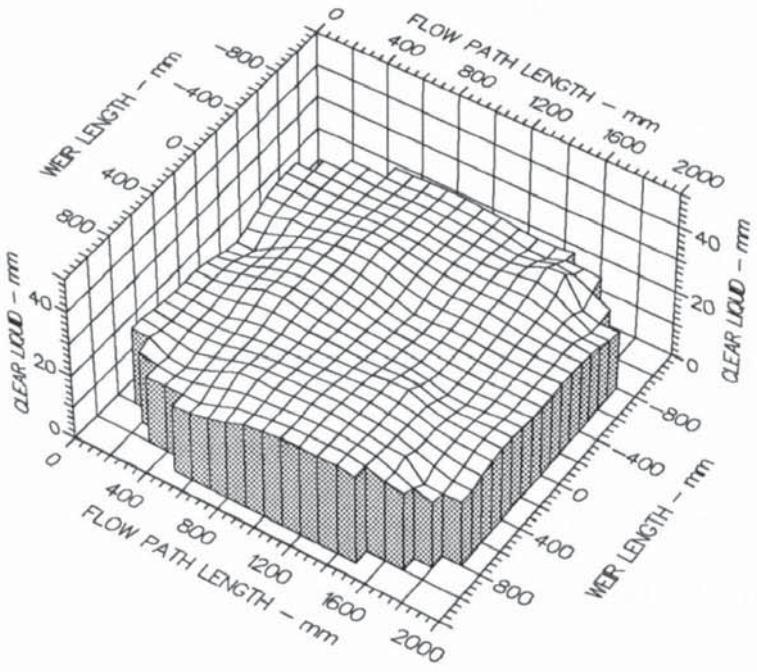

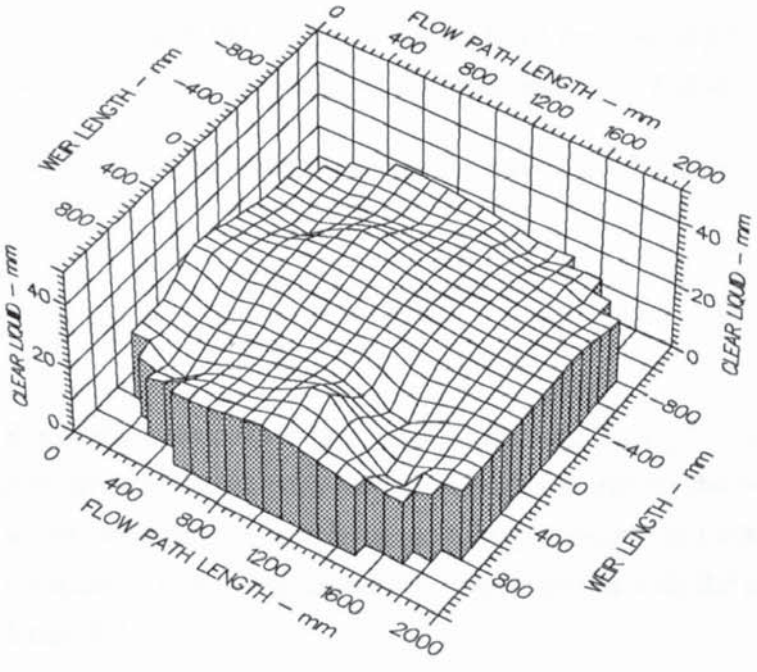

Figure 9.9b Examples of height of clear liquid profiles with an uneven surface across the whole tray during the simulation of moderate pressure distillation (designation N).

It was assumed that these correlations would produce accurate results since the input parameters required include hole diameter, tray free area, flow ratio group for each flow regime, and outlet weir height. Thus the experimental data from the simulated pressure experiments were incorporated into the following height of clear liquid expressions:-

For the spray regime: $$h_L = 0.015 \cdot f_a^{-1.61} \cdot w^{0.50} \cdot d_0^{0.33} \quad (9.7)$$

For the mixed regime: $$h_L = 0.091 \cdot f_a^{-0.70} \cdot w^{0.63} \cdot \psi^{0.33} \quad (9.8)$$

For the froth regime: $$h_L = 0.084 \cdot f_a^{-0.36} \cdot w^{0.64} \cdot \psi^{0.35} \cdot d_0^{-0.19} \quad (9.9)$$

The three equations defined are only valid when;

f_a = 0.045–0.144 m^2/m^2; w = 0.025–0.075 m; d_0 = 0.003–0.0127 m;
v_a = 0.37–3.43 ms^{-1}; and L_w = 0.0003–0.016 $m^3/(m.s)$

All mathematical notation are defined in the nomenclature section at the end of the thesis.

One problem with the input of experimental data into the above correlations, is that the outlet weir heights used for the simulation of vacuum and atmospheric pressure distillation lie just outside the permitted weir height range. In addition the height of clear liquid measurements in the emulsion flow regime, (moderate pressure simulation), were compared with the predicted results from the froth regime correlation even though it was unclear as to the definition of the froth regime by Bekassy-Molnar.

The flow ratio group for each of the three flow regimes, (simulated pressures), is defined as:

$$\psi = \frac{L_w}{v_a}\sqrt{\frac{\rho_L}{\rho_V}} \quad (9.10)$$

Since the water flow rate to air velocity, (L_w/v_a), was constant for each simulated pressure, the most convenient way of comparing the measured height of clear liquid results with the predicted values, was to average the measured results for each simulated pressures. The comparison of measured results with the predicted values are presented in Table 9.4.

On the whole, there were significant differences between the two sets of results. That is, the average measured height of clear liquid for vacuum simulation was greater than the

predicted result by an order of magnitude of 17 %. Furthermore, the measured results during the atmospheric and moderate pressure simulations were less than the predicted results by an order of magnitude of 7 and 60 % respectively. These discrepancies can be attributed to a number of factors. For instance, the outlet weir heights used for the simulation of vacuum (spray regime) and atmospheric pressure (mixed regime) were not valid for the corresponding spray and mixed regime correlations. In addition, it was probably inappropiate to compare height of clear liquid results obtained in the emulsion flow regime, during moderate pressure simulation, with those predicted from the froth regime correlation since the definition of the froth regime by Bekassy-Molnar was unclear.

Comparison of Measured Height of Clear Liquid Results with Predicted Results of Bekassy-Molnar (1991)					
Simulated Pressure and Flow Regime	IG / OW heights - mm	Flow Ratio Group - ψ	Average Height of Clear Liquid- mm		Percent Difference - %
			Measured	Predicted	
Vacuum (Spray)	10,10	0.00125	13.80	11.51	16.6
Atmospheric Pressure (Mixed)	20,20	0.171	20.31	21.66	6.60
Moderate Pressure (Emulsified)	50,50	0.285	29.72	47.68	60.4

Table 9.4 Comparison of measured height of clear liquid results with predicted results of Bekassy-Molnar (1991).

Finally the above results suggest that the height of clear liquid correlations, proposed by Bekassy-Molnar, based on experimental measurements made on 400 mm diameter trays might not be representative of that found on commercial trays. Thus correlations based on experimental data, in the spray, mixed and emulsion flow regimes, on commercial size trays need to be further developed in order to make more meaningful comparisons with the measured height of clear liquid results for each simulated pressure.

Conclusion

The height of clear liquid experiments have shown that the level of non-uniform liquid head profiles increased as the simulated pressure changed from vacuum to moderate pressure. However, there were no substantial differences between the liquid head surface of the slower moving or circulating liquid at the sides of the tray compared to that for the faster moving liquid in the middle. This demonstrates that the technique does not

'distinguish' between slow forward flow and circulation at the sides of the tray, and is not sensitive enough for highlighting small differences around circulating regions.

On the whole, there was little agreement between the measured height of clear liquid results obtained in the simulated pressure experiments compared with those predicted from the correlations of Bekassy-Molnar (1991). This suggests that the predicted height of clear liquid results using correlations, derived from data on small scale trays for different flow regimes, may be unrepresentative of that found on commercial trays. Thus it is proposed with some confidence that the measured height of clear liquid results presented in this chapter, may be representative of that found on commercial size trays used in industry.

9.4 Comparison of Experimental Temperature Isotherms with Predicted Concentration Profiles From the Stagnant Regions Model

So far, the effect of flow patterns on mass transfer have been determined using the water-cooling technique which utilizes an analogy between heat and mass transfer to simulate distillation. The reduced temperature profile isotherms generated during water-cooling, are related to concentration profiles found in distillation, with the coldest water temperature regions on the tray corresponding to longer liquid residence times.

The aim of this section was to compare temperature profile isotherms, from each pressure simulation experiment, with concentration profiles predicted from the stagnant regions model, or SRM, Porter et al., (1972). (A description, including the mathematical development of the model is presented in Chapter 2). In addition, by using data from the water-cooling experiments as input into the theoretical model, the computed tray efficiencies can be compared with those obtained experimentally.

9.4.1 Computer Prediction of Concentration Profiles and Efficiencies

In the water-cooling experiments, use was made of reduced temperature profile isotherms in order to compare experimental results on an equal basis. This concept was also used in the SRM so as to calculate concentration profiles using the reduced, or dimensionless, concentration X_r, which is given by,

$$X_r = \frac{x - x_{eot}}{x_i - x_{eot}} \qquad (9.11)$$

To compare the reduced concentration profiles with the reduced temperature isotherms for the same experimental conditions, input parameters such as the tray dimensions and the froth properties were incorporated into the SRM computer programme. The tray data included the weir length, tray diameter, weir height, hole diameter, and the fractional free area of the tray. Data concerning the froth included the vapour and liquid flow rates, experimental λ, N_{Pe}, experimental E_{OG}, ρ_L, ρ_V, and the average height of clear liquid. The original SRM computer programme was modified (Walton, 1993) such that there were no dramatic stepwise changes in the liquid concentration from the tray inlet to the tray outlet.

From this information, liquid velocity profiles were calculated, starting on the tray centreline from the inlet downcomer, followed by point to point calculations of the reduced concentration profiles. These in turn were used for the calculation of theoretical tray efficiencies.

The calculated reduced concentration profiles were computer processed, using the UNIRAS suite of plotting routines, to yield two and three-dimensional concentration field displays. A complete set of all the predicted concentration profiles, for each pressure simulation experiment, are shown in Appendix 11.0.

9.4.2 Comparison of Predicted Concentration Profiles with Experimental Temperature Profiles

The computed concentration profiles, presented in Figures 9.10a and 9.11a, are similar to the transverse and severe "U-shaped" temperature profiles, shown in the corresponding Figures 9.10b and 9.11b, for the simulation of atmospheric and moderate pressure distillation, where the SRM is expected to be applicable. The "U-shaped" concentration profiles are indicative of a rapid depletion of the most volatile component to the vapour rising through the sides of the tray. This is a very interesting result since the theoretical model assumes that the liquid at the sides of the tray is stagnant, ie in between slow forward flow and a reverse flow in which circulating flow occurs near the column wall.

For vacuum simulation, the predicted concentration profiles, from the SRM were "U-shaped" compared with the straight and parallel reduced temperature isotherms obtained experimentally, (see Figures 9.12a and 9.12b). Figure 9.12b shows that the "U-shaped" concentration profiles are indicative of a severe loss of the most volatile component to the vapour rising through the sides of the tray such that the reduced concentration profile in this region was almost zero. This implies that for this set of experimental conditions, the

SRM is not valid for vacuum distillation, since the "U-shaped concentration profiles are expected to correspond to liquid channelling along the middle of an operating tray associated with stagnant zones at the sides. Since the experimental isotherms were parallel to the downcomers, it implies that there may be a different flow mechanism for vacuum distillation, ie spray regime operation, whereas the SRM is applicable to trays operating in the bubbly or froth regime only.

9.4.3 Comparison of Predicted Efficiencies with Experimental Efficiencies

All of the results are presented in Table 9.5. The computed tray efficiencies were remarkably similar to those obtained experimentally during the higher presssure simulations despite the "U-shaped" appearance of the calculated concentration profiles, indicative of the rapid depletion of the most volatile component at the sides of the tray.

However, there was less agreement, between the computed and experimental tray efficiencies for vacuum simulation and was probably due to the reasons outlined above. Furthermore, the computed enhancement of point efficiency, E_{MV}/E_{OG}, results were greater than the experimental E_{MV}/E_{OG} results, during the higher flow rate range vacuum simulation, which was opposite to that produced for the higher pressure simulations. This is further evidence of the SRM being invalid for the calculation of concentration profiles and tray efficiencies when the tray is operating in the spray regime during the simulation of vacuum distillation.

Simulated Pressure	Vacuum				Atmospheric Pressure				Moderate Pressure			
IG/OW - mm	10,10				20,20				50,50			
Superficial Velocity - ms^{-1}	1.00	1.50	2.00	2.50	1.00	1.50	2.00	2.50	1.25	1.50	2.00	2.50
10^3 .Average Clear Liquid Height - m	15.3	15.4	13.5	11.0	22.8	23.1	21.1	14.2	36.6	35.8	23.7	22.8
10^4 .Liquid Rate, Q_L - m^3/s per m of weir	12.5	18.5	25.0	31.0	60.0	90.0	120	150	100	150	200	250
Experimental λ	4.96				1.20				0.62			
Calculated N_{Pe}	137	103	94.5	80.2	184	138	120	150	86.7	80.0	97.2	85.4
Experimental E_{OG}	0.36	0.41	0.45	0.47	0.77	0.86	0.82	0.81	0.88	0.94	0.87	0.83
Experimental E_{MV}	0.68	0.75	0.80	0.93	0.99	1.15	1.05	1.00	1.03	1.06	0.95	0.92
Experimental E_{MV}/E_{OG}	1.90	1.83	1.78	1.95	1.29	1.34	1.28	1.24	1.17	1.13	1.09	1.11
Computed E_{MV}	0.59	0.75	0.89	0.97	0.89	1.05	0.99	0.96	0.95	1.03	0.93	0.89
Computed E_{MV}/E_{OG}	1.64	1.82	1.98	2.07	1.15	1.22	1.20	1.19	1.08	1.10	1.07	1.08

Table 9.5 Comparison of experimental tray efficiencies with predicted efficiencies from the stagnant regions model.

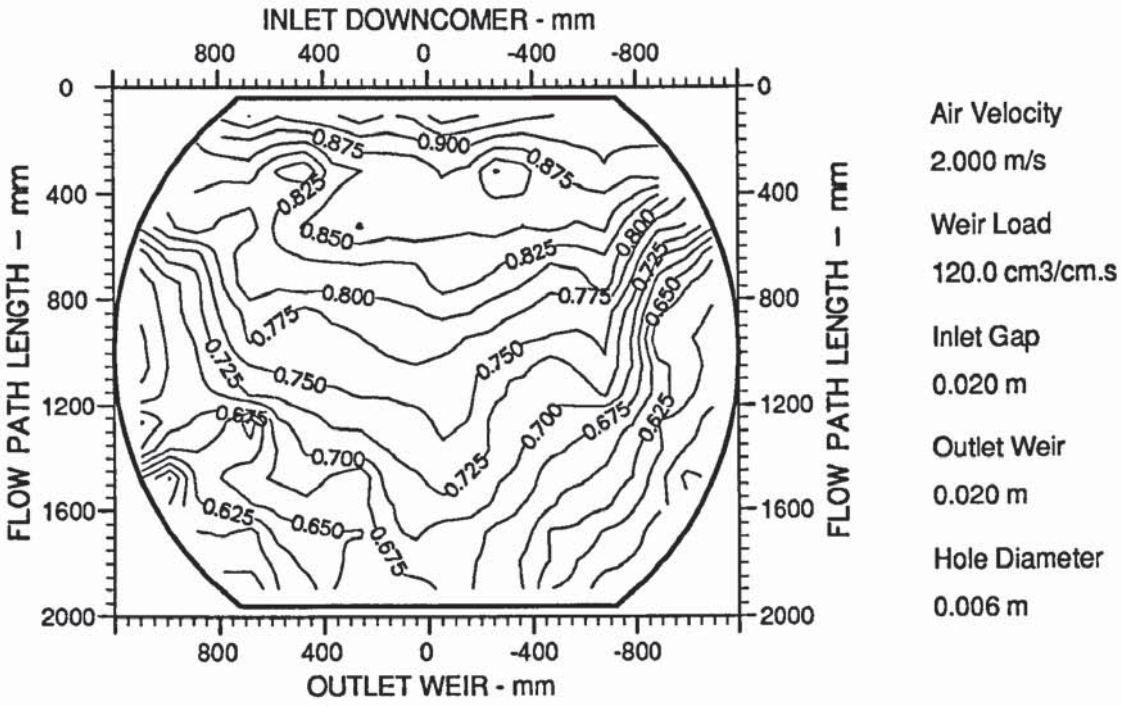

Figure 9.10a An example of a two-dimensional reduced temperature profile diagram showing transverse "U-shapes" during atmospheric pressure simulation.

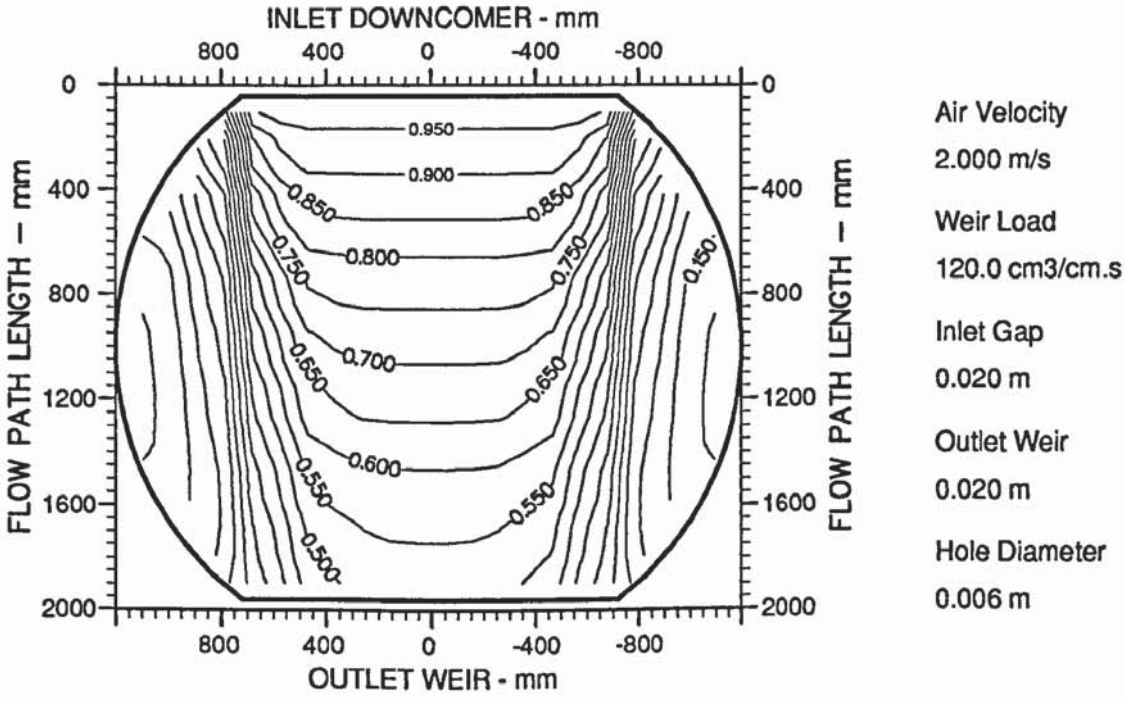

Figure 9.10b An example of a two-dimensional reduced concentration profile diagram showing transverse "U-shapes" during atmospheric pressure simulation.

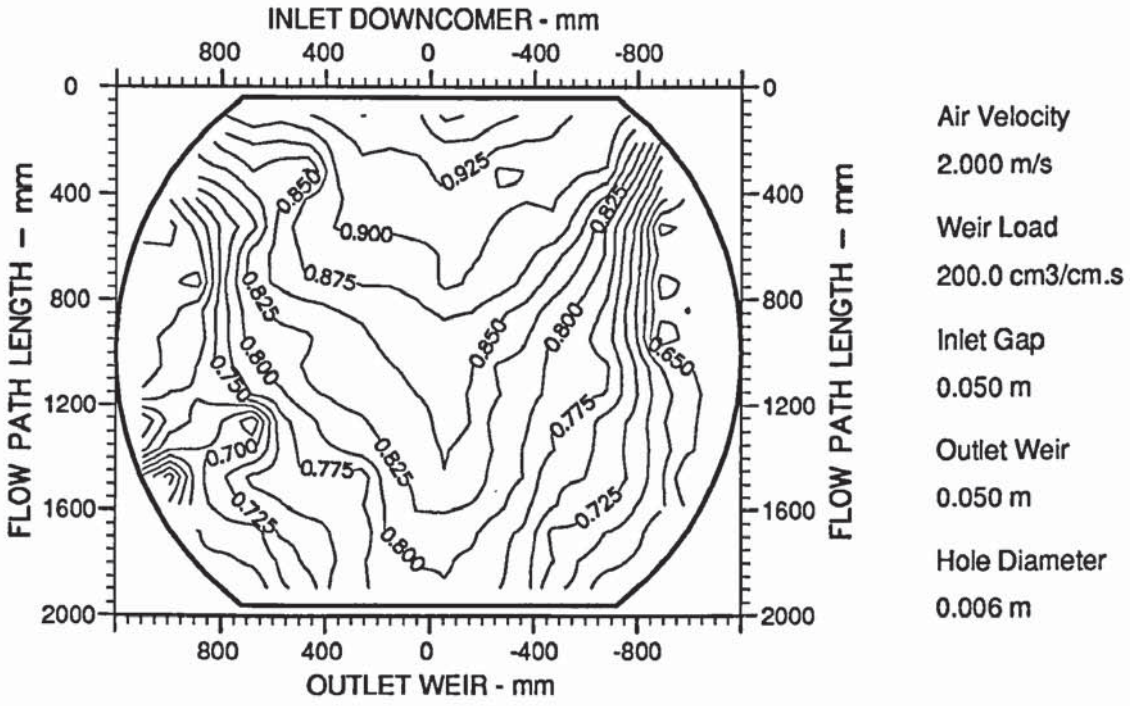

Figure 9.11a An example of a two-dimensional reduced temperature profile diagram showing distinctive "U-shapes" during moderate pressure simulation.

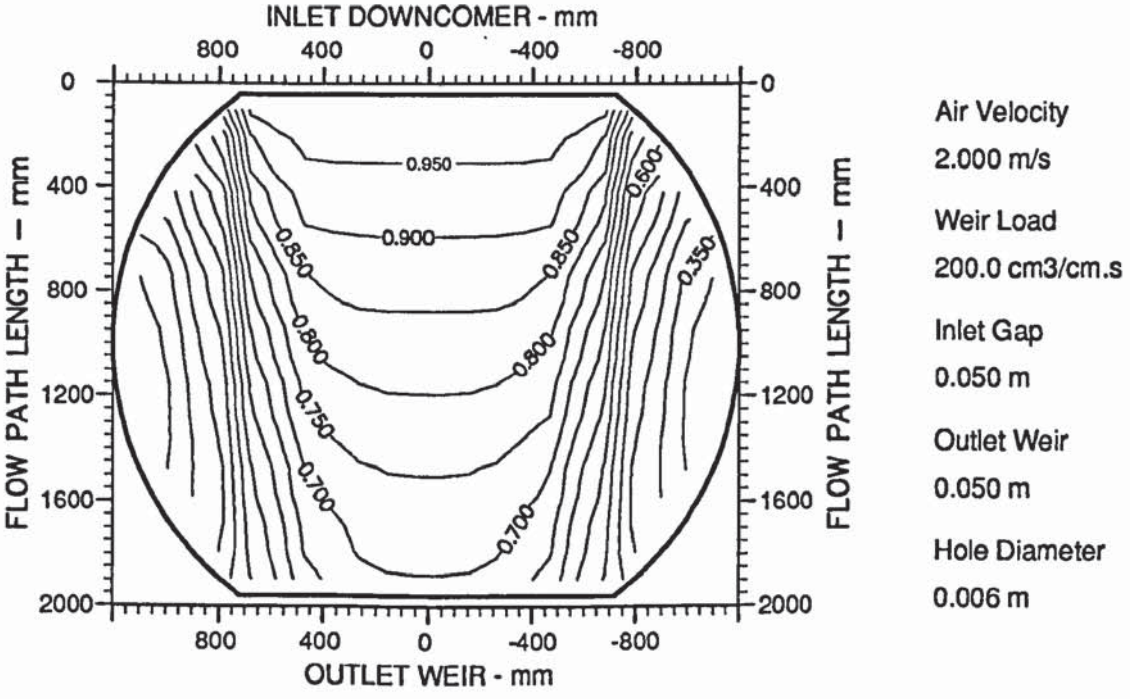

Figure 9.11b An example of a two-dimensional reduced concentration profile diagram showing distinctive "U-shapes" during moderate pressure simulation.

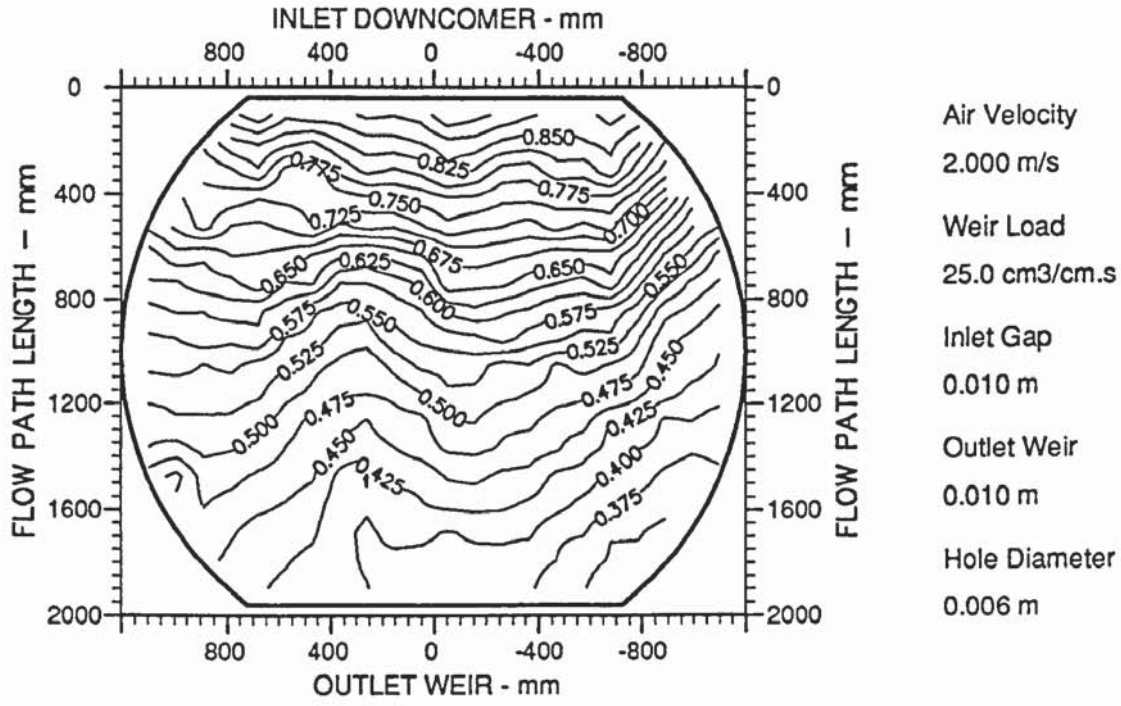

Figure 9.12a An example of a two-dimensional reduced temperature profile diagram showing parallel isotherms during vacuum simulation.

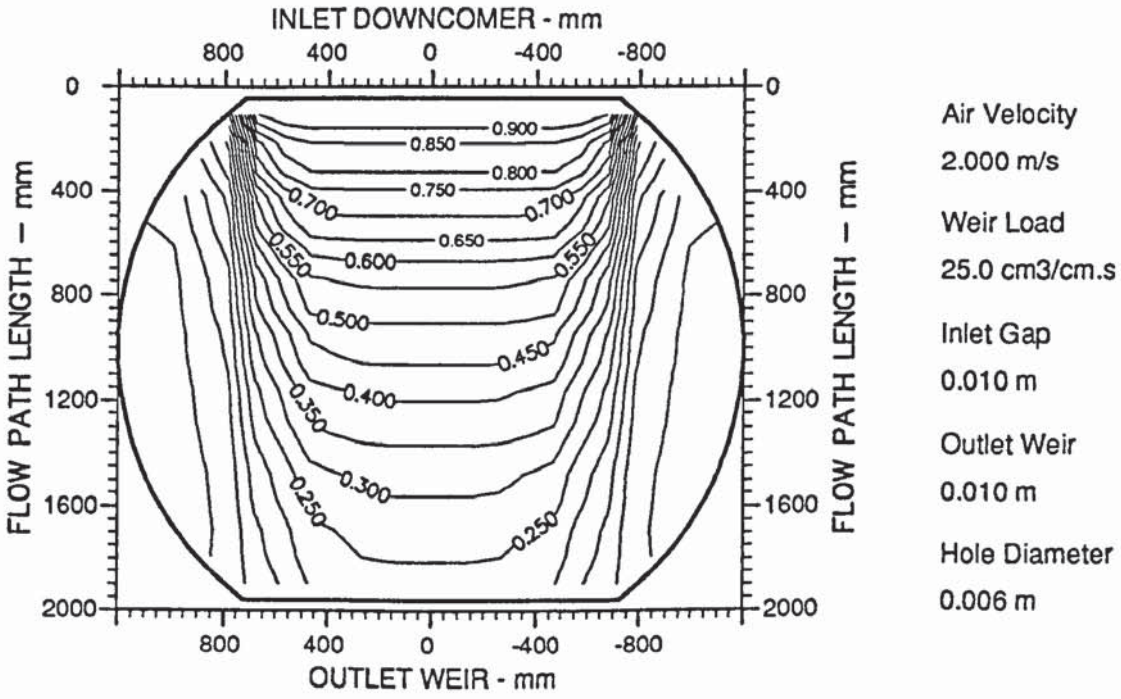

Figure 8.12b An example of a two-dimensional reduced concentration profile diagram showing shallow "U-shapes" during vacuum simulation.

9.4.4 Discussion of Results

The results presented above show that the SRM was applicable for conditions used in the atmospheric and moderate pressure simulations, but was not valid for the vacuum simulation. This can be expained as follows:-

The similarity between the predicted concentration profiles and tray efficiencies with that obtained experimentally for atmospheric and moderate pressure simulations, is an interesting result since the hypothetical flow pattern described in the SRM is oversimplified. That is, it is assumed that there are no circulating eddies and that there is no bulk liquid flow in the stagnant regions at the sides of the tray. However, random vapour-liquid agitation into the stagnant regions by transverse diffusional mixing occurs over a limiting distance of 0.30-0.60 m and is independent of column diameter. In contrast the liquid was slowly moving forward at the sides of the tray during the pressure simulation experiments.

Although the predicted and experimental results are very similar, it can be seen, from Figures 9.10a, 9.10b, 9.11a, 9.11b, 9.12a, and 9.12b, that the calculated reduced concentration profiles at the sides of the tray were much less than the experimental reduced temperature isotherms. This implies that the SRM under-predicted liquid concentration profiles at the sides of the tray which means that beyond the mixing zone, stagnant liquid is not the same as the slow moving liquid observed in the pressure simulation experiments.

The width of the mixing zone concept from the SRM is important in considering the effects of scale-up on tray efficiency. For small diameter trays, stagnant zones are smaller than the mixing zone which means that volatile material is continuously replenished as it is stripped by the vapour. This process is repeated on larger diameter trays except that the stagnant zones are much larger with liquid in these regions rapidly approaching equilibrium with the vapour passing through it. Further vapour passage through the stagnant zones undergoes no composition changes, and since the duty of the tray is to change the vapour composition, this reduces tray efficiency. This is significant since it was predicted that in a column of large diameter single pass trays placed one above the other, this effect produces a much greater reduction in both tray and column efficiency than for a single tray (Lockett et al., 1973).

The results for vacuum simulation show that the SRM is not applicable which implies that there may be a different flow mechanism for this flowrate ratio, (high gas rate and low

liquid rate), ie spray regime operation. Liquid flow in the spray regime was modelled in terms of a spray diffusion model, (Porter, Safekourdi, and Lockett, 1977), which utilizes point heights of clear liquid on the tray, analagous to concentration in molecular diffusion, to yield a more uniform flow pattern.

However, experimental measurements, (Porter et al., 1977) of liquid mixing on the tray to determine the diffusion coefficient for use in the spray diffusion model shows that there is a limit to liquid flow by spray diffusion. Hence, it was not possible to calculate concentration profiles using the experimental conditions for vacuum distillation, since the diffusion model is only valid for Peclet Numbers, N_{Pes} upto and including 1.25. This limiting value was calculated on the assumption that spray exists as a large body of liquid droplets dispersed in a continuous vapour stream which move about in a random manner.

If this assumption on the flow of spray is accepted, an estimate of N_{Pes} at the spray regime limit can be made by referring to the liquid mixing results plotted on a graph of eddy diffusivity against superficial gas velocity, (Porter et al., 1977). By using the superficial air velocity of 1.50 ms^{-1} and a clear liquid height of 0.0154 m from the vacuum simulation experiments, which is close to the spray-to-mixed regime transition, N_{Pes} ($= ZL/WD_{es}\rho_L h_i'$) was estimated to be 31. The result indicates that there may be another mechanism contributing to the liquid flow in the spray regime, and suggests that the flow of spray at the limt (i.e., close to the spray-to-mixed flow regime boundary) is essentially plug flow, a phenomenon reported by Raper et al., (1984).

From the vacuum simulation experiments, observations of the biphase dispersion showed that the tray floor was completely covered with aerated liquid and that frequent jetting of the liquid produced coarse drops immediately above the liquid continuous medium. This suggests that assumption of a mass of fine droplets suspended in a gas continuous medium in the spray diffusion model is oversimplified. Furthermore, the coarse spray was in forward flow at all points on the tray during the vacuum simulation experiments, which tends to support the observations of Raper (1984).

Overall, the spray diffusion model needs to be modified by first addressing the question of "how does liquid flow in the spray regime?" in order to calculate concentration profiles for the spray regime, and thus make meaningful comparisons with the vacuum simulation temperature profiles. Such activities are currently underway at The University of Aston in Birmingham. Nevertheless, the concentration profiles in Figure 2.7 of Chapter 2, calculated from the spray diffusion model, show that the spray regime produces a more uniform liquid flow pattern compared with the that using the SRM.

9.4.5 Conclusion

In this section, it has been shown that the predicted concentration profiles and tray efficiencies, from the SRM, were very similar to that found experimentally at the simulated higher pressures, whereas this was not the case for the simulation of vacuum distillation. This proved to be an interesting result given the imperfections of the experiments and the oversimplified hypothetical flow pattern in the SRM. The SRM was not valid for the vacuum simulation since there may be a different flow mechanism for this flowrate ratio, in that the tray was operating in the spray regime.

On the whole, this section has shown that it is unwise to fit experimental data, from the three pressure simulations, into the same tray efficiency design equations since flow pattern changes at different pressures will result in changes in the tray efficiency. (Using experimental data in the same tray efficiency design equations is a procedure adopted by Fractionation Research Incorporated (F.R.I.)).

9.5 Overall Conclusion

In this chapter, the air-water flow pattern results for the simulation of distillation, showed that most of the tray area was occupied by forward flow, i.e., in the direction from the inlet downcomer to the outlet weir. However, at the higher weir load simulations of atmospheric and moderate pressure distillation, the velocity of flow near the column wall was less than that in the middle of the tray between the downcomers.

This was important when interpretating the water temperature profiles, since slow forward flow in most of the experiments corresponded to colder regions at the sides of the tray where the liquid has a longer residence time, thus yielding relatively low tray efficiencies.

The colder, slow moving liquid on the tray was complemented by the height of clear liquid results which were, on the whole, higher at the sides than in the middle on the tray inlet. Furthermore, the liquid head became increasingly non-uniform as the simulated pressure was increased from vacuum to a moderate pressure.

The experimentally determined efficiencies and height of clear liquid results were compared against published data, obtained both experimentally and by the use of mathematical correlations, for similar operating conditions. A comparison of point

efficiency results, from the vacuum simulation experiments, with those of Prado and Fair (1990), were unrealistic since their apparatus was small scale, and the high E_{OG} results computed are probably not typical of that found on commercial size trays. However the low E_{OG} results, from the vacuum simulation experiments do reflect the curent trend of efficiencies found in practice. This suggests that the flow pattern might yet be improved and may be the subject of further work. The measured height of clear liquid results obtained in the simulated pressure experiments, showed very little agreement with those predicted from the correlations of Bekassy-Molnar et al., (1991). This implies that the liquid head results produced on the 2.44 m diameter test tray may be more realistic of that found on real trays in commercial scale columns.

Finally, it has been shown that for the same operating conditions on a single tray, the experimental temperature profiles can be compared with computed concentration profiles from an appropiate theoretical model. That is, the predicted concentration profiles and tray efficiencies, from the SRM, were very similar to that obtained experimentally at the higher pressure simulations. This proved to be an interesting result given the imperfections of the experiments and the oversimplified hypothetical flow patterns in the SRM. The SRM was not valid for vacuum simulation which implies that there may be a different flow mechanism for this flowrate ratio, such that the tray was operating in the spray regime. This needs to be modelled for comparison with the vacuum simulation temperature profiles.

In this chapter , considerable progress has been made in gaining a deeper insight into the controlling phenomena of two phase flow patterns produced using conditions to simulate distillation at different operating pressures on a single tray. However, this work, aswell as that reported in Chapters 6, and 8, needs to be extended to more than one tray, in order to simulate flow patterns that are likely to occur in industrial trayed columns. This is the subject of the studies pursued in Chapter 10.

CHAPTER 10

EFFECT OF THE GAS FLOW ON THE LIQUID FLOW PATTERN ON TWO TRAYS

10.1 Introduction

Since it has been established that the direction of the gas flow beneath one tray may influence the direction of liquid flow, it was necessary to investigate whether the gas flow emerging from the liquid movement on one tray may influence the direction of liquid flow on a second tray placed directly above. Thus two test trays were incorporated into the test facility at the lowest possible tray spacing of 300 mm (the exception being that in air separation where a typical tray spacing of 150 mm is used). This limited the range of industrial flow rates used in the experiments so as to prevent downcomer flooding.

In the time available, it was decided to use an integral beam tray as the second test tray since they are widely used in practice and the flow patterns produced may be representative of that found on commercial trays of this type. Furthermore, it is quite possible that the integral beams may change the inter-tray gas flow pattern and thus change the liquid flow pattern on the tray deck. Since the second tray was supported on a variable support ring and rod system, it was envisaged that gas-liquid flow patterns can be studied at various tray spacings from 300 mm up to and including 600 mm.

In these experiments, does gas-driven liquid circulation appear on the second tray, or are the two phase flow patterns the same or different to that observed on one tray? If they are different, what are the implications on the theoretical description required for a more scientific approach to tray design? It is essential to address this problem in order to incorporate these effects into a new and more mechanistic theoretical model. If there are no inter-tray gas flow pattern effects on the liquid flow patterns, then there is a need only to model the tray liquid flow pattern.

If this situation arises, then the following question needs to be addressed. That is, does the gas flow inhibit the separation of liquid flow on two trays in the same way as that observed on one tray, or does it produce more circulation? Furthermore, since commercial trays are operated under different pressures, are the flow patterns on two trays, using flow conditions chosen to simulate distillation, the same as that for one tray?

In this chapter, it will be shown that a surprising result emerged in that the inter-tray gas flow pattern had little effect on changing the direction of liquid flow on the upper tray compared with that reported on one tray. However, the effect of the gas flow on inhibiting the separation of liquid flow, was similar to that reported on one tray. Furthermore, results from the simulated pressure experiments on the two trays were similar to that produced on one tray. Despite these similarities, some differences in the flow patterns were noted in that the velocities of forward flow and circulating flow on the two trays were less than that produced on the one tray, for the same flow rates.

Finally, it will be shown that the results provide a promising start in determining the approach required to model flow patterns in trayed columns. Furthermore, the study of gas-liquid interactions on tray liquid flow patterns and their effect on mass transfer, by water cooling, at this and other tray spacings, will be the subject of future work.

10.2 Flow Pattern Studies on Two Trays by Direct Observation

Direct observation of the air-water flow patterns on the top tray of the two tray setup, by gas-liquid contacting, was achieved using the established technique of directional flow pointers and overhead video camera described in Chapter 5. Details of each direct observation experiment are presented below.

10.2.1 Programme of Experiments

The programme of experiments was in three parts:

a) Visual study to determine whether the gas flow emerging from the liquid flow on the lower tray changed the direction of liquid flow on the upper tray, i.e does the liquid flow in the opposite direction to forward flow? In these experiments, liquid flow patterns were monitored using the same flow rates as that detailed in Chapter 6.

b) The monitoring of the separation of flow during the air-water contacting experiments. That is, at several fixed air velocities, the water weir load was increased and the change in the biphase flow pattern from forward flow to reverse flow recorded. In these experiments, the combination of liquid backup in the downcomer and the small tray spacing limited the flow rate range used. That is, the weir load was restricted to 150 $cm^3/cm.s$ while the air velocity did not exceed 2.00 ms^{-1} so as to prevent

downcomer flooding. Nevertheless the flow rates and downcomer settings used are representative of those used in practice.

c) Visual study of air-water flow patterns during the gas-liquid contacting experiments in which distillation was simulated at three different pressures using the same flow rates and downcomer settings as those described in Chapter 9. As with the previous investigation, the flow rate range was limited to prevent downcomer flooding.

Each direct observation investigation is described in more detail below.

10.2.2 Effect of Inter-Tray Gas Flow Patterns on the Top Tray Liquid Flow Pattern

The approach adopted concerning the possible influence of inter-tray gas flow patterns on the upper tray liquid flow pattern, involved the concept of gas resistance to a liquid cross flow during the development of a turbulent single phase flow model, (Yu et al., 1991). In this model, it was assumed that the vertically rising gas enters the froth on a tray, and acquires a horizontal velocity component equal to that of the liquid flow before leaving the froth. The momentum required to accelerate the gas horizontally provides an additional resistance to the liquid flow which is much greater than the frictional drag resistance of the liquid along the tray floor.

When applied to two trays, it is possible that the gas, on leaving the froth on the lower tray, may circulate backwards due to the close tray spacing (see Figure 10.1), and thus produce a significant change on the liquid flow on the top tray.

Figure 10.1 Simplified diagram of the assumption made on the gas flow when forced through the liquid flow (Yu et al., 1991).

In the following investigations, the flow patterns generated will be described in terms of experiments performed at large froth heights and low froth heights.

A summary of the flow rates used in these experiments is presented in Table 10.1.

Experimental Investigation	Air Velocity - ms^{-1}	Weir load - $10^4.m^3/m.s$	Inlet Gap - mm	Outlet Weir - mm
	1.000	18.52		
Direct observation	1.243	27.78	10	10
using directional	1.523	37.04	20	20
flow pointers	1.760	46.30	50	50
	1.969	55.55		

Table 10.1 Summary of flow rates and tray configurations used in the air - water contacting experiments.

Flow Pattern Results

For all flow rates in both the large and small froth height experiments, a surprising result was obtained. That is, forward flow at all points on the tray in the direction from the inlet downcomer towards the outlet weir was produced (see Figure 10.2a). Furthermore, evidence of reverse or circulating flow close to the ends of the outlet weir even at large froth heights was negligible. This was significant since gas flow effects on changing the direction of liquid flow, which led to gas driven liquid circulation, was most severe at large froth heights for the same flow conditions on one tray. It was assumed that since the large inlet gap produced a low liquid velocity across the tray, the slow moving froth would have been more susceptible to changes in flow direction by the rising gas flow. The results for the large froth height experiments show that this was not the case.

At small froth heights, there was a relatively small level of flow separation at the ends of the inlet downcomer which produced a small area of circulating liquid especially at the highest fixed weir load setting of 55.55 $cm^3/cm.s$ (see Figure 10.2b). This may be attributed to the higher liquid velocity entering the tray from the smallest inlet downcomer clearance height of 10 mm. The circulating flow occupied no more than 10% of the total tray area for several flow rates during the low froth height experiments.

On the whole, the diverging/converging alignment of flow pointers on the tray, including those on the tray segments at the sides, revealed the presence of a velocity distribution profile for all flow rates. That is, the liquid forward flow was moving with a much lower velocity compared with the liquid flow along the tray centreline. In some cases,

particularly during the large froth height experiments, the froth appeared non-moving on the tray segments at a distance of approximately 800-1200 mm from the inlet downcomer, (refer to Figure 10.2a). The effect was most significant on increasing the superficial air velocity from a low to a high value.

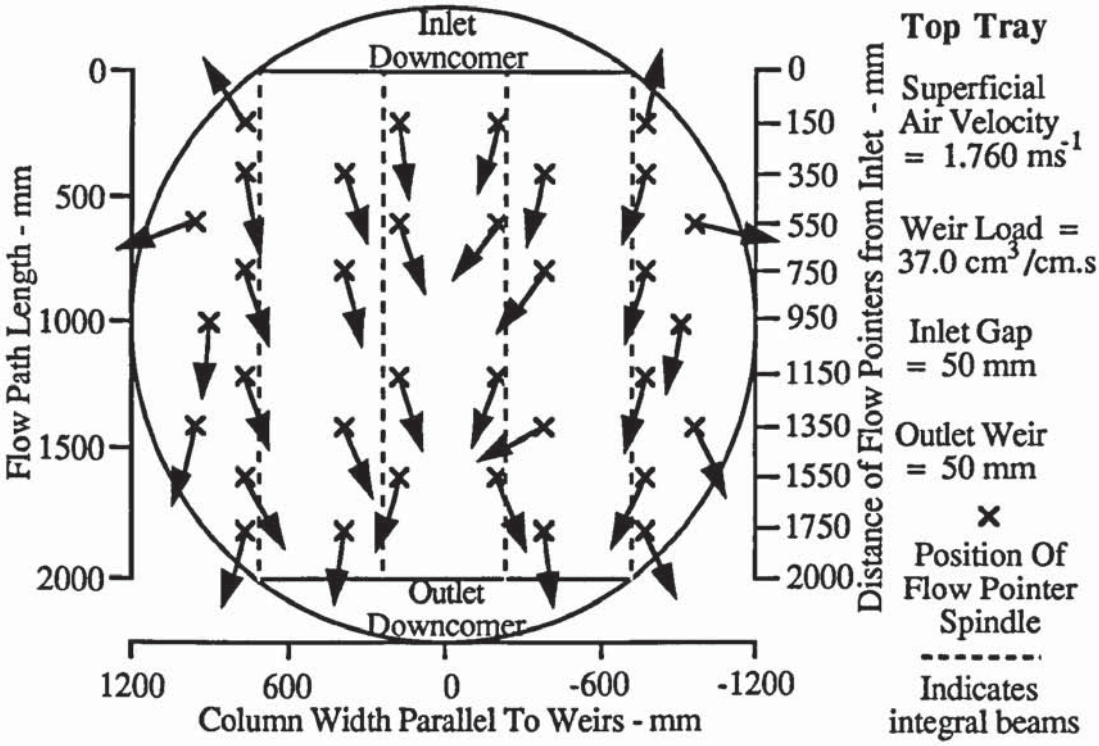

Figure 10.2a Flow pointer arrangement showing forward only flow and no evidence of gas driven liquid circulation.

The slow moving or non-moving liquid was caused by the longer liquid flow path at the sides of the tray compared with that in the middle between the downcomers. However, it is important to stress that the alignment of flow pointers do not give a measure of the liquid velocity profile across the tray.

Although, for most experiments, there was no reverse flow on the tray segments, a number of flow pointers were facing towards the column wall, indicative of sideways flow of froth. This was caused by the support ring effect described in previous chapters, (see Figure 9.2b).

Two important features of the biphase flow on the upper tray were the extent of turbulence and mixing of the liquid by the gas flow and the observation of swirling liquid drops in the vertical plane above the integral beam and joggle regions of the tray.

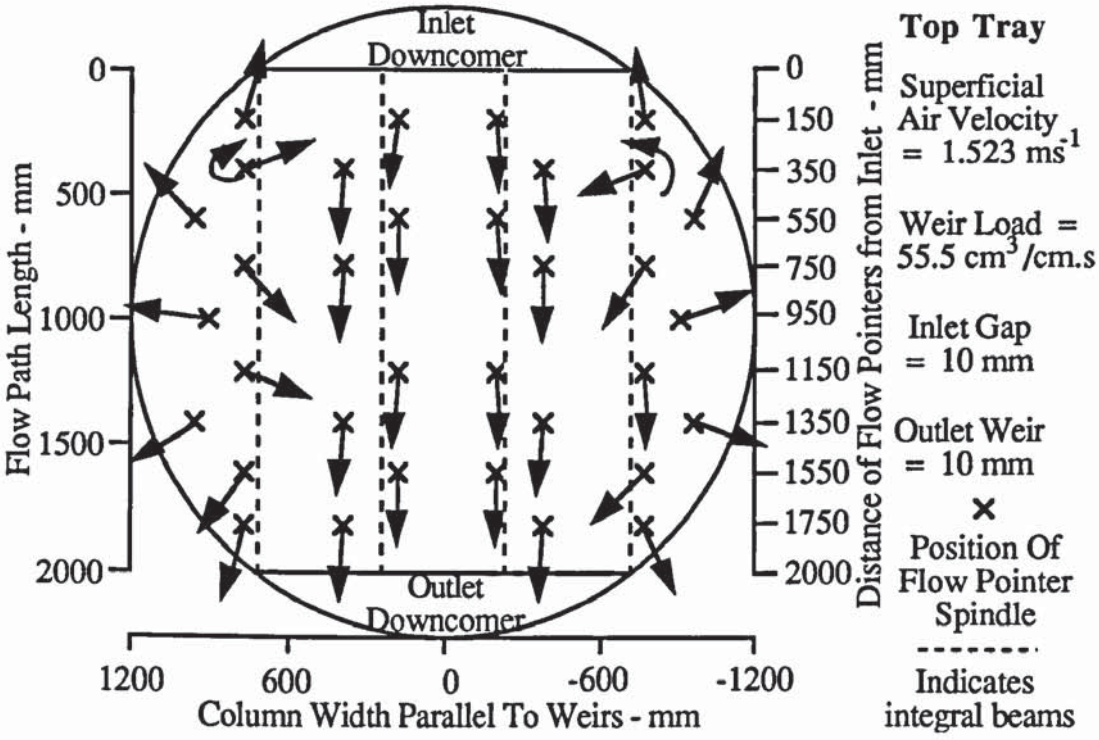

Figure 10.2b Flow pointer arrangement showing forward flow associated with a small inlet circulation and no evidence of gas driven liquid circulation.

The level of gas-liquid turbulence for all experiments increased with increasing superficial air velocity, and was reflected in the randomised alignment of flow pointers across the tray. This can be attributed to the liquid velocity across the tray being lower at large froth heights compared with that at low froth heights.

Swirling liquid droplets in the vertical plane, for most of the experiments, were observed above the non-perforated joggle sections. For the same air-water flow rates, liquid swirling was greatest at low froth heights and least at high froth heights as a result of the greater depth of liquid on the tray. On increasing the air flow rate, liquid swirling became much clearer due to the increased rotational velocity, but did not increase in size.

Vertical swirling above each integral beam and joggle unit was confirmed by the swirling nature of a ribbon flow pointer during air-only flow experiments. Air issuing from the tray perforations closest to the joggle sections may have produced circulating eddies as a result of the non-perforated surface of each joggle (see Figure 10.3).

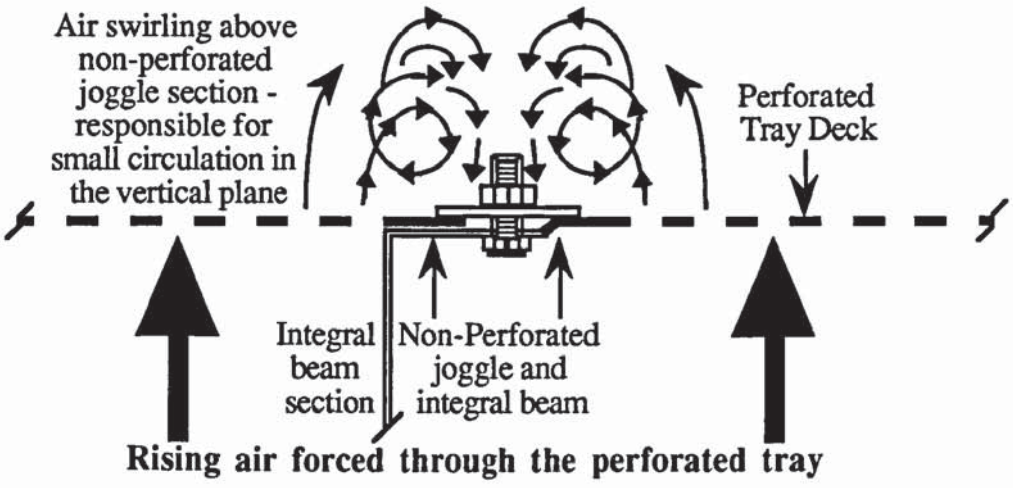

Figure 10.3 Simplified diagram, from an end view of the integral beam tray, of the swirling air flow above the non-perforated joggle section.

Discussion of Results

The results of the gas-liquid contacting experiments show that the inter-tray gas flow pattern emerging from the liquid flow on the one tray has an effect on the liquid flow pattern on a second tray placed 300 mm directly above. However an unexpected result was produced in that the gas flow appeared to have little effect on changing the direction of liquid flow on the upper tray in the same way as that observed on the one tray, for the same flow conditions. (Compare Figure 10.2a with Figure 6.3a of Chapter 6 for the one tray). Instead, forward only flow at all points on the tray associated with a high level of gas-liquid turbulence, particularly at large froth heights, was produced in all of the experiments. In addition circulating flow was found to be negligible at the ends of the inlet and outlet downcomers. A large proportion of the tray area at the sides was occupied by very slow or non-moving froth.

A summary of all the flow pattern results are presented on the modified vapour load factor verses weir load diagram as shown in Figures 10.4, 10.5, and 10.6. The air-water flow rates and flow pattern information are presented in a matrix format.

From the above evidence, it appeared that the inter-tray gas flow pattern had little effect on changing the direction of liquid flow on the top tray and that there was no evidence of gas-driven liquid circulation. This suggests that the flow patterns on two trays are superior to that on the one tray, and that the air-water interactions on the lower tray may have produced a more uniform air flow pattern prior to entering the upper tray.

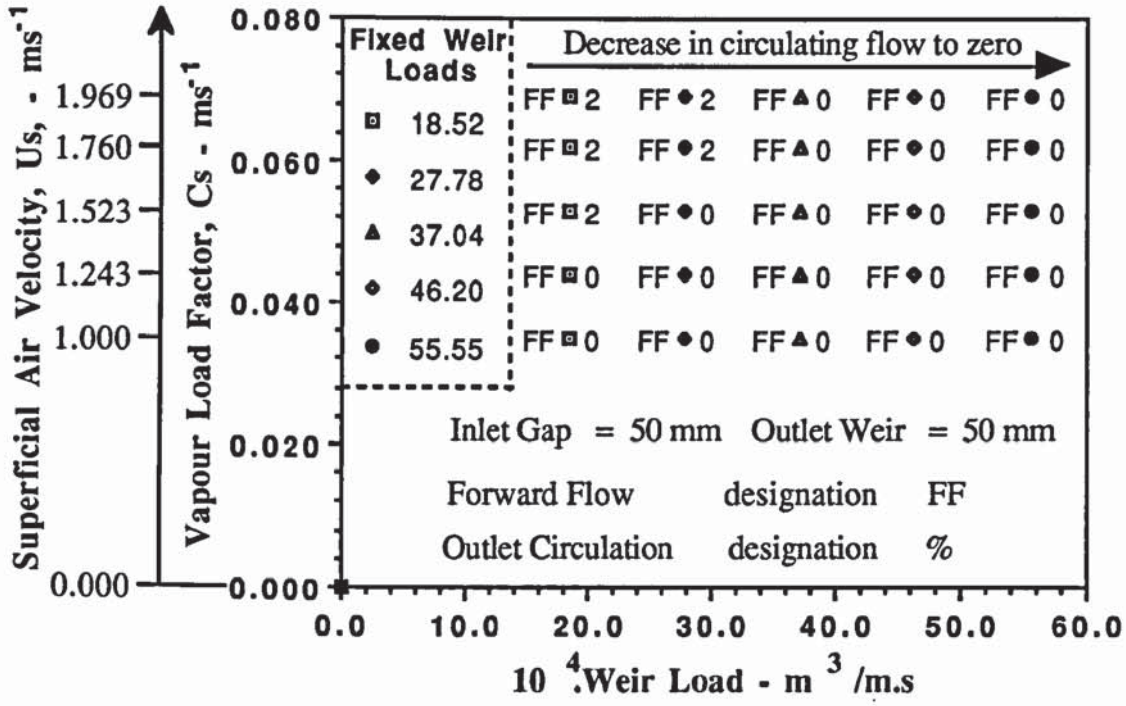

Figure 10.4 Summary of flow patterns for the top tray on a load factor verses weir load diagram.

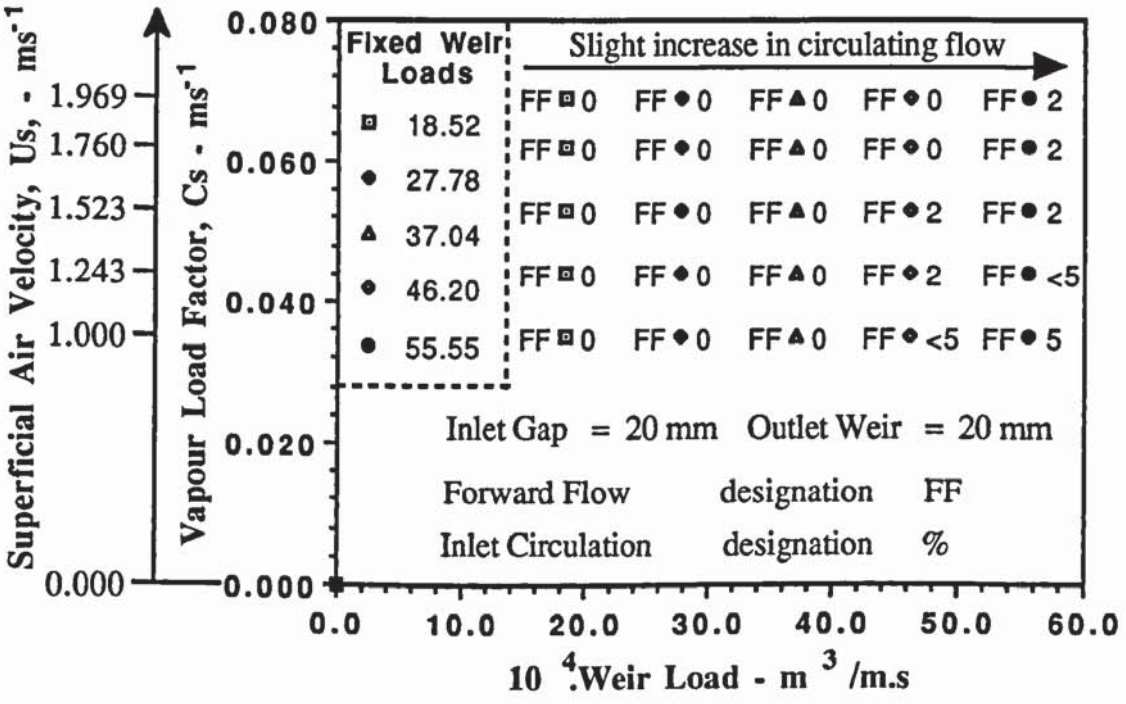

Figure 10.5 Summary of flow patterns for the top tray on a load factor verses weir load diagram.

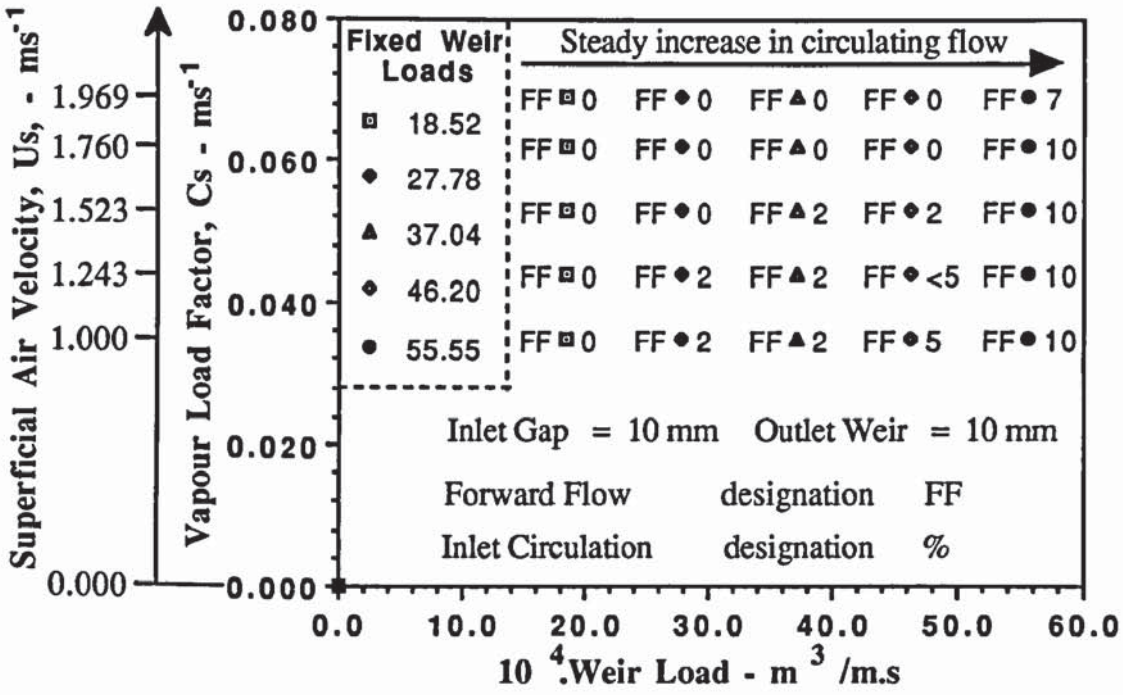

Figure 10.6 Summary of flow patterns for the top tray on a load factor verses weir load diagram.

That is, the air flow on leaving the liquid on the lower tray may have acquired a vertical velocity component which is much greater than that in the horizontal direction. This contradicts the assumption in the single phase turbulence model of Yu et al., (1991).

To test the validity of the assumption made by Yu, an approximate estimation of the liquid cross flow velocity can be made, to determine whether the liquid momentum, on the bottom tray, changes the magnitude and direction of the air rising through it. Using the flow rates from all of the gas-liquid contacting studies, liquid cross flow velocities were calculated from a knowledge of the average clear liquid height for each experiment and by assuming the tray to be a rectangular channel of uniform width. That is,

$$V_{Water} = \frac{\text{Volumetric Liquid Flow Rate}}{\text{Average HCL} \times \text{Average Width of Channel}} = \frac{Q_L}{h_{cl} \times W'} \qquad (10.1)$$

where $W' = (W + D)/2$.

The range of liquid cross flow velocities varied between 0.051- 0.157 ms^{-1} at large froth heights and 0.129 - 0.243 ms^{-1} at the lowest froth heights. Thus if the assumption of Yu is accepted as correct, then for this set of experiments, the low liquid cross flow velocity may have imparted insufficient momentum to distort the gas flow in the horizontal direction on passing through the liquid on the bottom tray. Although the gas flow will

have acquired a horizontal velocity component when accelerated by the liquid flow, the magnitude and direction of the gas was not sufficient to change the direction of liquid flow on the second tray.

Another possible reason for the absence of gas-driven liquid circulation on the top tray, is that the integral beams may have affected the inter-tray gas flow pattern. That is, they may have prevented the possible formation of circulating air eddies throughout the inter-tray space. In addition, the direction of gas flow, emerging from the liquid flow on the bottom tray, may have entered the top tray at an angle such that it opposes the forward flow of liquid. Hence, it appears that the gas resistance may have been responsible for the observation of very slow moving or stationary froth across the tray, especially on the longer liquid flow path at the sides. This is similar to the liquid forward flow with stagnant regions hypothetical flow pattern predicted by Porter et al., (1972).

Conclusion

The air-water flow patterns generated in all of the experiments showed that the liquid was in forward flow at all points on the upper tray of the two tray setup, and that there was no evidence of gas-influenced liquid flow patterns. This is in direct contrast to the gas-influenced liquid flow patterns produced for the same experimental conditions on the single tray, and suggests that the flow patterns on two trays are superior to that on one tray. Thus from these experimental results, the effect of the gas flow on changing the direction of liquid flow may only occur on the first tray above the vapour feed inlet in a commercial scale column.

10.2.3 Effect of the Gas Flow on the Separation of Liquid Flow on the Top Tray

From the above experiments it was noted that the weir loadings were varied over a narrow range. This may have affected the magnitude of the horizontal velocity component of the gas when leaving the froth in relation to that in the vertical direction according to the assumptions made by Yu. Thus by varying the weir load over a wide range for a fixed air velocity, it is possible that the inter-tray gas flow, on leaving the liquid flow on the lower tray, may be forced to circulate backwards. This means that Yu's assumption, (see Section 10.2.2), may apply for this set of flow conditions.

Alternatively, the effect of the gas flow on the tray liquid flow pattern may only prevent the onset of flow separation compared with water-only flow, and produce results similar to that reported on the one tray. Either flow phenomenon will have a significant effect on

the approach required for modelling flow patterns on trays.

A summary of the flow rates used in these experiments, are presented in Table 10.2.

Experimental Investigation	Air Velocity - ms^{-1}	Weir load - $10^4.m^3/m.s$	Inlet Gap - mm	Outlet Weir - mm
	1.00	25.0		
Direct observation	1.25	50.0	10	10
using directional	1.50	100.0	20	20
flow pointers	2.00	150.0	50	50

Table 10.2 Summary of flow rates and downcomer settings used in the air - water contacting experiments.

Flow Pattern Results

For all flow rates both at the large and small froth heights, the liquid flow on the tray outlet was not distorted by the inter-tray gas flow. To justify this, liquid cross flow velocities for the higher weir loadings were calculated, to determine whether the liquid momentum, on the bottom tray, changes the magnitude and direction of the air rising through it. The range of liquid cross flow velocities varied between 0.136- 0.816 ms^{-1} at the lowest froth heights and 0.119 - 0.266 ms^{-1} at large froth heights. Although the results were higher than in the previous studies, they were less than the air velocity passing through the liquid on the bottom tray. This means that from Yu's assumption, the magnitude and direction of the gas flow was still not sufficient to change the direction of liquid flow on the top tray and the above arguements concerning the resistance of the gas flow to the liquid flow still apply.

Instead the flow patterns generated were similar to that observed on the one tray. At both the large and small froth heights, the air-water flow pattern was in forward flow at all points on the tray for weir loads upto and including 50.0 $cm^3/cm.s$. The randomised appearance of flow pointers across the tray showed that the velocity of the liquid around the longer liquid flow paths at the sides of the tray was slower than that on the shorter flow path in the middle of the tray. In many of the experiments, the froth appeared non-moving on the tray segments at a distance of between 900-1300 mm from the inlet downcomer. These observations were similar to that produced on one tray.

However, gas-liquid turbulence appeared to be greater on two trays compared with that on the one tray. For the same flow rates the level of gas-liquid turbulence was greatest at

large froth heights (lowest liquid cross flow velocity) and least at small froth heights (highest liquid cross flow velocity). The reasons for this are the same as that described in Section 10.2.2.

As with the one tray experiments, the effect of the gas flow on the tray liquid flow pattern at low weir loadings inhibited the onset of flow separation. On increasing the weir load upto and including 150 $cm^3/cm.s$, flow separation occurred such that forward flow associated with circulation emanating from the ends of the inlet downcomer was produced. The extent of circulating flow along the tray segments, however, was strongly dependant on the inlet liquid velocity entering the tray from beneath the inlet downcomer. Thus, when the tray was configured with an inlet gap and outlet weir height of 10 mm, the size of circulating flow at the sides grew steadily until a maximum of 30% liquid circulation was produced (see Figure 10.7a).

However, unlike the one tray experiments, the inter-tray gas flow pattern reduced the velocity of forward and circulating flow, especially on the tray outlet. The resistance of the rising gas to the liquid flow increased with increasing superficial air velocity such that the maximum circulation was not achieved at the superfical air velocity of 2.00 ms^{-1}.

Similar observations were made at the inlet gap and outlet weir height of 20 mm, except that the lower liquid cross flow velocity combined with the gas flow resistance on the tray outlet decreased the size of circulating flow. The maximum circulation size at the highest weir load of 150 $cm^3/cm.s$ and the lowest fixed air velocity setting, was 22% as shown in Figure 10.7b.

At the larger froth heights, the lower liquid cross flow velocities combined with the gas resistance had a significant effect on the circulating flow. That is, liquid circulation was reduced to 12% of the total tray area at the highest weir loading and lowest superficial air velocity (see Figure 10.7c). Although this observation was similar to that observed on the one tray, the gas resistance had a greater effect on the slow moving, large depth of liquid on two trays compared with that on one tray. That is, a significant level of gas-liquid turbulence was observed, in which liquid mixing and splashing over most of the tray area was produced. This steadily increased at the higher superficial air velocities such that a given area of circulation on two trays was less than that produced on the one tray.

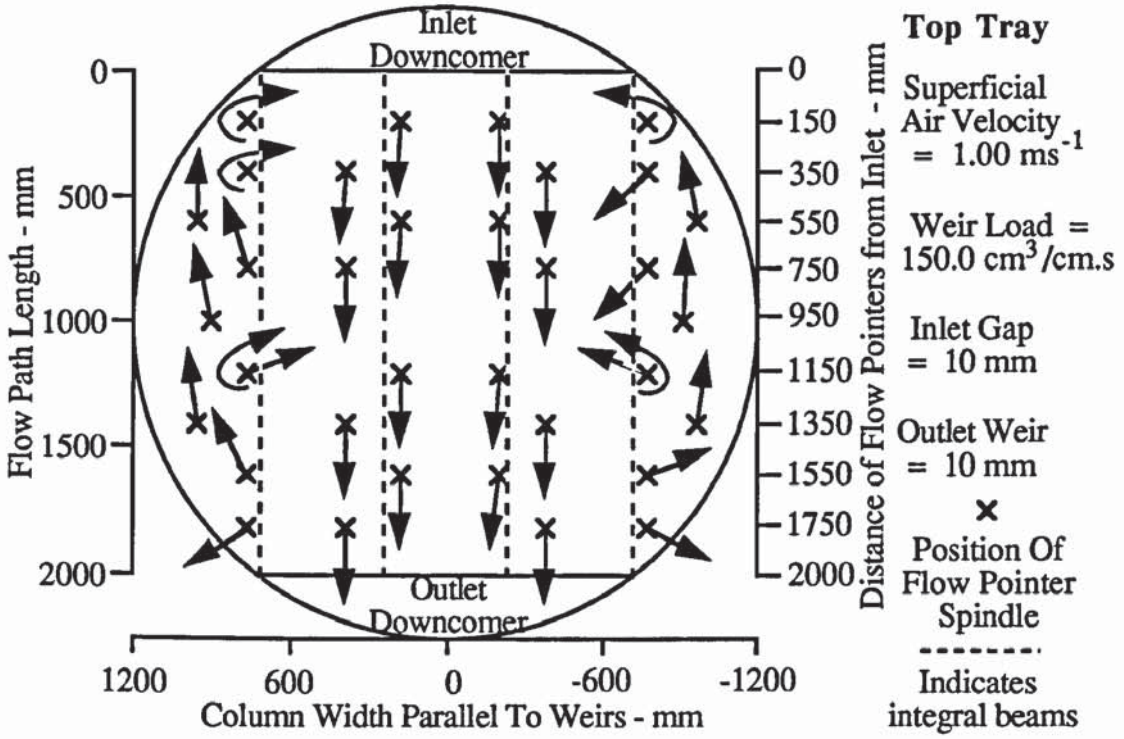

Figure 10.7a Flow pointer arrangement showing forward associated with a maximum of 30 % liquid circulation.

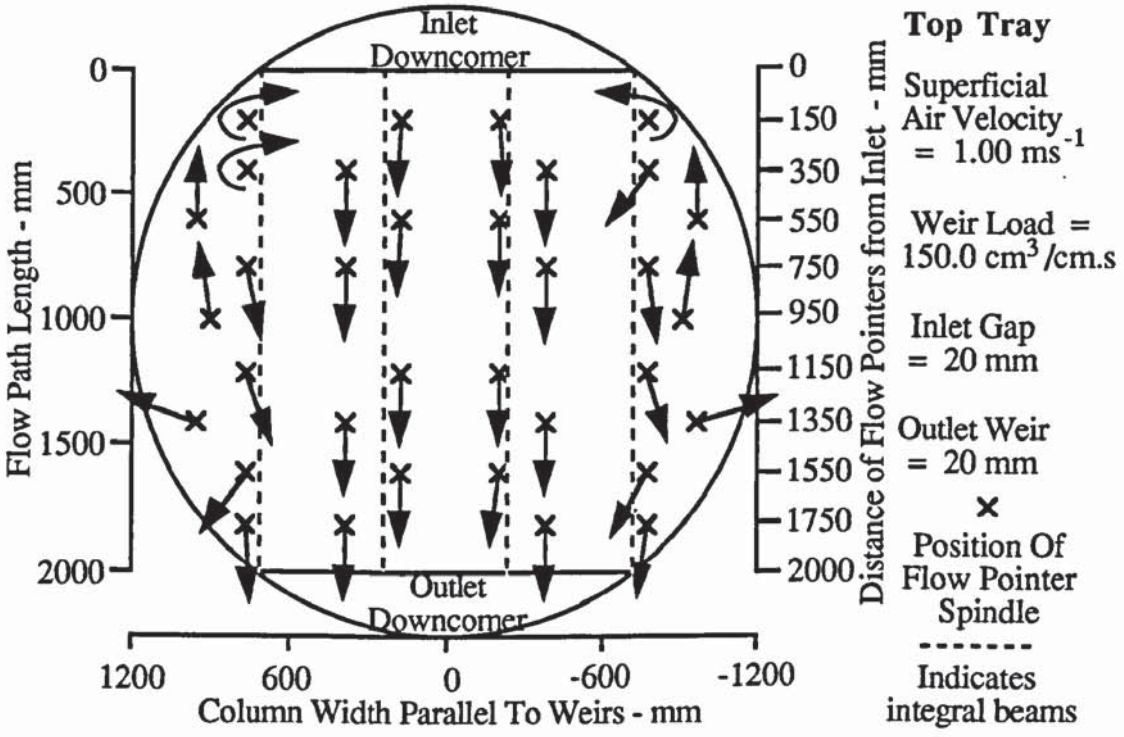

Figure 10.7b Flow pointer arrangement showing forward flow associated with 22 % liquid circulation.

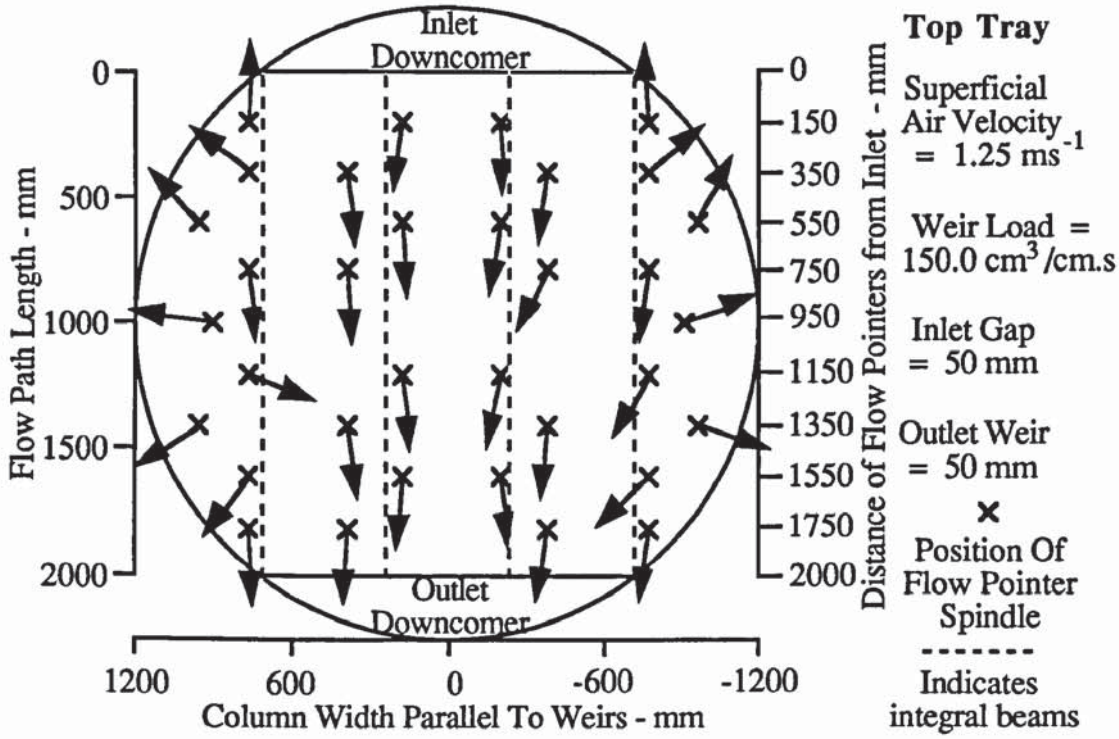

Figure 10.7c Flow pointer arrangement showing forward flow associated with 12 % liquid circulation.

Summaries of all the flow patterns generated are presented on a modified vapour load factor verses weir load diagram as shown in Figures 10.8, 10.9 and 10.10.

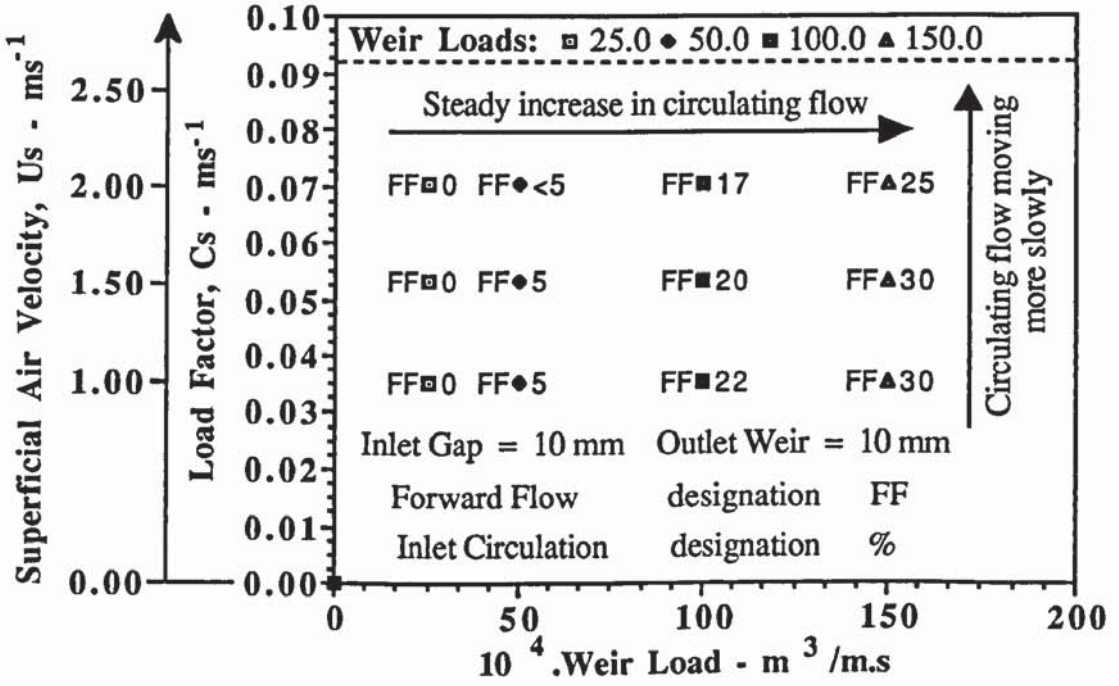

Figure 10.8 Summary of flow patterns for the top tray on a load factor verses weir load diagram.

In these diagrams are shown the percentage of tray area occupied by circulating liquid for each air-water flowrate combination.

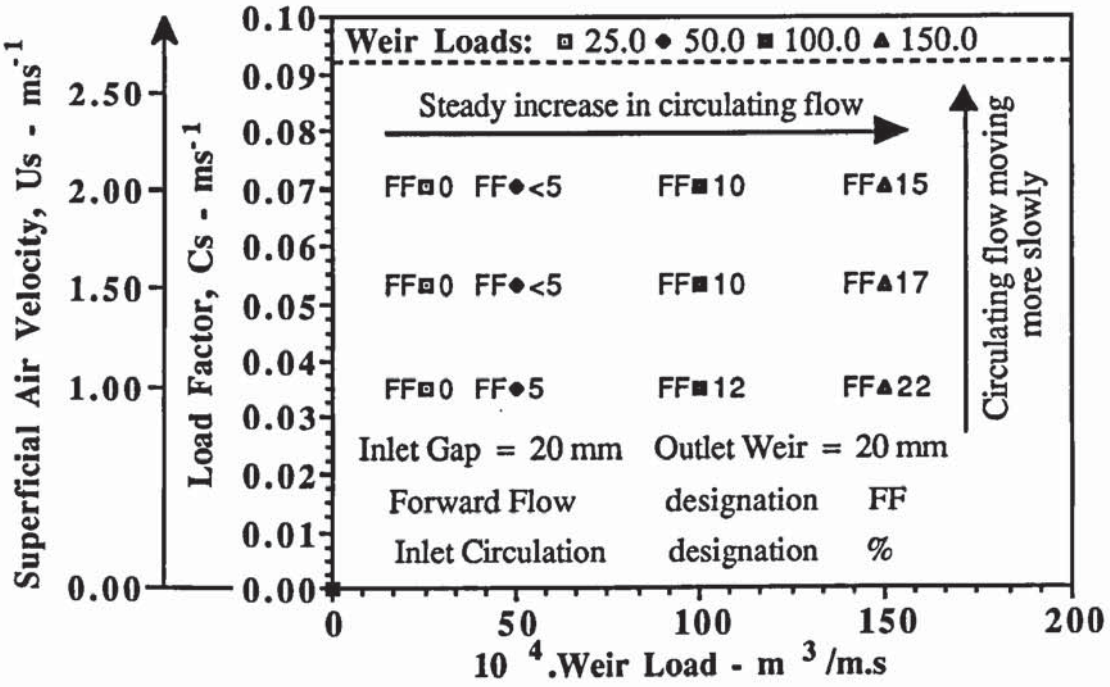

Figure 10.9 Summary of flow patterns for the top tray on a load factor verses weir load diagram.

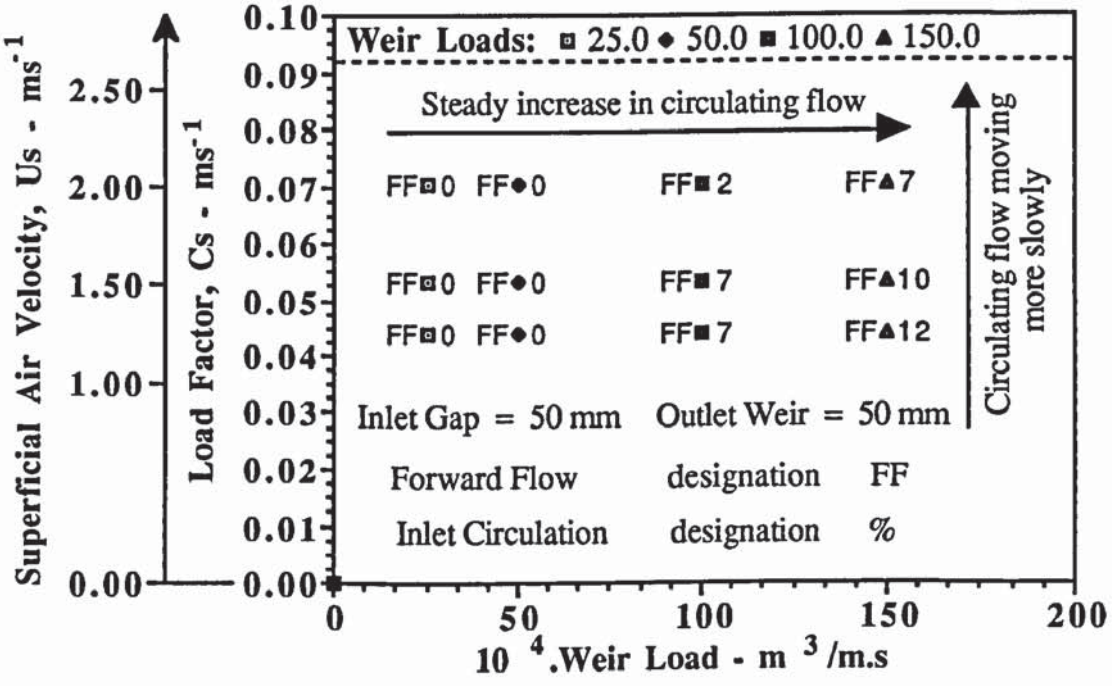

Figure 10.10 Summary of flow patterns for the top tray on a load factor verses weir load diagram.

Discussion of Results

The results presented in this gas-liquid contacting study showed that the inter-tray gas flow pattern had little effect on changing the direction of liquid flow on the upper tray even for the highest weir loadings. Although the liquid cross flow velocities were, in some cases, higher than in the previous study, they were less than the air velocity passing through the liquid on the bottom tray. This implies, from Yu's assumption, that the liquid may have imparted insufficient momentum to distort the gas flow in the horizontal direction. Hence the magnitude and direction of the gas flow may not have been sufficient to change the direction of liquid flow on the second tray.

Instead the flow pattern results were similar to those produced on the one tray experiments. That is, the effect of forcing the gas through the liquid delayed the onset of flow separation, which only occurred at high liquid inlet velocities produced from small clearance heights beneath the inlet downcomer. The rate of increase of circulating flow associated with increasing weir load, was less than that for water-only flow and was strongly dependant on the inlet downcomer gap through which the liquid entered the tray. Hence the larger the inlet gap, the smaller the velocity of liquid entering the tray, and the larger the weir load required to produce a given area of circulating flow.

However, some differences in the flow patterns were noted in that the velocity of forward only flow at all points on the upper tray of the two tray setup was less than that on the one tray during non-separated flow. In addition, the velocity of forward and circulating flow on the two trays during the separation of flow was less than that produced on the one tray, for the same flow rates. This suggests that the gas resistance to forward flow and the growth of circulating regions at the sides had a significant effect on the two trays.

Conclusion

From this study, it has been shown that there was no evidence of gas-influenced liquid flow on the upper tray. Instead the gas had a significant effect on the separation of liquid flow such that the results were similar to those obtained on the single tray. The effect of forcing the gas through the liquid on the tray prevented flow separation, which only occurred at high liquid inlet velocities produced from small gaps beneath the inlet downcomer compared with the separated water-only flow patterns. However it appeared that the resistance to liquid flow by the rising gas was greater for the two tray experiments compared to that on the one tray for the same operating conditions. From the above evidence it appears that the flow patterns on two trays are superior to those generated on

the one tray, particularly at the higher weir loadings.

10.2.4 Flow Pattern Results at Different Simulated Pressures on the Top Tray

Since commercial tray columns are operated under different pressures, the gas-liquid contacting studies were extended to two trays to study flow patterns generated using flow conditions chosen to simulate distillation at different pressures. In these experiments, flow rates were varied at a fixed ratio of liquid flow to air velocity, such that three flow rate ratios represented distillation under vacuum, at atmospheric pressure, and at a moderate pressure. The flow rate and the downcomer settings are presented in Table 10.3.

Simulated Pressure					
Vacuum		Atmospheric Pressure		Moderate Pressure	
Inlet Gap = 10 mm Outlet Weir = 10 mm		Inlet Gap = 20 mm Outlet Weir = 20 mm		Inlet Gap = 50 mm Outlet Weir = 50 mm	
Air Velocity - ms^{-1}	Weir load - 10^4 $m^3/m.s$	Air Velocity - ms^{-1}	Weir load - 10^4 $m^3/m.s$	Air Velocity - ms^{-1}	Weir load - 10^4 $m^3/m.s$
1.00	12.5	1.00	60.0	1.25	100.0
1.50	18.5	1.50	90.0	1.50	150.0
2.00	25.0	1.75	102.0	1.75	175.0
2.50	31.0	2.00	120.0	-	-

Table 10.3 Summary of flow rates chosen for the simulation of distillation experiments at three different pressures.

Flow Pattern Results

For all flow rates during the simulation of vacuum distillation, forward only flow was produced at most points on the tray including the segmental regions at the sides (see Figure 10.11a). This was reflected by most of the flow pointers facing towards the outlet weir despite their random appearance, especially on the tray inlet and at the sides.

At the higher pressure simulations, the flow pointers showed forward flow between the downcomers, associated with a mixture of slow forward flow, stationary liquid and circulating flow on the tray segments as shown in Figures 10.11b and 10.11c. However, unlike the one tray experiments, a mixture of slow forward flow in the regions close to the ends of the outlet weir, and two large areas of stationary froth were observed at the sides of the tray. In addition, a relatively small liquid circulation emanating from the ends of the inlet downcomer was produced, which for most experiments occupied no more than 12% of the total tray area.

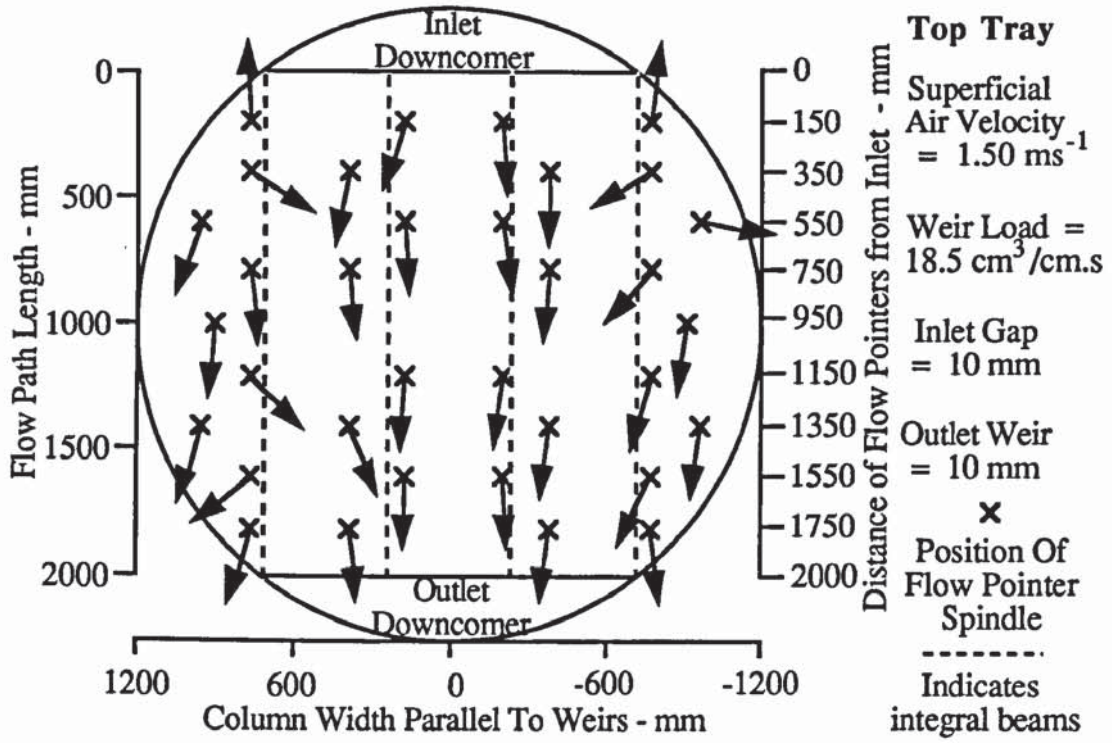

Figure 10.11a Flow pointer arrangement showing forward only flow during the simulation of vacuum distillation.

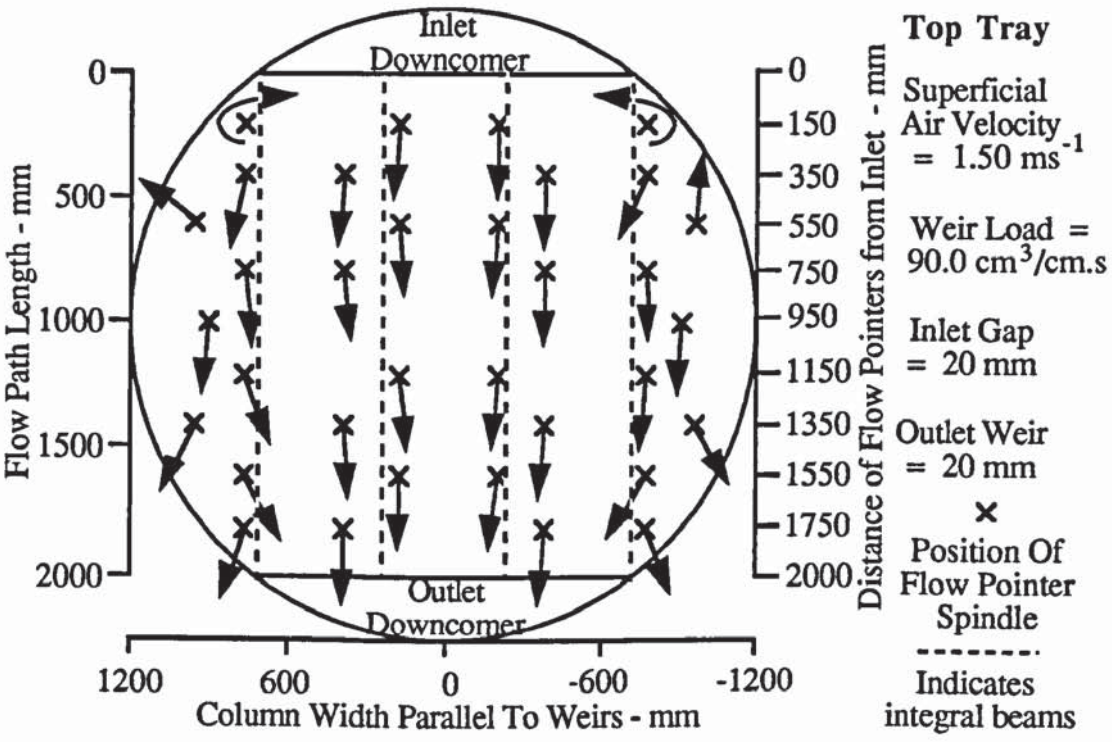

Figure 10.11b Flow pointer arrangement showing forward flow associated with 10 % circulation during the simulation of atmospheric pressure distillation.

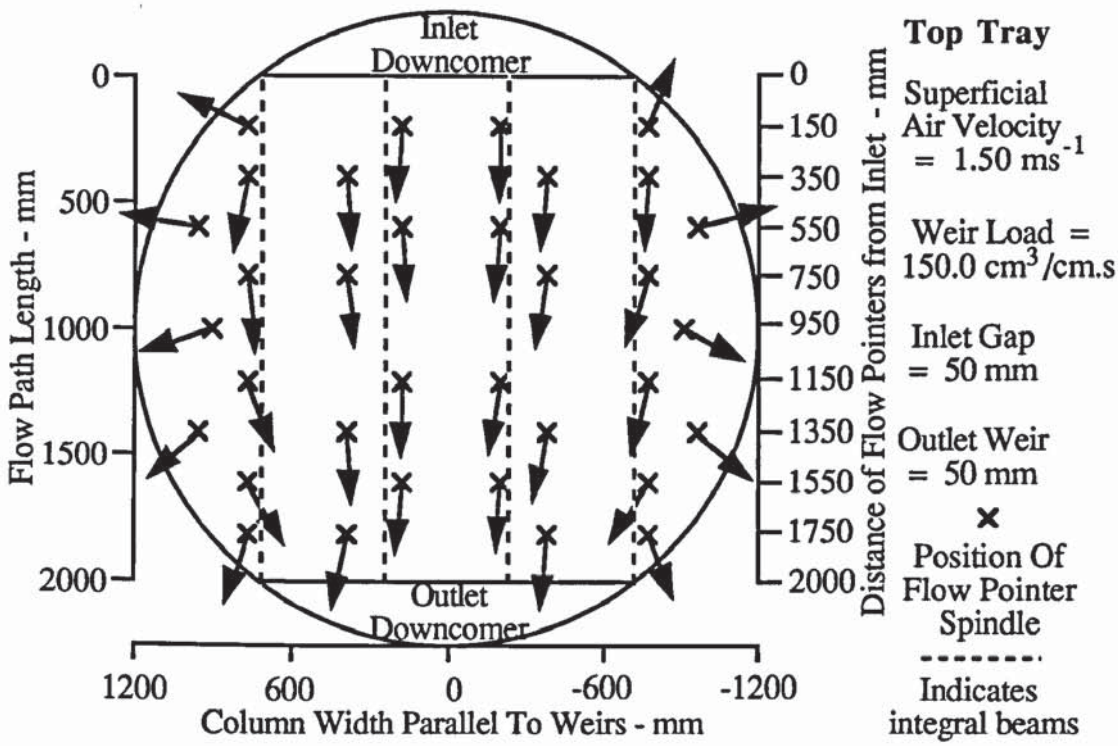

Figure 10.11c Flow pointer arrangement showing forward flow associated with 12 % circulation during the simulation of moderate pressure distillation.

Discussion of Results

Flow patterns have been summarised in a similar manner to that used in the one tray experiments and is presented in Figure 10.12. (Note that the flow regime transition lines for the 12.5 mm hole tray have been included on the load factor verses weir load diagram, the reasons for which are explained in Chapter 9). The percentages of tray area occupied by circulating liquid are shown on the three sloped lines representing each simulated pressure. Figure 10.12 shows that in the simulation of vacuum distillation, forward only flow was produced at all points on the tray. For the simulation of atmospheric and moderate pressure distillation, circulating flow in many cases did not exceed 12%.

Although precise comparisons of flow patterns cannot be made for the same flow conditions used in both the one and two tray experiments, the direct observation experiments showed an increased level of gas-liquid turbulence particularly at the higher pressure simulations. In addition, the velocity of forward and circulating flow on the two trays was less than that produced on the one tray. This suggests that the resistance of the gas flow to liquid forward flow and the growth of circulating regions had a significant effect on the two trays, especially on the longer liquid flow path at the sides.

From the above evidence it appears that the flow patterns on two trays are superior to

those generated on the one tray, particularly at the higher pressure simulations in that the velocity and size of the circulating flow was less than that on the one tray.

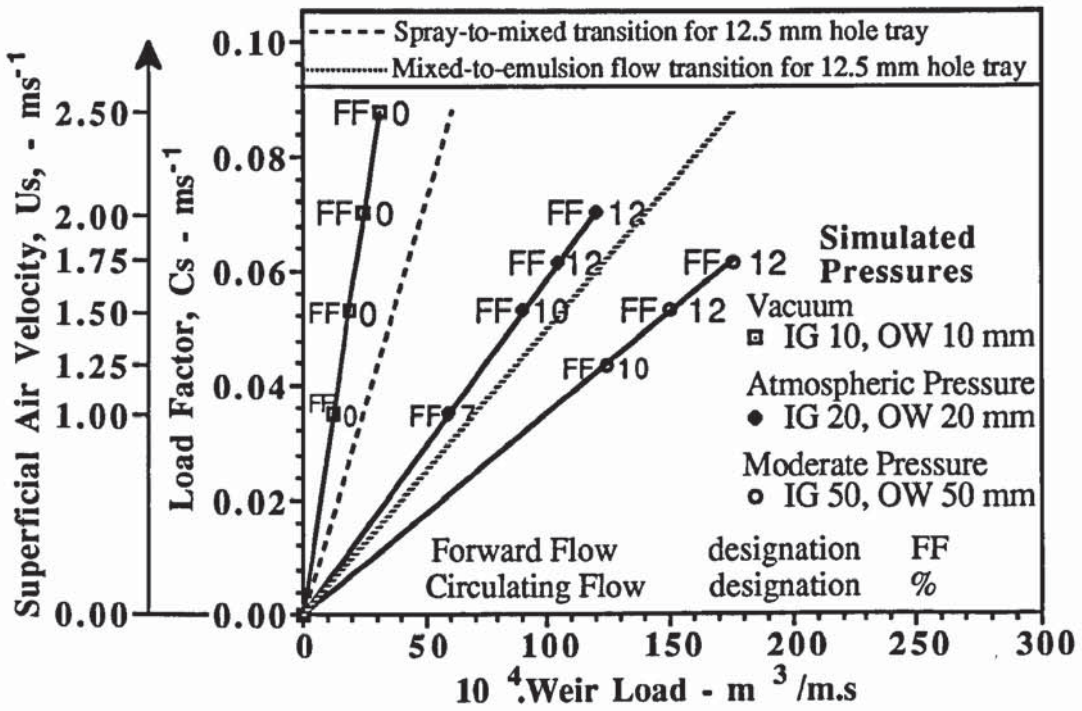

Figure 10.12 Summary of biphase flow patterns obtained in the simulation of distillation experiments at three different presssures.

Conclusion

The air-water flow patterns generated during the simulation of distillation on two trays were on the whole similar to those obtained on the one tray. That is, most of the tray area was occupied by forward flow towards the outlet weir. In addition the velocity of liquid flow near the column wall was less than that in the middle of the tray between the downcomers. However, the level of gas-liquid turbulence on two trays was greater than that observed on the one tray.

Summary of Results from the Direct Observation Experiments

At this point, the direct observation experiments have shown that the inter-tray gas flow pattern emerging from the liquid flow on the one tray produced an unexpected result on a second tray placed 300 mm directly above. That is the gas flow appeared to have little effect on changing the direction of liquid flow on the two trays in the same way as that observed on the one tray in Chapter 6 for the same flow conditions. Instead, forward only flow at all points on the tray associated with a considerable level of gas-liquid turbulence, particularly at large froth heights, was produced in all of the experiments.

Investigations into gas flow effects on the separation of liquid flow and the simulation of distillation at different pressures, showed that the flow pattern results were, on the whole, similar to those produced on the one tray. That is, the effect of the air flow delayed the onset of flow separation which only occurred at much higher water flow rates and small inlet gap heights. In addition, liquid was in forward flow over most of the tray during the pressure simulation experiments. However, for all of the experiments, the velocity of forward and circulating flow was less than that on the one tray, and may have been caused by a higher level of gas-liquid turbulence on the two trays.

On the whole, the flow patterns generated on two trays during each of the three experimental investigations described above, are superior to that produced on the one tray. That is, the size and velocity of reverse or circulating flow was less than that observed on the one tray. In several experiments, the observation of forward flow associated with non-moving liquid at the sides of the tray is similar to the stagnant regions hypothetical flow pattern predicted by Porter et al., (1972). It is possible that the integral beams of the second tray might have produced a uniform inter-tray gas flow pattern by reducing any circulation tendancy between the two trays.

Evidence to support this was the estimation of liquid cross flow velocities on the bottom tray all of which were lower than the superficial velocity of the air passing through the liquid even for the highest weir loadings. This suggests that from the assumption of Yu, the momentum exchange from the liquid to the gas was insufficient to accelerate the gas such that it escaped from the liquid surface with a horizontal velocity component equal to that of the liquid. Thus, the vertical air velocity component appears to be greater than the horizontal air velocity component, and may be responsible for the high level of gas-liquid turbulence. This, in turn, may have caused the liquid to flow with a lower velocity on the two trays compared with that on the one tray.

Alternatively, it is possible the integral beams may have split any circulating air flow into smaller circulating eddies. This may have caused a significant amount of liquid mixing in all directions over many points across the tray. If this was the case, the gas-liquid mixing behaviour appears to contradict the assumption of Lockett et al., (1975) in that the gas flow may be considered unmixed between large diameter single pass trays. Lockett reported that vapour mixing was ineffective in reducing vapour bypassing through stagnant zones on large diameter trays, which, in turn, has an adverse effect on tray efficiency.

Overall, it is clear that the inter-tray gas flow pattern and its effect on liquid flow patterns

is not yet understood. Thus, the gas flow pattern at this and other tray spacings needs to be determined since this will influence the way in which theoretical models are developed in order to explain the flow patterns that are produced in industrial scale practical distillation. One method would be to study the effects of the gas-liquid interactions on mass transfer for the two trays using the water cooling technique.

10.3 Flow Pattern Studies on Two Trays by Height of Clear Liquid Measurements

The direct observation experiments provided very little information about the effect of the gas-liquid interactions on two trays in terms of the variation in liquid head profiles. Liquid head profiles were determined by measurement of the clear liquid height across the tray, for the different flow patterns generated. A complete description of the height of clear liquid experiment is presented in Chapter 5.

10.3.1 Height of Clear Liquid Results

As with the one tray experiments, the liquid head profiles were identified using the same designations, described in Chapter 5. A complete set of height of clear liquid data for each experimental investigation is presented in Appendix 12.0.

10.3.2 Effect of the Inter-Tray Gas Flow Pattern on the Liquid Head Profile on the Two Trays

The height of clear liquid results show that at low air-water flow rates, relatively flat liquid head profiles were produced, indicative of forward only flow at all points on the tray, as shown in Figure 10.13. On increasing the superficial air velocity for a fixed weir loading, the height of clear liquid profiles were transformed from a horizontal to an uneven liquid head surface which occupied part or all of the tray bubbling area (see Figure 10.14). In these experiments, the uneven liquid head surface across the two trays consisted of a number of peaks and troughs over the active bubbling area, which can be attributed to the increased level of gas-liquid turbulence especially at larger froth heights. However, it is possible that the uneven liquid head surface may have been affected by the non-perforated joggle regions directly above the integral beam units on the tray.

A summary of all the height of clear liquid profiles are summarised on the modified load factor verses weir load diagram as shown in Figures 10.15a, 10.15b and 10.15c.

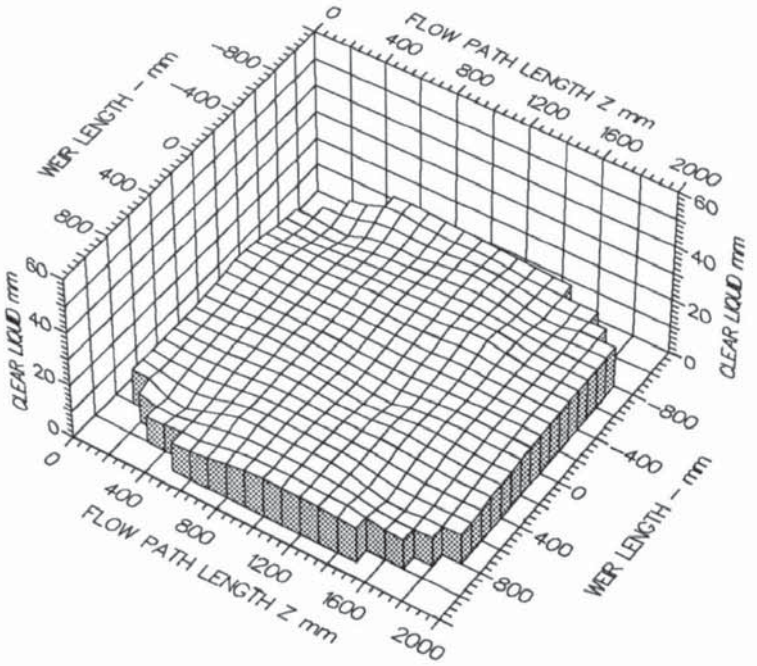

TOP TRAY 1

Air Velocity
1.000 m/s

Weir Load
27.8 cm3/cm.s

Inlet Gap
0.010 m

Outlet Weir
0.010 m

Hole Diameter
0.006 m

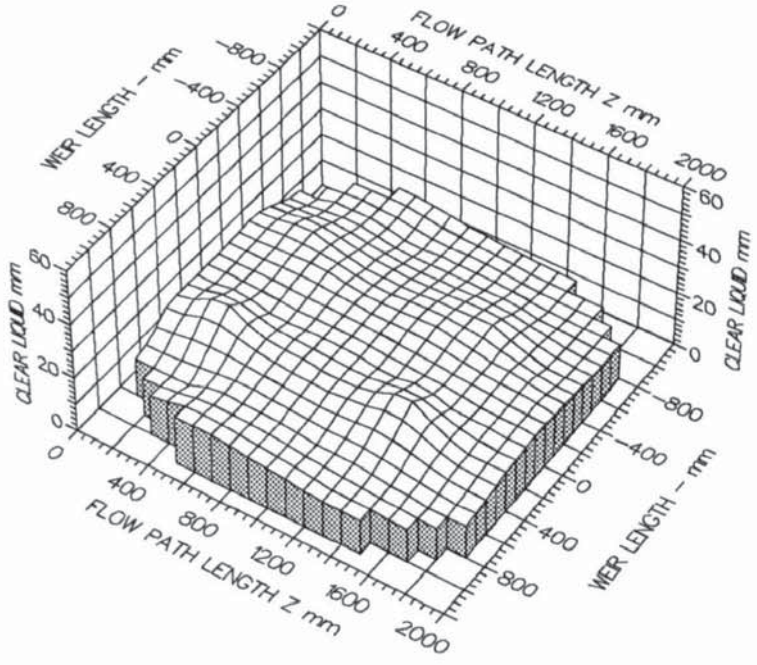

BOTTOM TRAY 2

Air Velocity
1.000 m/s

Weir Load
27.8 cm3/cm.s

Inlet Gap
0.010 m

Outlet Weir
0.010 m

Hole Diameter
0.006 m

Figure 10.13 Examples of comparatively flat height of clear liquid profiles, at low froth heights on the upper tray (designation H) and lower tray (designation H/N).

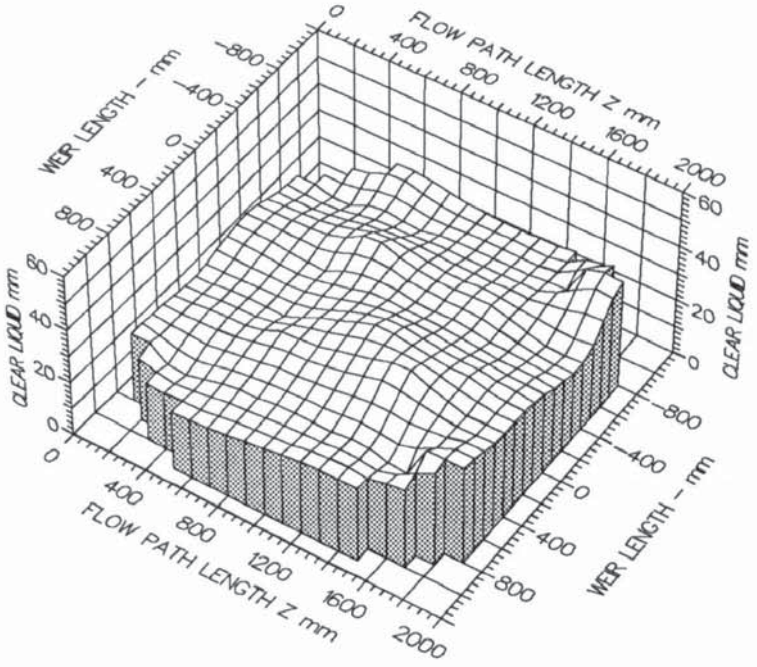

TOP TRAY 1

Air Velocity
1.520 m/s

Weir Load
37.0 cm3/cm.s

Inlet Gap
0.050 m

Outlet Weir
0.050 m

Hole Diameter
0.006 m

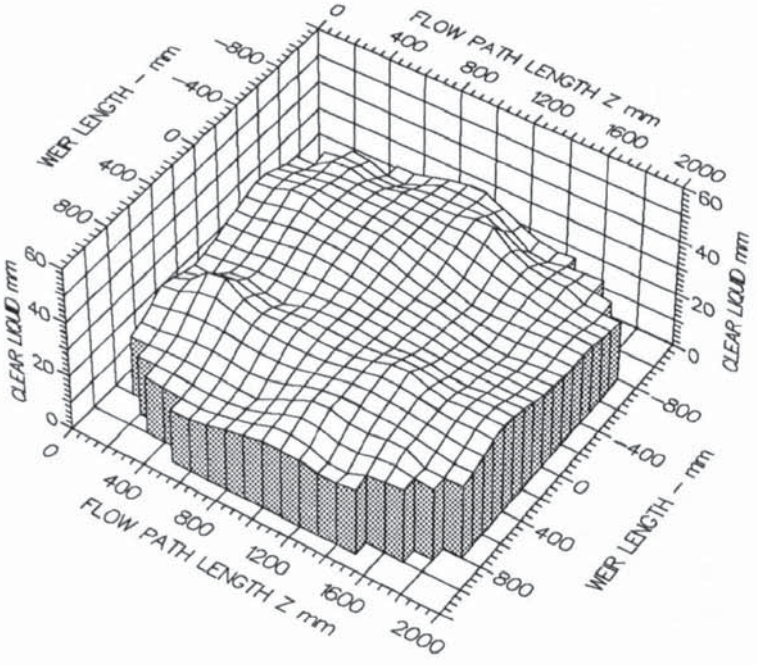

BOTTOM TRAY 2

Air Velocity
1.520 m/s

Weir Load
37.0 cm3/cm.s

Inlet Gap
0.050 m

Outlet Weir
0.050 m

Hole Diameter
0.006 m

Figure 10.14 Examples of height of clear liquid profiles with an uneven surface at medium froth heights on the upper tray (designation NO) and lower tray (designation N).

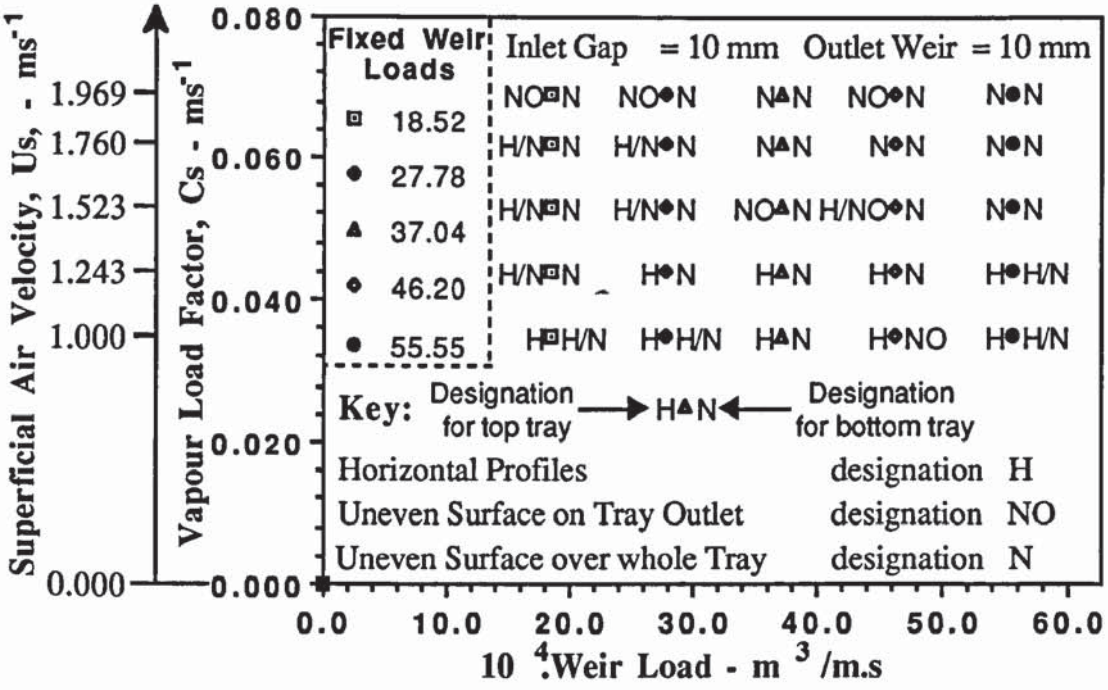

Figure 10.15a Summary of liquid head profiles on a load factor verses weir load diagram.

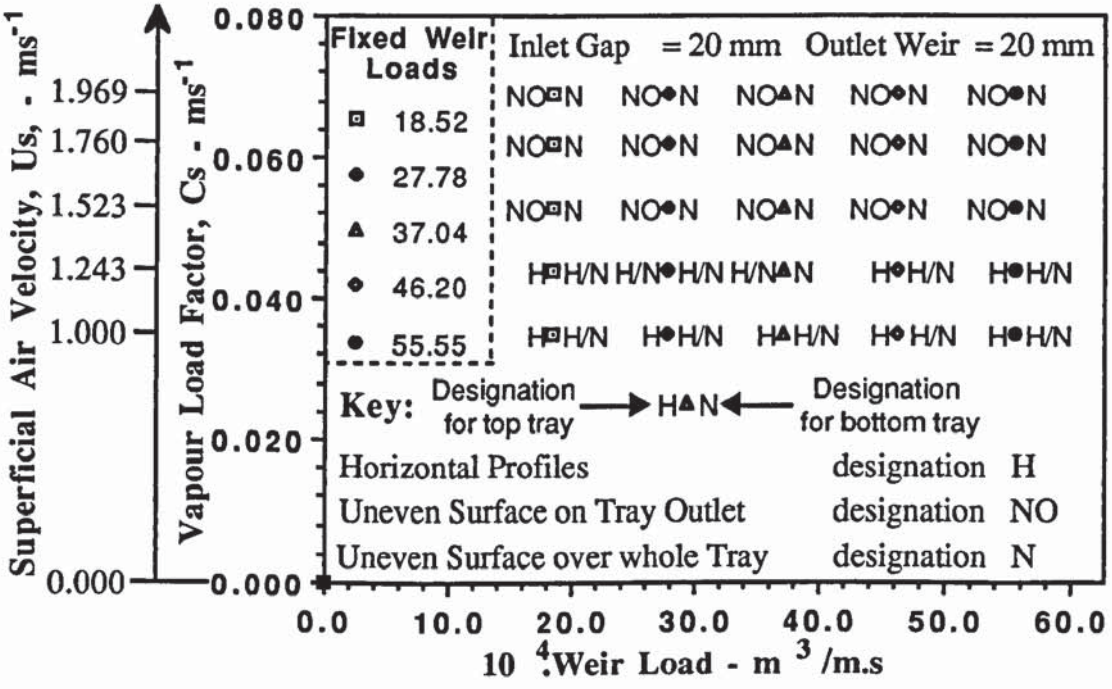

Figure 10.15b Summary of liquid head profiles on a load factor verses weir load diagram.

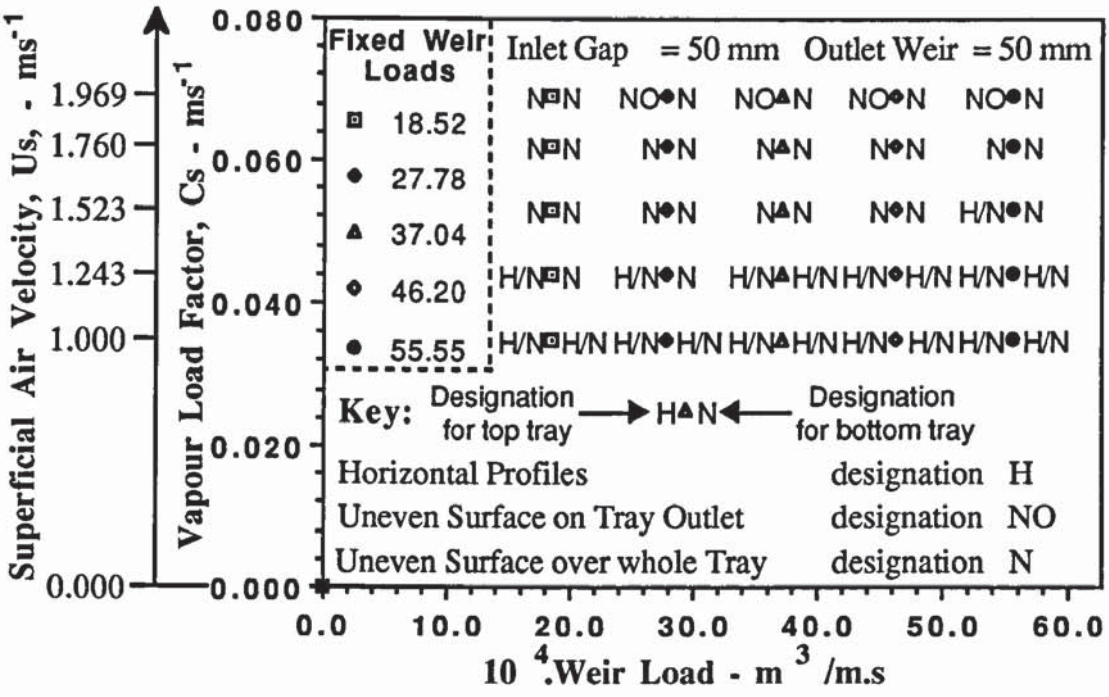

Figure 10.15c Summary of liquid head profiles on a load factor verses weir load diagram.

Conclusion

Although the liquid was completely aerated on the two trays, the height of clear liquid results show that the liquid head surface changed from a relatively flat profile to an uneven profile over most of the tray area. The uneven liquid head profiles consisted of peaks and troughs particularly during the large froth height experiments, and at the high air flow-low liquid flow rates, which was indicative of the increased level of gas-liquid turbulence.

10.3.3 Effect of Non-Separated and Separated Flow Patterns on the Liquid Head Profile on the Two Trays

In spite of no large variations in the point to point height of clear liquid measurements, as a result of the liquid being completely aerated over the whole tray, the separation of liquid flow had a noticeable effect on the liquid head profiles. On the whole, horizontal profiles were produced at low weir loadings on both trays, indicative of forward only flow in the non-separated flow patterns, as shown in Figure 10.16. At the higher weir loadings such that circulating flow became the dominant flow pattern, the height of clear liquid on the tray segments was greater than that in front of the inlet downcomer. This was most evident during the extreme case of liquid channelling associated with the maximum

circulation of 30% which occurred mainly at the inlet gap and outlet weir heights of 10 mm. In these cases, liquid appeared to be jetting from the inlet gap and did not become fully aerated until approximately 200 mm downstream from the inlet downcomer, as shown in Figure 10.17.

As the superficial air velocity was increased, the bubbling action of the gas through the liquid on the two trays increased the level of gas-liquid turbulence. This was reflected in the greater number of peaks and troughs in the liquid head surface across the tray especially at large froth heights, (see Figure 10.18).

In general, for the same flow conditions, the relatively flat liquid head profiles produced on the lower tray of the two trays, during the separation of flow, were dissimilar to that produced on the single tray. That is, the liquid head profiles showed that there were some differences between the uneven liquid head surface on the one tray compared with that on the lower tray of the two trays. For instance, by comparing Figure 8.20b from Chapter 8 with Figure 10.17, the difference in the liquid head surface at the sides of the tray compared with that in the middle on the one tray was far greater than that observed on the lower tray in the two tray experiments.

This may have been caused by an uneven flow of liquid onto the lower tray from the downcomer although this is unlikely since downcomer backup measurements either side of the tray centreline were relatively uniform. One possible explanation for the differences in the liquid head profiles on the two trays is that the gas-liquid interactions on the lower tray, of the two tray setup, may have been influenced by the gas flow pattern emerging from that tray. This may be significantly different to the behaviour of the relatively uniform gas flow entering the liquid on the one tray for the same flow conditions. However, this needs to be investigated experimentally in the future.

A summary of all the height of clear liquid profiles are summarised on the modified load factor verses weir load diagram as shown in Figures 10.19a, 10.19b and 10.19c.

Conclusion

The above height of clear liquid experiments on the two trays have shown that the liquid head profiles became increasingly non-uniform with increasing air and water flow rates. In general, the height of clear liquid profile of the slower moving or circulating liquid along the sides of the tray inlet, was greater than that of the faster moving liquid along the middle of the tray. However this is not as distinct as that produced on the one tray which suggests that flow patterns on the two trays are superior to those on the one tray.

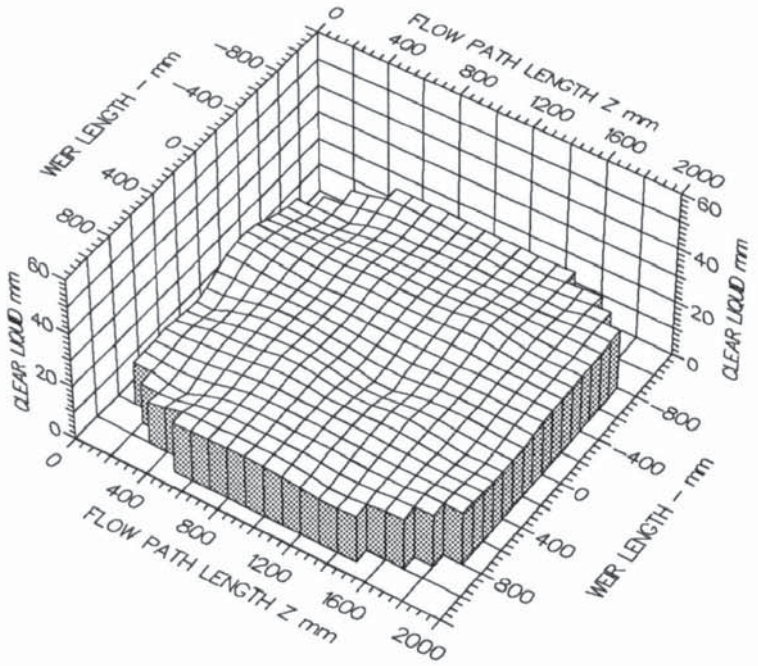

TOP TRAY 1

Air Velocity
1.000 m/s

Weir Load
50.0 cm3/cm.s

Inlet Gap
0.020 m

Outlet Weir
0.020 m

Hole Diameter
0.006 m

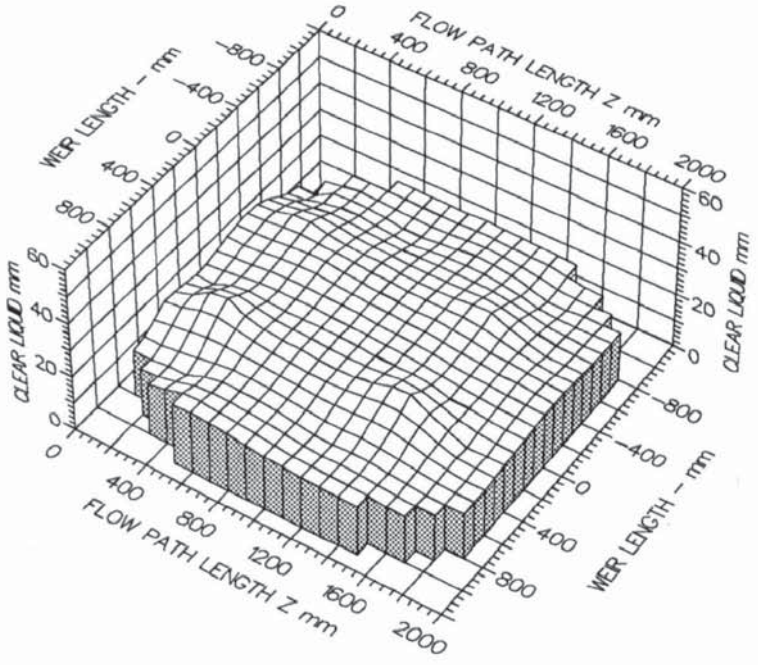

BOTTOM TRAY 2

Air Velocity
1.000 m/s

Weir Load
50.0 cm3/cm.s

Inlet Gap
0.020 m

Outlet Weir
0.020 m

Hole Diameter
0.006 m

Figure 10.16 Examples of comparatively flat height of clear liquid profiles, at medium froth heights on the upper tray (designation H) and lower tray (designation H/NI).

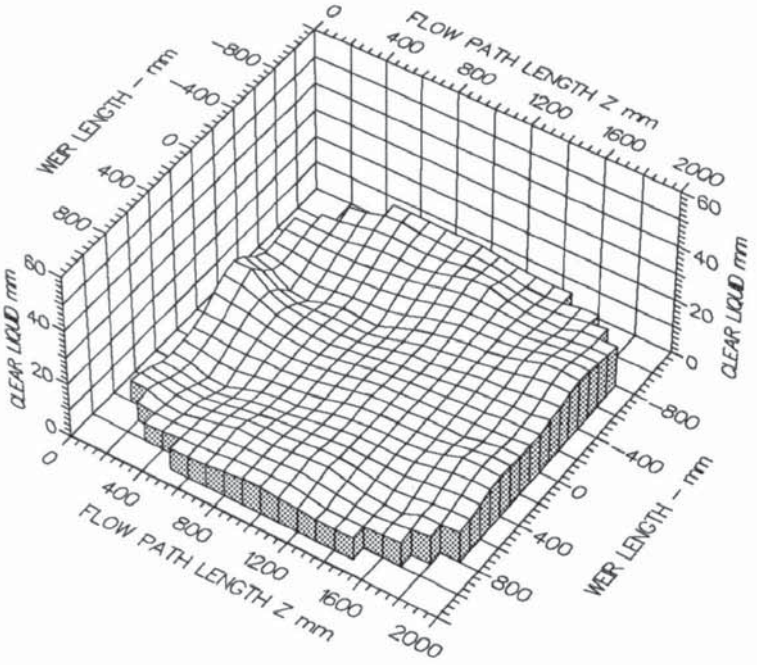

TOP TRAY 1

Air Velocity
1.000 m/s

Weir Load
150.0 cm3/cm.s

Inlet Gap
0.010 m

Outlet Weir
0.010 m

Hole Diameter
0.006 m

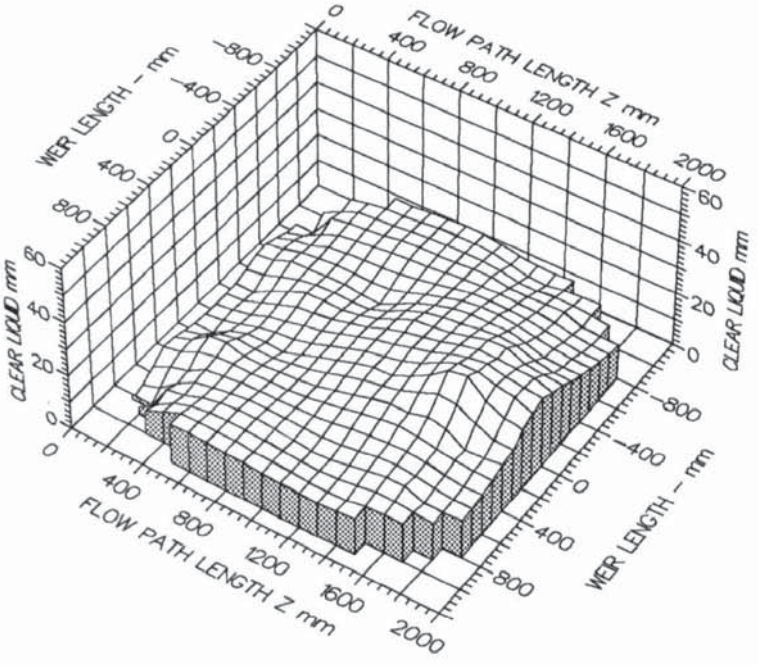

BOTTOM TRAY 2

Air Velocity
1.000 m/s

Weir Load
150.0 cm3/cm.s

Inlet Gap
0.010 m

Outlet Weir
0.010 m

Hole Diameter
0.006 m

Figure 10.17 Examples of height of clear liquid profiles with an uneven surface at low froth heights on the upper tray (designation NI) and lower tray (designation NI).

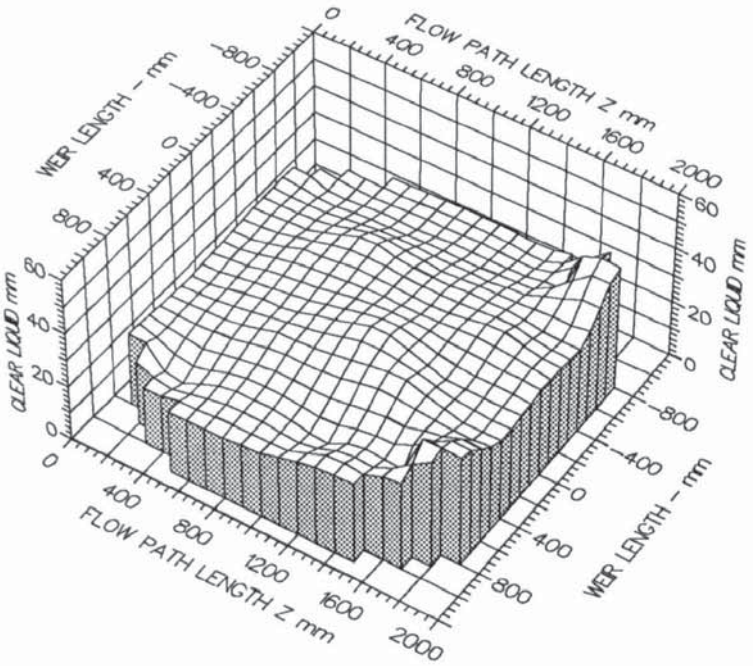

TOP TRAY 1

Air Velocity
1.500 m/s

Weir Load
150.0 cm3/cm.s

Inlet Gap
0.050 m

Outlet Weir
0.050 m

Hole Diameter
0.006 m

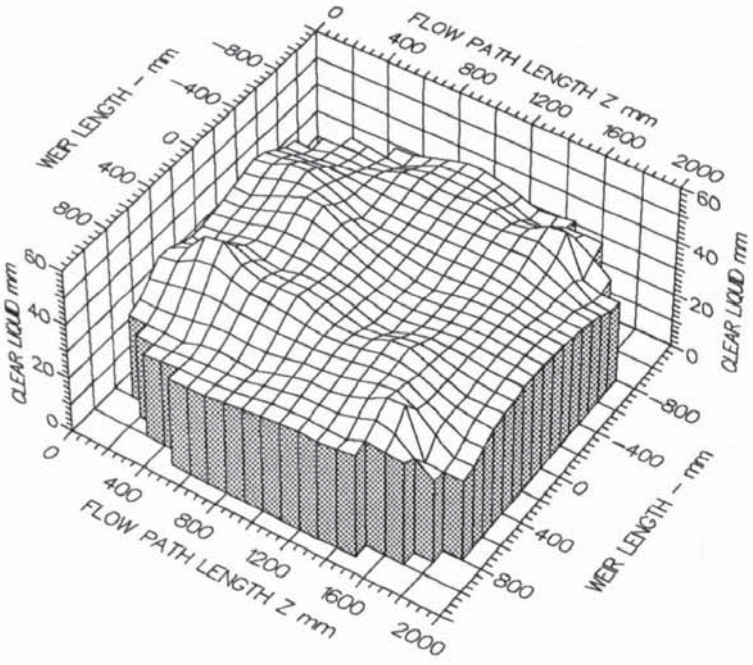

BOTTOM TRAY 2

Air Velocity
1.500 m/s

Weir Load
150.0 cm3/cm.s

Inlet Gap
0.050 m

Outlet Weir
0.050 m

Hole Diameter
0.006 m

Figure 10.18 Examples of height of clear liquid profiles with an uneven surface at large froth heights on the upper tray (designation H/NO) and lower tray (designation N).

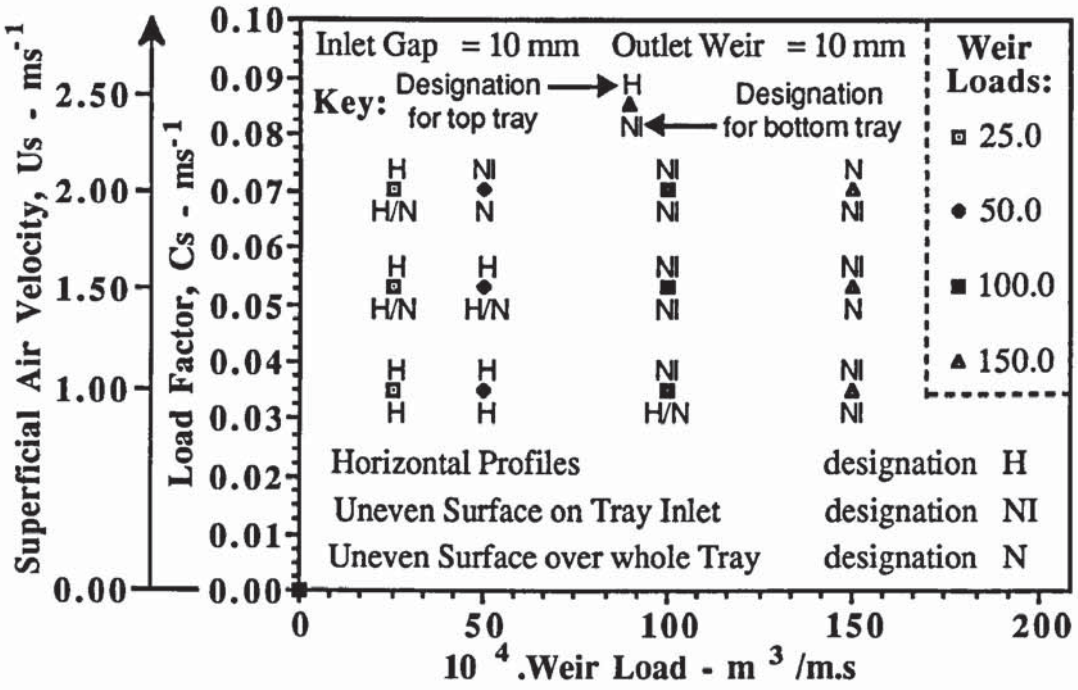

Figure 10.19a Summary of liquid head profiles on a load factor verses weir load diagram.

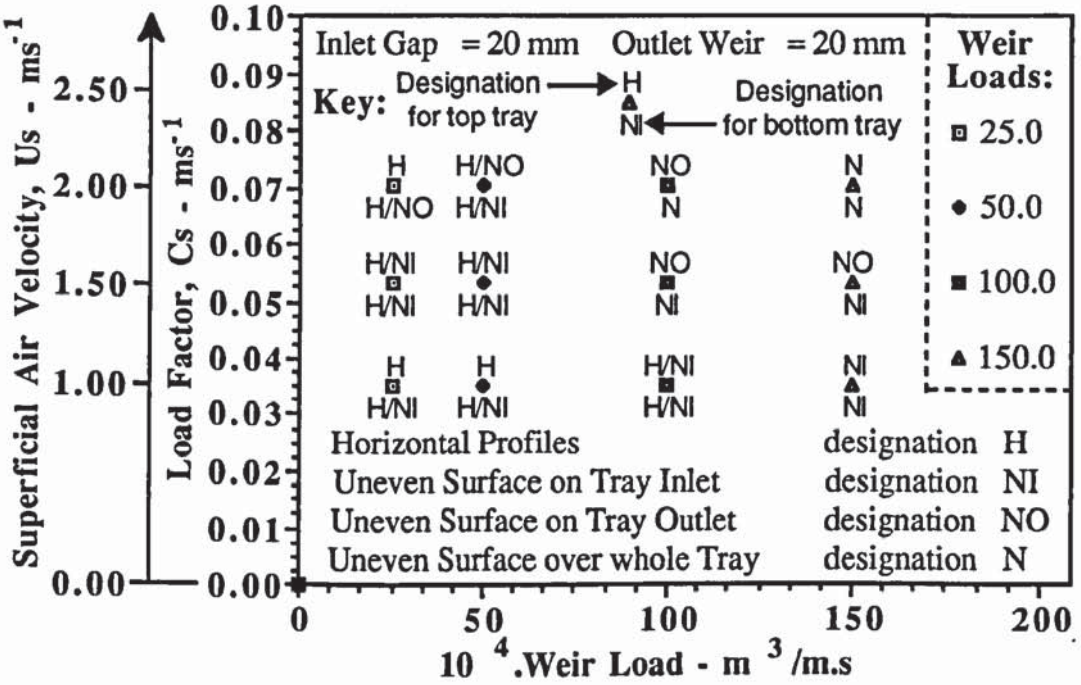

Figure 10.19b Summary of liquid head profiles on a load factor verses weir load diagram.

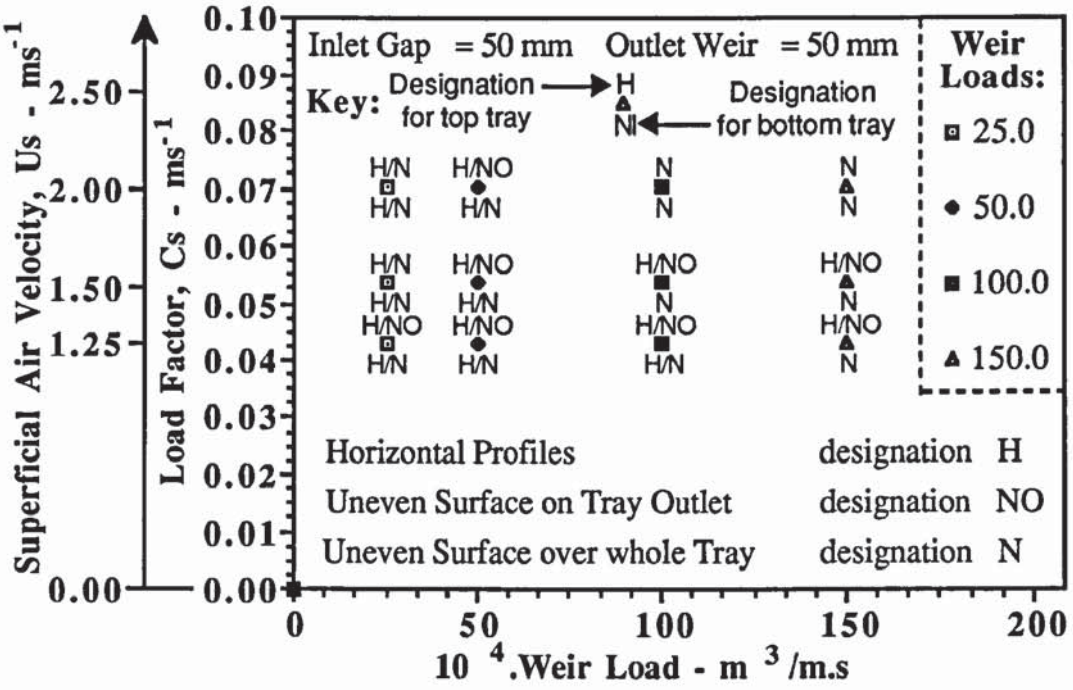

Figure 10.19c Summary of liquid head profiles on a load factor verses weir load diagram.

10.3.4 Effect of Flow Pattern Results at Different Simulated Pressures on the Liquid Head Profile on the Two Trays

In general, horizontal profiles on both trays were produced during the vacuum simulation experiments, indicative of forward only flow at all points on the tray (see Figure 10.20). At the higher weir load pressure simulation experiments, the uneven liquid head surface was found initially on the inlet tray section, but this spread out to the tray outlet section at the higher air flow to liquid flow operating range during the moderate pressure simulation experiments (see Figure 10.21). This can be attributed to the increased level of gas-liquid turbulence within the larger froth heights produced during the simulation of moderate pressure distillation. All of the height of clear liquid results, for each simulated pressure, are presented on the load factor verses weir load diagram as shown in Figure 10.22.

Liquid head profiles on the lower tray were dissimilar to that produced on the single tray for the same air-water flowrates, in that the variation of point to point height of clear liquid profiles on the lower tray of the two tray setup were greater than that produced on the one tray. This was deduced by comparing Figure 9.9b of Chapter 9 with Figure 10.21. The reasons for this phenomenon are similar to those outlined in Section 10.3.3.

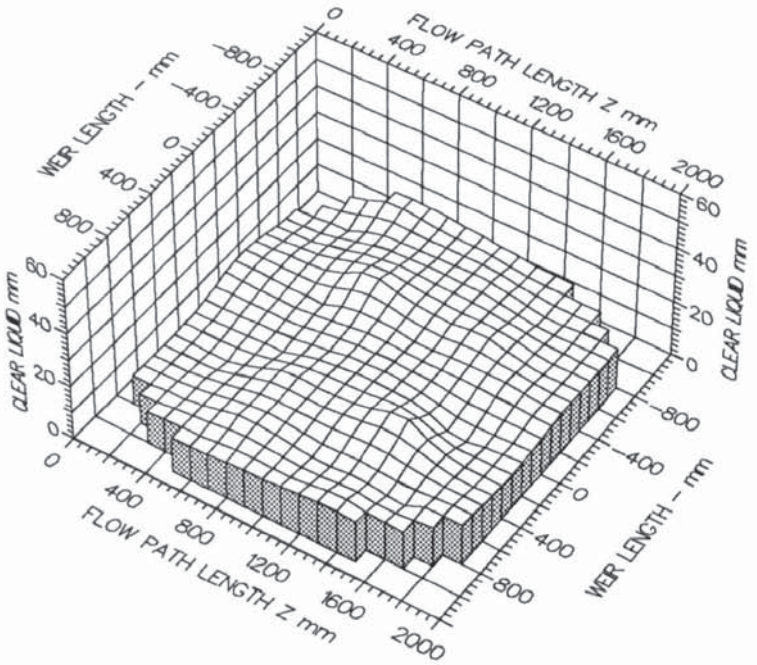

TOP TRAY 1

Air Velocity
1.500 m/s

Weir Load
18.5 cm3/cm.s

Inlet Gap
0.010 m

Outlet Weir
0.010 m

Hole Diameter
0.006 m

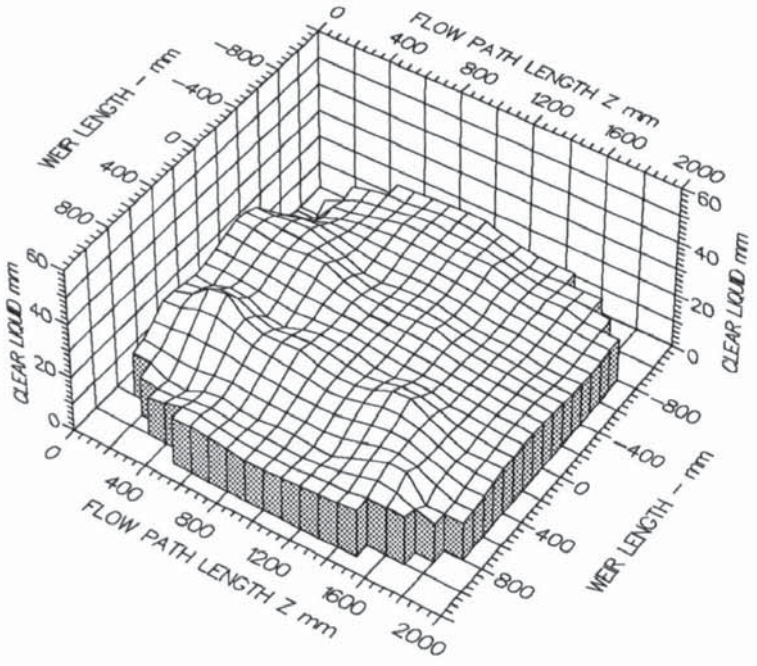

BOTTOM TRAY 2

Air Velocity
1.500 m/s

Weir Load
18.5 cm3/cm.s

Inlet Gap
0.010 m

Outlet Weir
0.010 m

Hole Diameter
0.006 m

Figure 10.20 Examples of comparatively flat height of clear liquid profiles, during vacuum simulation on the upper tray (designation H) and lower tray (designation H/NI).

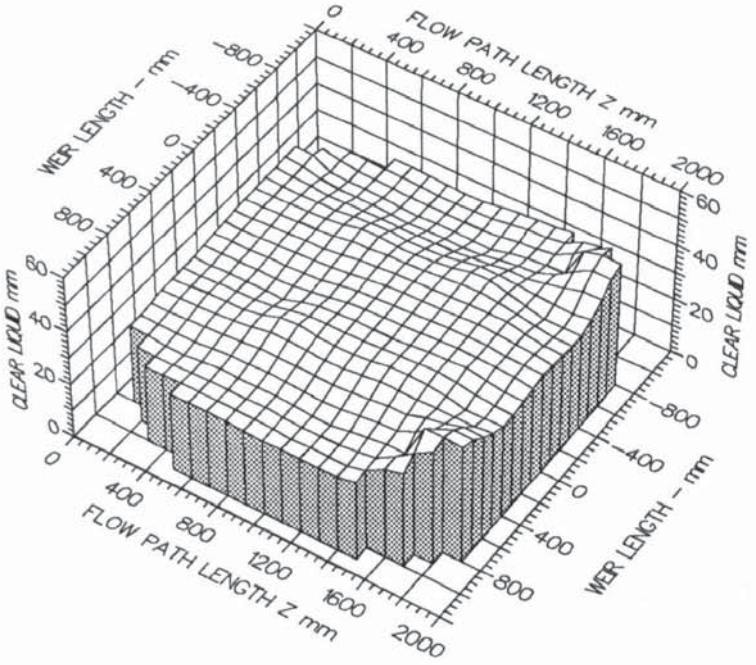

TOP TRAY 1

Air Velocity
1.250 m/s

Weir Load
100.0 cm3/cm.s

Inlet Gap
0.050 m

Outlet Weir
0.050 m

Hole Diameter
0.006 m

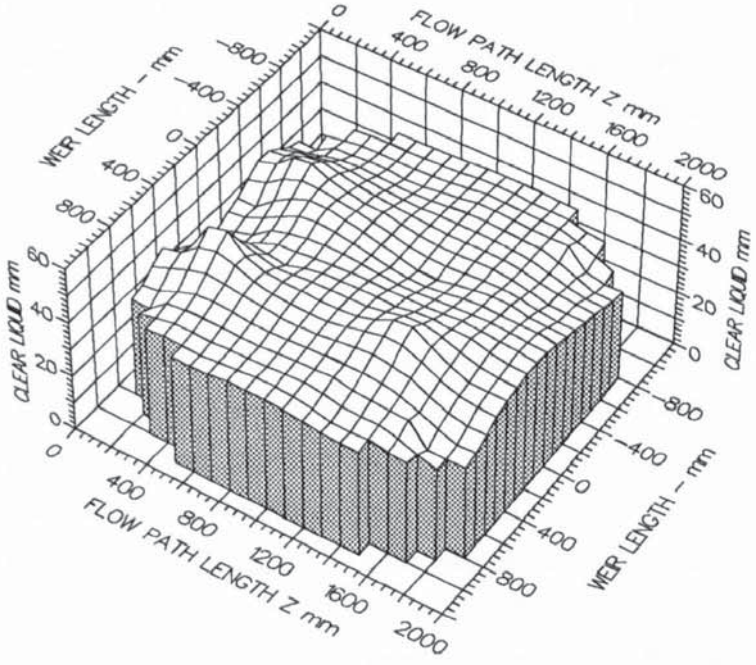

BOTTOM TRAY 2

Air Velocity
1.250 m/s

Weir Load
100.0 cm3/cm.s

Inlet Gap
0.050 m

Outlet Weir
0.050 m

Hole Diameter
0.006 m

Figure 10.21 Examples of height of clear liquid profiles with an uneven surface during moderate pressure simulation on the upper tray (designation H/N) and lower tray (designation NI).

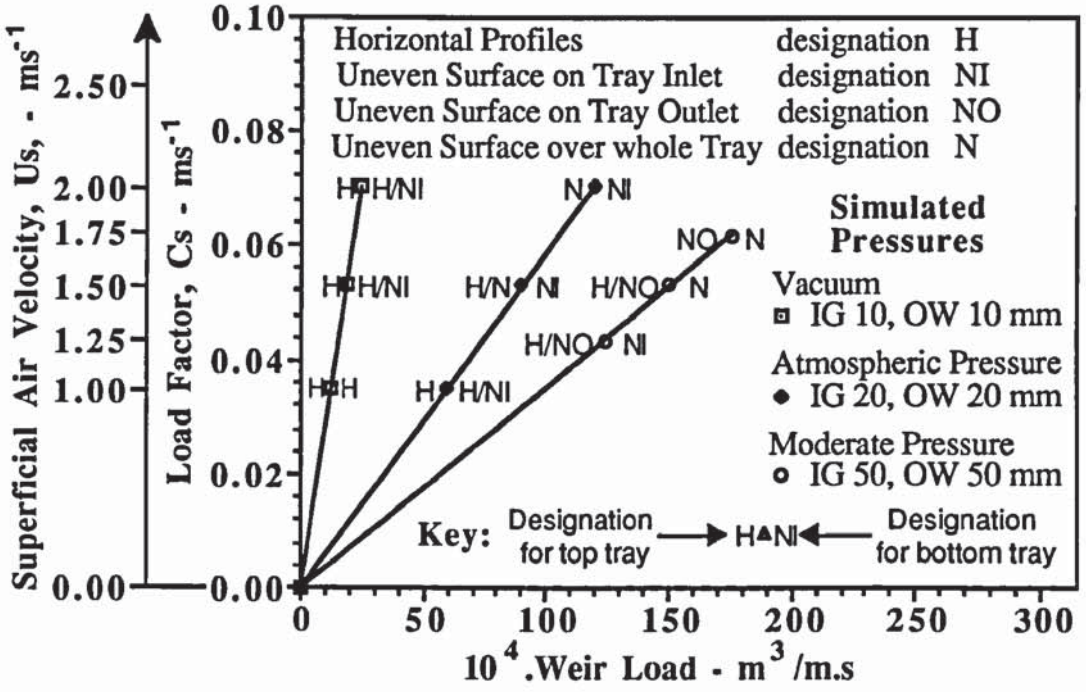

Figure 10.22 Summary of liquid head profiles on a load factor verses weir load diagram.

Conclusion

The height of clear liquid experiments on two trays have shown that the liquid head profiles became increasingly non-uniform as the simulated pressure changed from vacuum to moderate pressure. On the whole, the height of clear liquid profiles for the slower moving, stationary or circulating liquid at the sides of the diverging tray inlet section, were greater than that for the faster moving liquid along the middle of the tray.

10.4 Overall Conclusions

In this chapter it has been shown that the inter-tray gas flow pattern emerging from the liquid flow on one tray had a surprising effect on the liquid flow pattern on a second tray placed 300 mm directly above. That is, the gas flow appeared to have little effect on changing the direction of liquid flow on the two trays in the same way as that reported for the one tray in Chapter 6. This implies that for a real tray column, gas-influenced liquid flow patterns may only occur on the first tray above the vapour feed inlet. This means that there may be a need to model the tray liquid flow patterns only.

The effect of the gas flow on the separation of liquid flow and in the simulation of distillation at different pressures, showed that the flow pattern results were, on the whole,

similar to those produced on the one tray. However, in all of the experiments, the velocity of forward and circulating flow was less than that on the one tray, which may have been the result of a higher level of gas-liquid turbulence on the two trays.

On the whole, the flow patterns generated on two trays, appear to be superior to that produced on one tray in that the velocity and size of circulating flow was less for the same operating conditions. In several experiments, the observation of forward flow associated with stationary liquid at the sides of the tray is similar to the stagnant regions hypothetical flow pattern predicted by Porter et al., (1972). It is possible that the integral beams of the second tray might have produced a uniform inter-tray gas flow pattern by reducing any circulation tendancy between the two trays.

Evidence to support this was the estimation of liquid cross flow velocities on the bottom tray all of which were lower than the superficial velocity of the air passing through the liquid even for the highest weir loadings. This means that if the assumption of Yu is accepted, the momentum imparted to the gas from the liquid flow on the lower tray was insufficient to accelerate the gas with a horizontal velocity component equal to that of the liquid. In addition the magnitude and direction of the gas flow was not sufficient to change the direction of liquid flow on the top tray. Thus, it is possible that the vertical air velocity component is greater than the horizontal air velocity component, even for the highest weir loadings and may be responsible for the high level of gas-liquid turbulence. This, in turn, may have resulted in the liquid flow moving with a lower velocity on the two trays compared to that on the one tray.

Alternatively, the integral beams may have split any circulating air flow into smaller circulating eddies. This might have caused liquid mixing and splashing in all directions over many points across the tray. If this was the case, the gas-liquid mixing behaviour appears to contradict the assumption of Lockett et al., (1975) that the gas flow may be considered unmixed between large diameter single pass trays. Lockett reported that vapour mixing was ineffective in reducing vapour bypassing through stagnant regions on large diameter trays, which, in turn, has an adverse effect on tray efficiency.

On the whole the results, have provided a promising start in gaining a deeper understanding of flow patterns that may occur in real trayed columns. However, the nature of the inter-tray vapour flow pattern, including possible changes in the vapour concentration profiles is not yet understood. Studies of gas flow patterns at this and other tray spacings are required since this will influence the way in which future theoretical models are developed to explain the flow patterns that occur in practice.

If, on the one hand, the gas flow pattern changes the direction of liquid flow on more than one tray, then the new theoretical model will need to explain the fluid mechanics of the vapour-liquid interactions throughout the whole column. Alternatively, if the gas flow changes the direction of liquid flow on only one tray, then this may be due to gas entrance effects from the vapour feed inlet to the column. Hence the theoretical model will concentrate on the fluid mechanics of liquid only flow on trays stacked in a column.

Investigations into gas-liquid interactions on the two trays such as the water cooling technique, to determine their effect on mass transfer, is the subject of future work.

CHAPTER 11

DISCUSSION

11.1 Introduction

The empiricism of tray design and the lack of understanding on how two phase flow dispersions flow across distillation trays, has necessitated the need for a new fundamental approach in order to overcome these deficiencies from first principles. This can be achieved by the development of a more mechanistic theoretical model to explain how and why vapour-liquid dispersions flow in a certain manner across commercial trays of various geometries. These effects can be incorporated into future efficiency models such that the effect of the two phase flow pattern (formed in a particular flow regime) on mass transfer efficiency can be predicted for use in the more scientific approach to tray design.

To develop these theoretical models, a "flow pattern data bank" needs to be established based on a comprehensive set of experimental investigations on a number of tray types, starting with sieve trays, in which the diameter can vary from 1.0 to 10.0 m. Sieve trays are the simplest and cheapest separating device which continue to enjoy a considerable amount of popularity in the petrochemical and associated industries.

Since the bubbling action of the vapour when forced through a horizontal liquid cross flow is highly complex, the flow phenomenon is an "open channel two phase flow" problem. Thus to simplify matters, the effect of the vapour flow on the liquid flow pattern can be investigated by comparing water-only flow across an unperforated tray with air-water flow patterns on perforated trays of various hole sizes. These include 1.0 mm holes, used in air-separation; intermediate hole size trays ranging from 4.50 mm to 6.35 mm, used in the chemical industry; and 12.7 mm hole trays, which are the most widely used trays in the petrochemical industry.

Results from water-only flow experiments and air-water contacting on a 1.0 mm hole tray (Hine, 1990) showed that flow separation at the ends of the inlet downcomer occurred on both trays, thus causing large circulating zones at the sides. However, on forcing the air through the liquid flow on the 1.0 mm hole tray, flow separation and circulating flow was inhibited such that it only occurred at high water inlet velocities.

At this point, it is worth noting that some work has already been carried out on larger hole

sieve trays in which some remarkable flow patterns were produced. For instance, Porter et al., (1987), reported non-uniform liquid flow patterns, in the form of severely distorted "U-shaped" temperature isotherms during water-cooling, on a 1.22 m diameter, 4.5 mm hole sieve tray, and was thought to be the result of the gas flow pattern beneath the tray. This was in direct contrast to that obtained on 1.0 and 12.0 mm hole trays for the same operating conditions. In addition the gas flow, beneath a 6.35 mm hole tray of diameter 2.44 m, changed the direction of liquid flow, Ayvaz (1990), such that it forced the liquid to circulate on the tray outlet. Thus it was established that non-uniform liquid flow, on trays of hole diameters 4.50-6.35 mm, may have been caused by gas flow effects and as far as is known this is the first time that this phenomenon has been observed.

Thus the discussion of results presented in this chapter, were essentially concerned with two sets of experiments to investigate the effect of the gas flow on the liquid flow for a 6.35 mm hole tray. In the first set does the effect of the gas flow beneath the test tray change the direction of liquid flow such that gas-driven liquid circulation is produced? If gas-driven liquid circulation does occur what measures were taken to remove these effects? With the removal of gas distribution effects, does the gas behave as a resistance force to the separation of liquid flow across the tray for a wide range of operating conditions in the second set of experiments. This includes those operating conditions selected for the simulation of distillation at three different pressures. Finally, in order to describe the two phase flow patterns that occur in practice, it is necessary to determine the whether the behaviour of gas-liquid interactions on more than one tray are similar or different to that observed on one tray. Hence the above investigations were repeated on two trays starting with the smallest possible tray spacing of 300 mm for large hole trays.

11.2 Gas Flow Pattern Effects on Liquid Flow Patterns Generated on the One Test Tray

In the first set of gas-liquid contacting studies, does the gas flow pattern change the direction of liquid flow such that it forces the liquid to circulate in a similar manner to that observed by Ayvaz (1990)?

From the direct-observation of flow pointers the presence of gas-driven liquid circulation was clearly shown in which two large symmetrical circulating zones were produced on the tray outlet (see Figure 6.3a). In some cases, a maximum of 30% circulation was recorded, for this tray configuration where the ratio of the weir length to tray diameter is

0.60. Gas-driven liquid circulation was favoured at the high-air flow to low-liquid flow operating range, and at large froth heights. No gas-driven liquid circulation was produced at the higher water weir loadings. The result supports the observations of Ayvaz, and as far as is known, this is the first time that gas-influenced liquid flow patterns have been observed on perforated trays.

The above observations were reflected in the water-cooling results, in which gas-influenced liquid flow patterns had a dramatic effect on the water temperature profiles and the driving forces for mass transfer. The gas-driven liquid circulating flow pattern, at large froth heights, showed up as very tightly packed elongated "U-shaped" isotherms associated with closed looped contours. The latter corresponded to the coldest liquid regions on the tray, where the liquid has a longer residence time compared with other parts of the tray (see Figures 6.9a and 6.9b). Consequently, a dramatic fall-off in tray efficiency was observed such that in some experiments where a maximum gas-driven liquid circulation was produced, the computed tray efficiency was less than the point efficiency.

At low froth heights, particularly at the inlet gap and outlet weir height of 10 mm, the gas flow had a minimal effect on the liquid flow pattern, and this was reflected in the higher tray efficiency results compared with that produced at large froth heights. However, even for the lowest froth heights, the complex nature of the mixed or confused temperature isotherms from the water-cooling experiments, show that the biphase flow pattern is non-uniform (see Figures 6.5a, 6.5b, 6.7a, and 6.7b).

By identifying the problem of gas-driven liquid circulation, was it caused by a non-uniform gas flow pattern beneath the tray and if so, what causes the flow non-uniformity.

An explanation into the cause of circulating liquid is that the gas flow circulates beneath the test tray. The test facility was fitted with a gas distributor, (see Figure 4.6 in Chapter 4), from which the air entered the tray column shell through 130 risers, of diameter 50 mm, on a plate situated immediately above the air distribution shell. Previous work had shown that the flow of air through each riser was essentially the same. In this work, the air-only flow studies, by direct-observation of ribbon flow pointers, and by air velocity measurements, using a hot wire anemometer, showed a very high air flow through the middle of the distributor plate with very little flow at the sides.

It is important to note at this stage, that the diameter of the distributor plate was less than the test tray, and that the distributor had only been installed across the internal cylinder

flow chamber. Thus, the unperforated horizontal plane of the annulus between the perimeter wall of the distributor plate and the tray column wall was unaccounted for in the original air distribution design, and had a significant effect on the inter-tray gas flow pattern. That is, the air flow was non-uniform in that it consisted of diverging air cones in the middle of the distributor plate and large circulating eddies above the annulus at the sides, as shown in Figure 6.12. This is analogous to fluid separation at an interface between a narrow and a wide cross section of a conduit, such as a pipe, in which forward and reverse velocity components are produced in the same domain.

These effects coupled with the assumption that the gas enters the tray at an angle may have produced a reverse flow of liquid. The experimental observations show that the gas-influenced reverse flow became powerful enough to force the liquid to circulate in a closed loop on the tray outlet section with minimal replenishment of liquid from the bulk forward flow of froth.

Another important result from the gas-liquid contacting experiments is that the liquid entrance velocity to the tray, from the inlet downcomer, and froth height over the tray bubbling area, may also have important implications on gas-influenced liquid flow patterns. This can be explained as follows:-

On entering the tray, the inlet liquid velocity, through the large inlet downcomer clearance of 50 mm was much less than that produced from smaller inlet gap heights. Furthermore, as the liquid crossed the tray from the inlet to the outlet, the horizontal velocity of the liquid decreased until a critical point was reached where the magnitude and direction of the liquid flow changed to produce reverse flow. Factors which caused this change included the gas resistance rising through the froth, and the large froth height produced using a large outlet weir. This, in turn, produced a large liquid head across the tray which resulted in a low liquid velocity.

With the tray configured at smaller inlet gap and outlet weir heights, the above mentioned effects were substantially reduced. That is, the resistance of the rising gas through the liquid was less significant owing to the faster inlet liquid velocity from the smaller inlet downcomer clearances and the reduced gas residence time within the lower froth height.

The above observations confirmed that a non-uniform air flow in the inter-tray space above the gas distributor plate, was responsible for gas-driven liquid circulation.

11.3 Methods of Improving the Gas Flow Pattern By Distributor Design

By identifying the problem of a non-uniform gas flow effect from the original gas distribution design, what methods can be used to improve the distribution system? The problem of obtaining a uniform gas flow pattern throughout the cross section of a large diameter column is notorious. Hence before discussing the options considered for improving the non-uniform gas flow pattern, described above, it is worth noting the reasons for using original gas distribution system of annular and cross baffles for an inlet tangential air feed.

The gas distribution system was based on the observations of Ali (1984), in which the effects of various gas distributor designs on the gas distribution through a 1.2 m diameter shallow random packed bed were investigated. (The 1.2 m diameter test facility is a geometrically scaled down version of a 7.3 m vacuum crude distillation column in which vapour and liquid distribution are of great importance.) The level of non-uniform gas flow was measured in terms of a maldistribution factor, ϕ, for straight and tangential air feeds to the column. It was found that ϕ was far higher for the internal cylinder distributor compared with a system of radial baffles inside the annulus of the internal cylinder and cross baffles within the inner flow chamber.

Hence the system of annular and cross baffles were incorporated into the air distribution shell of the test facility (see Figures 4.2 and 4.3), with the chimney distributor tray serving to remove any weeped liquid from the intertray space aswell as providing a uniform flow of air to the test tray (see Figures 4.6 and 4.7). The problem with this system was that the diameter of the chimney tray and internal flow chamber was 0.44 m less than the test tray (of diameter 2.44 m). This resulted in a high flow of air through the middle of the tray with no air flow at the sides, thus permitting the formation of circulating gas eddies above the annulus sections in the inter-tray space.

A number of measures were therefore taken to increase the flow of air to the sides above the annulus to see whether there was an improvement in the gas flow pattern within the inter-tray space and a reduction in gas-driven liquid circulation. These included:-

a) Raising the air riser (chimney) distributor plate 36 mm above the annulus.

b) Removing the distributor plate completely from the inner cylinder flow chamber.

c) Fitting the test tray with mock integral beams, with a view to reduce any circulating

tendency of the gas flow beneath the sieve tray.

d) The installation of a 10% free area perforated tray, of hole diameter 1.80 mm, 150 mm above the annulus.

In each case the effect of the gas flow on changing the direction of liquid flow on the test tray was monitored by forcing air through a fixed pool of liquid.

The distributor design modifications, in the first three cases, changed the gas flow pattern such that a greater flow of air at the sides of the column, above the annulus, was achieved. This was associated with a lower air velocity through the middle of the gas distributor. However, the ribbon flow pointers showed the continued presence of circulating eddies above the annulus, although they appeared to be less intense than that produced above the original gas distributor. In addition, the observation of smaller gas-liquid circulating eddies in the fixed liquid pool experiments showed a slight improvement in the gas-influenced liquid flow pattern compared with that observed in the initial gas-liquid contacting experiments.

With the installation of a small hole, high free area perforated tray spread over the whole cross-section of the tray column including the annulus, there was a significant reduction in the size of circulating eddies. This was complemented by an increase in the number of air jets over a greater area of the distributor tray. The improvement in the inter-tray gas flow pattern brought about the elimination of gas-driven liquid circulation on the test tray during the fixed liquid pool experiments.

Overall, the above distributor design tests have shown that the most suitable gas distributor for reducing or eliminating the effects of gas-driven liquid circulation on the test tray, was the 1.80 mm hole, 10% free area perforated tray.

Based on the above observations, a proposal was suggested in Chapter 6 as to why the small hole perforated gas distributor eliminated gas-driven liquid circulation An important feature of the distributor was that the tray thickness is approximately equal to the small hole diameter, thus producing square orifices in the cross section. This will tend to reduce or remove the horizontal velocity component of the gas stream and increase the vertical velocity component of the gas above the tray. Hence the tendency to produce large circulating eddies in the inter-tray region had diminished and was confined to zones close to the column wall. This needs to be investigated further by measuring inter-tray gas velocity profiles using Laser Doppler Anemometry (LDA).

On the whole, this work has shown that under certain conditions, the gas flow pattern beneath the test tray, can have a significant effect on the tray liquid flow pattern and that this was a function of this particular air-water simulator design. Non-uniform gas flow effects were subsequently removed by modification of the gas distribution system.

11.4 Effect of Gas Flow Pattern on the Separation of Liquid Flow on One Tray

With the effects of gas infuenced liquid flow patterns removed, does the gas flow pattern inhibit the separation of liquid flow in a similar manner to that observed on the 1.0 mm hole tray? Before discussing the results, it is worth recalling the definitions of separated and non-separated flow.

Definition of Separated and Non-Separated Flow

The definition of separated and non-separated flow was described in some detail in Chapter 8. The fundamental difference between the two is that in a conduit of constant width and flow depth, forward only flow is found during non-separated flow, whereas in separated flow, both forward and reverse flow are produced in the same domain.

Gas Flow Effects on the Separation of Flow

The gas-liquid contacting studies, in which the weir load was varied over a wide range for a fixed air velocity, showed that the passage of air through water, flowing over the perforated test tray had significant effect on the developed flow patterns. When as a single phase, the water flowed across a rapidly diverging/converging channel, formed by a single pass tray, such that flow separation was produced at the ends of the inlet downcomer. In most cases, with the exception of very low weir loads, this resulted in the formation of circulating regions along the sides of the tray (Hine, 1990).

The effect of forcing the gas through the liquid was to delay the onset of flow separation, which only occurred at much higher weir loads and with smaller gaps under the inlet downcomer, (i.e. high liquid inlet velocities), as shown in Figures 8.2 and 8.3. Thus when the tray was configured with inlet gap heights of 10 and 20 mm, the weir loads required to produce a maximum of 30% circulation along the segments, at the sides of the tray were 120 and 250 $cm^3/cm.s$ respectively. With an inlet gap of 50 mm, the maximum area on the tray occupied by circulating liquid was in most cases 15% but no more than

20%, even at a weir load of 300 $cm^3/cm.s$ (see Figure 8.6b).

Overall, the rate of increase of circulating flow associated with increasing weir load, was less than that for the water-only experiments and showed a strong dependance on the inlet downcomer gap through which the liquid entered the tray. Hence the larger the inlet gap, the smaller the velocity of the liquid entering the tray, and the larger the weir load required to produce a given area of circulating flow.

The prevention of flow separation by the vertically rising gas, such that forward only flow was produced, was reflected in the comparatively straight reduced temperature isotherms which ran parallel to the downcomers (see Figure 8.11a). This resulted in relatively high calculated tray efficiencies. At higher weir loads, where flow separation occurred, a significant proportion of the tray occupied by circulating flow showed up as "U-shaped" isotherms associated with contours lines forming a closed boundary at the sides of the tray. In the most extreme case of liquid channelling associated with a maximum circulation of 30%, the highly transverse "U-shaped" isotherms revealed a plugflow of liquid between the downcomers. The closed looped contours on the tray segments indicated a steep temperature gradient with the coldest liquid being found near the ends of the inlet downcomer (see Figure 8.11b).

The presence of colder regions on the tray as a result of slow moving or circulating liquid, showed that these regions had a longer residence time. This reduced the driving force for mass transfer and in some cases, caused a dramatic fall-off in tray efficiency. Slow moving and circulating flow during the separation of flow, was confirmed by the relatively large height of clear liquid measurements along the tray sides at the ends of the inlet downcomer compared with those in the middle of the tray (see Figure 8.17b).

The results described above, are similar to the predictions of the stagnant regions model, (Porter et al., 1972) in which the calculated concentration profiles give a measure of the driving force for mass transfer. In this model, it was shown that as the tray diameter increased for a single pass tray, the increased size of the stagnant zones resulted in vapour bypassing with no concentration change, and ultimately caused a fall-off in efficiency. This is significant since it was predicted that in a column of single pass trays placed one above the other, this effect produces a much greater reduction in both tray and column efficiency than for a single tray (Lockett et al., 1973).

The results obtained on the single tray are similar to those generated on the 1.00 mm hole tray (Hine, 1990) with one distinct exception. That is, a smaller area of the 6.35mm hole

tray was occupied by circulating liquid at the higher air velocities of 2.00 and 2.50 ms^{-1}, unlike the 1.00 mm hole tray. On the whole, the use of larger holes increased the gas density and gas resistance within the liquid flow, thus decreasing the growth and velocity of circulating liquid.

The input of experimental data, from above, into a turbulent two phase flow mathematical model for computing tray liquid flow patterns, by considering the vapour flow as a resisting force, provided a promising start at a new theoretical description of the flow phenomena. The model needs to be developed further since many of the computational procedures used in the calculation of flow patterns were based on single phase flow. (The validity of these procedures needs to be investigated experimentally). Nevertheless, the computed flow patterns revealed forward flow between the downcomers with very slow or non-moving liquid at the sides of the tray. In some cases the computed flow pattern contained reverse flow near the column wall, (see Figure 8.23), which was fairly similar to the experimental flow pattern for the same operating conditions.

Overall the above results have shown that increasing the inlet gap can reduce the effect of the liquid channelling. In other work not reported here, the use of empirical corrective techniques, such as the use of a seal pan or an inlet weir infront of the inlet downcomer, are used in trayed columns. Both of these modifications will have a significant effect in reducing the momentum of the liquid entering the froth.

11.5 Simulation of Distillation at Three Different Pressures on the One Tray

An extension of the above set of investigations is to determine whether any flow separation occurs using flow conditions to simulate industrial scale practical distillation. That is, by selecting flow rates to simulate distillation at three different operating pressures, does circulating flow occur, or is the liquid in forward flow at all points on the tray?

In most cases, the tray area was occupied by forward only flow, i.e. in the direction from the inlet downcomer to the outlet weir. (Figures 9.1, 9.2a and 9.2b show forward only flow during vacuum simulation). At the higher weir load simulations of atmospheric and moderate pressure, the velocity of flow on the tray segments near the column wall, was much less than that in the middle between the downcomers, as shown in Figures 9.3 and 9.4. These observations are important when interpretating the water temperature profiles.

The temperature isotherms were staight an parallel to the downcomers during vacuum simulation, as shown in Figure 9.7a. This implies a similar liquid residence time distribution over the whole tray cross section. At the higher pressure simulations, the slow forward flow corresponded to colder regions at the sides of the tray where the liquid has a longer residence time. The longer liquid flow path at the sides of the tray means that the coldest liquid was found near the ends of the outlet weir (see Figures 9.7b and 9.7c), which, in turn, yielded relatively low tray efficiencies.

The colder, slower moving liquid on the tray was complemented by liquid head surface profiles which, on the whole, were higher at the sides than in the middle in front of the inlet downcomer, as shown in Figures 9.9a and 9.9b. Furthermore, the liquid head became increasingly non-uniform as the simulated pressure was increased from vacuum to a moderate pressure.

The experimentally determined efficiencies and height of clear liquid results were compared against published data, obtained both experimentally and by the use of mathematical correlations, for similar operating conditions. A comparison of point efficiency results, from the vacuum simulation experiments, with those of Prado and Fair (1990), were shown to be unrealistic as their apparatus was small scale. In addition, the high E_{OG} results computed are probably not typical of that found on commercial size trays, whereas the low E_{OG} results, from the vacuum simulation experiments reflect the curent trend of efficiencies found in practice. This suggests that the flow pattern might yet be improved and may be the subject of further work. The measured height of clear liquid results obtained in the simulated pressure experiments, showed very little agreement with those predicted from the correlations of Bekassy-Molnar et al., (1991). This implies that the liquid head results produced on the 2.44 m diameter test tray might be more realistic to that found on real trays in commercial scale columns.

During the simulation of distillation, data concerning the flow rates, froth properties, and tray geometry, was used as input to generate concentration profiles, predicted from the SRM, (Porter et al., 1972) for a single tray. The computed concentration profiles are similar to the transverse and severe "U-shaped" isotherms, obtained with both forward flow and with a region of circulating flow at the sides of the tray, for the conditions of atmospheric and moderate pressure distillation, where the model is expected to be applicable. This proved to be a very interesting result since the theoretical model assumes that the liquid at the sides of the tray is stagnant, ie in between slow forward moving and reverse flow adjacent to the column walls.

Although the predicted and experimental results are very similar, it can be seen, from Figures 9.10a, 9.10b, 9.11a, 9.11b, 9.12a, and 9.12b, that the calculated reduced concentration profiles at the sides of the tray were much less than the experimental reduced temperature isotherms. This implies that the SRM under-predicted liquid concentration profiles at the sides of the tray which means that beyond the mixing zone, stagnant liquid is not the same as slow moving liquid observed in the pressure simulation experiments.

For vacuum simulation, the predicted concentration profiles, from the SRM, were "U-shaped" compared to the straight and parallel reduced temperature isotherms obtained experimentally. This implies that for this set of experimental conditions, the SRM is not valid for vacuum distillation and that there may be a different flow mechanism across the tray, ie operation in the spray regime. It should be noted that concentration profiles predicted from the spray diffusion model of Porter, Safekourdi, and Lockett, 1977, are similar to the straight and parallel isotherms from the vacuum simulation experiments. However, experimental measurements of liquid mixing on the tray to determine the diffusion coefficient for use in the spray diffusion model show that there is a limit to liquid flow by spray diffusion. Thus the model needs to be further developed in the future for comparison with the vacuum simulation temperature profiles.

On the whole, the incorporation of experimental data into an appropiate theoretical model has shown that it is unwise to fit experimental data, from the three pressure simulations, into the same tray efficiency design equations since flow pattern changes at different pressures will result in changes in the tray efficiency. (Using experimental data in the same tray efficiency design equations is a procedure adopted by Fractionation Research Incorporated (F.R.I.)).

11.6 Effect of the Gas Flow Pattern on Liquid Flow Patterns Produced on Two Trays

Since it has been established that the direction of the gas flow beneath one tray may influence the direction of liquid flow, does the gas flow emerging from the liquid movement on one tray influence the direction of liquid flow on a second tray placed directly above? Alternatively, are the two phase flow patterns the same or different to that observed on one tray? It is important to address this problem since this will influence the way in which future theoretical models are developed to explain the flow patterns that

occur in industrial scale practical distillation columns.

Thus two test trays were incorporated into the test facility at a low tray spacing of 300 mm. This limited the range of industrial flow rates used in the experiments so as to prevent downcomer choking and flooding. In the time available, it was decided to use an integral beam tray as a second test tray since they are widely used in practice and the flow patterns produced may be representative of that found on commercial trays of this type. Furthermore, do the integral beam units of the tray change the inter-tray gas flow pattern and thus change the liquid flow pattern on the tray deck?

With the above factors in mind, the approach adopted involved the concept of gas resistance to a liquid cross flow on a tray during the development of a turbulent single phase flow model, (Yu et al., 1991). From this model, it was assumed that the gas enters the froth on the tray, in a vertical direction and acquires a horizontal velocity component equal to that of the liquid flow before leaving the froth. Thus, the momentum required to accelerate the gas in the horizontal direction provides an additional resistance to the liquid flow which is much greater than the frictional drag resistance of the liquid along the tray floor.

When applied to the two tray set up, it is possible that the gas, on disengaging from the froth on the bottom tray, may circulate backwards as a result of the close tray spacing (see Figure 10.1). The circulating gas may, in turn, yield a significant change on the liquid flow on the top tray.

Overall a surprising result was observed in that the inter-tray gas flow appeared to have little effect on changing the direction of liquid flow on the two trays in the same way as that observed on the one tray, for the same flow conditions (compare Figure 10.2a from this work with Figure 6.3a for the one tray). Instead, forward only flow at all points on the tray associated with a considerable level of gas-liquid turbulence, particularly at the large froth heights, was produced in all of the experiments. This suggests that the flow patterns are superior to those obtained on the one tray in that the size and velocity of reverse or circulating flow was less on two trays for the same flow conditions (see Figures 10.2a, 10.2b, 10.13, 10.14, and 10.15).

One possible reason for the absence of gas-driven liquid circulation on the top tray, is that the integral beams may have affected the inter-tray gas flow pattern. That is, they may have prevented the possible formation of circulating air eddies throughout the inter-tray space. In addition, the direction of gas flow, emerging from the liquid flow on the

bottom tray, may have entered the top tray at an angle such that it opposes the forward flow of liquid. Hence, it appears that the gas resistance may have been responsible for the observation of slow moving or stationary froth over most of the tray, especially on the longer liquid flow path at the sides. This is similar to the liquid forward flow associated with stagnant regions hypothetical flow pattern predicted by Porter et al., (1972). Further studies into the inter-tray gas flow pattern need to be carried out in the future.

Since there was no evidence of gas-influenced liquid flow on two trays, are the two phase flow patterns the same or different to that observed on one tray? Overall, the flow pattern results were similar to those produced on the single tray. That is, the effect of the air flow delayed the onset of flow separation and circulating flow which only appeared at higher water inlet velocities and small inlet gap heights (see Figures 10.7a, 10.7b, and 10.7c). In the experiments to simulate distillation, the liquid was in forward flow over most of the tray area, as shown in Figures 10.11a, 10.11b, and 10.11c.

However, some differences in the flow patterns were noted in that the velocities of forward flow and circulating flow on the two trays were less than that produced on the one tray, for the same flow rates. This was reflected in the greater number of peaks and troughs within the uneven liquid head profiles over the whole of the tray cross section and appeared to be the result of an increased level of gas-liquid turbulence (see Figures 10.16, 10.17, 10.18, 10.20, and 10.21).

One possible explanation for the above observations is as follows. If the assumption of Yu et al., (1991) is accepted to be correct, the momentum imparted to the gas from the liquid flow on the lower tray was insufficient to accelerate the gas with a horizontal velocity component equal to that of the liquid, even for the highest weir loadings. Thus the magnitude and direction of the gas flow was not sufficient to change the direction of liquid flow on the top tray. It is possible, therefore, that the vertical air velocity component is greater than the horizontal air velocity component, even for the highest weir loadings and may be responsible for the high level of gas-liquid turbulence.

On the whole the results on one and two trays, have provided a promising start in gaining a deeper understanding of flow patterns that are likely to occur in real trayed columns. However, the nature of the inter-tray vapour flow pattern, including possible changes in the vapour concentration profiles is not yet understood. Studies of gas flow patterns at this and other tray spacings need to be determined since this will influence the way in which future theoretical models are developed to explain the flow patterns that occur in industrial scale practical distillation.

If, on the one hand, the gas flow pattern changes the direction of liquid flow on more than one tray, then the new theoretical model will need to explain the fluid mechanics of the vapour-liquid interactions throughout the column as a whole. On the other hand, if the gas flow has an effect on changing the direction of liquid flow on only the one tray, then the phenomenon is due to the gas entrance effect from the vapour feed inlet to the column. Hence the theoretical model will need to concentrate on the fluid mechanics of liquid only flow across trays stacked in a column.

Finally, experimental investigations into gas-liquid interactions on two trays by two-dimensional, (to determine the effect of gas-liquid flow patterns on mass transfer), direct-observation, and the measurement of inter-tray gas velocity profiles using LDA, will be the subject of future work.

CHAPTER 12

CONCLUSIONS

The main conclusions from the experimental work can be summarised as follows:

1. A fundamental gas-liquid contacting study of liquid flow patterns, on sieve trays, of hole diameter 6.35 mm, has shown that the passage of the gas through the liquid has a significant effect on the liquid flow. When, as a single phase, the liquid flows through a divergent / convergent open channel formed by a single pass tray, except for very low weir loads, the flow separates at the ends of the inlet downcomer and forms circulating regions throughout the segments at the sides of the tray. The effect of forcing the gas through the liquid was to prevent the onset of flow separation and circulation which only occurred at much higher weir loads and with smaller gaps under the inlet downcomer (i.e. at high liquid inlet velocities). At very high weir loads, circulating liquid occupied the whole of the segments at the sides of the tray, which corresponds to 30% of the total tray area. Overall, the results were similar to that reported on the 1.00 mm hole tray (Hine, 1990).

2. In the simulation of distillation, where the inlet velocity of the liquid was reduced in order to decrease the liquid backup to levels found in practical ditillation, the liquid was in forward flow over most of the tray, i.e. in the direction from the inlet downcomer to the outlet weir. This was particularly so for the simulation of vacuum distillation. For the higher weir load simulations of atmospheric and moderate pressure distillation, it was observed that the velocity of flow on the tray segments was much less than that in the middle of the tray between the downcomers. This is important in interpreting the results from the water-cooling experiments.

3. For most experiments where heat transfer by water-cooling was carried out, the liquid head profile across the tray was measured and was found to be non-uniform. In general, the clear liquid height profile of the slower moving or circulating liquid at the sides of the tray, at the ends of the inlet downcomer, was greater than that for the faster moving liquid along the middle of the tray.

4. During water-cooling, for the case of flow separation and circulating flow, the reduced water temperature isotherms were "U-shaped" with the coldest liquid found

near the ends of the inlet downcomer. However, in situations where the liquid was in forward flow over most of the tray (e.g. the pressure simulation experiments), the coldest liquid was found at the sides near the ends of the outlet downcomer. These colder regions on the tray have confirmed that the driving force for mass transfer is reduced in regions, where the liquid is either circulating or in forward flow across long liquid flow paths, thus causing the liquid to have a longer residence time.

5. The reduced water temperature profiles for vacuum distillation were approximately straight and parallel to the downcomers, whereas those obtained with both forward flow and with a region of circulating flow during the simulations of distillation at higher pressures were distinctly "U-shaped". The parallel isotherms imply that the liquid residence time distribution would be similar, both at the sides and in the middle of the tray , whilst the "U-shaped" isotherms, in the higher pressure simulations, are caused by the longer flow path length near the column wall and also the lower liquid velocity in this region.

6. Data from the heat transfer experiments, during the simulation of distillation, was used as input to calculate concentration profiles, using the stagnant regions theoretical model, SRM, (Porter et al., 1972) for a single tray. The computed concentration profiles are similar to the transverse and severe "U-shaped" isotherms, obtained with both forward flow and with a region of circulating flow at the sides of the tray, for the conditions of atmospheric and moderate pressure distillation, where the model is expected to be applicable. This proved to be a very interesting result since the theoretical model assumes that the liquid at the sides of the tray is stagnant. That is, the liquid is in between slow forward flow at the sides of the tray and a reverse flow in which circulating flow occurs near the column wall.

7. For vacuum simulation, the predicted concentration profiles, from the SRM, were "U-shaped" compared to the straight and parallel reduced temperature isotherms obtained experimentally. This implies that for this set of experimental conditions, the SRM is not valid for vacuum distillation. Since the experimental isotherms were straight and parallel to the downcomers, it implies that there may be a different flow mechanism for vacuum distillation, i.e. operating in the spray regime. However, it should be noted that the concentration profiles predicted for the spray regime, from the spray diffusion model of Porter, Safekourdi, and Lockett, (1977), are similar to the straight and parallel isotherms for vacuum simulation, using the above experimental conditions.

8. For a wide operating range in both the simple gas-liquid contacting and pressure simulation experiments the calculated point efficiencies increased with higher weir loadings. Increasing the weir load has the effect of increasing the clear liquid height, and thus the gas residence time within the froth.

9. A comparison of E_{OG} results from the vacuum simulation experiments with those of Prado and Fair (1990) showed that their results may be unrepresentative of that found on commercial scale trays due to the small scale apparatus used. The E_{OG} results from the vacuum simulation experiments reflect the expected point efficiencies found in practice. Similar arguements apply to the height of clear liquid results when compared against those obtained from correlations derived for the spray, mixed and froth regimes (Bekassy-Molnar and Mustafa, 1991). These observations justify the need to obtain a comprehensive set of experimental data on commercial size trays in the laboratory so as to gain a deeper understanding of the two phase flow behaviour occurring in practical distillation.

10. From investigations into the effect of the gas flow pattern on changing the liquid flow pattern, the initial gas-liquid contacting studies on the single test tray produced an unusual circulating flow on the tray outlet. The effect of the gas flow, beneath the test tray, forced the liquid to flow in the opposite direction, to that of forward flow, from the outlet downcomer to the inlet downcomer. The observation of gas influenced liquid circulation was first reported by Ayvaz (1990). The result was confirmed during this study which showed that gas influenced liquid circulation occured at the high air flow to low liquid flow operating range. However, very little or no circulating flow on the tray outlet was observed at much higher weir loadings. All these observations were made using the original air distributor (chimney) tray. There was no evidence in the open literature as to whether this phenomenon has been observed before.

11. Air only flow studies, by observing the motion of the gas on interaction with a fixed pool of liquid, using the original gas distributor, showed a high gas flow through the middle of the plate, with very little flow at the sides. Hence the gas flow pattern was modified, using a 10% free area, 1.80 mm hole diameter perforated plate, until the effect of gas - driven liquid circulation on the tray outlet was shown to be negligible.

12. From the water-cooling experiments, the observation of gas driven liquid circulation was confirmed by the appearance of very large elongated "U-shaped" reduced temperature isotherms associated with closed looped contours. The closed looped

isotherms extended to the column wall on the inlet and outlet tray segments. These colder regions on the tray confirmed that the driving force for mass transfer is reduced in circulating regions, in which the liquid has a longer residence time. This has an adverse effect on efficiency such that, in some cases, the tray efficiency was found to be less than the point efficiency.

13. The flow patterns obtained on the two test trays, at a spacing of 300 mm, using the modified gas distributor, were on the whole different to those obtained on the one tray. The inter tray gas flow did not have a significant effect on changing the liquid flow pattern on the top tray compared with that on the one tray, for this particular tray spacing. However, it is quite possible that gas flow pattern effects may appear in the inter tray region at higher tray spacings, and thus change the direction of liquid flow on the top tray.

14. Studies into the effect of the gas flow on preventing the separation of liquid flow and the pressure simulation experiments showed that the developed flow patterns on the top tray were superior to that produced on the one tray. That is, the velocity and size of reverse or circulating flow was less than that produced on the one tray, such that in many cases the froth appeared stationary at the sides. This flow pattern is similar to the stagnant regions hypothetical liquid flow pattern of Porter et al., (1972). Overall the above observations may be attributed to the inter tray gas flow pattern providing a significant level of resistance to the liquid flow on the upper tray.

15. On the whole, the experiments have shown that the presence of gas driven circulation was confined only to the bottom test tray and was caused by a non-uniform flow of air from the gas distributor. Hence, in a real tray column, the effect of the gas flow on changing the direction of liquid flow may occur on the first tray above the vapour feed inlet only. Nevertheless it is quite possible that the inter tray gas flow pattern may change the liquid flow on all trays within the column, at higher tray spacings. This is the subject of future work.

Recommendations for Future Work

1. To investigate further the inter tray gas flow pattern at various tray spacings, starting with 300 mm using various experimental techniques. Is the effect of gas influenced liquid circulation only confined to one tray, or does it occur on trays where one is placed above the other? The answer to this question will influence the way in which

future theoretical models are developed.

If, on the one hand, the gas flow pattern changes the direction of liquid flow on more than one tray, then the new theoretical model will need to explain the fluid mechanics the interactions of the vapour-liquid traffic throughout the column as a whole. On the other hand, if the gas flow has an effect on changing the direction of liquid flow on only the one tray, then the phenomenon is due to the gas entrance effect from the vapour feed inlet to the column. Hence the theoretical model will concentrate on the fluid mechanics of liquid only flow across trays stacked in a column.

2. To use the experimental observations from this work as a guide for the more scientific approach required for tray designs used in practice.

3. To repeat all the above studies, into the effect of the gas flow on liquid flow patterns, on sieve trays of hole diameter 12.7 mm.

4. To incorporate the results from this work into the development of a fundamental theory which explains the behaviour of two phase flow on a divergent/convergent open channel formed by a sieve tray.

5. To test the validity of this new theory by identifying those parameters which can be used to improve the computation procedures for use in future theoretical mass transfer models based on "open channel two phase flow" so that flow patterns that occur in real tray columns may be predicted.

6. To develop and test new flow control straightener devices based on a better understanding of the two phase flow phenomena on sieve trays.

NOMENCLATURE

a	Interfacial area per volume of two-phase mixture	$[m^2/m^3]$
a	Length of perimeter section to be blocked when the distributor plate is raised	[m]
A	Effective transfer area	$[m^2]$
A_B	Active area of tray	$[m^2]$
A_D	Downcomer area	$[m^2]$
A_T	Column cross-sectional area	$[m^2]$
C_1, C_2, C_m	Constants	[-]
C_{air}	Specific heat capacity of air	[kJ/kg K]
C_{wat}	Specific heat of water vapour	[kJ/kg K]
Cp	Specific heat capacity	[kJ/kg K]
C_{SB}	Bubbling area capacity factor = $u_s / [\rho_V/(\rho_L - \rho_V)]^{0.5}$	$[ms^{-1}]$
C_s	Load factor = $u_s.[\rho_V/(\rho_L - \rho_V)]^{0.5}$	$[ms^{-1}]$
D	Tray diameter	[m]
D	Kinematic viscosity (Eddy viscosity)	$[m^2/s]$
De	Eddy diffusion coefficient	$[m^2/s]$
De_w	Eddy diffusion coefficient in w direction	$[m^2/s]$
De_z	Eddy diffusion coefficient in z direction	$[m^2/s]$
d_{ann}	Diameter of the annulus inside the column wall	[m]
d_h	Diameter of tray perforations	[m]
d_i	Diameter of the distributor tray	[m]
d_O	Hole diameter	[m]
d_r	Diameter of a chimney riser	[m]
E_{ML}	Murphree tray efficiency, based on liquid phase	[-]
E_{MV}	Murphree tray efficiency, based on vapour phase	[-]
E_O	Overall column efficiency	[-]
E_{OG}	Murphree point efficiency, based on overall vapour phase resistance	[-]
E_{OL}	Murphree point efficiency, based on overall liquid phase resistance	[-]
F	Flooding factor in tray design	[-]
F	Superficial F - Factor = $u_s.(\rho_g)^{0.5}$	$[m/s.(kg/m^3)^{0.5}]$
f_a	Free area on the active area of the tray	$[m^2/m^2]$
F_{lv}	Flow parameter = $L/G.(\rho_v/\rho_l)^{0.5}$	[-]
G	Total air (vapour) mass flowrate	[kg/s]

h_{cl}	Height of clear liquid	[m of H_2O]
h_{DT}	Dry tray pressure drop	[m of H_2O]
h_F	Froth height	[m]
h_R	Residual pressure drop	[m of H_2O]
h_{ow}	Height of outlet weir	[m]
h_w	Heat transfer coefficient in the liquid phase	[kJ/m^2.s.K]
h_{WT}	Wet tray pressure drop	[m of H_2O]
H_{FG}	Latent heat of water	[kJ/kg]
$\overline{H_2}$	Average outlet enthalpy of air leaving the froth	[kJ/kg]
H_1	Average inlet enthalpy of air	[kJ/kg]
H_{2i}	Outlet enthalpy of air from position i on a tray	[kJ/kg]
H_{in}	Average inlet enthalpy of air	[kJ/kg]
H_{g1}	Inlet air enthalpy to water cooling tower	[kJ/kg]
H_{g2}	Exit air enthalpy from water cooling tower	[kJ/kg]
H^*_{Ti}	Enthalpy of air in equilibrium with water at temperature T_i	kJ/kg]
H^*_{Tout}	Enthalpy of air in equilibrium with water at temperature T_{out}	[kJ/kg]
$H_{(Tdb,wb)}$	Humidity of air under dry/wet bulb conditions	[-]
$H_{(Tout)}$	Humidity of air at average outlet water temperature	[-]
IG	Height of gap under the inlet downcomer	[m]
k	Turbulent kinetc energy, $\frac{1}{2}\overline{u_i' u_j'}$	[J]
k_G'	Mass transfer coefficient in the gas (vapour) phase	[ms^{-1}]
k_L	Mass transfer coefficient in the liquid phase	[ms^{-1}]
k_T	Heat transfer coefficient in the gas (vapour) phase	[kJ/m^2.s.K]
K	Constant	[-]
K_{OG}	Overall mass transfer coefficient based on the gas phase	[ms^{-1}]
K_T	Overall heat transfer coefficient based on air-water surface	[kJ/m^2.s.K]
L	Total Liquid mass flowrate	[kg/s]
Le	Lewis number (Sc / Pr)	[-]
L_w	Liquid flow rate per unit weir length	[m^3/(m.s)]
m	Gradient of equilibrium line in mass transfer	[-]
m	Gradient of saturation enthalpy line in heat transfer	[-]
m_1	Moisture content of inlet air to water cooling tower	[kg/kg dry air]
m_2	Moisture content of exiting air from water cooling tower	[kg/kg dry air]
n	Line normal to column wall	[-]
n	Number of chimney risers on the distributor tray	[-]
N	Number of passes in tray design	[-]

N_{OG}	Number of overall transfer units in the gas phase	[-]
N_{Pe}	Peclet Number	[-]
N_{Pes}	Peclet Number in the spray regime	[-]
OW	Outlet weir height	[m]
p	Pressure	[N/m^2]
Q	Heat flux through an air-water interface	[kJ]
Q_G	Vapour volumetric flowrate	[m^3/s]
Q_L	Liquid volumetric flowrate	[m^3/s]
S	Foam or "ignorance derating" factor in tray design	[-]
t	Time	[s]
t	Height at which distributor plate is raised	[m]
t_L	Average liquid contact time	[s]
t_G	Mean residence time of gas in dispersion	[s]
t_w	Water temperature	[K]
t_{w1}	Inlet water temperature to water cooling tower	[K]
t_{w2}	Outlet water temperature from water cooling tower	[K]
T	Dimensionless liquid temperature	[-]
T_{db}	Air dry bulb temperature	[K]
T_i	Temperature of water at position i on a tray	[K]
$\overline{T_{in}}$	Average inlet water temperature entering the tray	[K]
$\overline{T_{out}}$	Average outlet water temperature entering the tray	[K]
T_r	Reduced temperature driving force	[-]
T_{wb}	Air wet bulb temperature	[K]
u	Mean componental velocity in x direction	[ms^{-1}]
U_{DF}	Downcomer velocity of vapour-liquid mixture	[ms^{-1}]
u_i	Mean componental velocity in x_i direction	[ms^{-1}]
u_j	Mean componental velocity in x_j direction	[ms^{-1}]
u_i, u_j	Fluctuating componental velocity in x_i and x_j directions directions	[ms^{-1}]
u_h	Hole gas velocity through tray	[ms^{-1}]
u_s	Superficial (empty tower) velocity	[ms^{-1}]
u_{SB}	Superficial velocity based on tray bubbling area	[ms^{-1}]
v	Mean componental velocity in y direction	[ms^{-1}]
$\overline{V}$	Volumetric vapour flow rate (used in total flows chart)	[m^3/s]
v_a	Gas velocity through the tray bubbling area	[ms^{-1}]
V_w	Liquid velocity in w direction	[ms^{-1}]
V_z	Liquid velocity in z direction	[ms^{-1}]

w'	Coordinate perpendicular to z' direction	[-]
w	Dimensionless coordinate parallel to flow path length	[-]
W	Weir length	[m]
W_G	Total air (vapour) mass flowrate	[kg/s]
W_L	Total water (liquid) mass flowrate	[kg/s]
x	Cartesian coordinate of the tray in the main flow direction	[-]
x	Liquid concentration	[kmol/kg]
X	Dimensionless liquid concentration	[-]
X_+	Dimensionless liquid concentration, just above a zero length coordinate	[-]
x_{eot}	Liquid concentration in equilibrium with the inlet vapour	[kmol/kg]
$\underline{x}_n$	Composition of liquid leaving stage n	[kmol/kg]
$\bar{x}_{n+1}$	Average composition of liquid leaving stage n+1	[kmol/kg]
$\bar{x}_n$	Average composition of liquid leaving stage n	[kmol/kg]
x_n^*	Composition of liquid in equilibrium with vapour composition y_n	[kmol/kg]
X_r	Reduced or dimensionless concentration	[-]
y	Cartesian coordinate of the tray perpendicular to the x - direction	[-]
y_n	Composition of vapour leaving stage n	[kmol/kg]
$\underline{y}_{n-1}$	Composition of vapour leaving stage n-1	[kmol/kg]
$\bar{y}_n$	Average composition of vapour leaving stage n	[kmol/kg]
$\bar{y}_{n-1}$	Average composition of vapour leaving stage n-1	[kmol/kg]
y_n^*	Composition of vapour in equilibrium with liquid composition x_n	[kmol/kg]
z'	Coordinate parallel to flow path length	[-]
z	Dimensionless coordinate perpendicular to z' direction	[-]
Z	Flow Path Length	[m]

Greek Letters

α	Relative volatility of a binary mixture	[-]
δ	Kroneeker function	
ΔT	Temperature difference	[K]
ΔH_m	Mean Enthalpy driving force	[kJ/kg]
ε	Dissipation rate of turbulent energy	[J/s]
ρ_L	Liquid density	[kg/m^3]

ρ_G	Vapour density	[kg/m^3]
ρ_f	Froth density	[-]
η	$\frac{N_{Pe}}{2}\cdot\left[\sqrt{1+\frac{4\cdot\lambda\cdot E_{OG}}{N_{Pe}}}-1\right]$	[-]
λ	Ratio of gradient of equilibrium line to operatingline (= mG/L)	[-]
σ_k , σ_s	Constants	[-]
ϕ	Gas maldistribution factor (Ali, 1984)	[-]
ψ	Flow ratio group, $L_w/v_a(\rho_L/\rho_G)^{0.5}$	[m]

Subscripts

1,2	Pertaining to inlet and outlet conditions used in enthalpy balance	[-]
1,2	Refers to tray numbering scheme starting from the bottom of the column, i.e., first tray is assigned number 1	[-]
db	Dry bulb	[-]
cl	Clear liquid	[m]
f	Froth	
g	Gas or vapour	[-]
in	Inlet	[-]
i	Defined as a point value	[-]
i,j	i and j defined as the direction perpendicular and parallel to the inlet and outlet downcomers	[-]
l	Liquid	[-]
L	Pertaining to the average liquid contact time	
MV	Murphree efficiency for the whole tray based on the vapour concentrations	[-]
o	Outlet	[-]
OG	Overall resistance to mass transfer based on gas (vapour) phase resistance forces	[-]
out	Outlet	[-]
r	Reduced (for concentration and temperature)	[-]
wb	Wet bulb	[-]

Superscripts

*	Pertaining to equilibrium conditions	[-]

REFERENCES

A.I.ChemE., Bubble Tray Design Manual "Prediction of Fractionation Efficiency", AIChE J., New York, (1958).

Ashley, M. J. and Haselden, G. G., 1970, "The calculation of plate efficiency under conditions of finite mixing in both phases in multiplate columns, and the potential advantage of parallel flow", Chem. Engng. Sci., **25**, 1665.

Ayvaz, Z., 1990, "Gas-liquid contacting studies on a 2.4 m diameter sieve tray ", Aston University Internal Report on Advanced Studies in Distillation.

Aleksandrov, A. and Vybronov, V. G., 1971, "Investigation of the hydrodynamic pattern of liquid flow on cross-flow trays", Teor. Osnovy. Kim. Tekh., **5**,(2) 339.

Ali, Q. H., 1984, "Gas Distribution in Shallow Large Diameter Packed Beds", Ph.D. Thesis, University of Aston in Birmingham, Birmingham, England.

Ani, C. C., 1988, "Flow Patterns, Performance and Scale-Up of Distillation Trays", Ph.D. Thesis, University of Aston in Birmingham, Birmingham, England.

Bekassy-Molnar, E. and Mustafa, H., 1991, "Clear liquid height on sieve plates in the froth, mixed and spray regimes", Chem. Eng. Res. Des., **69**,(Part A), 289.

Bell, R. L., 1972, "Experimental determination of residence time distributions on commercial scale distillation trays using a fibre optic technique", AIChE J., **18**,(3) 491.

Bell, R. L., 1972, "Residence time and fluid mixing on commercial scale sieve trays", AIChE J., **18**,(3), 498.

Bell, R. L. and Solari, R. B., 1974, "Effect of non-uniform velocity fields and retrograde flow on distillation plate efficiency", AIChE J., **20**,(4), 688.

Biddulph, M. W., Kler, S. C. and Lavin, J. T., 1990, "Double-expanded metal distillation tray", US Patent 5091 119.

Biddulph, M. W. and Bultitude, D. P., 1990, "Flow characteristics of a small-hole sieve tray", AIChE J., **36**, (12), 1913.

Bruin, S. and Freije, A. D., 1974, "A simple liquid mixing model for distillation plates with stagnant zones", Trans. IChemE., **52**, 75.

Darton, R.C., 1992, "Distillation and absorption technology: current market and new developments ", Closing address, IChemE. Symp. Ser., **n128**, A385.

Enjugu, B. A., 1986, "Flow Patterns and Performance of Distillation Trays", Ph.D. Thesis, University of Aston in Birmingham, Birmingham, England.

Fair, J. R., 1961, "How to predict sieve tray performance and flooding", Petro/Chem. Engineer, **33**,(10),45.

Foss, A. S., Gerster, J. A. and Pigford, R. L., 1958, "Effect of liquid mixing on the performance of bubble trays", AIChE J., **4**,(2), 231.

French, R. H., 1986, "Open Channel Hydraulics", McGraw-Hill, New York.

Gautreaux, M. F. and O'Connell, H. E., 1955, "Effect of length of liquid path on plate efficiency", Chem. Engng. Prog., **51**,(5), 232.

Gerster, J. A., Hill, A. B., Hochgraf, N. N. and Robinson, D. G., 1958, "Tray efficiencies in distillation columns", Final Report, University of Delaware, AIChE., New York.

Goederen, C. W. J. De., 1965, "Distillation tray efficiency and interfacial area", Chem. Engng. Sci., **20**, 1115.

Hine, C. J., 1990, "Effect of Liquid Flow Patterns on Distillation Trays", Ph.D.Thesis, University of Aston in Birmingham, Birmingham, England.

Hofhuis, P. A. M. and Zuiderweg, F. J., 1979, "Sieve trays: Dispersion density and flow regimes", IChemE. Symp. Ser., **n56**, 2.2/1 - 2.2/27.

IUSC (Inter University Software Committee), Information Graphics Working Party, 1988, Newsletter, n2.

Kafarov, V. V., Shestopalov, V. V. and Komissarov, Y. A., 1979, "Vapour-liquid flow structure on bubbler plates", IChemE. Symp. Ser., **n56**, 2.3/79.

Katayama, H. and Imoto, T., 1972, "Effect of vapour mixing on the tray efficiency of distillation columns", J.Chem.Soc. Japan, **9**, 1745.

Keller, R. D., 1973, "Apparatus for liquid and vapour or gas mass transfer", US Patent 3 729 179.

Kirkpatrick, R. D. and Weiler, D. W., 1978, "Liquid-gas contacting tray", US Patent 4 101 610.

Kirschbaum, E., 1934, "Efficiency of rectification and appropriate path for liquid flow", Forsch. Gebiete Ingenieur, **5**, 245.

Kirschbaum, E., 1948, "Distillation and Rectification", Chemical Publishing Co., New York, 276.

Kouri, R. J. and Sohlo, J. J., 1985, "Effect of developing liquid flow patterns on distillation plate efficiency", Chem. Eng. Res. Des., **63**,(2), 117.

Launder, B. E. and Spalding, D. B., 1972, "Lectures in mathematical models of turbulence", Academic Press.

Launder, B. E. and Spalding, D. B., 1974, "The numerical computation of turbulent flows", Comp. Math. Appl. Mech. Engng., **3**,269.

Lavin, J. T., 1986, "Improvements in distillation trays", UK Patent 2 160 788.

Legg, R., 1986, "Energy Management Focus", December, (9), 2.

Lewis, W. K., 1936, "Rectification of binary mixtures", Ind. Engng. Chem., **28**,(4), 399.

Lewis, W. K., 1922, Trans. ASME., **44**, 325.

Lim, C. T., Porter, K. E. and Lockett, M. J., 1974, "The effect of liquid channelling on two pass distillation plate efficiency", Trans. IChemE., **52**, 193.

Lockett, M. J., 1986, "Distillation Tray Fundamentals", Cambridge University Press.

Lockett, M. J., 1981, "The froth to spray transition on sieve trays", Trans. IChemE., **59**, 26.

Lockett, M. J., and Dhulesia, H. A., 1980, "Murphree plate efficiency with non-uniform vapour distribution", Chem. Engng. J. **19**, 183.

Lockett, M. J., Lim, C. T. and Porter, K. E., 1973, "The effect of liquid channelling on

distillation column efficiency in the absence of vapour mixing", Trans. IChemE., **51**, 61.

Lockett, M. J., Porter, K. E. and Bassoon, K.S., 1975, "The effect of vapour mixing on distillation plate efficiency when liquid channelling occurs", Trans. IChemE., **53**, 125.

Lockett, M. J., Spiller, G. T. and Porter, K. E., 1976, "The effect of the operating regime on entrainment from sieve trays", Trans. IChemE., **54**, 202.

Lockett, M. J. and Safekourdi, A., 1976, "The effect of the liquid flow pattern on distillation plate efficiency", Chem. Engng. J. **11**, 111.

Matsch, L. C., 1973, "Liquid-gas contact tray", US Patent 3 759 498.

McCabe, W. L. and Smith, J. C., 1956, "Unit Operations of Chemical Engineering", McGraw-Hill, New York.

Merkel, F., 1925, "Verdunstungskuhling", Forscharb. Ingwes. Heft 275.

Muller, R. L. and Prince, R. G. H., 1972, "Regimes of bubbling and jetting from submerged orifices", Chem. Engng. Sci. **27**, 1583.

Murphree, E. V., 1925, "Rectifying Column Calculations", Ind. Engng Chem., **17**,(7), 747.

Murphy, J. D., " Turbulence Modelling ", NASA. TM 8 5889 (1984).

Payne, G. J. and Prince, R. G. H., 1977, "The relationship between the froth and spray regimes, and the orifice processes occurring on perforated distillation plates", Trans. IChemE., **55**, 266.

Pinczewski, W. V. and Fell, C .J. D., 1972, "The transition from froth-to-spray regime on commercially loaded sieve trays", Trans. IChemE., **50**, 102.

Pinczewski, W. V. and Fell, C. J. D., 1977, "Droplet sizes on sieve plates operating in the spray regime", Trans. IChemE., **55**, 46.

Porter, K. E., 1973, "Destillations oder Adsorptionskolonne", German Patent 2 322 895.

Porter, K. E., 1992, Opening address, IChemE. Symp. Ser. in Birmingham, **n128**.

Porter, K. E., Davies, B., Enjugu, B. A. and Ani, C. C., 1987, " Investigating the effect

of the liquid flow pattern on sieve tray performance by means of the water-cooling technique", IChemE. Symp. Ser., **n104**, 569.

Porter, K. E. and Jenkins, J. D., 1979, "The interrelationship between industrial practice and academic research in distillation and absorption", IChemE. Symp. Ser., **n56**, 5.1/1.

Porter, K. E. and Lan, R., 1991, "Gas driven liquid circulation on perforated trays ", Aston University Internal Report on Advanced Studies in Distillation.

Porter, K. E., Lockett, M. J. and Lim, C. T., 1972, "The effect of liquid channelling on distillation plate efficiency", Trans. IChemE., **50**, 91.

Porter, K. E., O'Donnell, K. A. and Latipifour, M., 1982, "The use of water-cooling to investigate flow pattern effects on tray efficiency", IChemE. Jubilee Symp. Ser., **No.73**:L33.

Porter, K. E., Safekourdi, A., and Lockett, M. J., 1977, "Plate efficiency in the spray Regime", Trans.I ChemE., **55**, 190.

Porter, K. E. and Wong, P. F. Y., 1969, "Transition from spray to bubbling on sieve plates ", IChemE. Symp. Ser., **No. 32**, p.2:22.

Porter, K. E., Yu, K. T., Chambers, S. and Zhang, M. Q., 1992, "Flow patterns and temperature profiles on a 2.44 m sieve tray ", I.ChemE. Symposium Series **No. 128**: A257.

Prado, M. and Fair, J. R., 1990, "Fundamental model for the prediction of sieve tray efficiency ", Ind. Eng. Chem. Res., **29**, p.1031

Raper, J. A., Hai, N. T., Pinczewski, W. V. and Fell, C. J. D., 1984, "Liquid passage on sieve trays operating in the spray regime", Chem. Eng. Res. Des., **62**,(2), 111.

Rush, F. E. Jr., 1979, "Energy saving alternatives to conventional distillation", IChemE Symp. Ser., **56**, 4.1/1.

Sakata, M. and Yanagi, T., 1979, "Performance of a commercial scale tray", IChemE Symp. Ser., **n56**, 3.2/21.

Smith, V. C. and Delnicki, W. V., 1975, "Optimum sieve tray design", Chem.Engng Prog. **71** (8) 6.

Sohlo, J. J. and Kinnunen, S., 1977, "Dispersion and flow phenomena on a sieve plate", Chem. Engng. Sci., **55**,(2), 71.

Sohlo, J. and Kouri, R. J., 1982, "An analysis of enhanced transverse dispersion on distillation plates", Chem. Engng. Sci., **37**,(2), 193.

Solari, R. B. and Bell, R. L., 1986, "Fluid flow patterns and velocity distribution on comercial scale sieve trays", AIChE J., **32**,(4), 640.

Solari, R., Saez, E., D'Apollo, I. and Bellet, A., 1982, "Velocity distribution and liquid flow patterns on industrial sieve trays", Chem. Engng. Comm. **13**, 369.

Stichlmair, J. and Ulbrich, S., 1987, "Liquid channelling on trays and its effect on plate efficiency", IChemE. Symp. Ser., **n104**, 555.

Stichlmair, J. and Weisshuhn, E., 1973, "Untersuchungen zum bodenwirkungsgrad unter besonderer berucksichtigung der flussigkeitsvermischung", Chem. Ing. Tech., **45**,(5), 242.

Taylor, J. R., 1982, "An Introduction to Error Analysis", University Science books, Mill Valley, CA, USA.

Urua, I. J., Lavin, J. T. and Biddulph M. W., 1992, "A new high performance flow control tray ", I.ChemE. Symposium Series **No. 128**: A345.

Walton, A. G.,1993, "Computer simulation of liquid flow patterns on distillation trays", Report submitted to members of the Consortium for Advanced Studies in Distillation (A.S.I.D.).

Weiler, D. W., Bonnet, F. W. and Leavitt, F. W., 1971, "Slotted sieve trays", Chem. Engng. Prog., **67**,(9), 86.

Weiler, D. W., Delnicki, W. V. and England, B. L., 1973, "Flow hydraulics of large diameter trays", Chem. Engng. Prog., **69**,(10), 67.

Williams, B. and Yendall, E. F., 1963, "Improvements in and relating to liquid-gas contact tray", GB Patent 941 783.

Williams, B. and Yendall, E. F., 1968, "Apparatus for liquid-gas contacting tray", US Patent 3 417 975.

Yanagi, T. and Scott, B.D., 1973, "Effects of liquid mixing on commercial scale sieve tray efficiency", AIChE J., Meeting, March, New Orleans.

Urua, I. J., Lavin, J. T. and Biddulph M. W., 1992, "A new high performance flow control tray ", I.ChemE. Symposium Series **No. 128**: A345.

Yu, K. T., 1992, "Some progress of Distillation Research and industrial applications in China", I.ChemE. Symposium Series **No. 128**: A139.

Yu, K. T., Huang, J., Li, J. L. and Song, H. H., 1990, "Two-dimensional flow and eddy diffusion on a sieve tray", Chem. Engng. Sci., **45**,(9), 2901.

Yu, K. T., Huang, J. and Zhang, Z. T., 1982, "The residence time distributions and efficiencies of large trays", Proceedings of Joint Meeting of Chemical Engineering, Beijing, China, **2**, 425.

Yu, K. T., Huang, J. and Zhang, Z. T., 1986, "Residence time profile and plate efficiency for a large tray with single-pass or two-pass liquid flow", J. Chem. Ind. Engng (China), **2**, 151.

Yu, K.T., Song, H.H. and Huang, J., 1991, "A three dimensional non-equilibrium pool model for the simulation of a tray column", J.Chem. Ind. Eng (China), **42**,653.

Yu, K.T. and Zhang, M. Q., 1991, "Theoretical computation of a two dimensional model of liquid phase flow on a tray", Private communication.

Zuiderweg, F. J., 1982, "Sieve trays - a view on the state of the art", Chem. Engng. Sci., **37**,(10), 1441.